DOI: 10.31577/ahs-2023-0024.02.0018

ACTA HYDROLOGICA SLOVACA

Volume 24, No. 2, 2023, 161 – 172

Evaluation of water dissolved oxygen under climate change and its modeling in Bodrog River at Streda nad Bodrogom

Veronika BAČOVÁ MITKOVÁ*

The oxygen is one of indicators of water quality that plays a crucial role in affecting the biological processes in surface water. In the context of the climate change, there are also changes in the oxygen regime of the water in the streams. The paper presents an evaluation of the changes in long-term data of the dissolved oxygen (DO), water temperature T_w, biochemical oxygen demand (BOD) and chemical oxygen demand (COD), and flows (Q) in the Bodrog River at Streda nad Bodrogom, during the period of 1965–2021. The aim of the study is to detect whether significant trends occur in the time series of analyzed data. The first part of the paper dealt with the trend analyses of monthly and annual data. The results can be useful to quantify the possible threat to its balanced regime. The study shoved an increasing trend in the long-term trend of the DO and a decreasing trend in biochemical oxygen demand. The following section is focused on regression between selected components of the hydrosphere and modelling them. The ability to model the components of the hydrosphere is an essential part of water resource management.

KEY WORDS: flow, oxygen water regime, water temperature, long-term trends, interrelationships

Introduction

Water is a renewable but limited natural source, an important component of natural ecosystems. As a result of human activity and climate change, growing of the extreme hydrological and meteorological phenomena in their frequency of occurrence, duration and severity are expected (Dai, 2013; Trenberth et al., 2014; Alfieri et al., 2017; Baiardi and Morana, 2021; Gorbachova and Khrystiuk 2021 or Blaškovičová et al., 2022). That may directly or indirectly affects water quality in surface waters. Due to the multifunctional and multiple use of water, inconsistency between the temporal and spatial distribution of the water sources and requirements as well as from water reuse along the streams it is necessary to coordinate the water managements and use of water resources (Vitaku et al., 2013). In practice, the efforts of all participating actors should be focused on the use, development and protection of water resources in a fair and appropriate way, by applying the concept of sustainable development in the field of water management using the most modern methods at least at the European level (Heinz et al., 2007).

In October 2000 the Water framework Directive (WFD 2000/60/ES) of the EU parliament was adopted. The implicate objective of the Directive is to achieve good status for all water bodies. The EU Water Framework Directive (WFD 2000/60/EC) applies the principle "one-out-all-out" it means that good status must be achieved by each monitored element. The many EU Member States have „forgotten" to work with the concepts of quantity/quality/condition/potential of surface waters, their interrelationship and interconnection. The EU Water Resources Concept (COM, 2012) states „it is important to recognize that water quality and quantity are closely linked in terms of good condition". On 12th May 2021, the European Commission adopted the EU Action Plan: „Towards zero air, water and soil pollution" (COM, 2021).

Slovak Hydrometeorological Institute (SHMI) provides the national monitoring and assessment of hydrological characteristics and water quality in Slovakia according to NV No. 269/2010 Z. z. Regulation of the Government of the Slovak Republic. Pekárová et al. (2004) processed a method for identifying long-term trends of individual water quality indicators in surface streams. The methodology was based on the requirements of Directive 2000/60/EC and existing data from the database of the SHMI. In recent years, the evaluation of quality elements on selected profiles of Slovak rivers or the transport of pollution in surface waters was investigated by Pekárová et al. (2009); Noskovič et al. (2013); Hrdlicová (2016); Ondrejka Harbuľáková et al. (2017) or Siman and Velísková (2017). These works concluded that the state of water quality after 1989 has generally improved. However, it is still necessary to monitor trends in water temperature, surface pollution

and, in the case of small streams, the trend of pollution by organic or inorganic substances. The type and concentration of chemical elements in the surface waters of streams are changed due to different types of natural processes, which depends on environmental factors influenced by still changing natural and anthropogenic activities. Monitoring of the trends in surface water quantity and quality deserves special attention in the research to quantify the possible threat to its balanced regime.

The DO concentration of the water is one of the important indicators of the water ecosystems status. The oxygen is essential for respiration and survival of the aquatic organisms. The source of the oxygen in water comes primarily from atmosphere by physical diffusion between water-air interface. This process is substantially enhanced by the turbulent mixing of water with air, facilitated by wind and water waves. The oxygen uptake is significantly higher in fast flowing, large and turbulent streams compared with slow-moving streams and lakes. Gas-transfer modelling (Gualtieri and Pulci Doria, 2012) or, if the transferred gas is oxygen, reaeration is most relevant in water quality modelling. Air-water gas transfer velocity determines the transport rate of oxygen, carbon dioxide, methane, and volatile pollutants entering or leaving streams and rivers via the free surface (Raymond et al., 2012). This, affects basic ecological processes in water and has tremendous implications for the global climate system (Bernhardt et al., 2018; Ulseth et al., 2019). Wang et al. (2021) presented physically based scaling models to predict gas transfer velocity for 35 streams and small to medium-sized rivers in the United States based on DO data using an inverse modelling approach.

It is also known that the concentration of DO in water is affected by water temperature, where oxygen has a greater solubility in colder water than in warmer water. As the result of this, the concentration values of DO in the rivers during the colder seasons are higher than during the warmer seasons. The concentration of the DO can be further reduced by adding oxygen-demanding organics to the river systems (e.g. sewage, agricultural waste, lawn clippings, etc.). The impact of climate change on water temperature and oxygen regime has been addressed in papers by Harvey et al. (2011); Danladi et al. (2017) or Rajesh and Rehana (2022). The effects of water pollution are complex and vary depending on the nature and concentration of contaminants (Artemiadou and Lazaridou, 2005).

Understanding and analysing their interconnectedness and dependencies deserves equal attention. As was mentioned above, the climate change and anthropogenic activities affect the water quantity and quality with negative impact on hydrological regime of streams. Therefore, it is necessary to know and analyse their changes and the mutual relationship of quantitative characteristics and indicators of water quality. Such knowledge enables prevention and response to a crisis phenomenon and is one of the prerequisites for a quick and correct solution in elimination of its consequences. While the potential impacts of climate change on water availability have been widely studied in recent decades, their impact on water quality is still less researched.

The first objective of the paper is to detect and analyse the changes in the long-term trends of the oxygen regime of surface water in the selected river: Bodrog at the Streda nad Bodrogom station to quantify the possible threat to his balanced regime for the period 1965–2021. The input data were monthly samples of selected water quality indicators (dissolved oxygen DO, water temperature T_w, biochemical and chemical oxygen demand (BOD and COD) and the corresponding daily flows (Q_d) on the sampling days. In addition, analysed water temperatures are those at the time of the sampling for water quality.

The second part of the paper is focused on the cross-correlation analysis of selected components of the hydrosphere and to model them effectively. An autoregressive model with a selected regressor was tested in the presented work. For modelling dissolved oxygen depending on water temperature, the model is designed to capture and account for patterns and trends within time series data, including seasonality and periodicity. The ability to model the components of the hydrosphere is an essential part of water resource management.

Material and methods

Study area and data

To analyse the development, assessment and interrelationship of selected components of the hydrosphere and taking into account the length of observations of the selected components we selected the Bodrog River at the Streda nad Bodrogom station. The period of 56 years (1965–2021) was analysed. From a hydrological point of view, the Bodrog river basin represents a complex river system of four main rivers (Latorica, Laborec, Uh, Ondava). These main rivers meeting each other in a small area, which has an adverse impact on the formation of large waters and flood situations in this location. The Bodrog River itself is formed by the confluence of the rivers Ondava and Latorica near Zemplín. It is a right-hand tributary of the Tisa River. Bodrog has a length of 65 km to the mouth of the Tisza, of which only 15 km is in Slovakia area. Bodrog leaves our territory at an altitude of 94 m a. s. l., which represents the lowest place in Slovakia and crosses the border with Hungary near the villages of Klin nad Bodrogom and Borša. The Bodrog River is the only waterway in Eastern Slovakia (Fig. 1) (it is navigable by larger ships; depending on the water level it reaches a depth of at least 230 cm).

Hydrological conditions of the Bodrog River in the Streda nad Bodrogom station 1950–2021

The year 2010 2010 (204.2 $m^3 s^{-1}$) we can classify as wettest year and the driest was 1961 (46.5 $m^3 s^{-1}$) at Bodrog in Stanica Streda nad Bodrogom. The highest flood in Bodrog was in 1979, when the peak flow reached a value of 1200 $m^3 s^{-1}$, but the longest-lasting flood wave occurred in 2006 with a peak flow of 846.4 $m^3 s^{-1}$ and

a duration of approx. 61 days. September is the driest month in Bodrog, with a share of 4.1% of the annual runoff. The wet months are March and April, when on average around 31% of the annual runoff flows. Fig. 2 shows the deviation of annual flows from the long-term annual flow for the period 1950–2021, as well as 5-year moving averages.

Development of selected indicators of the oxygen regime at Bodrog in Streda nad Bodrogom station

The input data for analysis were monthly samples of selected water quality indicators (dissolved oxygen, water temperature, biochemical and chemical oxygen demand) and the corresponding daily flows on the sampling days. In addition, analysed water temperatures are water temperatures at the time of sampling for water quality. Daily flow values on the day of water quality sampling on the Bodrog at the Streda nad Bodrogom station in the period 1965–2021 are plotted in Fig. 3. The long-term development of monthly values of selected water quality indicators of the Bodrog at the Streda nad Bodrogom station in the period 1965–2021 are plotted in Fig. 4. In order to obtain basic information about water quality, monthly sampling intervals can be considered sufficient, but the case of very significant transport of substances by a flood wave may not be captured.

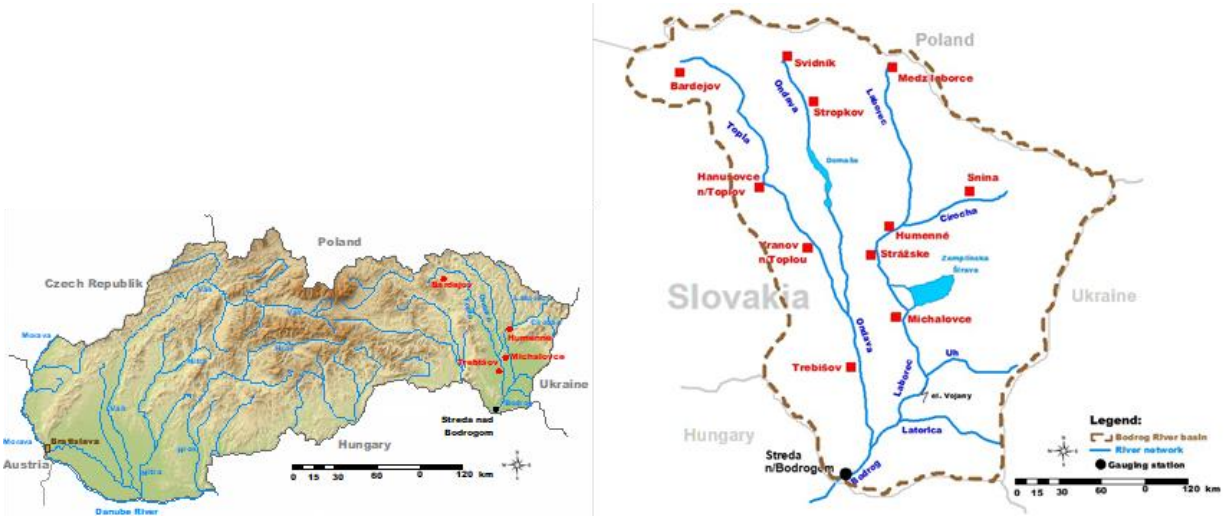

Fig. 1. Scheme of the main river network of Slovakia with Bodrog River location and scheme of the Bodrog river catchment.

Table 1. Basic geograpical characteristics of the Bodrog River: Streda nad Bodrogom

River	Gauging station	Catechment area [km^2]	River kilometer [r.km]	Elevation [m a. s. l]
Bodrog	Streda nad Bodrogom	11474.25	5.20	91.4

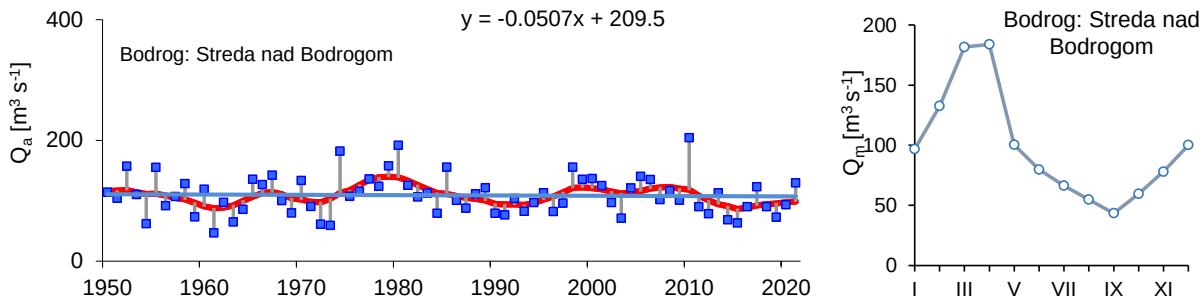

Fig. 2. Annual and monthly flows of the Bodrog River: Streda nad Bodrogom during the period 1950–2021 (red line – 5-year moving average).

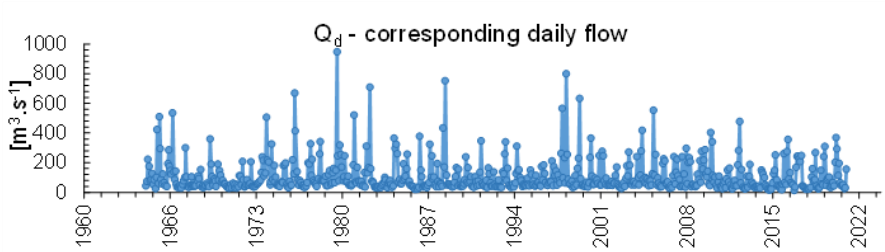

Fig. 3. The corresponding daily flows Q_d on the sampling days for water quality of the Bodrog River: Streda nad Bodrogom during the period 1965–2021, (black line – linear trend).

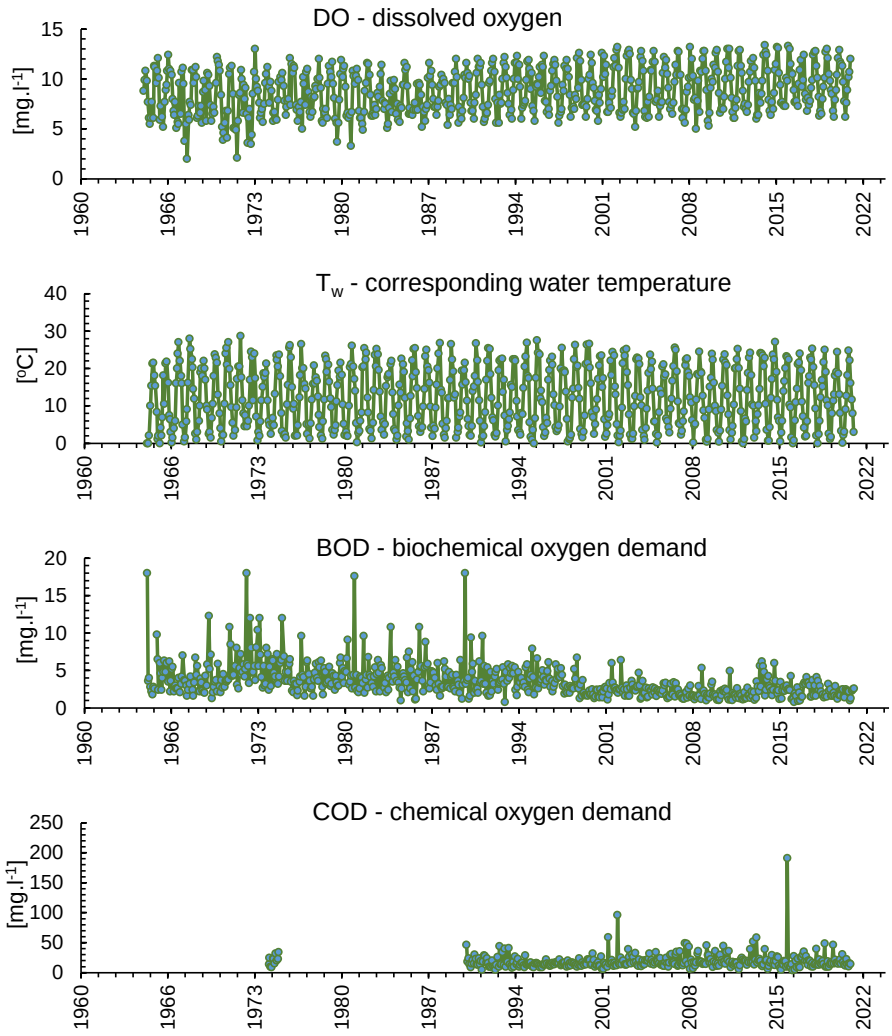

Fig. 4. Development of monthly values of selected water quality indicators DO, T_w, BOD and COD of the Bodrog River: Streda nad Bodrogom during the period 1965–2021.

Methods

Trend analysis of the selected monthly and annual oxygen indicators of the surface water

The Mann-Kendall nonparametric test (M-K test) was used for determining the significant trends detection of monthly and annual confrontations of selected indicators of oxygen river regime. The nonparametric tests are more suitable for the detection of trends in hydrological time series, which are usually irregular, with many extremes (Hamed, 2008; Yue, et al. 2002; Gilbert, 1987). MAKESENS 2-tailed test is used for four different α significance levels. The significance level of the test α- is a chosen number from the interval from 0 to 1, or 100% (the smaller the better, but α = 0.05 or 5%) is most often

used. A significance level of 0.05 means that there is a 5% probability that the values of xi are from a random distribution, and with that probability we make an error in rejecting H0 (the null hypothesis) of no trend. A significance level of 0.001 means that the existence of a monotonic trend is very likely.
We evaluated the significance of the trend in our study at selected significant levels or levels of trend significance).

*** – if the trend is at α = 0.001 – the validity of H0 is improbable,
** – if the trend is at α = 0.01–1% error in rejecting H0,
* – if the trend is at α = 0.05–5% error in rejecting H0,
+ – if the trend is at α = 0.1–10% error in rejecting H0,
Empty – the level of significance is greater than 0.1, we cannot rule out that H0 is true.

The most important trend is assigned three stars (***), with the gradual decrease in importance, the number of stars also decreases. Statistically, we evaluate the significance of a trend using the *Z* value. A positive *Z* value indicates an upward (growing) trend, while a negative value indicates a decreasing trend. If the absolute value of *Z* is less than the significance level, there is no trend.

Cross-correlation analysis of selected components of the hydrosphere

To assess the strength of interdependence between individual selected components of the hydrosphere, the equation (1) was used (Prohaska et al., 2000)

$$\sigma_R = \frac{1-R^2}{\sqrt{N}}\sigma \quad (1)$$

where
σ_R – correlation coefficient error *R*;
N – number of years included in the analysis.

For a significantly different correlation coefficient from zero, criterion (2) must be valid

$$|R| \geq 3.\sigma_R \quad (2)$$

By standardizing the random variables, we obtained a new dimensionless measure of dependence, which takes on values from the interval (−1; 1). The sign of the correlation coefficient depends on the covariance, according to which we interpret the value of the coefficient:
• $R(x,y) > 0 \Leftrightarrow$ direct dependence,
• $R(x,y) < 0 \Leftrightarrow$ indirect dependence,
• $R(x,y) = 0 \Leftrightarrow$ independence (correlation).

The most commonly developed models for predicting river oxygen concentrations may be difficult for calculation, e.g. dynamic mass balance models (Gelda et al., 2001), models of artificial neural networks (Rounds, 2002), or extended harmonic analysis, so-called algorithm models (Abdul-Aziz et al., 2007). The simplest model is the regression model, which indicates a linear relationship between water temperature T_w and DO:

$$O2 = \alpha_0 + a * Tw + \varepsilon \quad (3)$$
or
$$O2 = \alpha_0 + a * Tw + WL + \varepsilon \quad (4)$$

where
α_0, *a* – are the parameters of the regression curve,
T_w – is the water temperature,
WL – is the height of the water level (enters the equation if it is a significant element),
ε – is the error (residue).

Linear and nonlinear modelling for simultaneous prediction of DO and biochemical oxygen demand in surface water was analysed in Basant et al. (2010). Pekárova et al. (2020), used an empirical-regression relationship to indirectly estimate nitrate nitrogen concentrations based on the average daily flow in the sampling days.
Another type of models can be autoregressive models, which forecast future behavior based on past behavior data and there correlation between the time series values and their preceding and succeeding values exists (Faruk, 2010; Wongsathan and Seedadan, 2016; Soltani et al., 2021). For the modelling of DO depending on water temperature, an autoregressive ARIMA model with the selected regressor was tested. The model is designed to capture and account for patterns and trends within time series data, including seasonality and periodicity. The seasonal component is particularly important in the SARIMA model because it allows modelling data with seasonal fluctuations or cycles. The model involves fitting a regression equation to the data, where the dependent variable is the time series data and the independent variables are the series lags and lagged errors. The model is usually estimated using the maximum likelihood estimation, and the accuracy of the model can be evaluated using various statistical criteria. To identify this model, it is necessary to analyze the individual components of the time series in the following order:

- trend identification,
- choosing the type of model and determining the order of the model,
- estimation of model parameters,
- model validation.

The general form of the SARIMA(*p, d, q*)x(*P, D, Q*)*L* model takes the following form:

$$\varphi(B)\,\phi(B^L)\,\nabla^d\,\nabla^D{}_L\,Y_t = \Theta(B)\,\Theta(B^L)E_t, \quad (5)$$

where:
E_t – independent and normally distributed random variable with zero mean value μ=0 and variance σ_E^2;
p – trend autoregressive order,
d – trend difference order,
q – trend moving average order,

P – seasonal autoregressive order,
D – seasonal difference order,
Q – seasonal moving average order,
L – the number of time steps for a single seasonal period (an L of 12 for monthly data suggests a yearly seasonal cycle,
B – reversion shift operator defined as $BY_t = Y_{t-1}$,
∇^1 – the backwards difference operator,
φ – the regular AR (auto-regressive) operator of the order p,
Θ – is the regular SMA (moving average) operator of the order q,
$\nabla^D{}_L$ – the seasonal backwards difference operator,
$\boldsymbol{\varphi}$ – is the regular SAR (seasonal auto-regressive) operator of the order P,
$\boldsymbol{\Theta}$ – is the regular SMA (seasonal moving average) operator of the order Q.

Results and discussion

Trend analysis of selected monthly and annual indicators of the oxygen flow regime

The first part of the paper is aimed to evaluate water temperature development and oxygen regime of the Bodrog River at Streda nad Bodrogom during the period 1965–2021. Long-term monthly concentration of selected indicators and as well as water temperature are illustrated in Fig. 5a, b. The maximal long-term monthly concentration of DO was found from December to March. The minimum long-term monthly concentration of DO was observed in July. The analysed corresponding water temperatures show long-term maximum value in summer months (July and August). In terms of long-term monthly concentration of biochemical and chemical oxygen demand, the maximum reached the value 4.1 mg l^{-1} and 22 mg l^{-1}.

The development of annual concentrations of selected indicators and as well as water temperature are illustrated in Fig. 6a–d. The development of annual DO concentrations shows a significant increasing long-term trend during the period 1965–2021 (Fig. 6a) and Table 2). The development of annual biochemical oxygen demand concentrations shows a significant decreasing long-term trend during the period 1965–2021 (Fig. 6c) and Table 2). The annual values of water temperature in days of sampling and chemical oxygen demand do not indicate a change in the long-term trend (Fig. 6b, c).

The development of monthly concentrations of DO indicates a significant increasing long-term trend in all months of the year (Table 2). The development of monthly concentrations of DO and long-term linear trend in the selected months of February and August are plotted in Fig. 7 a, b. The development of monthly values of biochemical oxygen demand indicates a significant long-term decreasing trend in all months of the year (Table 3). The development of monthly concentrations of biochemical oxygen demand and the long-term linear trend in the selected months of October and August are plotted in Fig. 8 a, b.

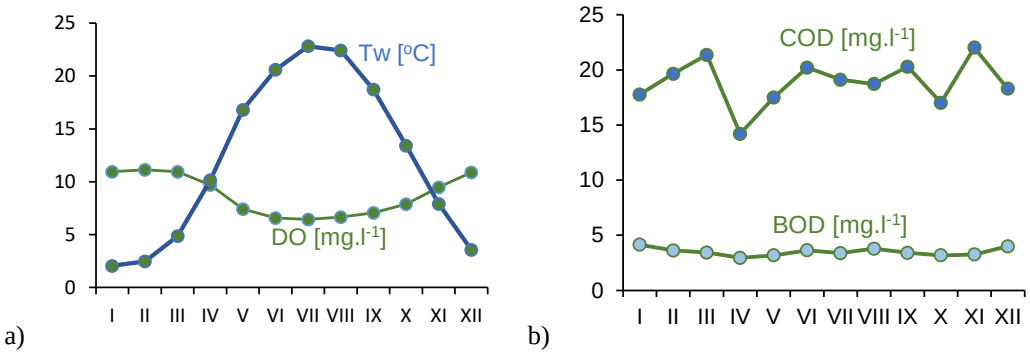

Fig. 5. Long-term monthly values of DO, water temperature T_w, biochemical oxygen demand (BOD) and chemical oxygen demand (COD) in the Bodrog River: Streda nad Bodrogom during the period 1965–2021.

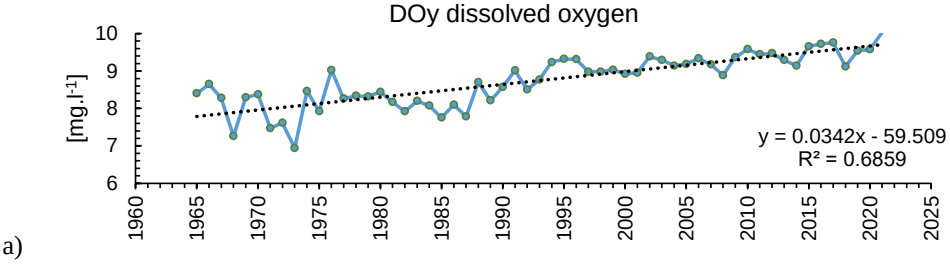

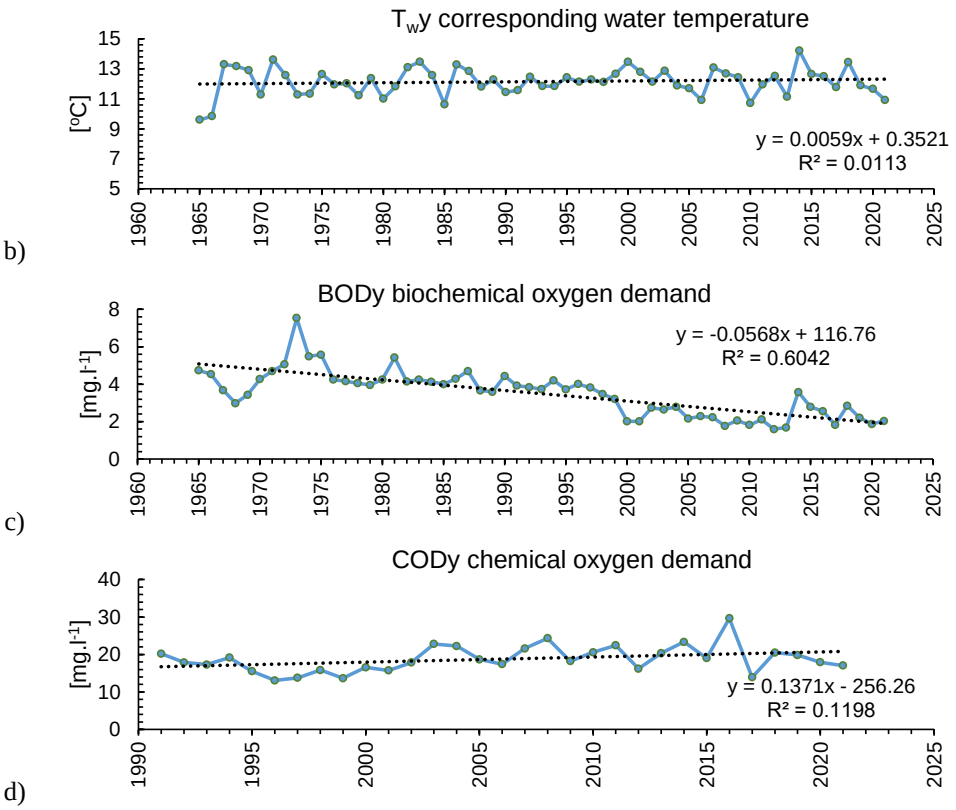

Fig. 6. Annual values of selected water quality indicators, in the Bodrog River: Streda nad Bodrogom during the periods 1965–2021 and1991–2021.

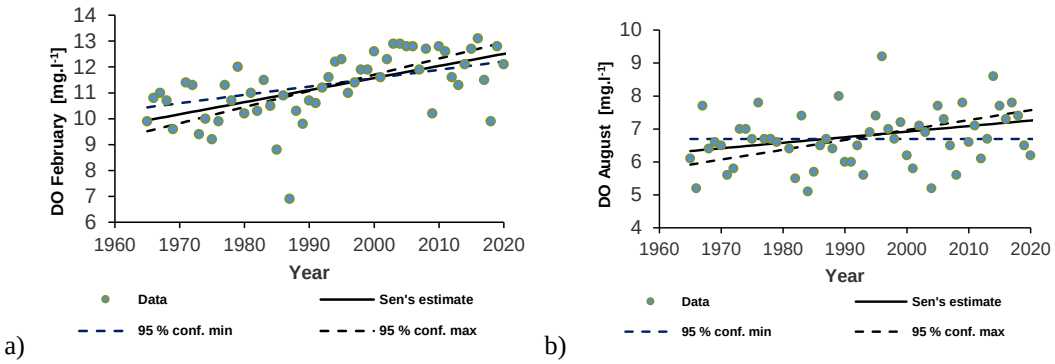

Fig. 7. Monthly concentration of the DO and long-term linear trend (black line) with confidence interval (dot line) in the Bodrog River: Streda nad Bodrogom during the period 1991–2021, a) January and b) August.

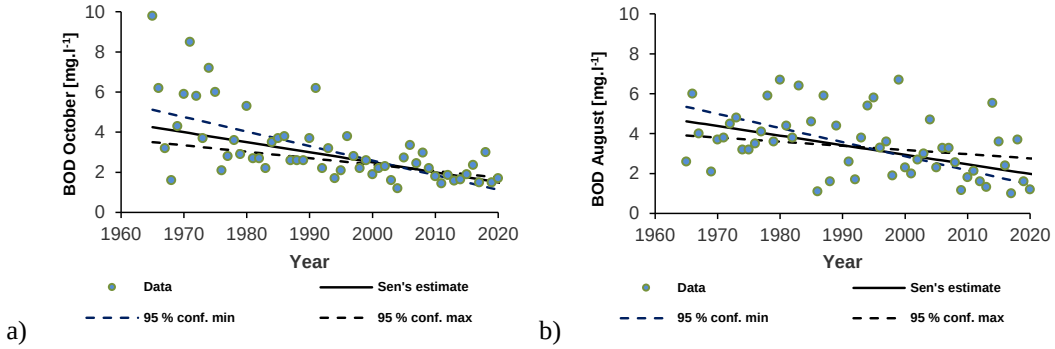

Fig. 8. Monthly concentration of the biochemical oxygen demand and long-term linear trend (black line) with confidence interval (dot line) in the Bodrog River: Streda nad Bodrogom during the period 1991–2021, a) October and b) August.

Table 2. Results of the M-K test for long-term trend of monthly and annual concentration of DO in the Bodrog River: Streda nad Bodrogom during the period 1991–2021

Month	First year	Last year	*n*	Test *Z*	Sign.	skew	Corell. *R*
January	1965	2021	57	4.52	***	0.056	0.55
February	1965	2021	57	4.97	***	0.047	0.57
March	1965	2021	57	2.50	*	0.023	0.38
April	1965	2021	57	2.59	**	0.021	0.33
May	1965	2021	57	3.44	***	0.033	0.46
June	1965	2021	57	3.23	**	0.022	0.44
July	1965	2021	57	1.95	+	0.013	0.32
August	1965	2021	57	2.26	*	0.017	0.30
September	1965	2021	57	2.99	**	0.029	0.41
October	1965	2021	57	5.35	***	0.059	0.58
November	1965	2021	57	3.52	***	0.035	0.47
December	1965	2021	57	4.10	***	0.039	0.55
Annual	1965	2021	57	6.90	***	0.034	0.83

Table 3. Results of the M-K test for long-term trend of monthly and annual concentration of BOD in the Bodrog River: Streda nad Bodrogom during the period 1991–2021

Month	First year	Last year	*n*	Test *Z*	Sign.	skew	Corell. *R*
January	1965	2021	57	-5.30	***	-0.076	0.55
February	1965	2021	57	-4.57	***	-0.059	0.54
March	1965	2021	57	-3.78	***	-0.044	0.48
April	1965	2021	57	-3.18	**	-0.028	0.37
May	1965	2021	57	-2.87	**	-0.027	0.35
June	1965	2021	57	-3.33	***	-0.037	0.40
July	1965	2021	57	-3.95	***	-0.042	0.44
August	1965	2021	57	-3.43	***	-0.048	0.31
September	1965	2021	57	-3.63	***	-0.047	0.37
October	1965	2021	57	-5.33	***	-0.050	0.64
November	1965	2021	57	-4.44	***	-0.051	0.58
December	1965	2021	57	-4.83	***	-0.078	0.55
Annual	1965	2021	57	-6.71	***	-0.057	0.78

Correlation analysis of the selected components of hydrosphere

The correlation coefficient between the flow rate Q_d and the selected qualitative indicators reached values in the interval -0.278 to 0.241 (Table 4). According to the criterion (2) some correlation coefficients were significantly different from zero (Table 5). The scatter plots of the dependencies of individual indicators showed, that more of them does not have a linear course. For example, the dependence between the flow Q_d and DO is plotted in Fig. 9 a. From the graphical comparison of all correlation dependencies, the highest linear correlation emerged between qualitative indicators: water temperature T_o and DO when R= -0.845 (Fig. 9b).

Modeling of the dissolved oxygen DO

Several auto regression models were tested to identify a suitable model that would model the DO concentration with water temperature as a regressor. Monthly DO concentrations and monthly corresponding water temperatures were used to calibrate an auto regression model for period 1990–2021. Monthly values of water temperature as a linear ($R_{DO\text{-}Tw}$=0.904) and exponential ($R_{DO\text{-}Tw}$=0.902) regressors were used. The period 2012–2021 was used for model validation.

Selected SARIMA auto regression models:

(A) SARIMA(0,0,0)x(0,1,1)$_{12\ constant}$ + 1 lin. regressor,

(B) SARIMA(0,0,0)x(0,1,1)$_{12\ constant}$ + 1 exp. regressor.

Table 4. **Correlation coefficient R between the selected components of the hydrosphere in the Bodrog River at the Streda nad Bodrogom station (1965–2021), (red values - criterion applies $|R| \geq 3.\sigma_R$)**

R	Q_d [m^3 s^{-1}]	DO [mg l^{-1}]	BOD [mg l^{-1}]	COD [mg l^{-1}]	T_w [°C]
Q_d [m^3 s^{-1}]	1.000				
DO [m^3 s^{-1}]	0.241	1.000			
BOD [m^3 s^{-1}]	-0.118	-0.158	1.000		
COD [m^3 s^{-1}]	0.166	-0.031	0.202	1.000	
T_w [°C]	-0.278	**-0.845**	-0.057	-0.004	1.000

Table 5. **Values $3.\sigma_R$ eteween selected components of the hydrosphere in the Bodrog River at the Streda nad Bodrogom station (1965–2021)**

R	Q_d [m^3 s^{-1}]	DO [mg l^{-1}]	BOD [mg l^{-1}]	COD [mg l^{-1}]	T_w [°C]
Q_d [m^3 s^{-1}]	0.000				
DO [m^3 s^{-1}]	0.103	0.000			
BOD [m^3 s^{-1}]	0.113	0.112	0.000		
COD [m^3 s^{-1}]	0.149	0.154	0.147	0.000	
T_w [°C]	0.106	0.034	0.115	0.154	0.000

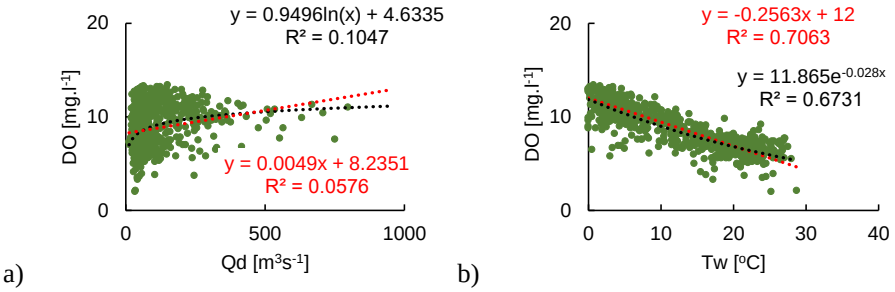

Fig. 9. Correlation a) linear and logarithmic between corresponding daily flows Q_d and DO, and b) linear and exponential between corresponding water temperature T_w and DO in the Bodrog River: Streda nad Bodrogom (1965–2021).

Table 6. **The model estimation errors of selected models and model parameters of the SARIMA (0,0,0) x (0,1,1)12 $_{\text{constant}}$ + 1 exp. regresor(T_w) used to model the DO in Bodrog at the Streda nad Bodrogom**

Model	RMSE	MAE	MAPE	ME	MPE
(A)	0.869626	0.655725	7.6103	0.020077	-0.724278
(B)	0.810823	0.599878	6.79626	-0.0145233	-0.957048
Model SARIMA (0,0,0) x (0,1,1)12 + 1 exp. regresor					
Parameter	Estimate	Stnd. Error		t	P-value
SMA(1)	0.905768	0.018092		50.0644	0.000000
exp. regres T_w	0.683492	0.101812		6.71327	0.000000
mean	0.0281473	0.0111421		2.52621	0.012218
Constant	0.0281473				

For both selected models the P-value values for in their estimated parameters as well as in the simulations were not statistically significant. The model estimation errors and model parameters SARIMA (0,0,0) x (0,1,1)12$_{\text{const}}$+1exp. regressor are listed in Table 6. The graphical result of the validation of the modelling of the monthly concentrations of DO depending on the water temperature by the selected model are illustrated in Fig. 10. The selected model subsequently can be used to predict the concentrations of DO depending on the water temperature T_w. Fig. 11 illustrates changes in the DO concentrations if the water temperature is higher about 2°C and long-term monthly residuals from the measured DO concentrations.

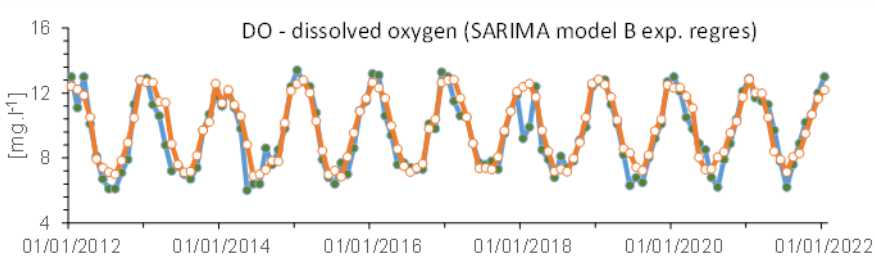

Fig. 10. Validation of the selected SARIMA model for modelling monthly DO concentrations with water temperature T_w as exponential regressor of the Bodrog: Streda nad Bodrog (2012–2021).

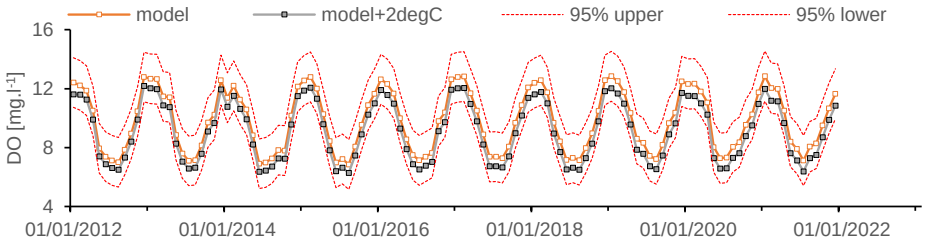

a)

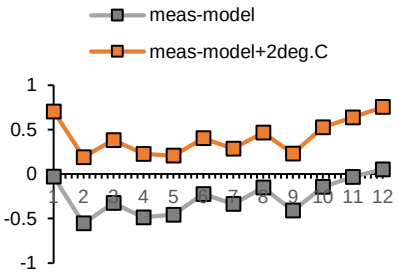

b)

Fig. 11. Comparison of modelled DO concentrations using the SARIMA(0,0,0) x (0,1,1)12const+1exp model, at recorded temperatures and when water temperature is higher about 2°C in river Bodrog: Streda nad Bodrogom (a) monthly concentrations, b) long-term monthly residuals).

Conclusion

The oxygen is one of the indicators of the water quality and plays kay role in biological processes in surface water. Organic substances in water cannot be monitored and determined individually, because they are capable of oxidation. But we can express their amount/sum by the amount of oxygen for their complete oxidation. Such substances can oxidize, either chemically or biochemically. Chemical oxygen demand is a qualitative estimate of organic water quality and should not be used as the sole parameter for measuring organic loading. Biochemical oxygen demand is an empirical test that measures oxygen demand by bacteria over 5 days. In connection with climate change, there are also changes in the oxygen regime of water in streams. Firstly, the present paper dealt with long-term trend analysis of monthly and annual selected oxygen indicators, corresponding water temperatures and daily flows in the Bodrog River at Streda nad Bodrogom during the period 1965–2021. The results of the long-term trend analysis of the development of the monitored indicators of the oxygen regime of the surface water showed a significant long-term increasing trend of annual concentrations of DO, while the indicator of biochemical oxygen demand showed a significant long-term decreasing trend in annual values. The similar course was detected in monthly concentrations of DO, and of biochemical oxygen demand. The indicator of chemical oxygen demand for the period 1991–2021 showed a balanced trend.

Secondly, we determined the correlation dependence of selected components of the hydrosphere and modelled the concentrations of DO in the flow depending on the selected regressor. The results of the correlation analysis showed the closest relationship between monthly concentrations of DO and corresponding water temperature Tw. The correlation coefficient for the entire period reached a significant value of R= -0.845 (the "–" sign indicates indirect dependence between the variables). The relationship between DO and water temperature is strongly negative (Harvey et al., 2011).

Johnson et al. (2016), state that the exponential model may be more suitable for modelling low DO concentrations at higher water temperatures such as polynomial relationship. The results of our analysis on the Bodrog River in the Streda nad Bodrogom station did not show a significant difference in the correlation coefficient of the linear and exponential dependence of the concentrations of DO and water temperature T_w up to 30°C.

Subsequently, we used an autoregressive model with a different mathematical expression of the water temperature T_w as a regressor on data for the period 1990–2021to model the monthly concentrations of DO depending on the water temperature of the Bodrog River at the Streda nad Bodrogom station. In the first model, the regressor T_w had linear expression and in the second, it had exponential expression. Model SARIMA(0,0,0) x (0,1,1)12const+1exp. the regressor achieved slightly better results in the statistical parameters of the estimation during validation with a good fit indicated by a high correlation coefficient of R=0.931. In conclusion, however, we can state that both selected regressors can subsequently be used to predict the concentrations of DO depending on the water temperature T_w up to 30°C. An autoregressive model with the appropriate selected regressor is able to model and predict dissolved oxygen as a function of water temperature, captures and takes into account trends in time series data, including seasonality and periodicity. The ability of this model can predict risk states associated with the increase in water temperature and subsequent changes in dissolved oxygen in the water, which allows for early implementation of economically less demanding environmental and water management measures to reduce their negative impacts.

Acknowledgement

This work was supported by the project VEGA No. 2/0015/23 "Comprehensive analysis of the quantity and quality of water regime development in streams and their mutual dependence in selected Slovak basins"; project APVV-20-0374 "Regional detection, attribution and projection of impacts of climate variability and climate change on runoff regimes in Slovakia"; and project WATSIM "Water temperature simulation during summer low flow conditions in the Danube basin".

References

Artemiadou, V., Lazaridou, M. (2005): Evaluation Score and Interpretation Index for the Ecological Quality of Running Waters in Central and Northern Hellas. Environmental monitoring assessment, 110, 1–40. https://link.springer.com/article/10.1007/s10661-005-6289-72016_17_2_Hrdlicova_157.pdf

Abdul-Aziz, O., Wilson, B., Gulliver, J. (2007): An extended stochastic harmonic analysis algorithm: application for dissolved oxygen. Water Resources Research, 43: 1–19. https://doi.org/10.1029/2006WR005530 articles/2017_18_1_Siman_39.pdf

Alfieri, L., Bisselink, B., Dottori, F., Naumann, G., de Roo, A., Salamon, P., Wyser, K., Feyen, L. (2017): Global projections of river flood risk in a warmer world. Earth's Future, 5(2), 171–182. doi.org/10.1002/2016EF000485.

Baiardi, D., Morana, C. (2021): Climate change awareness: Empirical evidence for the European Union. Energy Economics, 96, 105163. doi.org/10.1016/j.eneco.2021.105163.

Basant, N., Gupta, S., Malik, A., Singh, K. P. (2010): Linear and nonlinear modeling for simultaneous prediction of dissolved oxygen and biochemical oxygen demand of the surface water—a case study. Chemometrics and Intelligent Laboratory Systems, 104(2), 172–180. doi.org/10.1016/j.chemolab.2010.08.005

Bernhardt, E. S., Heffernan, J. B., Grimm, N. B., Stanley, E. H., Harvey, J., Arroita, M., et al. (2018): The metabolic regimes of flowing waters. Limnology & Oceanography, 63(S1), S99–S118. https://doi.org/10.1002/lno.10726.

Blaškovičová, L., Jeneiová, K., Melová, K., Poórová, J., Liová, S., Slivková, K., Síčová B. (2022): Changes in Selected Low-Flow Characteristics in the 2001–2015 Period Compared to the 1961–2000 Reference Period in Slovakia. Climate 10, no. 6: 81. https://doi.org/10.3390/cli10060081

COM (2012): Communication from the Commission to the European Parliament, the Council, the European Economic and Social Committee and the Committee of the Regions: A Blueprint to Safeguard Europe's Water Resources. COM/2012/673 final, Brusel.

COM (2021): Communication from the Commission to the European Parliament, the Council, the European Economic and Social Committee and the Committee of the Regions: Pathway to a Healthy Planet for All EU Action Plan: „Towards Zero Pollution for Air, Water and Soil" COM/2021/400 final.

Dai, A. (2013): Increased drought under global warming in observations and models. Nat. Clim. Change 3, 52–58. doi.org/10.1038/nclimate1633.

Danladi Bello, A. A., Hashim, N. B., Mohd Haniffah, M. R. (2017): Predicting impact of climate change on water temperature and dissolved oxygen in tropical rivers. Climate, 5(3), 58. https://doi.org/10.3390/cli5030058

Faruk, D. Ö. (2010): A hybrid neural network and ARIMA model for water quality time series prediction. Eng Appl Artif Intell, 23 (4), 586–594. https://doi.org/10.1016/j.engappai.2009.09.015

Gelda, R., Effler, W., Owens, E. (2001): River dissolved oxygen model with zebra mussel oxygen demand. Journal of Environmental Engineering. 127(9): 790–801. https://doi.org/10.1061/(ASCE)0733-9372(2001)127:9(79)

Gilbert, R. O. (1987): Statistical Methods for Environmental Pollution Monitoring. John Wiley & Sons, Inc., New York.

Gorbachova, L., Khrystiuk, B. (2021): Extreme low flow change analysis on the Tysa River within Ukraine. Acta Hydrologica Slovaca, 22(2), 200–206. doi: 10.31577/ahs-2021-0022.02.0023

Gualtieri C, Pulci Doria G (2012): Gas-transfer at unsheared free surfaces. In Gualtieri C, Mihailovic DT (Eds) In Fluid Mechanics of Environmental Interfaces, 2nd ed. CRC Press: Boca Raton, FL, USA, 143–177.

Hamed, K. H. (2008): Trend detection in hydrologic data: The Mann-Kendall trend test under the scaling hypothesis. Journal of Hydrology, 349(3–4), 2008, 350–363.

Harvey, R., Lye, L., Khan, A., Paterson, R. (2011): The influence of air temperature on water temperature and the concentration of dissolved oxygen in Newfoundland Rivers. Canadian Water Resources Journal, 36(2), 171–192. https://doi.org/10.4296/cwrj3602849

Heinz, I., Pulido-Velazquez, M., Lund, JR., Andreu, J., 2007. Hydro-economic Modeling in River Basin Management:

Implications and Applications for the European Water Framework Directive. Water Resour Manag, 21(7), 1103–1125. DOI:10.1007/s11269-006-9101-8.

Hrdlicová, E. (2016): Hodnotenie kvality vody vo vybraných monitorovaných profiloch rieky Myjavy. Acta Hydrologica Slovaca, Vol. 17, No. 2, 2016, 157–165. http://www.uh.sav.sk/ah_articles/

Johnson, H. E., Kular, B., Mur, L., Smith, A. R., Wang, T. L., Causton, D. R. (2016): The application of multivariate analysis of variance (MANOVA) to evaluate plant metabolomic data from factorially designed experiments. Metabolomics, 12, 191. https://doi.org/10.1007/s11306-005-0010-2

Noskovič, J., Rakovská, A., Porhajašová, J., Babošová, M., Čeryová, T. (2013): Biological Evaluation of the Water Quality in the Water flow in the Southwestern part of the Slovak Republic. Research Journal of Agricultural Science, 45 (2), 171–181.

NV č. 269/2010 Z. z. Nariadenie vlády Slovenskej republiky, ktorým sa ustanovujú požiadavky na dosiahnutie dobrého stavu vôd. (Regulation of the Government of the Slovak Republic establishing requirements for achieving good water status.) https://www.slov-lex.sk/pravne-predpisy/SK/ZZ/2010/269/ (in Slovak)

Ondrejka Harbuľáková, V., Zeleňáková, M., Rysulová, M., Repel, A., Simonová, D. (2017): Investigation of Selected Qualitative and Quantitative Water Parameters Using Correlation Analysis. Environmental Processes, 4(1), 163–177. DOI 10.1007/s40710-017-0228-9.

Pekárová, P., Miklánek, P., Rončák, P., Adamková, J., Chriastel, R., Metelkova, M., Pekár, J. (2004): Identification and assessment of long-term trends of surface water quality determinands in Slovakia for implementation of the EU WFD. Journal of Hydrology and Hydromechanics/Vodohospodársky Časopis, 52(4), 317–328.

Pekárová, P., Onderka, M., Pekár, J., Rončák, P., Miklánek, P. (2009): Prediction of Water Quality in the DanubeRiver under Extreme Hydrological and Temperature Conditions. J. Hydrol. Hydromech., 57(1), 3–15.

Pekárová, P., Miklánek, P., Pekár, J., Danáčová, Z. (2020): Long-term development of flow and nitrate concentrations in the Little Carpathians headwaters. Acta Hydrologica Slovaca, vol. 21, no.1, 48–55. 2644-4690. DOI: https://doi.org/10.31577/ahs-2020-0021.01.0006

Prohaska, S. (2000): Coincidence of flood flow of the Danube River and its tributaries. A Hydrological Monograph Follow-up Volume 4, 1st ed.; Research Institute of Water Management Bratislava, 2000, ISBN: 8096828231, 187.

Rajesh, M., Rehana, S. (2022): Impact of climate change on river water temperature and dissolved oxygen: Indian riverine thermal regimes. Scientific Reports, 12(1), 9222. https://doi.org/10.1038/s41598-022-12996-7

Raymond, P. A., Zappa, C. J., Butman, D., Bott, T. L., Potter, J., Mulholland, P., Laursen, A. E., McDowell W. H., Newbold, D. (2012): Scaling the gas transfer velocity and hydraulic geometry in streams and small rivers. Limnology and Oceanography: Fluids and Environments, 2(1), 41–53. https://doi.org/10.1215/ 21573689-1597669

Rounds, S. (2002): Development of a neural network model for dissolved oxygen in the Tualatin River, Oregon. Paper presented at the Second Federal Interagency Hydrologic Modeling Conference, Las Vegas, Nevada. 1–13. https://or.water.usgs.gov/tualatin/ann_proceedings.pdf

Siman, C., Velísková, Y. (2017): Transport znečistenia v povrchoých tokoch – základné pojmy a princípy modelovania. Acta Hydrologica Slovaca, Vol. 18, No. 1, 2017, 39 – 48. http://www.uh.sav.sk/ah (in Slovak)

Soltani, K., Amiri, A., Zeynoddin, M., Ebtehaj, I., Gharabaghi, B., Bonakdari, H. (2021): Forecasting monthly fluctuations of lake surface areas using remote sensing techniques and novel machine learning methods. Theor Appl Climatol 143, 713–735. https://doi.org/10.1007/s00704-020-03419-6

Trenberth, K. E., Dai, A., Van Der Schrier, G., Jones, P. D., Barichivich, J., Briffa, K. R., Sheffield, J. (2014): Global warming and changes in drought. Nat. Clim. Chang. 4 (1), 17–22. doi.org/10.1038/nature20584.

Ulseth, A. J., Hall, R. O., Canadell, M. B., Madinger, H. L., Niayifar, A., Battin, T. J. (2019): Distinct air–water gas exchange regimes in low-and high-energy streams. Nature Geoscience, 12(4), 259–263. https://doi.org/10.1038/s41561-019-0324-8.

Vitaku, A., Baruti, B., Malollari, I., Shala, F. (2013): Impact of polluted acidic waters flowd from Trepca Pb-Zn mines, Kosovo, on the pollution of cross-border rivers in the region. Journal of Environmental Protection and Ecology, 14(1), Thessaloniki, Greece, 29–34.

Wang, J., Bombardelli, F. A., Dong, X. (2021): Physically based scaling model to predict gas transfer velocity in streams and rivers. Water Resources Research 57(3):e2020WR028757.

WFD (2000): Directive 2000/60/EC of the European Parlament and of the Council of the 23 October 2000, establishing a framework for Community action in the field of water policy. https://www.eea.europa. eu/policy-documents/water-framework-directive-wfd-2000

Wongsathan, R., Seedadan, I. (2016): A hybrid ARIMA and neural networks model for PM-10 pollution estimation: The case of Chiang Mai city moat area. Procedia Computer Science, 86, 273–276. https://doi.org/10.1016/j.procs.2016.05.057

Yue, S., Pilon, P., Cavadias, G., (2002): Power of Mann-Kendall and Spearman's rho tests for detecting monotonic trends in hydrological series. J. of Hydrology, 259, 254–271. doi.org/10.1016/S0022-1694(01)00594-7

Ing. Veronika Bačová Mitková, PhD. (*corresponding author, e-mail: mitkova@uh.savba.sk)
Institute of Hydrology SAS
Dúbravská cesta 9
84104 Bratislava
Slovak Republic

DOI: 10.31577/ahs-2023-0024.02.0019

ACTA HYDROLOGICA SLOVACA

Volume 24, No. 2, 2023, 173 – 181

Comparison of saturation models in complex hillslopes

Touraj SABZEVARI*, Andrea PETROSELLI*, Ali Torabi HAGHIGHI, Hamidreza R. BABAALI

Hillslopes of natural catchment have a complex geometry. In complex hillslopes, combining different cases of plan shape (convergent, parallel and divergent) and profile curvature (concave, convex and straight) nine different geometries are created. In prediction of the surface and subsurface runoff of catchments based on saturation excess runoff mechanism, the saturated and unsaturated zones of hillslopes must be first separated. Subsurface travel time of hillslope is dependent on saturation attributes. In this research, a new saturation model, called Gamma, was developed to predict the saturated zone length and subsurface travel time in complex hillslopes. An analytical formula was introduced to calculate saturation zone length in Gamma model. Results of Gamma model, namely the saturation zone length and subsurface travel time, were compared with the results given by two other complex saturation models W and Sigma. The results of the three models were relatively close to each other in convergent and parallel hillslopes of different profile curvature type. However, due to the existence of an analytical equation for estimation of saturated zone length in the Gamma model, this model is recommended. It should be noted that for straight divergent and convex divergent hillslopes, the Gamma model is not suitable and Sigma or W model should be used.

KEY WORDS: saturation excess runoff mechanism, complex hillslope, subsurface travel time

Introduction

Investigating cathments‘ saturation and runoff production in hydrology is crucial for many applications. For instance, runoff formation is linked to flood mapping (Szolgay et al., 2003). Infiltration within soil generates the groundwater recharge (Aldarir et al., 2022). The presence of water in soils affects soil hydraulic properties, e.g. the soil retention curves (Kandra et al., 2015).

The infiltration (Hortonian) and saturation (Dunne-Black) excess are two of the main runoff formation mechanisms in catchments. In the latter, the subsurface flow produces saturated zone in downstream of the hillslope (Dunne and Black, 1970 a, b). These two runoff formation mechanisms can be found in a catchment at the same time. In hilly catchments with vegetation cover which have steep hillslopes, large part of the observed runoff usually comes from subsurface runoff (Hewlett and Hibbert, 1963; 1967; Anderson and Burt, 1978).

Due to their complex nature, separation of surface and subsurface flow in catchments is difficult and an accurate technique has not been provided for this purpose yet.

Many rainfall-runoff models used for simulation of catchment are based on the infiltration excess mechanism. Catchment surface becomes saturated in such models from upstream and the entire surface of a hillslope is usually assumed to contribute to runoff. Separation of saturated and unsaturated areas in hillslopes during rainfall is necessary to account for the infiltration excess mechanism of runoff formation. Estimation of these areas considering the temporal variability of rainfall intensity is more difficult.

The dynamic of interaction between saturated and unsaturated zones has been examined by several researchers using numerical simulations (Freeze and Harlan, 1969; Freeze, 1971;1972 a, b; Beven, 1982).

Subsurface flow and saturation of hillslopes are affected by many parameters such as soil specifications (porosity, soil hydraulic conductivity and soil thickness), recharge rate, vegetation cover, the geometry of hillslopes.

Hillslopes have different geometries. In terms of profile curvatures, hillslopes are divided into three cases which are concave, convex and straight, and, regarding the plan shape, they are grouped into convergent, parallel and divergent. Generally nine different geometries are considered for hillslopes which are called complex hillslopes. According to past investigations, this geometry can have a significant effect on the surface flow (Singh and Agiralioglu, 1981a, b; 1982; Noroozpour et al., 2014; Sabzevari and Noroozpour, 2014) and subsurface flow (O'Loughlin, 1981; Aryal et al., 2005; Hilberts et al., 2004; 2007; Berne et al., 2005; Troch et al., 2002; 2004; Sabzevari and Noroozpour, 2014).

O'Loughlin (1981) derived criteria for the existence of

saturated area on draining hillslopes in natural catchments. He showed that the size of saturated zone on undulating hillslopes with gradational soils strongly depends on topographic convergence or divergence. Takasao and Shiiba (1981) concluded that the effect of flow concentration on hydrological responses varies in convergent and divergent hillslopes, and with the magnitude of rainfall. They also noted that convergent hillslopes with deep soils had delayed runoff responses, whereas hillslopes with shallow soils produced highly peaked hydrographs. The analytical solutions to a kinematic wave equation which are expressed in terms of storage using the mapping method of Fan and Bras (1998) were evaluated through applying them to nine hillslopes with different plan shapes and profile curvatures by Troch et al. (2002). Troch et al. (2002) also found that dynamic response of the hillslopes is strongly dependent on plan shape and bedrock slope. It was concluded that convergent hillslopes tend to drain much more slowly than divergent ones due to a reduced flow domain near the outlet. Aryal et al. (2005) derived relationships describing response times for landscape saturation and subsurface flow for idealized hillslopes after a change happened in water balance in terms of similarity parameters given by their topographic, soil and climatic attributes. They investigated the effects of geometry of hillslopes on the amount of saturation in hillslopes, and then, by calculating the length of saturation zone (SZL) in steady rainfall condition, they estimated travel time of subsurface flow. According to their derived equations, each factor affecting the amount of saturation in hillslopes can influence the subsurface travel time (STT) too. Their results showed that the STT in divergent hillslopes is twice that of convergent hillslopes, and concave slopes tend to have lower travel times than planar or convex slopes. Sabzevari et al. (2010) determined the SZL of complex hillslopes based on the Sigma saturation index previously given by Troch et al. (2002). In their study, an analytical equation was presented according to the saturation model of complex hillslopes to calculate the travel time of subsurface flow. They related the saturation capacity, and subsurface travel time of complex hillslopes to soil parameters (thickness, porosity and hydraulic conductivity), geometric characteristics of hillslope (length, plane shape and profile curvature) and rainfall recharge rate. Based on their results, the convex hillslopes show smaller SZL than the concave hillslopes and take greater STT compared with straight and concave ones, whereas in convex-convergent hillslopes, due to their convergence, there is much inclination towards saturation. On average, the STT in divergent hillslopes is twice that for convergent hillslopes. The concave hillslopes saturate sooner in comparison with the straight and convex ones, with shorter STT. Sabzevari and Noroozpour (2014) introduced an instantaneous unit hydrograph model for simulating runoff hydrographs for complex hillslopes. The model is able to estimate surface and subsurface flows in catchments based on the saturation-excess mechanism. The model was used to predict the direct runoff hydrograph (DRH) and subsurface flow hydrograph in Walnut Gulch No. 125 catchment in Arizona, USA. Their results showed that the geometry can change the peak of DRH.

In this research, a saturation model, called Gamma model hereafter, is introduced which considers a simpler geometry in comparison with Sigma saturation model. The results of Gamma model were compared with those of saturation model results given by Sabzevari et al. (2010) and Aryal et al. (2005). The main goals of this research are to (1) provide a saturation model for complex hillslopes with a simpler geometry and to calculate subsurface travel time, and (2) compare the results of saturation models of Sigma and Gamma with that of W saturation model presented by Aryal et al. (2005).

Sigma model description

Evans (1980) provided a topography model to produce complex hillslopes as follows:

$$z(x, y) = E + H(1-x/L)^n + \omega y^2 \quad (1)$$

where z is the elevation, x is the horizontal distance lengthwise measured in the downstream length direction of the surface, y is the horizontal distance from the longitudinal axis in the direction perpendicular to the length direction (the width direction), E is the minimum elevation of the surface above an arbitrary datum, H is the maximum elevation difference defined by the surface, L is the horizontal length of the surface, n is the profile curvature parameter, and is the plan shape parameter.

Fig. 1 illustrates a convergent convex hillslope with soil thickness of D on the bedrock which has the same curvature as the soil surface.

This hillslope is recharged by a rainfall, and due to infiltration of water into the soil, soil moisture profile is formed. Soil moisture storage is related to soil characteristics, recharge rate, and geometry of hillslope (Troch et al., 2002). The width of the complex hillslopes is calculated from the following equation (Talebi et al., 2008):

$$W(x) = c_w \exp\left\{\frac{2\omega L^2}{n(2-n)H}\left(1-\frac{x}{L}\right)^{2-n}\right\} \quad (2)$$

where c_w defines the hillslope width at $x=L$. It is supposed that the soil thickness is the same throughout the hillslope.

The steady-state relative saturation function in Sigma model is given by Troch et al. (2002) and Talebi et al. (2008):

$$\sigma(x) = \frac{S(x)}{S_c(x)} = \frac{\left[\frac{fLN}{nkH}(1-\frac{x}{L})^{1-n} A(x)\right]}{\left[W(x)D(x)f\right]} \quad (3)$$

$$A(x) = \int_0^x W(u)du \quad (4)$$

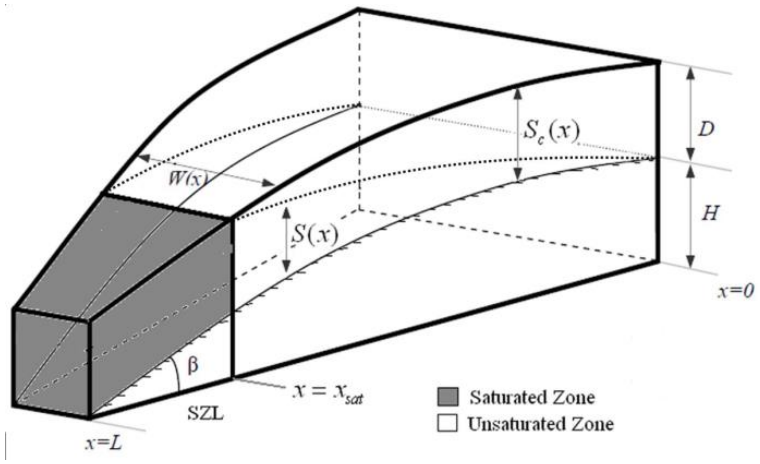

Fig. 1. Schematic of convergent convex hillslope.

where $S(x)$ is the soil moisture storage, $S_c(x)$ is the soil moisture storage capacity, $A(x)$ is the drainage area at the distance x, N is the recharge rate to the saturated layer, k is the saturated soil hydraulic conductivity, f is the drainable porosity, and $D(x)$ is the average soil thickness.

According to Fig. 1, any point of the hillslope with the moisture storage equal to the moisture storage capacity σ=1, belongs to the saturation zone (Sabzevari et al., 2010). By solving numerically of the equation [$\sigma(x)$-1=0], the SZL can be obtained.

In Eq. (4), except for n=1, the function of A(x) does not have an analytical solution and could only be solved numerically.

Subsurface flow travel time is a key parameter in some rainfall-runoff models to estimate the subsurface flow of catchment. In most catchments with high soil permeability, the contribution of subsurface flow to DRH is significant. Sabzevari et al. (2010) offered the Eq. (5) for calculation of SST in complex hillslopes based on the Sigma saturation model and Darcy equation:

$$T = \frac{L\, f\left[(1-\frac{x_{sat}}{L})^{2-n}-1\right]}{nk\bar{s}(n-2)} \tag{5}$$

where x_{sat} is the coordination of the saturated zone boundary. According to Eq. (5), the coordination of the saturated zone boundary in each hillslope is a key parameter in calculating STT.

W model description

Aryal et al. (2005) used the geometric equations of Zaslavsky and Rogowski (1969) for modelling of complex hillslopes. Eq. (6) describes the geometric profile of concave and convex hillslopes:

$$z = H[\frac{\tan^{-1}\{B(X-1)\}}{\tan^{-1}(B)}+1] \qquad Concave \quad B>0$$
$$z = H[\frac{\tan^{-1}\{BX\}}{\tan^{-1}(B)}] \qquad Convex \quad B<0 \tag{6}$$

where B is the curvature parameter and $X=1-(x/L)$ is the normalized distance.

Aryal et al. (2005) obtained the value of saturation zone boundary by solving the following equation:

$$\frac{X_s(2-X_s+X_sCR)}{1+CR} = 1-\frac{fDk\bar{s}}{NL}\frac{f(X_s)}{\lambda(X_s)} \tag{7}$$

$$\lambda(X_s) = (1+CR)/[2(1-X_s+X_sCR)]$$

where CR signifies the convergence degree of hillslope (CR>1 for convergent, CR<1 for divergent, and CR=1 for parallel hillslope) which is the ratio of upstream width to the width of hillslope at the outlet, $X_s=1-(x_{sat}/L)$ is the normalized length of saturation zone, $\lambda(x_s)$ is the plan shape function, $f(X_s)=dz/dx$ is the curvature profile function.

Aryal et al. (2005) presented the Eqs. (8) and (9) for calculation of STT in concave and convex hillslopes, respectively:

$$T = \frac{fL}{k\bar{s}}\tan^{-1}(B)[\frac{3+B^2}{3B}-(\frac{BX_s^{\,3}}{3}-BX_s^{\,2}+BX_s+\frac{X_s}{B})] \tag{8}$$

$$T = \frac{fL}{k\bar{s}}\tan^{-1}(B)[\frac{3+B^2}{3B}-(\frac{BX_s^{\,3}}{3}+\frac{X_s}{B})] \tag{9}$$

As the value of B approaches 0 (a straight hillslope), Eq. (8) reduces to $T=fL(1-X_s)/(k\bar{s})$.

Gamma model development

Gamma model introduced in this study is based on the topography model already used by Norbiato and Borga (2008) and Berne et al. (2005). Due to the dependence of the width function derived from Evans (1980) on both plan shape parameter (n) and profile curvature parameter (ω), the resultant drainage area equation ($A(x)$) can not be solved analytically for any n. This limitation is eliminated in Gamma model by assuming an exponential form for width function as:

$$W(x) = c\exp(ax) \tag{10}$$

where c corresponds to the surface width at the upstream ($W(x=0)$) and a is a shape parameter quantifying the degree of convergence ($a < 0$) or divergence ($a > 0$) of the hillslope. The hillslope drainage area function is obtained analytically by integrating Eq. (10) as:

$$A(x) = \frac{c}{a}[\exp(ax) - 1] \tag{11}$$

For investigation on subsurface flow of hillslopes based on Fan and Bras (1998) equation, Norbiato and Borga (2008) considered the equation of profile curvature in complex hillslopes as:

$$z(x) = \alpha + \beta x + \gamma x^2 \tag{12}$$

In Eq. (12), values of β are always negative, positive values of γ define concave profiles, negative values of γ produce convex profiles, and for $\gamma = 0$ the profile is straight. Comparing Eq. (12) and Eq. (1) for n=2, the relation between the parameters of two equations would be: $\alpha = E + H, \beta = -2H / L, \gamma = H / L^2$

For the surfaces defined by Eq. (12), the local slope at each point of hillslope, s*, is obtained from:

$$s^* = \frac{dz}{dx} = \beta + 2\gamma x \tag{13}$$

The subsurface flow rates can be described with a kinematic wave approximation of Darcy's law as (Troch et al., 2002):

$$Q = -k\frac{S(x)}{f}\frac{dz}{dx} \tag{14}$$

According to Fig. 1, any point of the hillslope with the storage equal to the storage capacity [$S(x)=S_c(x)$], belongs to the saturation zone. The steady-state subsurface flow rate would be $Q(x) = NA(x)$. According to the Eqs. (14) and (13), it could be written:

$$S(x_{sat}) = \frac{-NA(x_{sat})f}{k(\beta + 2\gamma x_{sat})} \tag{15}$$

Computing the boundary of saturation zone, the value $S(x)=S_c(x)=w(x_{sat})Df$ is considered. Therefore:

$$\frac{-NA(x_{sat})}{k(\beta + 2\gamma x_{sat})} = w(x_{sat})D \tag{16}$$

Replacing the Eqs. (10) and (11) into Eq. (16) and solving the final equation for the boundary of saturation zone yields:

$$x_{sat} = \frac{2lambertw\left\{\frac{N}{2Dk\gamma}\exp\left(\frac{N + Dak\beta}{2Dk\gamma}\right)\right\} \times Dk\gamma - N - Dak\beta}{2Dak\gamma} \tag{17}$$

where *lambertw(x)* evaluates Lambert's w function at the elements of x, a numeric matrix or a symbolic matrix. Lambert's *w* solves the equation $w\exp(w)=x$. So the SZL is obtained from the relation: $L_s=L-x_{sat}$.

Eq. (17) is an analytical equation of saturation zone boundary in Gamma model. Based on Gamma model, the STT can be computed more simply.

According to Darcy equation for porous media, the velocity of water into soil is calculated as:

$$v = \frac{k\,s^*}{f} = \frac{dx}{dt} \tag{18}$$

By substituting the value of s* from Eq. (13) in Eq. (18) and integrating with bounds $t = 0$ to T, and $x = 0$ to x_{sat} for travel time of the unsaturated zone, we obtain:

$$T = \frac{-f}{2k\gamma}\left[\ln\left(\frac{\beta + 2\gamma x_{sat}}{\beta}\right)\right] \tag{19}$$

Replacing x_{sat} from Eq. (17) into Eq. (19), the STT of the complex hillslopes can be computed.

Models application

To investigate the effect of geometry on saturation of complex hillslopes, the nine basic complex hillslopes considered by Sabzevari et al. (2010) are studied to investigate STT of complex hillslopes. Fig. 2 illustrates the nine basic hillslope types that are formed by combining three plan shapes and three profile curvatures. The geometrical parameters of Sigma model for the nine characterized hillslopes are listed in Table 1. The length of all hillslopes is 100 m, the maximum elevation difference defined by the surface is 26.8 m, the average slope is 0.27, and the maximum value for y is 25 m. The curvature shape factor for hillslopes varies between 0.5 and 1.5 and the plan shape factor between $\omega = -H / L^2$ (for divergent hillslope) and $\omega = +H / L^2$ (for convergent hillslope) (Troch et al., 2002; Talebi et al., 2008).

The straight hillslopes have profile curvature parameter of unity, while the plan shape factor for parallel hillslopes is zero. The geometric parameters of hillslope in natural catchment usually are calculated by using geographic international system (GIS) technique.

To make the results of the models W, Gamma, and Sigma, comparable, the geometric parameters of hillslopes as regards plan shape and curvature profile of the defined study scheme should be equivalent to each other. For this purpose, geometrical parameters of Table 1 should be changed to geometries of the Gamma and W models. To do this, hillslope area, length, average slope, and the upstream width in all three geometries are considered the same for nine cases and geometric parameters are calculated. For instance, Eqs. (1), (6), and (12) are curvature equations for three geometries so by comparing the results of the two latter with the former, curvature parameters B and γ could be evaluated.

Comparing curvature and plan shape equations, and their solutions for different values of n and ω, the parameters

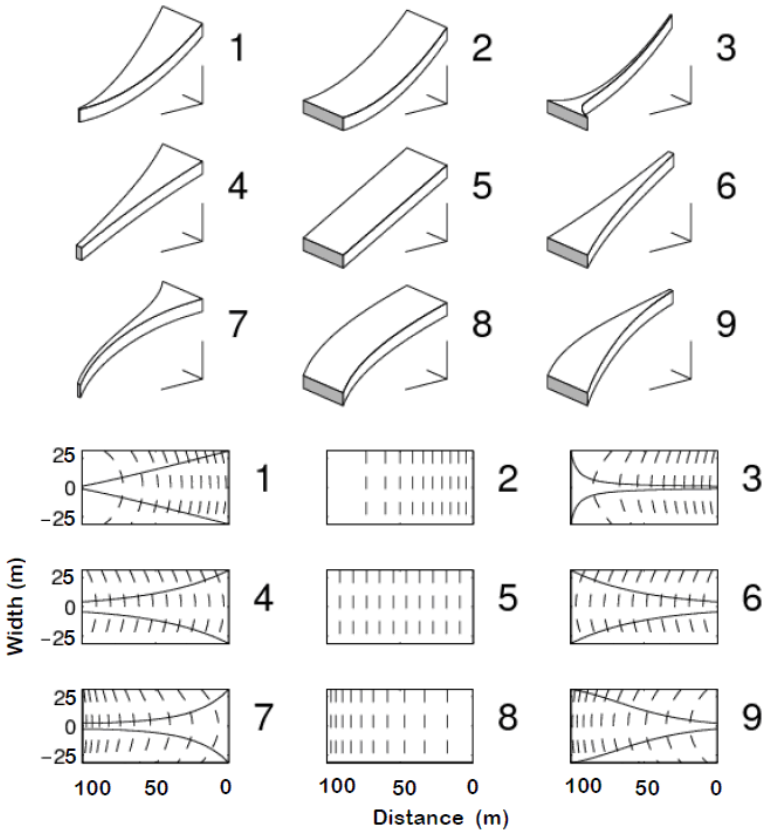

Fig. 2. A three-dimensional view (top) and a two-dimensional plot of the contour lines and slope divide the bottom of the nine hillslopes considered in this study (After Hilbert et al., 2004).

Table 1. Geometrical parameters for nine complex hillslopes (Sabzevari et al., 2010)

Hillslope Number	Profile Curvature	Plan Shape	n	$\omega[10^{-3}m^{-1}]$
1	Concave	Convergent	1.5	+2.7
2	Concave	Parallel	1.5	0
3	Concave	Divergent	1.5	-2.7
4	Straight	Convergent	1	+2.7
5	Straight	Parallel	1	0
6	Straight	Divergent	1	-2.7
7	Convex	Convergent	0.5	+2.7
8	Convex	Parallel	0.5	0
9	Convex	Divergent	0.5	-2.7

of models W and Gamma would be obtained as shown in Table 2. In model W, the convergence coefficient CR of complex hillslopes, is derived as:

$$CR = W(0)/c_w = \exp\left\{\frac{2\omega L^2}{n(2-n)H}\right\} \quad (20)$$

Considering equation $\omega=-H/L^2$, for divergent hillslopes, the CR coefficient would be $CR=\exp[-2/(n(2-n)]$, and for convergent hillslopes with $\omega=H/L^2$ it would be $CR=\exp[-2/(n(2-n)]$.

Results and discussion

In this section, the results of response of subsurface flow in complex hillslopes are discussed. Saturation rate and subsurface travel time of different hillslopes are compared according to the three models. Since choosing one model as more factual requires laboratory researches, in this study W model is taken as basis and the results of the other two models are compared with those of W model. The method of RMSE is used to compare the results. The value of RMSE is calculated from:

$$\mathrm{RMSE} = \sqrt{\frac{\sum_{i=1}^{m}(x_C - x_w)^2}{m}} \quad (21)$$

where x_c is the values from the Gamma or Sigma models, and x_w is the values from W model. The recharge rates into soil layer were considered so that the saturation level is observed at downstream of hillslopes. Since some hillslopes saturate too late (Sabzevari et al., 2010), the rainfall intensity should be assumed high enough. Figs. 3 and 4 show the values of saturated zone lenght (SZL) and subsurface travel time (SST) in complex hillslopes for different models. Table 3 presents the values of RMSE of two models W and Sigma.

To simulate the responses of convex-convergent hillslopes (Figs. 3g, 4g), recharge rates in the range of 35 to 60 mm day^{-1} were utilized because this hillslope saturates very much. For convex-convergent hillslope, The RMSE values for models of Gamma and Sigma are, respectively 32.1 mm day^{-1} and 31.3 mm day^{-1}, and RMSE for computation of STT of Gamma and Sigma are, respectively 187 hours and 209 hours. The results of Sigma and Gamma models in convex-convergent hillslope were close.

The results of saturation models of Gamma and Sigma under recharge rates 135 to 155 mm day^{-1} in straight-convergent hillslope were almost the same (Fig. 3d). RMSE values in models Gamma and Sigma for computation of SZL were, respectively 2.8 mm day^{-1} and 3.3 mm day^{-1}, and for computation of STT were 24 mm day^{-1} and 12 mm day^{-1} respectively (Fig. 4d). This shows that the three models are in relative agreement in estimation of SZL and STT of straight-convergent hillslopes. For this hillslope too, the Gamma and Sigma models have good conformity.

Table 2. Parameters of Gamma and W models

Hillslope Number	*B*	*CR*	*a*	*c*	β	γ
1	1.2	14.39	-0.016	50	-0.39	0.001
2	1.2	1	0	30	-0.39	0.001
3	1.2	0.0695	0.036	3	-0.39	0.001
4	0	7.389	-0.016	50	-0.27	0
5	0	1	0	30	-0.27	0
6	0	0.135	0.036	3	-0.27	0
7	-2.5	14.39	-0.016	50	-0.1	-0.001
8	-2.5	1	0	30	-0.1	-0.001
9	-2.5	0.0695	0.036	3	-0.1	-0.001

Table 3. Values of RMSE in Gamma and Sigma models

Hillslope Number	Profile Curvature	Plan Shape	SZL [m] Gamma	SZL [m] Sigma	STT [hours] Gamma	STT [hours] Sigma
1	Concave	Convergent	1.20	1.1	172	172
2	Concave	Parallel	59.3	52.0	135	104
3	Concave	Divergent	4.60	5.50	15.4	25.5
4	Straight	Convergent	2.80	3.30	24.0	12.0
5	Straight	Parallel	1.40	0.74	0.11	2.63
6	Straight	Divergent	--	6.00	--	6.20
7	Convex	Convergent	32.1	31.3	187	209
8	Convex	Parallel	4.30	9.0	3.60	10.3
9	Convex	Divergent	--	31.4	--	30.0

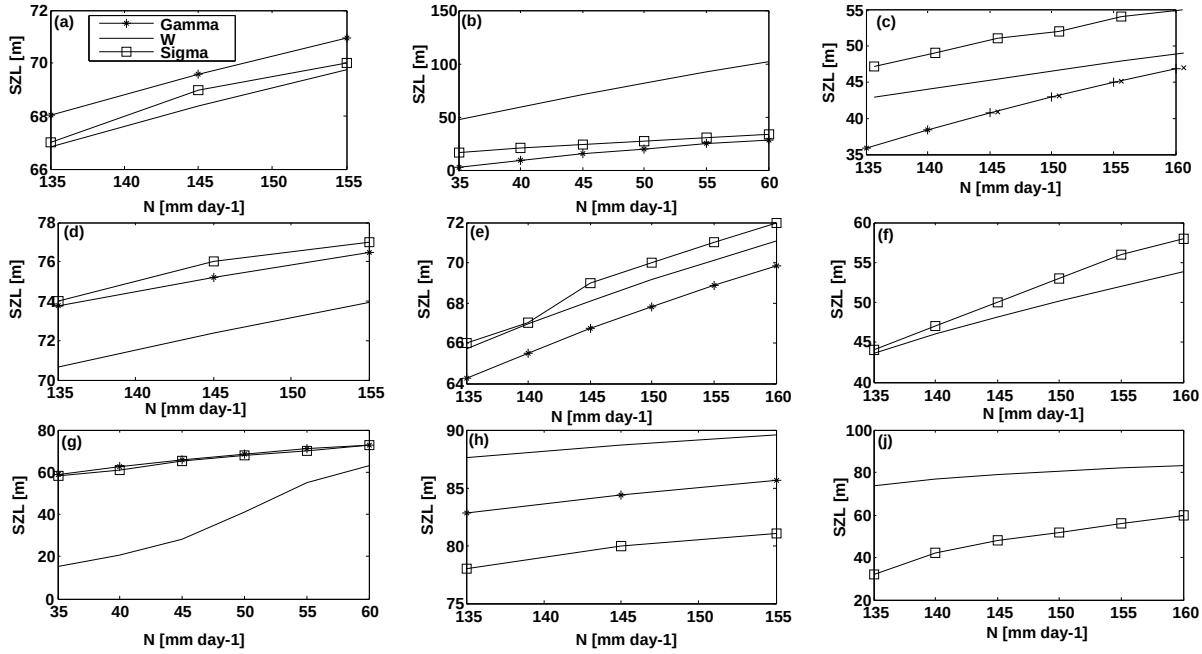

Fig. 3. Saturation zone length [m] in the hillslopes defined in Fig. 2 and Table 2; a) to i) correspond to hillslope numbers 1 to 9.

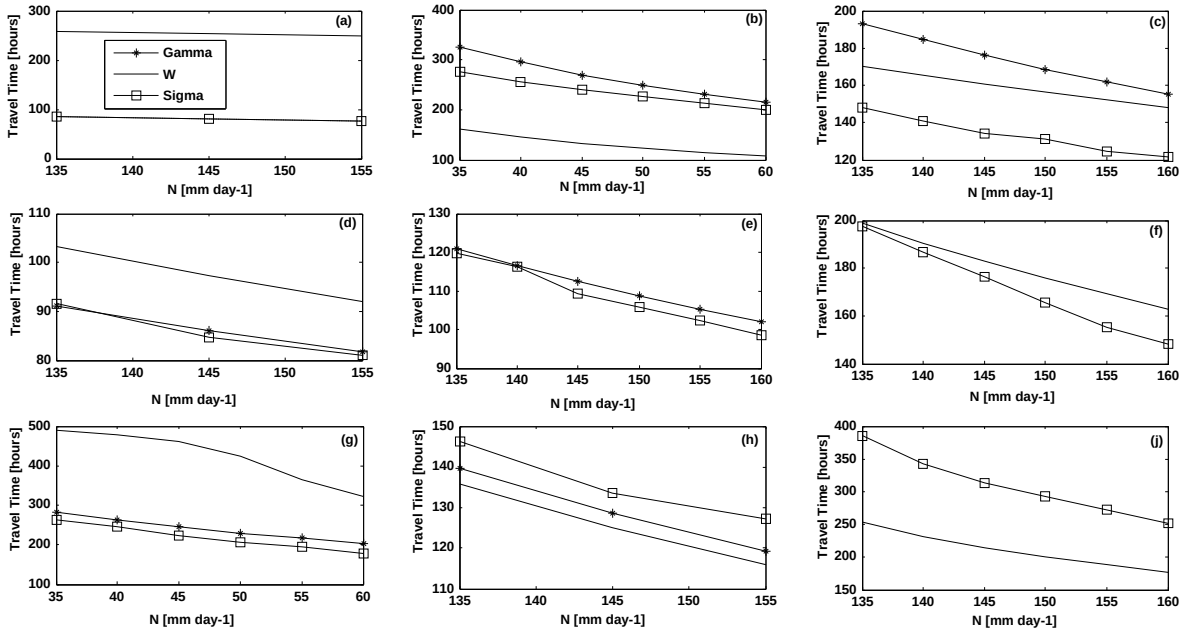

Fig. 4. Subsurface travel time [hours] in the hillslopes.

The results concerning SZL in the three models for concave-convergent hillslopes were similar (Fig. 3a). The values of RMSE in Gamma and Sigma models were, respectively 1.18 m and 1.1 m. As for the travel time, these two models showed total agreement while having many discrepancies with the W model (Fig. 4a). The value of RMSE of both Gamma and Sigma is 172 hours. Generally, for convergent hillslopes with different curvatures the model Gamma showed results very similar to those of the model Sigma.

For concave-parallel hillslopes, RMSE of SZL for the Gamma and Sigma models are, respectively, 59.3 m and 52 m, and the values of RMSE for evaluation of travel time are, respectively, 135 hours and 104 hours. In this type of hillslope the results for the two models are in accord (Figs. 3b, 4b). In convex-parallel hillslopes, the maximum values of SZL corresponded to the W model running in the range of 87 to 90 m, and the minimum values were of the Sigma model between 78 m and 82 m (Fig. 3h). The results of Gamma model

are similar to the averages of the other two models. The values of RMSE and of SZL for Gamma and Sigma model were 4.3 m and 9 m, respectively, and RMSE's for evaluation of STT were respectively, 3.6 hours and 10.3 hours (Fig. 4h). For straight-parallel hillslopes, RMSE and SZL values for Gamma and Sigma models are 1.4 m and 0.74 m respectively, and RMSE's for computation of travel time as 0.11 hours and 2.63 hours respectively. According to the results, all three models are in agreement regarding results for straight parallel hillslopes (Figs. 3e, 4e).

Finally for concave divergent hillslopes (Figs. 3c, 4c), the values concerning RMSE of SZL for Gamma and Sigma models are, respectively 4.6 m and 5.5 m, and those of RMSE for computation of travel time are 15.4 hours and 25.5 hours, respectively. By the obtained results it could be deduced that the Gamma model shows a better conformity with the W model for concave divergent hillslopes than the Sigma model.

The results of Gamma model for convex divergent hillslopes did not converge to a solution so the model could not evaluate appropriate results for these hillslopes (Figs. 3j, 4j). Having the RMSE value as 31.4 hours, Sigma model had significant differences in the results compared with W model. The results of Gamma model for straight divergent hillslopes did not converge to a solution (Figs. 3f, 4f).

Conclusions

In this study, a new saturation model, called Gamma model, based on a combined topography model, was introduced to separate the saturated and unsaturated zones and estimate subsurface travel time in complex hillslopes. The Gamma model is capable of considering the effects of plan shape and profile curvature upon saturation rate as well as subsurface travel time. Then, the results of three saturation models, Gamma, Sigma and W were compared. The geometric equations of hillslopes such as plan shape and profile curvature were different in each model. Gamma model has a simpler geometry and its results were compared to those of the other two models.

In Sigma and W models, the SZL was obtained by solving the saturation equations but in Gamma model, a new analytical equation was introduced to calculate the SZL in complex hillslope.

According to the results, the reactions of complex hillslopes in the three models are not the same. In Gamma or Sigma models, in general, in nine complex hillslopes no definite course of reaction was detected. In most hillslopes, the two models Gamma and Sigma had coinciding results and in convex divergent and straight divergent hillslopes, Gamma model was not efficient because the saturation equation of Gamma did not converge to a real solution.

The results of the three models were relatively close to each other in convergent and parallel hillslopes of different profile curvature type. However, due to the existence of an analytical equation for estimation of saturated zone length in the Gamma model, this model is recommended. It should be noted that for straight divergent and convex divergent, Gamma model is not suitable and Sigma or W model should be used. Undoubtedly, the most efficient model will be identified only by conducting experimental studies using laboratory models.

References

Aldarir, A., Fichtner, T., Gwiadowski, I. D., Blankenburg, R. Graeber, P. 2022. Estimation of limitations for groundwater recharge using the example of the Sarden site in Syria. Acta Hydrologica Slovaca, 23(1), 130–139.

Anderson, M. G., Burt, T. P. (1978): Towards more detailed field monitoring of variable source area. Water Resources Research 14, 1123–1131.

Aryal, S. K., O'Loughlin, E. M., Mein, R. G. (2005): A similarity approach to determine response times to steady-state saturation in landscapes. Adv. Water Resour., 28, 99–115.

Berne, A., Uijlenhoet, R., Troch, P. A. (2005): Similarity analysis of subsurface flow response of hillslopes with complex geometry, Water Resour. Res., 41, W09410.

Beven, K. (1982): On subsurface stormflow: prediction with simple kinematic theory for saturated and unsaturated flows, Water Resour. Res., 18 (6), 1627–1633.

Dunne, T., Black, R. D. (1970a): Partial-area contributions to storm runoff in a small New England watershed. Water Resources Research 6, 1296–1311.

Dunne, T., Black, R. D. (1970b): An experimental investigation of runoff production in permeable soil. Water Resources Research 6, 478–490.

Evans, I. S. (1980): An integrated system of terrain analysis and slope mapping. Zeitschrift fur Geomorphologie, Supplementband. 36, 274–295.

Fan, Y., Bras, R. (1998): Analytical solutions to hillslope subsurface storm flow and saturation overland flow. Water Resour Res, 34 (4), 921–927.

Freeze, R. A. (1971): Three-dimensional, transient, saturated-unsaturated flow in a groundwater catchment. Water Resour. Res., 7, 929–941.

Freeze, R. A. (1972a): Role of subsurface flow in generating surface runoff: 1. Baseflow contributions to channel flow. Water Resour. Res., 8, 609–623.

Freeze, R. A. (1972b): Role of subsurface flow in generating surface runoff: 2. Upstream source areas. Water Resour. Res., 8, 1272–1283.

Freeze, R. A., Harlan, R. L. (1969): Blueprint for a physically-based digitally simulated hydrologic response model. J. Hydrol., 9, 237–258.

Hewlett, J. D., Hibbert, A. R. (1963): Moisture and energy conditions within a sloping soil mass during drainage. Journal of Geophysical Research 68: 1080–1087.

Hewlett, J. D., Hibbert, A. R. (1967): Factors affecting the response of small watersheds to precipitation in humid areas. In International Symposium on Forest Hydrology, Sopper WE, Lull HW (eds). Pergamon Press: Oxford; 275–290.

Hilberts, A., Van Loon, E., Troch P. A., Paniconi, C. (2004): The hillslope-storage Boussinesq model for non-constant bedrock slope, J. Hydrol., 291, 160–173.

Hilberts, A., Troch, P. A., Paniconi, C., Boll, J. (2007): Low-dimensional modeling of hillslope subsurface flow: the relationship between rainfall, recharge, and unsaturated storage, Water Resour Res., 43, W03445.

Kandra, B., Pavelková, D., Tall, A. (2015): Determination of the soil retention curves with regard to the soil volume changes. Acta Hydrologica Slovaca, 16(2) 204–210.

Norbiato, D., Borga, M. (2008):. Analysis of hysteretic behaviour of a hillslope-storage kinematic wave model for subsurface flow , Advances in Water Resources journal, 31 , 118–131

Noroozpour, S., Saghafian, B., Akhondali, A. M., Radmanesh, F. (2014): Travel time of curved parallel hillslopes. Hydrol Res J 145(4), 190–199. doi:10.2166/nh.2013.171

O'Loughlin, E. M. (1981): Saturation regions in catchments and their relations to soil and topographic properties. J Hydrol; 53, 229–46.

Sabzevari, T., Talebi, A., Ardakanian, R. Shamsai, A. (2010): A steady-state saturation model to determine the subsurface travel time (STT) in complex hillslopes, Hydrol. Earth Syst. Sci.14, 891–900.

Sabzevari, T., Noroozpour, S. (2014): Effects of hillslope geometry on surface and subsurface flows, Hydrogeology Journal, 22, 1593–1604, DOI 10.1007/s10040-014-1149-6

Singh, V. P., Agiralioglu, N., (1981a): Diverging overland flow: analytical solutions. Nord Hydrol 12(2),81–89

Singh, V. P., Agiralioglu, N. (1981b): Diverging overland flow, application to natural watersheds. Nord Hydrol 12(2), 99–110

Singh, V. P., Agiralioglu, N. (1982): Lag time for diverging overland flow. Nordic Hydrol, 13, 39–48.

Szolgay, J., Hlavčová, K., Kohnová, S., Kubeš, R. Zvolenský M. (2003): Influence of antecedent basin saturation on extreme floods in the upper Hron River basin. Acta Hydrologica Slovaca, 4(2) 226–232.

Takasao, T., Shiiba, M. (1981): Incorporation of the effect of concentration of flow into the kinematic wave equations. Annuals of Disaster Prevention Research Institute, Kyoto University 12: 159–170 (in Japanese with English abstract).

Troch, P., van Loon, E., Hilberts, A. (2002): Analytical solutions to a hillslope-storage kinematic wave equation for subsurface flow. Adv. Water Resour. 25, 637–649.

Troch, P., van Loon, A., Hilberts, A. (2004): Analytical solution of the linearized hillslope-strorage Boussinesq equation for exponential hill- slope width functions, Water Resour. Res., 40, W08601.

Talebi, A., Troch, P. A., Uijlenhoet, R. (2008): A steady-state analytical hillslope stability model for complex hillslopes. Hydrol. Process, 22,546–553.

Zaslavsky, D., Rogowski, A. S. (1969): Hydrologic and morphologic implications of anisotropy and infiltration in soil profile development. Soil Sci Soc Am Proc; 33(4), 594–599.

Touraj Sabzevari, Associate Professor, (*corresponding author, e-mail: touraj.sabzevari@iau.ac.ir; tooraj.sabzevari@gmail.com)
Department of Civil Engineering, Estahban Branch
Islamic Azad University
Estahban
Iran

Andrea Petroselli, Associate Professor, (*corresponding author, e-mail: petro@unitus.it)
Department of Agriculture and Forest Sciences (DAFNE)
Tuscia University
01100 Viterbo
Italy

Ali Torabi Haghighi, Associate Professor
Water, Energy and Environmental Engineering Research Unit
University of Oulu
Finland

Hamid Reza Babaali, Assistant professor,
Department of Civil Engineering, Khorramabad Branch,
Islamic Azad University
Khorramabad
Iran

DOI: 10.31577/ahs-2023-0024.02.0020

ACTA HYDROLOGICA SLOVACA

Volume 24, No. 2, 2023, 182 – 186

Changes of drought indices in relation with the geographic altitude of the crop site

Ákos TARNAWA, Katalin M. KASSAI, Zoltán KENDE, Márton JOLÁNKAI*

The water availability of the crop site is a determining factor regarding plant growth and development. An assessment study has been done at the MATE University, Gödöllő to evaluate the magnitude of aridity in relaion with the geographic location of the crop site. Field crop species (Sugar beet Beta vulgaris, winter barley Hordeum vulgare, winter wheat Triticum aestivum, maize Zea mays, potato Solanum tuberosum, and alfalfa Medicago sativa) were examined in the study. Long term data of twelve meteorological stations (Békéscsaba, Budapest, Debrecen, Miskolc, Mosonmagyaróvár, Nagykanizsa, Nyíregyháza, Pécs, Siófok, Szeged, Szolnok, Szombathely) representing all regions of Hungary were used as a basis of evaluation. PAI indices of each station were processed with vulnerability indices of the field crops studied. The results obtained suggest, that of cereals proved to be the least susceptible, while potato and maize were proved to be highly influenced by aridity x vulnerability interactions. Strong climatic impact could be detected in the case of alfalfa and sugar beet. The geographic altitude of the crop site has shown negative correlation with the magnitude of drought indices.

KEY WORDS: drought, field crops, altitude, crop site, vulnerability

Introduction

Water availability provides bases for all live systems. Water availability of crop sites is a determining factor regarding plant growth and development. The two main factors determining that are the temperature and the precipitation of a certain crop site (Fig. 1). Land use patterns highly impact water availability of certain crop site. Quantifying the influence of land use changes on water and energy fluxes, it is necessary to evaluate their quantitative characteristics (Novák, 2023). Water deficiency of crops is labelled as aridity, however the physiological state my range from water scarcity to drought (Várallyay, 2006). All physiological processes are dedicated to the presence of moisture, like photosynthesis, osmosis, turgor, transpiration, respiration, as well as growth and development, and propagation. Water supply may have an influence in all of them. Aridity in general may obstruct growth and development, however drought is the most crucial from among all types of water scarcity.

Definition of droughts can be assessed in three main ways (Jolánkai et al., 2012):

(1) Meteorological drought is defined when there is a prolonged period with less than average precipitation. Meteorological drought usually precedes the other kinds of drought.
(2) Agricultural droughts affect crop production or the ecology of the area. This condition can also arise independently from any change in precipitation levels when soil conditions and erosion triggered by poorly planned agricultural endeavours cause a shortfall in water available to the crops. Drought is a phenomenon when a plant suffers irreversible physiological damages.
(3) Hydrological drought is defined when the water reserves available in sources such as aquifers, lakes, and reservoirs fall below the statistical average. Hydrological drought tends to show up more slowly because it involves stored water that is used but not replenished. Like an agricultural drought, this can be triggered by more than just a loss of rainfall.

There are various assessments for quantification of water scarcity. Aridity indices are numerical indicators of the degree of dryness of the climate at a given location. A number of indices have been used in various parts of the world, like Köppen and Thornthwaite indices (UNEP, 1992). Values of the aridity index are indicators of the water conditions of certain areas have been developed by researchers for water scarcity assessment (Rattayova et al., 2022). These indicators serve to identify, locate or delimit regions that suffer from a deficit of available water, a condition that can severely affect the effective use of the land for such activities as agriculture or stock-farming. In Hungary the Pálfai Drought Index (PAI) is extensively used in agrometeorology (Pálfai, 1990; Lakatos and Szalai, 2010). In all aridity indices climatic

components are expressed in mathematical formulas. Geographic locations in this context are very seldom examined upon the basis of crop site altitude, however the elevation may have a profound role in the utilization of natural water resources by the vegetation and so by the crop plants produced. Fig. 2 presents geographic altitude data of the Carpathian basin.

This tract of Europe is a part of the Danube river catchment area covering about ¼ million square kilometres, where over 60 percent of that area forms lowlands. The basin begins by Devin, Slovakia with an elevation of 134 m, and the lowest point of that is at the South-Eastern part of that, Portile de Fier, Romania with 61 m outflow level. Majority of the lowland areas are in the territory of Hungary, from which data of 12 meteorological stations have been used in this study.

Agricultural crops have diverse reactions to water availability conditions. According to their taxonomy, life cycle, evapotranspiration patterns and the crop site characteristics, crop plants can be clustered to various vulnerability groups. The present study is dealing with the interaction between aridity and climatic vulnerability of some of the major field crop species of Hungary, as well as to evaluate changes in the aridity indices in relation with the geographic altitude of the crop site.

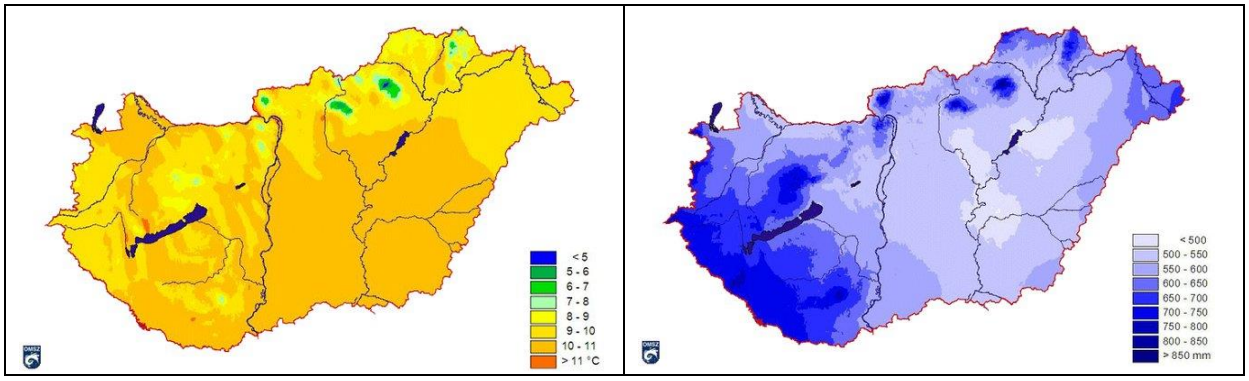

Fig. 1. Annual mean temperature and average precipitation in Hungary on a 30 years' timescale (OMSZ, 2022).

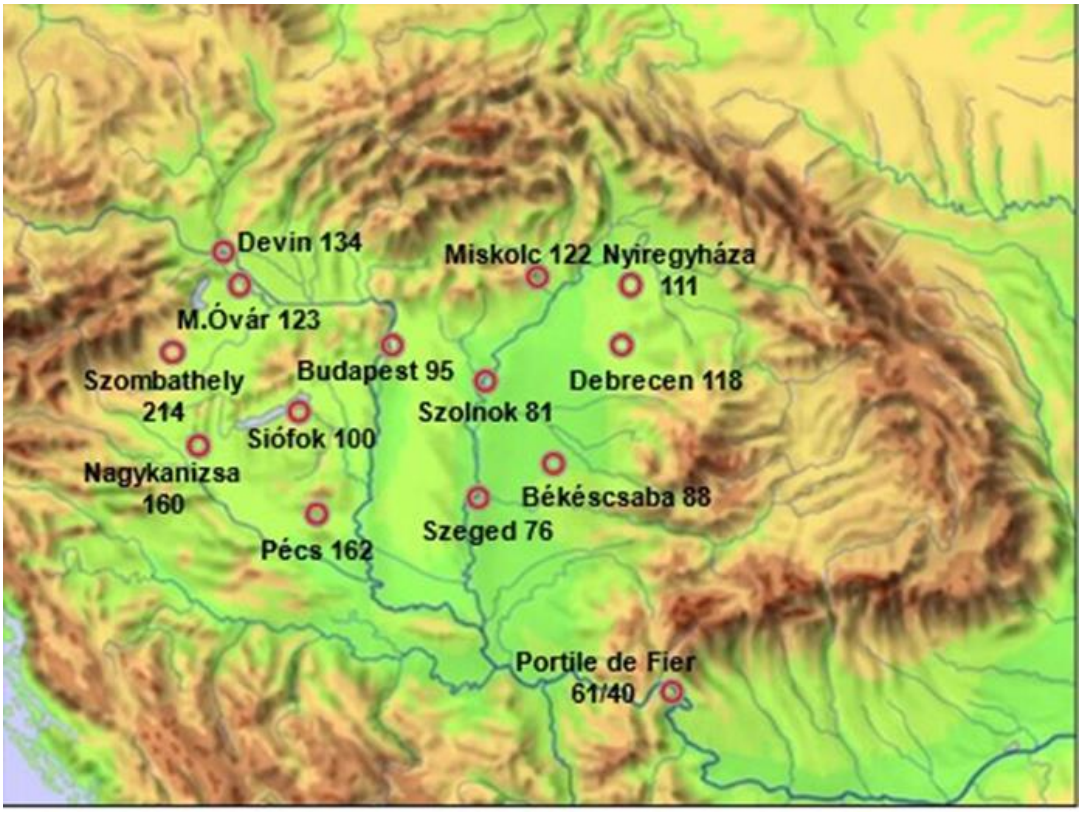

Fig. 2. Geographic altitude data of some meteorological stations in the Carpathian basin [m a.s.l.].

Material and methods

An assessment study has been conducted at the MATE University, Gödöllő to evaluate and identify the main factors of aridity. Almost all major field crop species were involved in the study, from which six species (Sugar beet *Beta vulgaris*, winter barley *Hordeum vulgare*, winter wheat *Triticum aestivum*, maize *Zea mays*, potato *Solanum tuberosum*, and alfalfa *Medicago sativa*) have been evaluated and presented. Crop vulnerability values were based on the mathematical model of Tarnawa et al. (2010). In the survey databases of the Hungarian Meteorological Service (OMSZ) and the Ministry of Agriculture (AM) have been used (KSH, 2022; OMSZ, 2022). The use of Pálfai Drought Index has been applied during the survey (Pálfai, 1990; Bihari et al., 2012). PAI values have been evaluated in a context of long-term databases. Regional evaluations were done respecting the databases of 12 meteorological stations chosen randomly to represent most of the regions of the territory of Hungary (Vermes, 2011; Tarnawa et al., 2012).
Evaluating the long-term data bases the methodology of the state of the World's land and water resources for food and agriculture – Systems at breaking point (FAO, 2021) was used. For statistical evaluations standard methods were applied; correlations, regression analysis, offered by Microsoft Office 2006.

Results and discussion

Pálfai Drought Indices of certain meteorological stations of the OMSZ Hungarian Meteorological Service (Békéscsaba, Budapest, Debrecen, Miskolc, Mosonmagyaróvár, Nagykanizsa, Nyíregyháza, Pécs, Siófok, Szeged, Szolnok and Szombathely) calculated on 50 years' averages were processed for each crop species studied. The results presented in Table 1 verify detectable differences between locations.
The twelve meteorological stations that were randomly chosen to represent various levels of drought probability. The highest PAI indices were found in the case the central and the South-eastern part of Hungary, while in the mountainous locations westward smaller figures were observed.
Studying the interactions between drought and vulnerability the data suggest that crop species in accordance with their water consumption patterns and physiological characteristics may have a rather diverse performance in relation with the crop site PAI values.
Fig. 3 presents data of the survey where the crop sites belonging to the certain meteorological stations were evaluated by the geographic altitude of them.
Yield performance of the six crop species had a reducing trend due to the geographic elevation of the crop site. PAI x VI interactions have shown constant reduction of the crop yields. The trend line of this reduction was labelled by a strong linear regression. The lowest altitude was that of the Szeged crop site with 76 m above sea level, while the highest one of Szombathely had a geographic elevation of 214 m. The reason of this trend may be due to the annual mean temperature and the average precipitation of the location as this can be detected by the data of Fig 1. Central part of the lowland proved to have a higher temperature mean belonging to the annual 10–11°C isotherm range, while the same locations received an annual 500–550 mm precipitation over the long term.

Table 1. Drought x crop vulnerability interactions regarding twelve meteorological stations and six field crop species based on 50 years' average

PAI [°C/100 mm]	VI indices	wheat	winter barley	maize	potato	alfalfa	sugar beet	mean
		5.6	5.8	7.3	6.5	7.6	7.7	6.75
Békéscsaba	5.47	5.5	5.6	6.4	6.0	6.5	6.6	6.11
Budapest	5.85	5.7	5.8	6.6	6.2	6.7	6.8	6.30
Debrecen	4.91	5.3	5.4	6.1	5.7	6.3	6.3	5.83
Miskolc	4.18	4.9	5.0	5.7	5.3	5.9	5.9	5.47
Mosonmagyaróvár	4.69	5.1	5.2	6.0	5.6	6.1	6.2	5.72
Nagykanizsa	3.79	4.7	4.8	5.5	5.1	5.7	5.7	5.27
Nyíregyháza	5.23	5.4	5.5	6.3	5.9	6.4	6.5	5.99
Pécs	4.22	4.9	5.0	5.8	5.4	5.9	6.0	5.49
Siófok	5.07	5.3	5.4	6.2	5.8	6.3	6.4	5.91
Szeged	5.88	5.7	5.8	6.6	6.2	6.7	6.8	6.32
Szolnok	6.02	5,8	5.9	6.7	6.3	6.8	6.9	6.39
Szombathely	3.79	4.7	4.8	5.5	5.1	5.7	5.7	527
mean	4.92	5.2	5.4	6.1	5.7	6.3	6.3	5.83

There were some alterations within the records since the most arid areas of the Great Plain belonging to the less than 500 mm range are located by the Szolnok station which is labelled by a higher PAI index than that of the Szeged crop site. Also, the highest altitude of this study at Szombathely with its 214 m had a medium level of PAI drought index. In the case of crop species the trends were almost consequest, but have shown detectable differences in accordance with their vulnerability. The results of the study support the postulated, that cereals were the least susceptible species, while potato and maize were proved to be highly influenced by drought x vulnerability interactions. Strong climatic impact could be detected in the case of alfalfa and sugar beet. Altitude of the crop site was in negative correlation with the magnitude of drought indices.

Fig. 4 presents the regression data of the PAI drought indices related to the altitude of the crop sites'

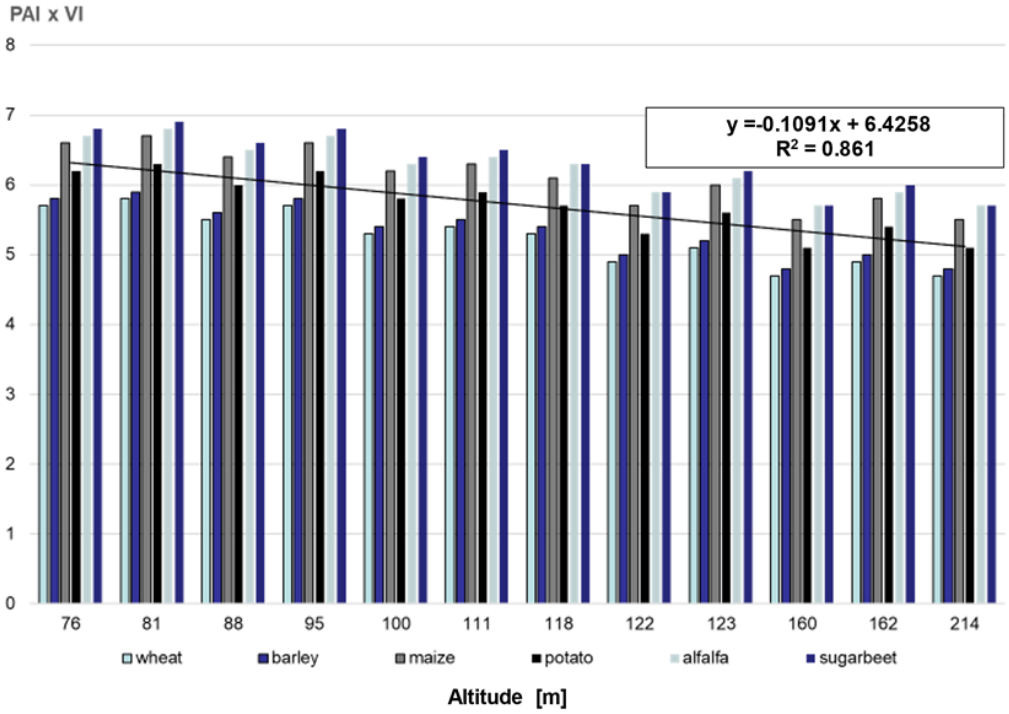

Fig. 3. Drought x crop vulnerability interactions of six field crop species by crop site altitude.

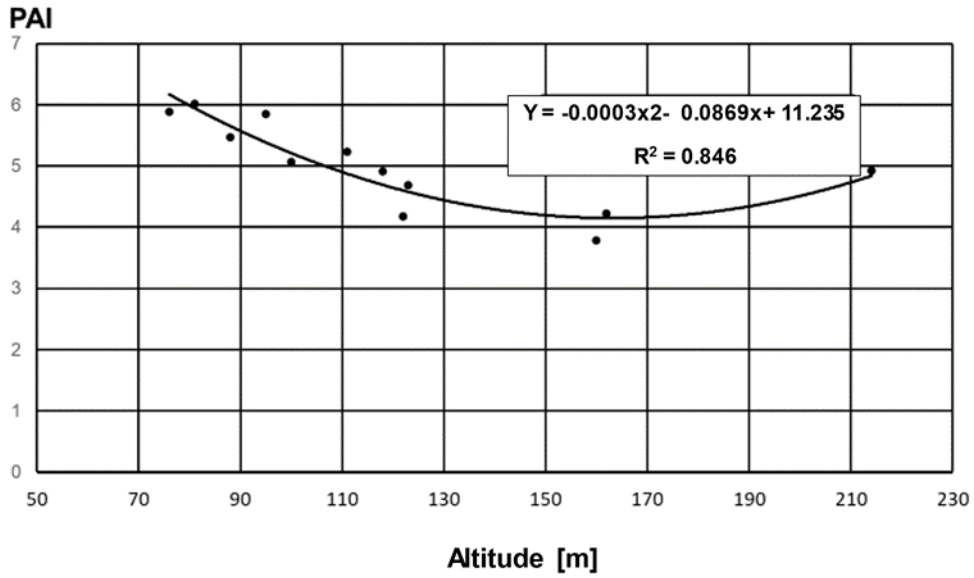

Fig. 4. Changes in the PAI indices due to the geographic elevation of crop sites.

meteorological station. The equation can be expressed by a polynomial equation that is having a rather strong statistical value.

Conclusion

As a conclusion of the study it can be stated, that the geographic location may have a strong influence for the performance of various crop plant species. Certain crops like cereals are less susceptible to crop site conditions, while others, especially those with higher water demand like maize and potato are more exposed to that. Alfalfa and sugar beet were definitely proven to be the most vulnerable crops in this study. The interaction between PAI and VI indices were proved to be useful for characterising the crop site.

Acknowledgement

The authors are indebted and would express their thanks for the support of the MATE Hungarian University of Agriculture and Life Sciences.

References

Bihari, Z. (Ed.) (2012): Délkelet-Európai Transznacionális Együttműködési Program. (South-East Europen Transnational Cooperation Programme). Országos Meteorológiai Szolgálat. Budapest. https://www.met.hu/doc/DMCSEE/DMCSEE_zaro_kiadvany.pdf

FAO (2021): The State of the World's Land and Water Resources for Food and Agriculture – Systems at breaking point (SOLAW 2021) Synthesis report 2021. https://www.fao.org/3/cb7654en/cb7654en.pdf

Jolánkai, M., Gyuricza, Cs., Tarnawa, Á., Pósa, B., Birkás, M. (2012): A drought assessment survey of Hungarian soils. Proceedings. 47th Croatian – 7th International Symposium on Agriculture. Ed.: M. Pospišil. Opatija. 492–496.

KSH (2022): Főbb növényi kultúrák terméseredményei. Crop yield of main field crops in Hungary. https://www.ksh.hu/docs/hun/xftp/stattukor/fobbnoveny/2020/index.html

Lakatos, M., Szalai, S. (2010): Aszályindex-számítás és –térképzés Magyarországra a DMCSEE keretében, Drought indexing and mapping in Hungary by DMCSEE. Agrofórum, 21. 8. 49–51.

Novák, V. (2023): The influence of land use change on transport of water and energy in ecosystem and climate change. Acta Hydrologica Slovaca. 24.(1) 3–8. DOI: 10.31577/ahs-2023-0024.01.0001

OMSZ (2022): Average annual precipitation and annual mean temperature. https:// www.met.hu/eghajlat/magyarorszag_eghajlata/altalanos_eghajlati_jellemzes/csapadek/

Pálfai, I. (1990): Description and forecasting of droughts in Hungary. Proc. of 14th Congress on Irrigation and Drainage (ICID), Rio de Janerio, 1990, Vol. 1-C, 151–158. https://www.springerprofessional.de/en/climate-change-and-european-water-bodies-a-review-of-existing-ga/5194598

Rattayová, V., Garaj, M., Hlavcová, K. (2022): Spatial and temporal variability of Aridity Index in lowland areas of Slovakia. Acta Hydrologica Slovaca. 23. (2) 273–281. DOI: 10.31577/ahs-2022-0023.02.0031

Tarnawa, Á., Gyuricza, Cs., Máté, A., Sallai, A., Pósa, B., Jolánkai, M. (2012): A drought assessment survey based on the evapotranspiration balance of major field crops in Hungary. In: Transport of water, chemicals and energy in the soil-plant-atmosphere system. Ed.: A. Celková. UH SAV. Bratislava. 786–791.

Tarnawa, Á., Klupács, H., Sallai, A., Szalay, K., Kassai, M. K., Nyárai, H. F., Jolánkai, M. (2010): Study on the impact of main climatic factors of crop production in a mathematical model. In: Transport of water, chemicals and energy in the soil-plant-atmosphere system. Ed: A. Celková. Institute of Hydrology, Bratislava, 566–571.

UNEP (1992): World Atlas of Desertification. https://wedocs.unep.org/handle/20.500.11822/42137

Várallyay, G. (2006): Soil degradation processes and extreme soil moisture regime as environmental problems in the Carpathian Basin. Agrokémia és Talajtan. 55. (1–2) 9–18. https://akjournals.com/view/journals /0088/55/1/article-p9.xml

Vermes, L. (Ed.) (2011): Aszálystratégia (Drought strategy). Manuscript VM, Budapest.

Ákos Tarnawa, PhD
Katalin M. Kassai, PhD
Zoltán Kende, PhD
Márton Jolánkai, DSc* (corresponding author, e-mail: jolankai.marton@uni-mate.hu)
Hungarian University of Agriculture and Life Sciences
H-2100 Gödöllő
Páter Károly utca 1
Hungary

DOI: 10.31577/ahs-2023-0024.02.0021

ACTA HYDROLOGICA SLOVACA

Volume 24, No. 2, 2023, 187 – 196

A comparative analysis of continuous and event-based hydrological modeling for streamflow hydrograph prediction

Mitra TANHAPOUR, Anna LIOVÁ, Kamila HLAVČOVÁ, Silvia KOHNOVÁ, Jaber SOLTANI*, Bahram MALEKMOHAMMADI, Hadi SHAKIBIAN

A precise evaluation of streamflow hydrographs and their attributes is one of the key components of hydrological applications. This research investigates a comparative analysis between event-based and continuous hydrological modeling of streamflow using the HBV rainfall-runoff model. The Dez river basin in southwest Iran was selected as a case study. Model performance was examined for a total of nine streamflow events during time period 2012–2019. The results of the model were compared for event-based and continuous simulations of streamflow using goodness-of-fit measures involving Nash-Sutcliff efficiency (NSE), normalized root mean square error (NRMSE), and mean absolute percentage error (MAPE). Besides, the most sensitive parameters were identified using sensitivity analysis. Results revealed that although HBV model has a reliable performance for both modeling approaches, continuous modeling of streamflow hydrographs slightly outperforms the EB simulation approach. These outcomes provide an efficient information to improve the operation of water systems and hydrological forecasts.

KEY WORDS: Streamflow hydrograph, HBV rainfall-runoff model, event-based simulation, continuous modeling

Introduction

Streamflow forecasting, as one of the main components of hydrological science, has great importance in water resources management in terms of optimal operation of reservoirs, water supply, flood risk management, and water structure design (Meshram et al., 2022). Rainfall-runoff (RR) models are commonly used to simulate streamflow (Wijayarathne and Coulibaly, 2020; Kumari et al., 2021). The process of converting rainfall to runoff is variable in different RR models. As described by Salvadore et al. (2015), RR models can be categorized based on their spatial variations (lumped, semi-distributed, and distributed), temporal changes (continuous and event-based modeling), and process definition (physical models or data-driven models). Similar classifications can be found in Okiria et al. (2022), Cunderlik (2003), and Lees et al. (2021). Therefore, RR models are selected based on the physical characteristics of basins and accessibility to data.

According to temporal category, event-based (EB) and continuous (CS) simulation approaches are the most well-known subcategories. EB modeling simulates the rainfall-runoff process in a catchment for an individual rainfall or streamflow event that may last several hours up to several days. In contrast, CS modeling simulates the rainfall-runoff process over a long period of time, from a few months to several years (Hossain et al., 2019).

Some scholars assessed the performance of different hydrological models to simulate EB and CS rainfall-runoff processes. In this regard, Hossain et al. (2019) carried out a comparative analysis using the storm water management model developed by the Environmental Protection Agency, USA (EPA-SWMM) in producing total runoff hydrographs and direct runoff hydrographs. They showed that EB modeling of runoff has more precision than CS modeling. A number of researchers have observed that an EB approach performs better than a CS approach for simulating runoff (Chu et al., 2009; De Silva et al., 2014; Azmat et al., 2017). In addition, Katwal et al. (2021) illustrated the reliability of the HEC-HMS model to forecast streamflow for both modeling approaches in the Zijinguan catchment in China. Cunderlik and Simonovic (2005) obtained a better fit using CS modeling of hydrological extremes in a southwestern Ontario river basin under future climate conditions.

Nowadays, various hydrological models, e.g., EPA-SWMM, soil and water assessment tool (SWAT), Hydrologic Engineering Center's Hydrological Modelling System (HEC-HMS), modular modeling system (MMS), and Hydrologiska Byrans Vattenbalansavdelning (HBV), have been developed to

estimate runoff worldwide (Hossain et al., 2019; Jaberzadeh et al., 2022). While each model has its own advantages and disadvantages, the HBV model is able to simulate RR modeling as CS and EB. This model has been used for water balance (Erlandsen et al., 2021), climate change (Djebbi and Dakhlaoui, 2023; Sabova and Kohnova, 2023), and related simulations concerning groundwater (Wang et al., 2021).

Previous studies revealed that the HBV model was successfully applied in different basins throughout the world due to its robustness, simplicity, and reliability. Moreover, it does not require a large number of input data (Krysanova et al., 1999). For instance, Tibangayuka et al. (2022) shown the proficiency of the HBV model in comparison with the data-driven model for simulating streamflow in a data-scarce high-humidity tropical catchment in Tanzania. In another study by Grillakis et al. (2010), the HBV model's performance was evaluated to predict flash floods in Slovenia. The results of their research represent the high efficiency of this model by producing values of the Nash-Sutcliffe coefficient in the range of 0.82-0.96. Besides, Kuban et al. (2021) analyzed the potential of the HBV model to simulate runoff using the satellite remote sensing of soil moisture (ASCAT) dataset over 209 catchments located in different climate zones of Austria. Based on the results of their research, a robust simulation of runoff was demonstrated in more than 27 percent of the studied catchments. Tanhapour et al. (2023) investigated the HBV model performance to forecast ensemble reservoir inflow under two scenarios, including ensemble forecasts (simulation using post-processed ensemble precipitation forecasts as input to the model) and deterministic forecasts (simulation using observed precipitation data). They indicated that ensemble forecasts are more reliable than deterministic forecasts to simulate reservoir inflow hydrographs. Therefore, previous studies have shown the successful application of the HBV model for forecasting streamflow.

To our knowledge, in none of the reviewed studies, the HBV hydrological model has been evaluated for CS and EB simulation of streamflow hydrographs. Therefore, the current research explores the accuracy of estimating streamflow using the HBV model based on CS and EB rainfall-runoff modeling approaches.

Material and methods

Case study

The Dez river basin, located upstream of the Dez reservoir, was selected as a case study. It is formed by the connection of the Bakhtiari and Sezar rivers in the south-western of Iran. This river is 120 km long and joins the Karun River in the area of Band-Ghir, downstream of the Dez reservoir. Fig. 1 demonstrates the location of the Dez basin, synoptic rainfall station, and hydrometric station.

The Dez basin has been located in the semi-arid mountainous region, in the range of latitudes from 32°, 35' to 34°, 07' North, and longitudes from 48°, 20' to 50°, 20' East. The basin shares its boundary with the Karkheh basin in the west, the Ghareh Chay basin in the north, and the Karun basin in the east and south (Tanhapour et al., 2023). The basin covers an area of 16213 km^2. The discharge data for the Taleh-Zang hydrometric station, upstream of the reservoir, was used to simulate streamflow hydrographs. The average annual discharge of Taleh-Zang hydrometric station is 193 m^3 s^{-1} during 2012–2019. Table 1 indicates the average annual precipitation and temperature of the synoptic stations during selected time period.

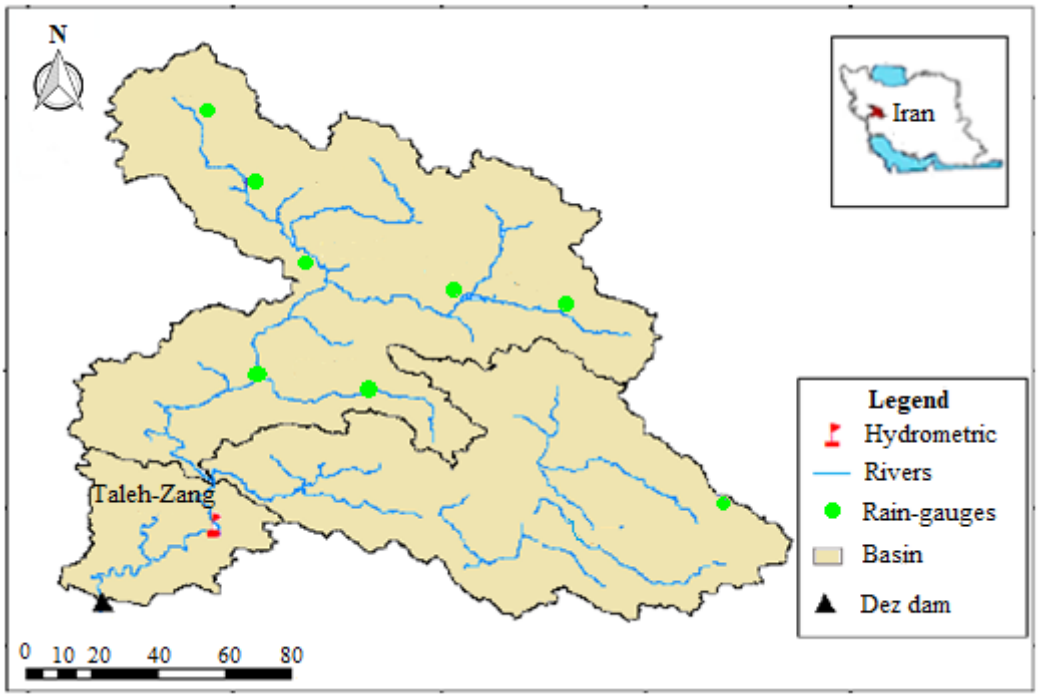

Fig. 1. The location of Dez river basin, hydrometric station, and rain gauges.

A set of variables, including precipitation, temperature, potential evapotranspiration, and discharge, were employed as inputs to the HBV hydrological model. Precipitation was interpolated uniformly all over the basin using the inverse distance weighting (IDW) method (Jeong et al., 2020). The temperature was estimated by interpolation between the temperature and elevation of synoptic stations. Besides, potential evapotranspiration was obtained using the empirical equation presented by Lawry-Johnson (Lowry and Johnson, 1942).

The input data were available at daily time steps during 2012–2019. The HBV model was calibrated during 2012–2015 and validated during 2016–2019. The model's efficiency was compared for two modeling approaches (CS and EB rainfall-runoff modeling) over the selected streamflow events, which were shown in Fig. 2. This figure indicates streamflow and precipitation time series in the calibration and validation stages. The streamflow events were chosen during peak flows. Table 2 displays the values of peak discharge for the streamflow events.

Table 1. Average annual precipitation and temperature of the synoptic stations

Station	Annual Precipitation [mm]	Annual Temperature [°C]
Aligudarz	727	13.41
Azna	496	13.12
Borujerd	541	15.94
Dorud	641	16.66
Shulabad	1048	15.3
Sepiddasht	679	20.64
Silakhor	491	15.1
Fereidunshahr	692	11.88

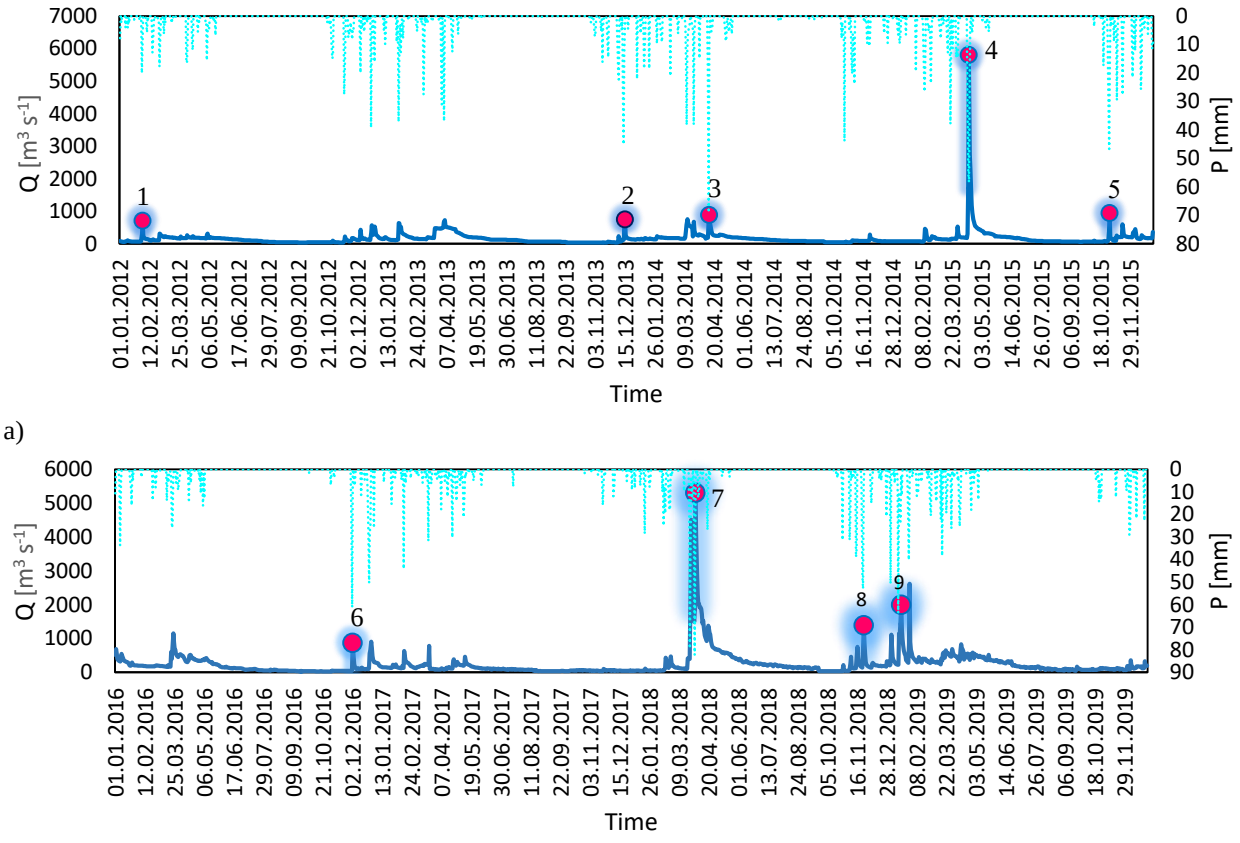

Fig. 2. Observed precipitation and streamflow time series in a) calibration period (2012–2015); b) validation period (2016–2019).

Rainfall-runoff model

The Hron hydrological model, as a modified version of the HBV model, was applied for simulating streamflow (Valent et al., 2012). This model includes three sub-models, e.g., snow accumulation and melt, soil moisture, and runoff response. Fig. 3 demonstrates the model's structure.

The model estimates runoff based on the parameters used in the snowmelt and soil moisture sub-models (see legend of Fig. 3). The runoff response sub-model transforms the estimated runoff into the discharge at the watershed outlet. In the runoff response, there are two storage zones, the upper storage zone and the lower storage zone. They are linked using constant percolation (perc). Runoff in the upper zone (Q_0) is swiftly triggered when the water level exceeds a threshold limit (L), while the other outlets are slow to respond. In the upper and lower zones, K_0, K_1, and K_2 represent recession coefficients that control runoff (Parra et al., 2018). Finally, it applies the triangular weight function (MAXBAS) for routing the produced runoff.

Calibration and validation of the model

The values of parameters were estimated automatically using genetic algorithms (GA). The Nash-Sutcliff efficiency (NSE) coefficient was used as an objective function to find the optimal values of the parameters based on the following equation (Nash and Sutcliffe, 1970):

Table 2. Selected streamflow events

Event No	Base-time	Time Period [day]	Peak flow [$m^3 s^{-1}$]
1	30 January–08 February, 2012	10	708
2	11 December–20 December, 2013	10	742
3	09 April–20 April, 2014	12	882
4	11 April–25 April, 2015	15	5799
5	26 October–04 November, 2015	10	938
6	28 November–07 December, 2016	10	858
7	30 March–06 April, 2018	8	5298
8	23 November –30 November, 2018	8	1381
9	12 January–27 January, 2019	16	1986

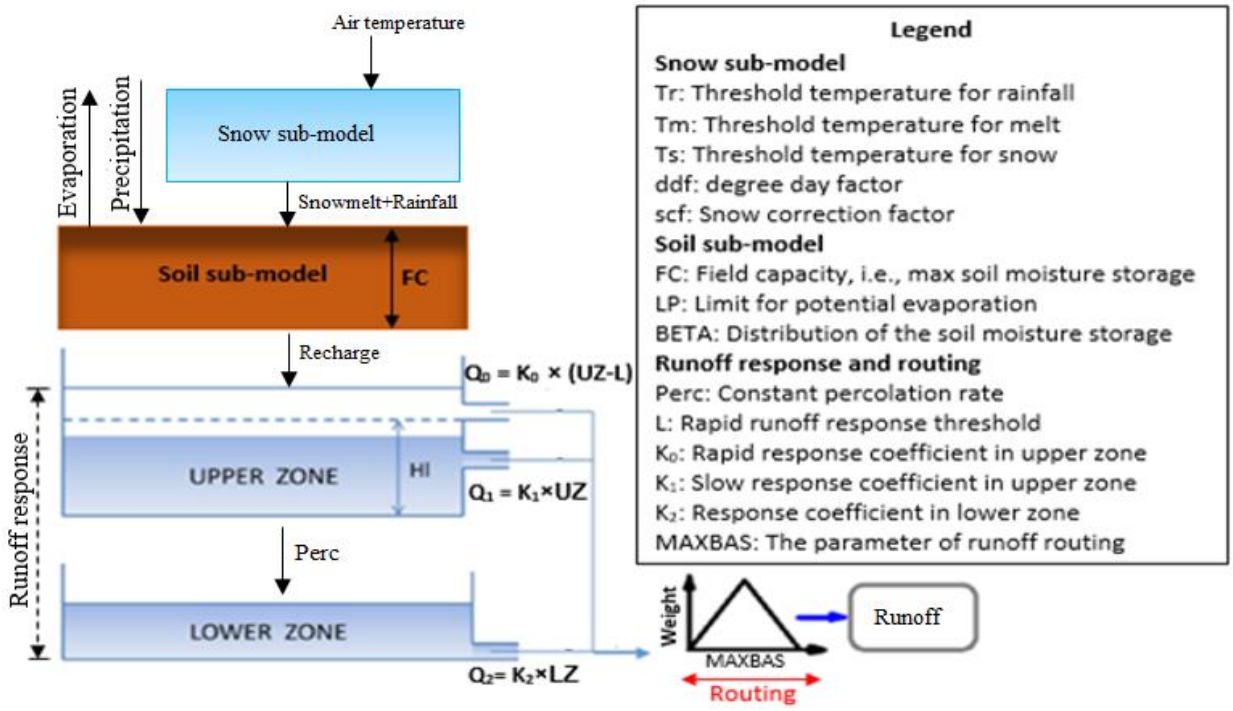

Fig. 3. The HBV model structure and parameters used in this study (Tanhapour et al., 2023).

$$NSE = 1 - \frac{\sum_{i=1}^{N}(Q_{sim}-Q_{obs})^2}{\sum_{i=1}^{N}(Q_{obs}-\bar{Q}_{obs})^2} \quad (1)$$

where

Q_{obs} and Q_{sim} – are observed and simulated flow [$m^3 s^{-1}$], respectively,

$\bar{Q}_{obs}$ – is the mean observed flow,

N – is the total number of records.

The model has been continuously calibrated for one month before the time period of streamflow events. For event-based calibration of the model, it was calibrated only during the base-time of selected events, which were shown in Table 2. The optimal values of the parameters were obtained using the calibration of the model for each modeling approach (Katwal et al., 2021). Moreover, to identify the most sensitive parameters, the values of the parameters were increased and decreased as much as 20% of their initial values. Then, it was investigated the maximum percentage of variations created in the model output using the variation of parameters (Tanhapour et al., 2022).

Continuous validation of the model has been carried out since two months before the time period of the selected events. In the next step, event-based validation of the model was performed during the streamflow events' base-time (Events 6–9). It is worthy to note that in both modeling methods, the optimal values of the parameters derived from calibration of similar streamflow events (with roughly the same peak flow) were used to investigate the validity of the model (Katwal et al., 2021).

Results and discussion

Continuous modeling of streamflow hydrograph

The results of the CS simulation of streamflow time series are depicted in Figs. 4 and 5 for the calibration and validation periods, respectively. Based on a visual comparison, it appears that the trend in the simulated time series is reasonably close to that of the observed series. However, it is obvious that there is a relative compatibility between simulated and observed peak flows. In addition, the results of sensitivity analysis of the parameters were presented in Table 3. The results indicated that the most sensitive parameters in reproducing streamflow are, respectively, L, maxbas, K1, scf, and BETA, considering the threshold limit for the NSE index of approximately 19–20% (Tanhapour et al., 2022). This means that by altering the values of the mentioned parameters, the NSE index was changed by a maximum of 20%. As a result, it can be inferred that these parameters greatly influence the model's precision compared to the others. Similar results were obtained by Brziak et al. (2021). They compared the lumped and semi-distributed versions of the HBV model in terms of the variations in the snowmelt sub-model parameters. This research was performed over 180 catchments in Austria. They divided the catchments into three groups based on their mean elevation. The results revealed the superiority of the semi-distributed versions of the HBV model compared to the lumped version.

Comparing continuous and event-based modeling of streamflow

Streamflow hydrographs were simulated as CS and EB using the HBV hydrological model. Fig. 6 shows the outcomes of the HBV model used for simulating streamflow during the calibration period. In this figure, the observed hydrograph along with CS and EB modeling of streamflow were displayed using blue, green, and red lines, respectively. As it can be seen, there is a little difference in the shape of stream hydrographs for both types of modeling approaches in the calibration period. However, in the majority of cases, the CS modeling approach has a better fit with observed streamflow in terms of peak flow, rising limb, and falling limb. In fact, it is possible for a model to take into account the antecedent status of a basin, e.g., antecedent rainfall, streamflow, and soil moisture, in CS modeling. For this reason, the model has higher efficiency for CS modeling compared to EB modeling. Moreover, CS modeling of streamflow considers both infiltration and evapotranspiration losses, whereas EB modeling only includes evapotranspiration losses.

The numerical results of the model's performance were presented in Table 4 for the calibration period. The average values of the NSE and NRMSE criteria, respectively, were estimated equal to 0.93 and 0.19 for the CS modeling approach. Similarly, they obtained 0.93 and 0.23 for the EB modeling approach, respectively. It represents the validity of the HBV model in reproducing streamflow hydrographs for both modeling approaches.

Fig. 7 indicates the graphical plot of streamflow hydrographs in the validation stage. It is clear that the model's error has been increased to estimate peak flow for both modeling approaches. Similar to the calibration stage, the simulated streamflow for CS modeling has a better match with the observed streamflow compared to the EB approach. It is worthy to note that hydrological processes and, subsequently, rainfall-runoff modeling are influenced by catchment urbanization and land use changes. Therefore, the streamflow generation process is different for diverse catchments. Consequently, it can be inferred that there is a clear distinction in hydrographs generated using models depending on the catchment characteristics. Consequentially, the models' performance is variable for CS and EB modeling of streamflow from one catchment to another.

Table 5 illustrates the values of goodness-of-fit measures to simulate streamflow in the validation stage. The average values of the NSE index for CS and EB modeling of streamflow have obtained 0.83 and 0.8, respectively, representing more accurate results of CS rainfall-runoff modeling. Generally, it can be said that the HBV model has robust efficiency for both modeling approaches in producing streamflow hydrographs.

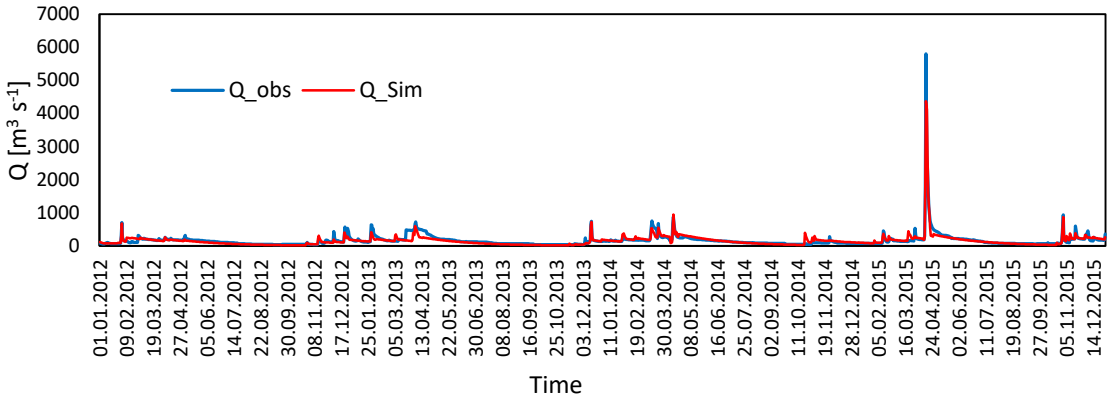

Fig. 4. Comparison of the CS simulation of the streamflow hydrograph and the observed hydrograph for the calibration period (2012–2015).

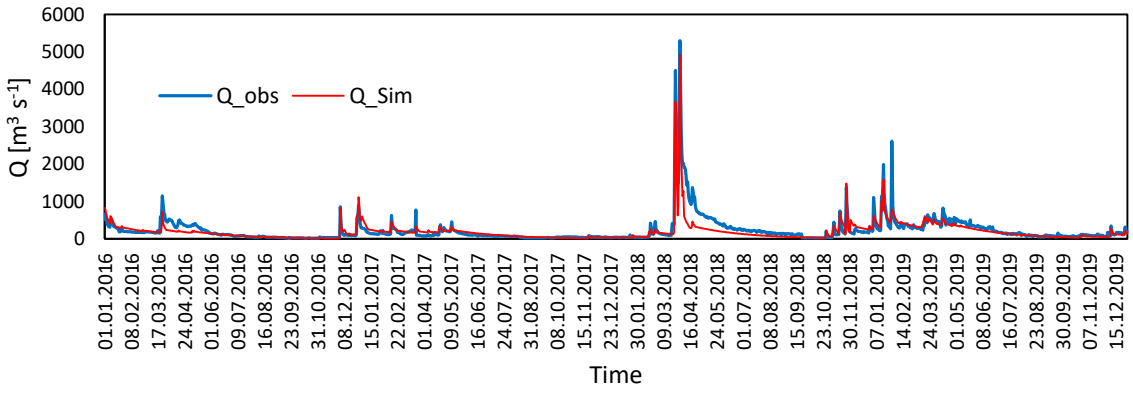

Fig. 5. Comparison of the CS simulation of the streamflow hydrograph and the observed hydrograph for the validation period (2016–2019).

Table 3. Maximum variations of the NSE index due to sensitivity analysis of the parameters

No	Parameter	Maximum variations of NSE index [%]	No	Parameter	Maximum variations of NSE index [%]
1	maxbas	20.4	8	ddf	16.9
2	scf	19	9	Ts	7.4
3	K2	17.8	10	Tm	13.5
4	K1	19.5	11	Tr	14
5	K0	14.1	12	L	21.6
6	LP	12.3	13	BETA	18.8
7	perc	15.3	14	Fc	10.8

Table 4. Goodness-of-fit measures for CS and EB modeling of streamflow hydrograph during calibration period

Streamflow events	Continuous			Event-based		
	NSE	NRMSE	MAPE	NSE	NRMSE	MAPE
Event 1	0.98	0.09	11.1	0.95	0.181	16.2
Event 2	0.98	0.11	12.5	0.94	0.19	25.9
Event 3	0.88	0.18	22.1	0.98	0.08	8.8
Event 4	0.85	0.41	24.1	0.86	0.39	22.5
Event 5	0.97	0.187	13.2	0.92	0.32	43.1

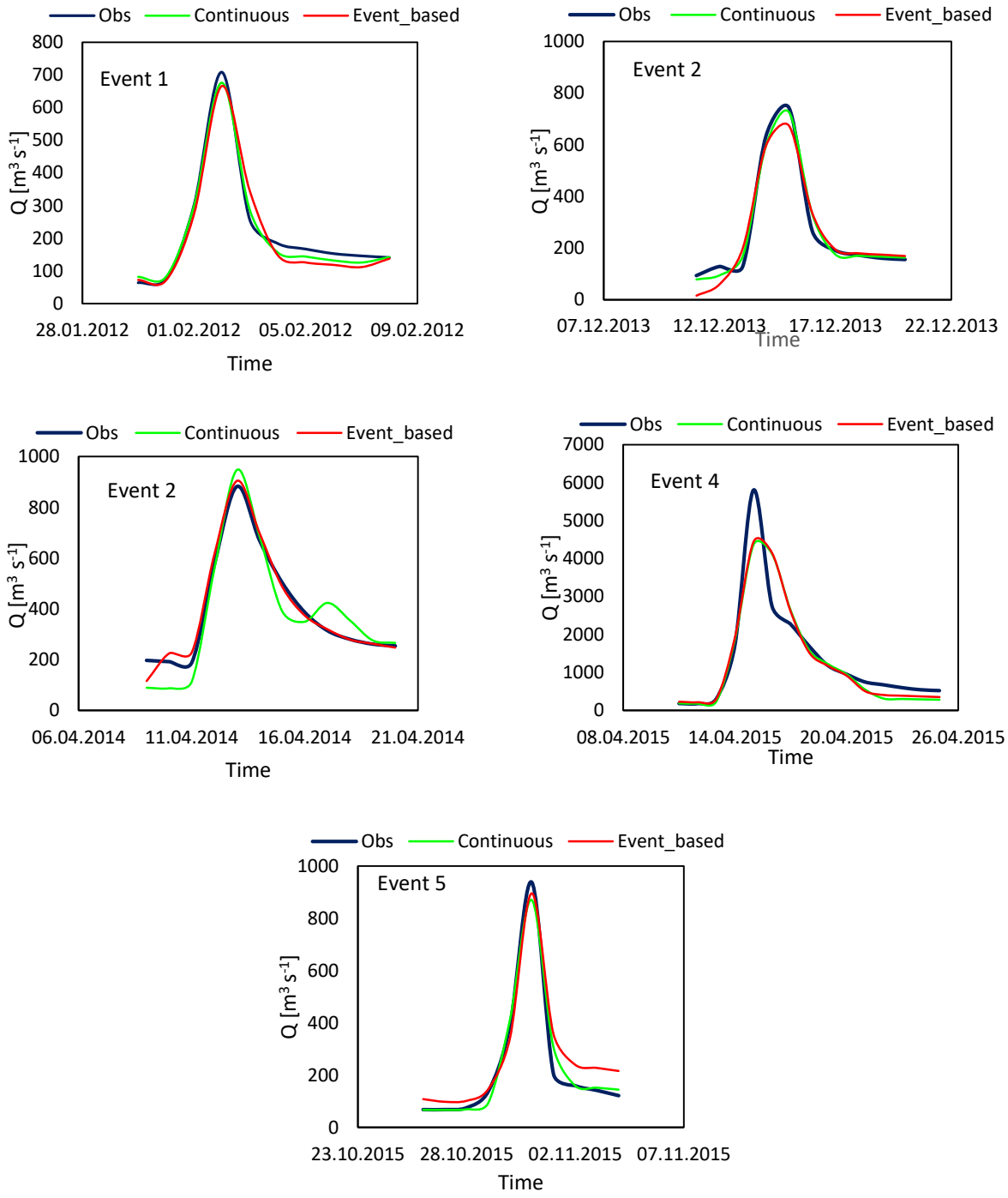

Fig. 6. Comparison of the CS and EB modeling of streamflow hydrograph during calibration period.

Table 5. Goodness-of-fit measures for CS and EB modeling of streamflow hydrograph during validation period

Streamflow events	Continuous			Event-based		
	NSE	NRMSE	MAPE	NSE	NRMSE	MAPE
Event 6	0.94	0.28	41.3	0.83	0.39	114.9
Event 7	0.77	0.21	23.4	0.72	0.23	26.6
Event 8	0.83	0.31	21.7	0.81	0.33	28.1
Event 9	0.76	0.32	30.1	0.87	0.23	28.9

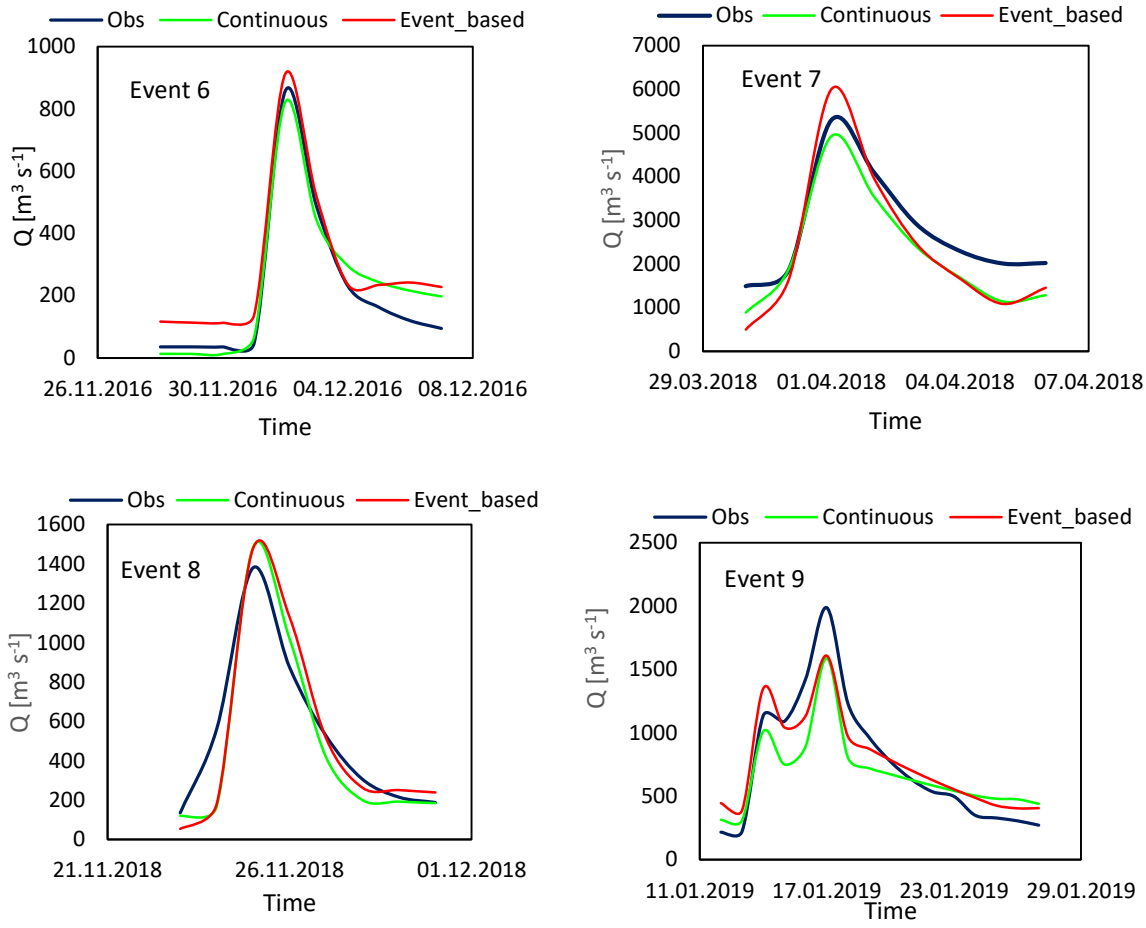

Fig. 7. Comparison of the CS and EB modeling of streamflow hydrograph during validation period.

Conclusion

This study compares the CS and EB simulations of streamflow hydrographs using the HBV model in the Dez River Basin. The results illustrated that the average values of the NSE index for CS and even-based simulation of streamflow respectively were obtained 0.83 and 0.8 in the validation stage. Besides, the average values of error for mentioned modelling approaches were estimated 0.28 and 0.3, respectively. Therefore, it can be concluded that the HBV model has an efficient performance for CS and EB modeling of streamflow hydrographs. However, the model performs slightly better for continues simulation of streamflow in comparison with EB modeling. Evaluation of the results showed that the most sensitive parameters were L, maxbas, K1, scf, and BETA to simulate streamflow in calibration period. Generally, the hydrological modeling used in this research facilitates subsequent hydrological studies in this basin. The results of this study is critical for flood warning and prediction in the next studies.

Acknowledgment

This research was supported by the Slovak Research and Development Agency under Contract No. APVV 19-0340 and the VEGA Grant Agency No. VEGA 1/0782/21.

References

Azmat, M., Qamar, M. U., Ahmed, S., Hussain, E., Umair, M. (2017): Application of HEC-HMS for the event and CS simulation in high altitude scarcely-gauged catchment under changing climate. European water, 57, 77–84.

Brziak, A., Kubáň, M., Kohnová, S., Szolgay, J. (2021): Comparison of the variability of snow cover parameters of the HBV model using lumped and distributed precipitation inputs and multi-basin calibration. Acta Hydrologica Slovaca, 22(1), 40–49.

Chu, X., Asce, A. M., Steinman, A. (2009): Event and CS modelling with HEC-HMS. J. Irrig. Drain. Eng. 135, 119–124.

Cunderlik, M. J. (2003): Hydrologic model selection for the CFCAS project: assessment of water resources risk and vulnerability to changing climatic conditions. The University of Western Ontario

Cunderlik, J. M., Simonovic, S. P. (2005): Hydrological extremes in a southwestern Ontario river basin under future climate conditions/Extrêmes hydrologiques dans UN basin versant du sud-ouest de l'Ontario sous conditions climatiques futures. Hydrological Sciences Journal, 50(4).

De Silva, M. M. G. T., Weerakoon, S. B., Herath, S. (2014): Modeling of event and CS flow hydrographs with HEC–HMS: case study in the Kelani River Basin, Sri Lanka. Journal of Hydrologic Engineering, 19(4), 800–806.

Djebbi, K., Dakhlaoui, H. (2023): Evaluating regional climate model simulations at Wadi El Abid catchment (northeastern Tunisia) using HBV rainfall-runoff model. Arabian Journal of Geosciences, 16(2), 139.

Erlandsen, H. B., Beldring, S., Eisner, S., Hisdal, H., Huang, S., Tallaksen, L. M. (2021): Constraining the HBV model for robust water balance assessments in a cold climate. Hydrology Research, 52(2), 356–372.

Grillakis, M. G., Tsanis, I. K., Koutroulis, A. G. (2010): Application of the HBV hydrological model in a flash flood case in Slovenia. Natural Hazards and Earth System Sciences, 10(12), 2713–2725.

Hossain, S., Hewa, G. A., Wella-Hewage, S. (2019): A comparison of CS and EB rainfall–runoff (RR) modelling using EPA-SWMM. Water, 11(3), 611.

Jaberzadeh, M., Saremi, A., Ghorbanizadeh Kharazi, H., Babazadeh, H. (2022): SWAT and IHACRES models for the simulation of rainfall-runoff of Dez watershed. Climate Dynamics, 1–13.

Jeong, H. G., Ahn, J. B., Lee, J., Shim, K. M., Jung, M. P. (2020): Improvement of daily precipitation estimations using PRISM with inverse-distance weighting. Theoretical and Applied Climatology, 139, 923–934.

Katwal, R., Li, J., Zhang, T., Hu, C., Rafique, M. A., Zheng, Y. (2021): EB and continous flood modeling in Zijinguan watershed, Northern China. Natural Hazards, 108, 733–753.

Krysanova, V., Bronstert, A., Müller-Wohlfeil, D. I. (1999): Modelling river discharge for large drainage basins: from lumped to distributed approach. Hydrological Sciences Journal, 44(2), 313–331.

Kubáň, M., Parajka, J., Tong, R., Pfeil, I., Vreugdenhil, M., Sleziak, P., Brziak, A., Szolgay, J., Kohnová, S., Hlavčová, K. (2021): Incorporating Advanced Scatterometer Surface and Root Zone Soil Moisture Products into the Calibration of a Conceptual Semi-Distributed Hydrological Model. Water, 13(23), 3366.

Kumari, N., Srivastava, A., Sahoo, B., Raghuwanshi, N. S., Bretreger, D. (2021): Identification of suitable hydrological models for streamflow assessment in the Kangsabati River Basin, India, by using different model selection scores. Natural Resources Research, 30(6), 4187–4205.

Lees, T., Buechel, M., Anderson, B., Slater, L., Reece, S., Coxon, G., Dadson, S. J. (2021): Benchmarking data-driven rainfall–runoff models in Great Britain: a comparison of long short-term memory (LSTM)-based models with four lumped conceptual models. Hydrology and Earth System Sciences, 25(10), 5517–5534.

Lowry Jr, R. L., Johnson, A. F. (1942): Consumptive use of water for agriculture. Transactions of the American Society of Civil Engineers, 107(1), 1243–1266.

Meshram, S. G., Meshram, C., Santos, C. A. G., Benzougagh, B., Khedher, K. M. (2022): Streamflow prediction based on artificial intelligence techniques. Iranian Journal of Science and Technology, Transactions of Civil Engineering, 46(3), 2393–2403.

Nash, J. E., Sutcliffe, J. V. (1970): River flow forecasting through conceptual models part I—A discussion of principles. Journal of hydrology, 10(3), 282–290.

Okiria, E., Okazawa, H., Noda, K., Kobayashi, Y., Suzuki, S., Yamazaki, Y. (2022): A Comparative Evaluation of Lumped and Semi-Distributed Conceptual Hydrological Models: Does Model Complexity Enhance Hydrograph Prediction?. Hydrology, 9(5), 89.

Parra, V., Fuentes-Aguilera, P., Muñoz, E. (2018): Identifying advantages and drawbacks of two hydrological models based on a sensitivity analysis: a study in two Chilean watersheds. Hydrological Sciences Journal, 63(12), 1831–1843.

Sabova, Z., Kohnova, S. (2023): On future changes in the long-term seasonal discharges in selected basins of Slovakia, Acta Hydrologica Slovaca, 24(1), 73–81.

Salvadore, E., Bronders, J., Batelaan, O. (2015): Hydrological modelling of urbanized catchments: A review and future directions. Journal of hydrology, 529, 62–81.

Tanhapour, M., Hlavcová, K., Soltani, J., Liová, A., Malekmohammadi, B. (2022): Sensitivity analysis and assessment of the performance of the HBV hydrological model for simulating reservoir inflow hydrograph. In Proceedings of the 16th Annual International Scientific Conference, Science of Youth, Banská Štiavnica, Slovakia, 1–3 June 2022; 115–124.

Tanhapour, M., Soltani, J., Malekmohammadi, B., Hlavcova, K., Kohnova, S., Petrakova, Z., Lotfi, S. (2023): Forecasting the Ensemble Hydrograph of the Reservoir Inflow based on Post-Processed TIGGE Precipitation Forecasts in a Coupled Atmospheric-Hydrological System. Water, 15(5), 887.

Tibangayuka, N., Mulungu, D. M., Izdori, F. (2022): Evaluating the performance of HBV, HEC-HMS and ANN models in simulating streamflow for a data scarce high-humid tropical catchment in Tanzania. Hydrological Sciences Journal, 67(14), 2191–2204.

Valent, P., Szolgay, J., Riverso, C. (2012): Assessment of the uncertainties of a conceptual hydrologic model by using artificially generated flows. Slovak journal of civil engineering, 20(4), 35–43.

Wang, S. J., Lee, C. H., Yeh, C. F., Choo, Y. F., Tseng, H. W. (2021): Evaluation of climate change impact on groundwater recharge in groundwater regions in Taiwan. Water, 13(9), 1153.

Wijayarathne, D. B., Coulibaly, P. (2020): Identification of hydrological models for operational flood forecasting in St. John's, Newfoundland, Canada. Journal of Hydrology: Regional Studies, 27, 100646.

Mitra Tanhapour, PhD graduated
Jaber Soltani, Associate Professor (*corresponding author, e-mail: jsoltani@ut.ac.ir)
Water Engineering Department
Faculty of Agricultural Technology
University College of Agriculture & Natural Resources
University of Tehran
Tehran
Iran

Anna Liová, PhD candidate
Kamila Hlavčová, Professor
Silvia Kohnová, Professor
Department of Land and Water Resources Management
Faculty of Civil Engineering
Slovak University of Technology
Bratislava
Slovak Republic

Bahram Malekmohammadi, Associate Professor
Department of Environmental Planning and Management
Graduate Faculty of Environment
University of Tehran
Tehran
Iran

Hadi Shakibian, Assistant Professor
Department of Computer Engineering
Faculty of Engineering, Alzahra University
Tehran
Iran

DOI: 10.31577/ahs-2023-0024.02.0022

ACTA HYDROLOGICA SLOVACA

Volume 24, No. 2, 2023, 197 – 204

Estimation of water temperature changes in the Ipeľ River based on future scenarios

Zbyněk BAJTEK*, Pavla PEKÁROVÁ, Katarína JENEIOVÁ, Pavol MIKLÁNEK

Water is an irreplaceable resource for life and ecosystems, and among its key parameters is its temperature. The temperature of water and its fluctuations have a significant impact on aquatic ecosystems, highlighting the need for accurate prediction and monitoring. Therefore this study focuses on the analysis and simulation of monthly and daily water temperatures in the Ipeľ River Basin at two measuring stations. The first part of the study deals with the statistical analysis of daily water and air temperature values. The second part examines regression models for predicting daily and monthly water temperatures in the Ipeľ River Basin. The results of this analysis indicate that due to climate change, there is a gradual increase in temperatures in the Ipeľ River. This trend can have a negative impact on aquatic ecosystems and biodiversity, especially in extreme scenarios. Additionally, elevated water temperatures can affect water management and the utilization of the Ipeľ River, including the availability of drinking water and the quality of water sources. Overall, this study holds significant importance for the protection of aquatic ecosystems, and the insights gained can serve as a foundation for future strategies and measures to adapt to changing conditions and safeguard the valuable aquatic environment of the Ipeľ River Basin.

KEY WORDS: prediction of water temperature, change in water temperature, Ipeľ River, climatic scenarios

Introduction

Water temperature in rivers is not only a physical property, but also an important environmental factor and indicator of water quality and aquatic habitats (Grbić et al., 2013; Lešková and Skoda, 2003). Through the influence of water temperature on chemical processes, it indirectly affects key ecosystem processes (Hannah et al., 2008), such as primary production, decomposition and nutrient cycling in rivers (Friberg et al., 2009). These parameters and processes influence dissolved oxygen levels and, of course, have a major impact on water quality (Beaufort et al., 2016). In addition to ecological importance, water temperature in rivers also affects socio-economic concerns such as industry (cooling), drinking water production (Varga et al., 2023); (Varga and Velísková, 2021), sanitation, bacterial contamination, and fisheries (Hannah and Garner, 2015). Therefore, changes in the water temperature of a river can significantly alter the hydro-ecological and socio-economic conditions of the river and its catchment. Assessing changes in this variable and its drivers is essential to take action to manage impacts and enable preventative measures. Direct measurements of water temperature are often limited to gauge profiles, and the availability of longer series of measurements is limited to wake profiles. For optimised water management, it will be essential to derive how river water temperatures will evolve in the future, especially when considering global climate change processes. For example, predicting river temperatures a few days in advance can have a significant impact on possible countermeasures. Knowing the expected water temperature for the next few days is therefore an advantage. An important step in this context is the development of suitable model concepts for predicting river water temperature, describing thermal regimes and investigating the thermal evolution of the river. Among the variables that have the greatest influence on the temperature of the water in the river we can include meteorological conditions, especially air temperature, then wind speed, solar radiation and humidity. These determine the heat exchange and fluxes that take place at the surface of the river (Sleziak et al., 2023). In regression analysis of river water temperature, air temperature is often used as the only independent variable because it can be used as a proxy for net heat exchange fluxes affecting the water surface and also because air temperature is widely measured and more readily available than other parameters (Mohseni and Stefan, 1998), (Webb et al., 2008). Many water temperature prediction models have been successfully developed and applied in the past. Deterministic water temperature models simulate spatial and temporal changes in river water temperature based on the energy balance of heat fluxes and the mass balance of currents in

the river. They require a large number of input variables and are often impractical and time consuming due to their complexity. On the other hand, because they are relatively simple and require less input data, statistical models are widely used. These include linear regression models (Morrill et al., 2005), nonlinear regression models (Bajtek et al., 2022; Mohseni and Stefan, 1998; van Vliet et al., 2023) and stochastic models (Ahmadi-Nedushan et al., 2007) for data over different time scales. Simultaneously, artificial neural network (ANN) models have recently been widely used to predict water temperature. DeWeber and Wagner, (2014) developed an ensemble ANN model for the prediction of daily mean water temperature with the use of air temperature and topography. With a particular focus on stream water temperature prediction, a recent study (Feigl et al., 2021) employed machine learning techniques to analyse the water temperature regime of the Danube River and its tributaries in Austria. In this study, the water temperature patterns of the Danube River and its tributaries were examined and predicted using advanced machine learning algorithms such as artificial neural networks and random forests. An important aspect is that it may be beneficial to consider the time lag of the influence of air temperature on practical temperature predictions (Benyahya et al., 2007), as stream water temperature does not respond instantaneously to changes in air temperature due to thermal inertia relative to hydrological regime fluxes (Isaak et al., 2017). This is broken down into two different parts: a long-term periodic part and a short-term variable part. In terms of land use change, many studies suggest that forest cover reduction (or vegetation shading reduction) (Pekárová et al., 2011) can have a significant impact on river water temperature change. Although the relationship between air temperature and water temperature is generally strong, the strength of these relationships varies regionally and temporally, and can change based on a number of external and internal aspects (Cisty and Soldanova, 2018; DeWeber and Wagner, 2014). For this reason, we set ourselves two objectives: the first one was to better analyse the variation of water temperature during the year, and the second one was to look for a suitable model to simulate the relationship between air temperature and water temperature. The catchment area of the Ipel River with its tributaries was chosen as the study area. The Cran R programming language (R Core Team, 2022) was chosen for the statistics and plotting of graphs because it provides a comprehensive set of analysis tools, as well as a great ability to visualise the results.

Material and methods

River basin description and data

The Ipeľ River (Fig. 1, 2) (Ipoly in Hungarian, Ipell in German) is the third largest river in Slovakia and a part of it forms the border between Slovakia and Hungary. The Ipeľ rises in the Low Tatras and flows for 232.5 km through central Slovakia, 140 km of which forms the aforementioned border with Hungary. The river basin extends into Hungarian territory and covers an area of 5,151 km². The most important tributaries of the Ipeľ in Slovakia include the Krupinica, which rises in the Javorie Mountains at the western foot of Veľký Lysec (886.4 m above sea level), is 65.4 km long, has an average discharge of 2.2 $m^3 s^{-1}$ (near the village of Plášť'ovce) and a catchment area of 551 km².

The Štiavnica River, which flows through the Krupina Plateau, is about 54.6 km long and has a catchment area of 441 km². It is a highland-lowland river. The Krivánský Brook is sometimes called the Lučenský Brook. With a length of 48.2 km and a catchment area of 204.89 km², it is an important right tributary of the Ipeľ River. It is a third-order stream, with a fan-shaped course and a regulated channel, and rises in the Ostrôžky Mountains, on the north-eastern slope of Baranie Hill (726.8 m above sea level), at an altitude of about 670 m above sea level. The Tisovník River, which flows through the territory of

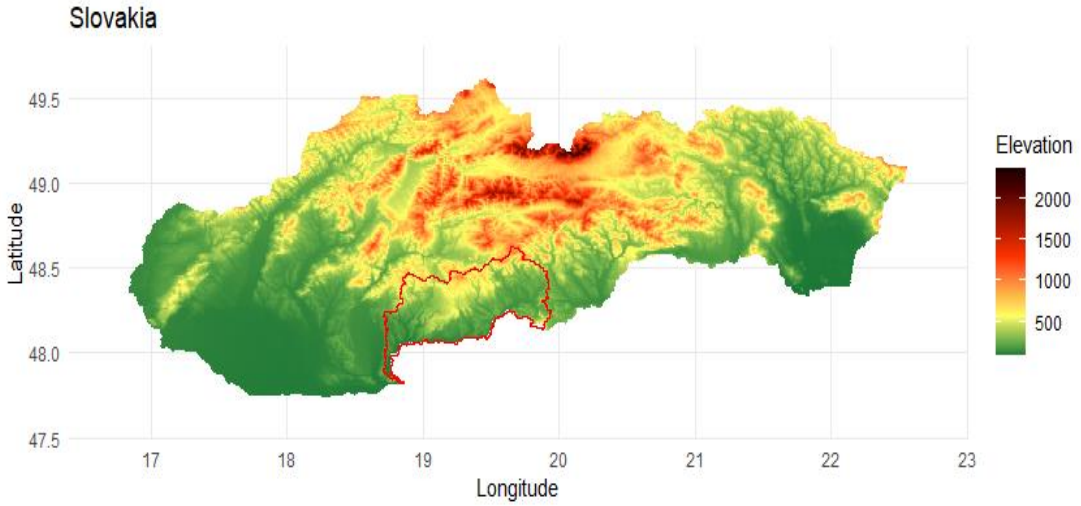

Fig. 1. Ipeľ River Basin, Slovakia map.

the Detva and Veľký Krtíš districts, is an important right tributary of the Ipeľ River with a length of 41 km and a catchment area of 441.1 km².

Methods

In our research we worked with data that included water temperatures from two water gauging stations, namely Slovenské Ďarmoty and Kalinovo, and one climatic station, namely Bzovík, with which the air temperature was used (Fig. 2).

In the framework of data preparation, we chose the period from 2005 to 2020, when the measurements in these two stations were automated and the daily water temperature value was computed as the average value of daily measurements in an hourly step (Fig. 3). Then we divided the data into two sets in 80 to 20 ratio, where the first set (80%) was used to train the model and the second set (20%) was used to test the model.

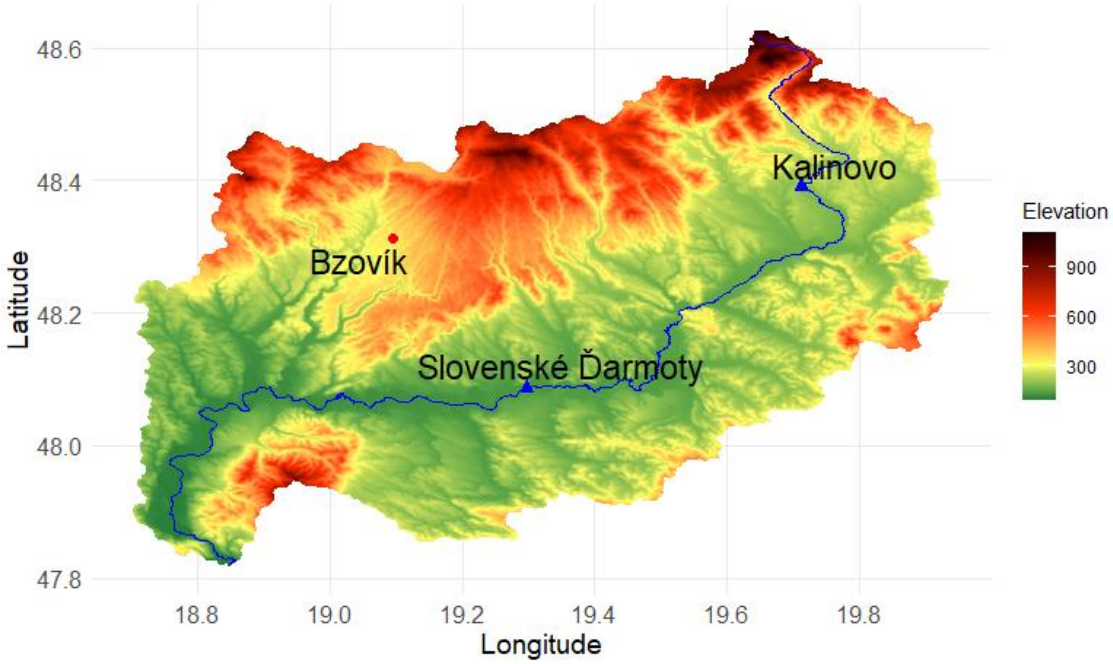

Fig. 2. Scheme of the Ipeľ River Basin, Gauging station Slovenské Ďarmoty, Kalinovo, and Bzovík climatic station.

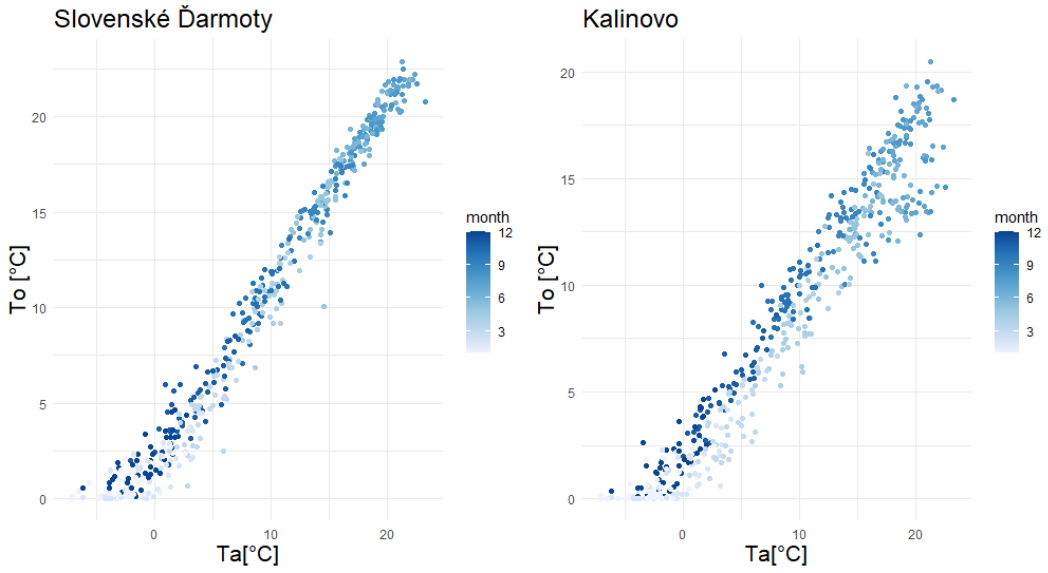

Fig. 3. Water temperature To and air temperature Ta dependence for "Slovenské Ďarmoty and Kalinovo" gauging station.

To build the model, we used non-linear multiple regression models, which are statistical models that are used to analyse the relationship between two or more independent variables and the dependent variable. Multiple regression models can be used to test hypotheses, make predictions and identify significant predictors of the outcome variable. The model used here is a version of the model (a four parameter non-linear function of air temperature) that was originally proposed by Mohseni et al., (1998) for the estimation of weekly stream temperatures over an annual cycle. According to this method, a continuous function of the form S curve' can describe the relationship between water and air, and its parameters have physical meaning:

$$To=\mu+((\alpha-\mu))/(1+e^{\gamma(\beta-Ta)}), \quad (1)$$

where
To – daily water temperature [°C],
Ta – daily air temperature [°C],
μ – lower asymptote of the dependent variable,
α – upper asymptote of the dependent variable,
β – inflection point of the dependent variable growth,
γ – slope of the curve at the inflection point.

We usually estimate the model using least squares regression, which minimizes the sum of squared differences between the observed and predicted values of the dependent variables.
We built the model for both stations based on a full year of data (Fig. 4a, b). The second alternative we tested was to further split the training data based on months and then create a model for each month separately (see Fig. 4c, d). To evaluate the models, we used statistical metrics that are often used to evaluate the performance of regression models, including those used in hydrologic prediction, specifically MAE (Mean Absolute Error), MSE (Mean Squared Error), RMSE (Root Mean Squared Error), and R-squared. The resulting values can be seen in Table 1.
In the next step, we focused on predicting daily water temperature values in the Ipeľ River using four climate scenarios for future periods: RCP2.6 (2031–2060), RCP2.6 (2071–2100), RCP8.5 (2031–2060) and RCP8.5 (2071–2100). We calibrated non-L multiple regression models for two stations (see Table 1): Kalinovo and Slovenské Ďarmoty. We used air temperature scenarios S1 to S4 according to Table 2. During the calibrations, we used the monthly water temperature and air temperature series in the base period from 2005 to 2020.

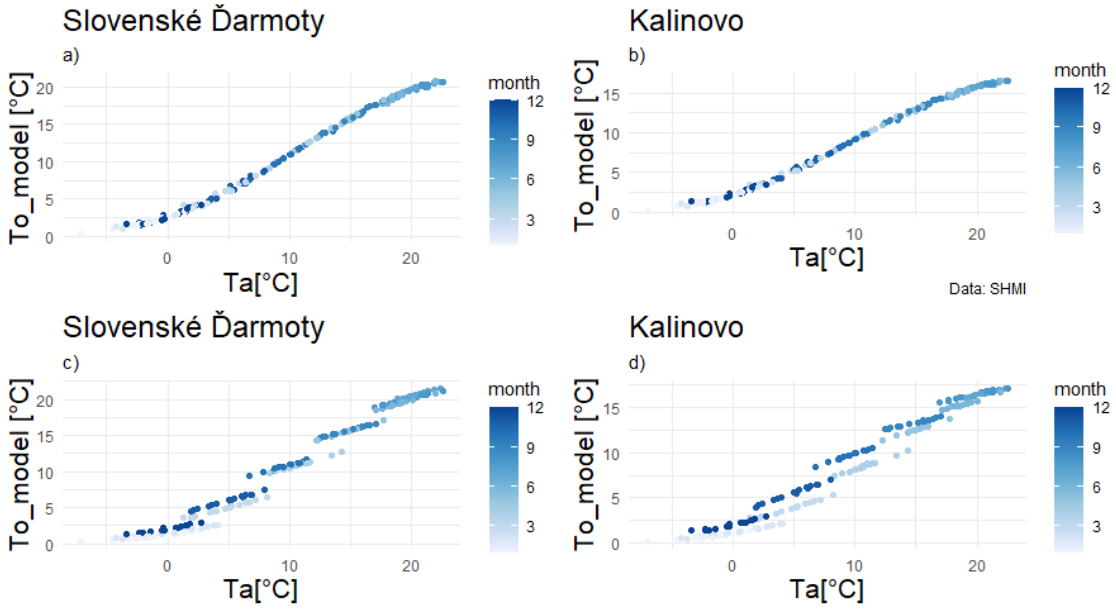

Fig. 4. Dependence of modelled water temperature To model and air temperature Ta for Slovenské Ďarmoty and Kalinovo water gauging stations. a, b) model for the whole year and c, d) models by months.

Table 1. Model parameters summarised

Station/model	MAE	MSE	RMSE	R-squared
Slovenské Ďarmoty (model for the whole year)	1.748	5.025	2.242	0.913
Slovenské Ďarmoty (models by months)	1.276	2.648	1.627	0.957
Kalinovo (model for the whole year)	1.737	4.697	2.167	0.862
Kalinovo (models by months)	1.526	3.631	1.906	0.897

Results and discussion

This study aimed to predict water temperature and its changes in two gauge profiles of the Ipeľ River using statistical approaches. Two different modelling methods were used, one using annual data and the other using monthly data. Non-linear multiple regression models were tested. The models were then used to predict water temperature on the basis of air temperature change scenarios derived from EURO-CORDEX simulations by Probst and Mauser, (2023). The results (Fig. 5, 6, 7) showed that the mean monthly water temperature in the Ipeľ River is predicted to increase under scenarios S1 to S4. The model working with annual data predicted the greatest increase of the water temperature at the station Slovenské Ďarmoty in the month of April, with a maximum increase of 4.01°C in the scenario S4. Conversely, models using monthly data predicted the largest increase at Slovenské Ďarmoty in the month of June, with a maximum increase of 2.1°C for scenario S4.

Table 2. Seasonal scenarios S1 to S4 of the air temperature for future periods

	Temperature [°C]			
Emission Scenario	Spring	Summer	Autumn	Winter
S1, RCP2.6 (2031–2060)	1.2	1.1	1.1	1.4
S2 RCP2.6 (2071–2100)	1.4	1.0	0.9	1.4
S3, RCP8.5 (2031–2060)	2.2	2.1	2.0	2.5
S4, RCP8.5 (2071–2100)	3.9	4.4	3.8	4.7

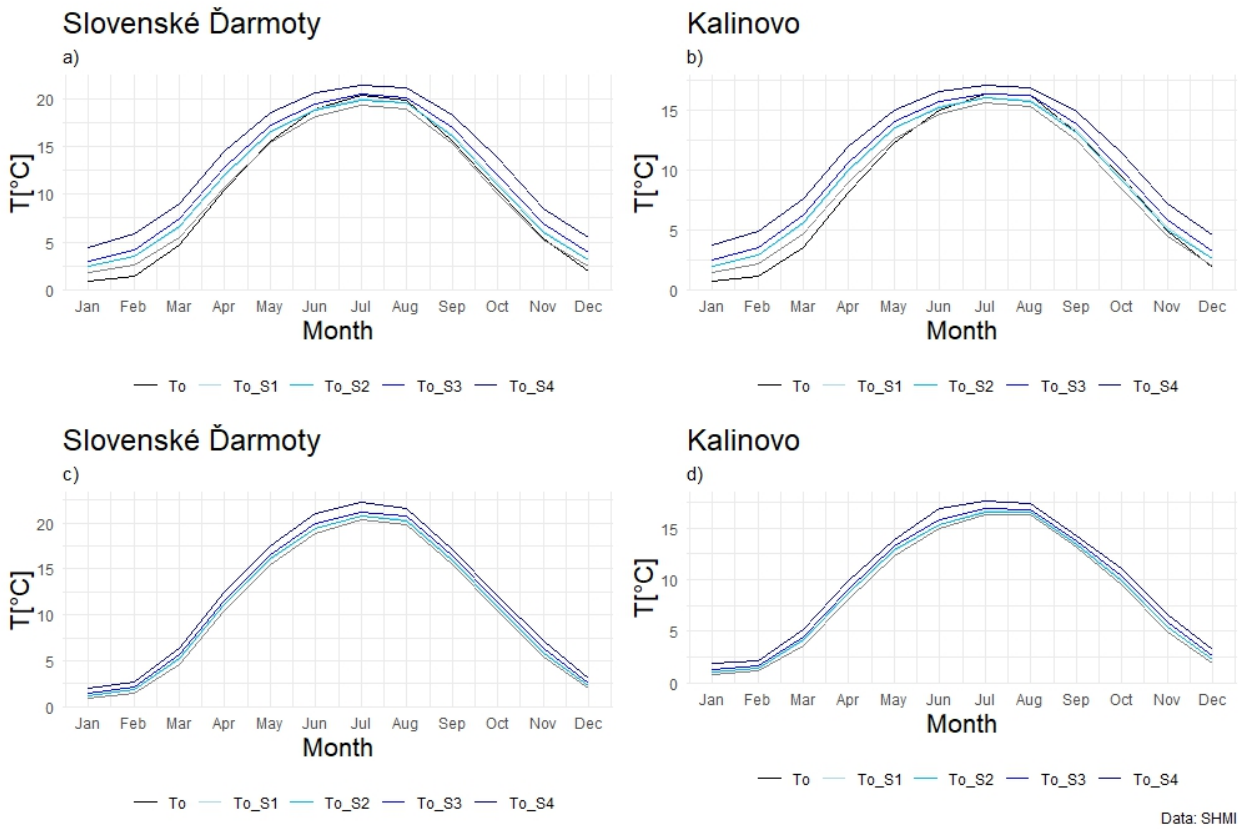

Fig. 5. Comparison of predicted monthly To according to scenarios S1 to S4 for stations Slovenské Ďarmoty and Kalinovo; a, b) model for the whole year and c, d) models by months.

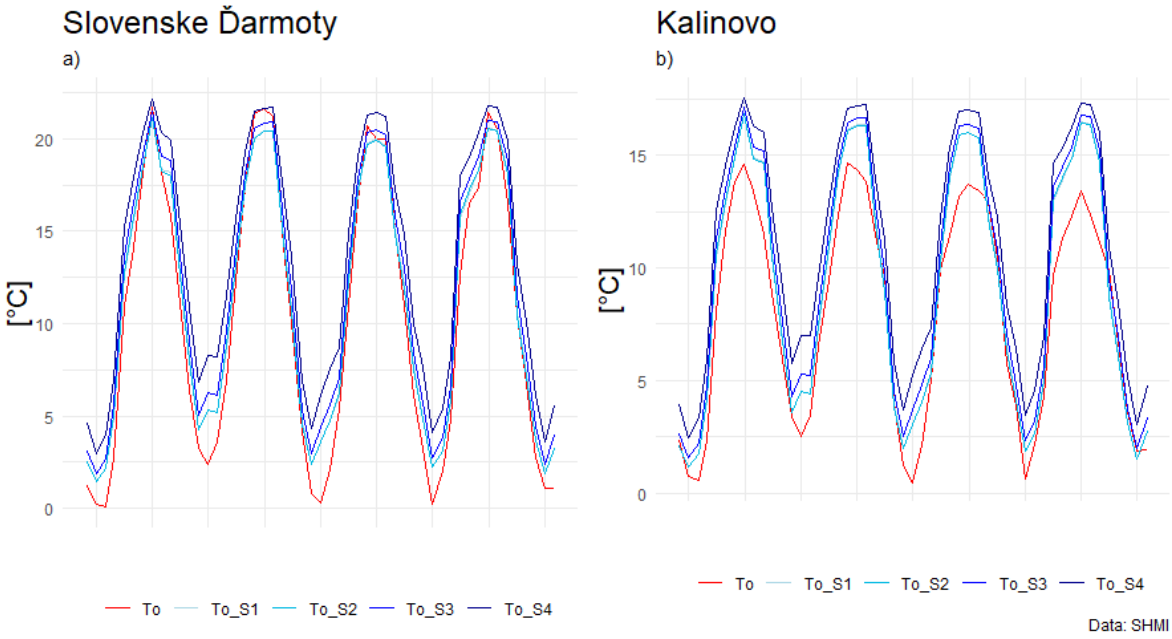

Fig. 6. Comparison between measured and modelled monthly water temperature values in the Ipeľ River at Slovenské Ďarmoty and Kalinovo stations using model under scenarios S1 to S4. (model for the whole year).

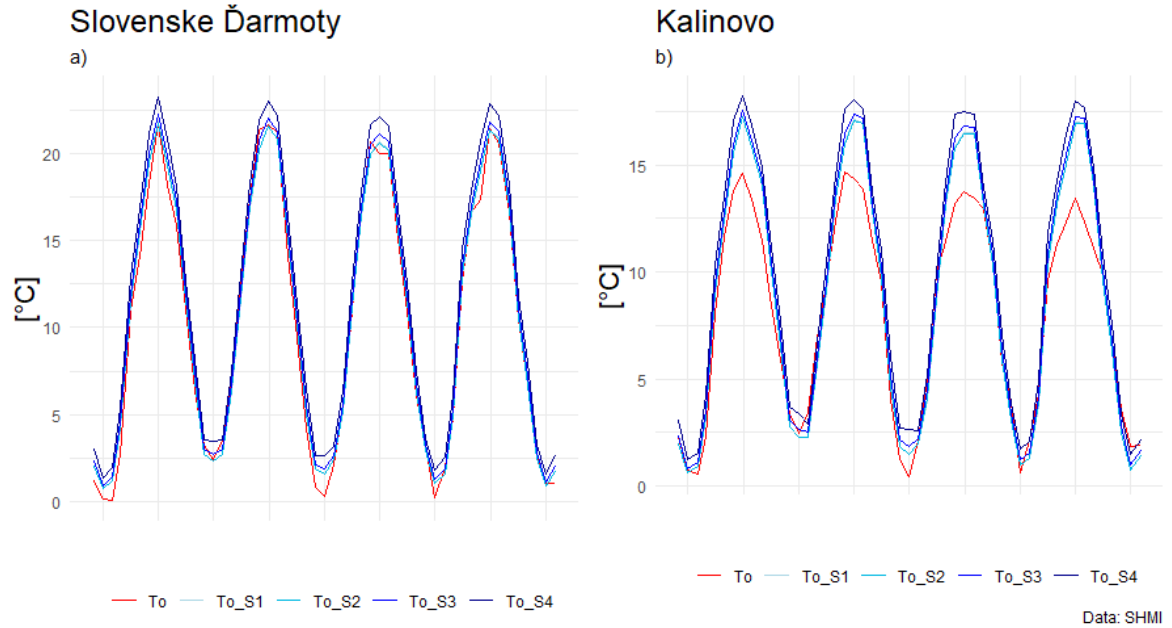

Fig. 7. Comparison between measured and modelled monthly water temperature values in the Ipeľ River at Slovenské Ďarmoty and Kalinovo stations using model under scenarios S1 to S4 (models by months).

Conclusion

To predict water temperature and its changes in two gauge profiles of the Ipeľ River, statistical approaches were used. Two types of non-linear multiple regression models were used to predict the monthly water temperature in the Ipeľ River at the Slovenské Ďarmoty and Kalinovo stations using the air temperature from the Bzovík station, where in the first case the model worked with annual data and in the second case with monthly step data. The air temperature was used to model the monthly mean water temperature. In the second phase, in order to

predict the impact on water temperature, a climate change scenario derived from EURO-CORDEX simulations was used. According to the models, monthly mean water temperature in Ipeľ will increase under scenarios S1 to S4. For the model working with the whole annual data series, the largest increase in water temperature at the station Slovenské Ďarmoty is 4.01°C in the month of April for S4. Conversely, models working with monthly data predict the largest increase in S4 at the Slovenské Ďarmoty station in the month of June at 2.1°C. According to the models for the whole year, the absolute smallest increase may occur in summer, while the largest increase is expected in the months of February, March and April at both stations. For both stations, the monthly models show smaller monthly increases in water temperature. Overall, in modelling the monthly water temperature variations in the Ipeľ River, the month-by-month model has shown greater stability and efficiency. It appears to be a useful tool for prediction of water temperatures in rivers without measurements, but for modelling future development it has some limitations which make this model less useful.

Acknowledgement

This research is supported by the project WATSIM "Water temperature simulation during summer low flow conditions in the Danube basin", and project APVV-20-0374 "Regional detection, attribution and projection of impacts of climate variability and climate change on runoff regimes in Slovakia" and projects VEGA No. 2/0015/23 "Comprehensive analysis of the quantity and quality of water regime development in streams and their mutual dependence in selected Slovak basins" APVV No. 20-0374 "Regional detection, attribution and projection of impacts of climate variability and climate change on runoff regimes in Slovakia".

References

Ahmadi-Nedushan, B., St-Hilaire, A., Ouarda, T. B. M. J., Bilodeau, L., Robichaud, É., Thiémonge, N., Bobée, B., (2007): Predicting river water temperatures using stochastic models: case study of the Moisie River (Québec, Canada). Hydrol. Process. 21, 21–34. https://doi.org/10.1002/hyp.6353

Bajtek, Z., Pekárová, P., Jeneiová, K., Ridzoň, J. (2022): Analysis of the water temperature in the Litava River. Acta Hydrologica Slovaca 23, 296–304. https://doi.org/10.31577/ahs-2022-0023.02.0034

Beaufort, A., Moatar, F., Curie, F., Ducharne, A., Bustillo, V., Thiéry, D. (2016): River Temperature Modelling by Strahler Order at the Regional Scale in the Loire River Basin, France. River Res. Appl. 32, 597–609. https://doi.org/10.1002/rra.2888

Benyahya, L., St-Hilaire, A., Quarda, T. B. M. J., Bobée, B., Ahmadi-Nedushan, B. (2007): Modeling of water temperatures based on stochastic approaches: case study of the Deschutes River. J. Environ. Eng. Sci. 6, 437–448. https://doi.org/10.1139/s06-067

Cisty, M., Soldanova, V. (2018): Flow Prediction Versus Flow Simulation Using Machine Learning Algorithms, in: Perner, P. (Ed.), Machine Learning and Data Mining in Pattern Recognition, Lecture Notes in Computer Science. Springer International Publishing, Cham, 369–382. https://doi.org/10.1007/978-3-319-96133-0_28

DeWeber, J. T., Wagner, T. (2014): A regional neural network ensemble for predicting mean daily river water temperature. J. Hydrol. 517, 187–200. https://doi.org/10.1016/j.jhydrol.2014.05.035

Feigl, M., Lebiedzinski, K., Herrnegger, M., Schulz, K. (2021): Machine learning methods for stream water temperature prediction (preprint). Rivers and Lakes/Modelling approaches. https://doi.org/10.5194/hess-2020-670

Friberg, N., DybkjÆr, J. B., Olafsson, J. S., Gislason, G. M., Larsen, Sø. E., Lauridsen, T. L. (2009): Relationships between structure and function in streams contrasting in temperature. Freshw. Biol. 54, 2051–2068. https://doi.org/10.1111/j.1365-2427.2009.02234.x

Grbić, R., Kurtagić, D., Slišković, D. (2013): Stream water temperature prediction based on Gaussian process regression. Expert Syst. Appl. 40, 7407–7414. https://doi.org/10.1016/j.eswa.2013.06.077

Hannah, D. M., Garner, G. (2015): A climate change report card for water Working Technical Paper.

Hannah, D. M., Webb, B. W., Nobilis, F. (2008): River and stream temperature: dynamics, processes, models and implications. Hydrol. Process. 22, 899–901. https://doi.org/10.1002/hyp.6997

Isaak, D. J., Wenger, S. J., Peterson, E. E., Ver Hoef, J. M., Nagel, D. E., Luce, C. H., Hostetler, S. W., Dunham, J. B., Roper, B. B., Wollrab, S. P., Chandler, G. L., Horan, D. L., Parkes-Payne, S. (2017): The NorWeST Summer Stream Temperature Model and Scenarios for the Western U.S.: A Crowd-Sourced Database and New Geospatial Tools Foster a User Community and Predict Broad Climate Warming of Rivers and Streams. Water Resour. Res. 53, 9181–9205. https://doi.org/10.1002/2017WR020969

Lešková, D., Skoda, P. (2003): Temperature series trends of Slovak rivers. Meteorological Journal 6, 13–17.

Mohseni, O., Stefan, H. G., Erickson, T. R. (1998): A nonlinear regression model for weekly stream temperatures. Water Resour. Res. 34, 2685–2692. https://doi.org/10.1029/98WR01877

Mohseni, Stefan, H. G. (1998): Stream temperature/air temperature relationship: A physical interpretation.

Morrill, J. C., Bales, R. C., Conklin, M. H. (2005): Estimating Stream Temperature from Air Temperature: Implications for Future Water Quality. J. Environ. Eng. 131, 139–146. https://doi.org/10.1061/(ASCE)0733-9372(2005)131:1(139)

Pekárová, P., Miklánek, P., Halmová, D., Onderka, M., Pekár, J., Kučárová, K., Liová, S., Škoda, P. (2011): Long-term trend and multi-annual variability of water temperature in the pristine Bela River basin (Slovakia). J. Hydrol. 400, 333–340. https://doi.org/10.1016/j.jhydrol.2011.01.048

Probst, E., Mauser, W. (2023): Climate Change Impacts on Water Resources in the Danube River Basin: A Hydrological Modelling Study Using EURO-CORDEX Climate Scenarios. Water 15, 8. https://doi.org/10.3390/w15010008

R Core Team (2022): R: A Language and Environment for Statistical Computing. R Foundation for Statistical Computing, Vienna, Austria.

Sleziak, P., Jančo, M., Danko, M. (2023): Dynamics of water temperature in a small mountain catchment. Acta Hydrol. Slovaca 24, 43–51. https://doi.org/10.31577/ahs-2023-0024.01.0006

van Vliet, M. T. H., Thorslund, J., Strokal, M., Hofstra, N., Flörke, M., Ehalt Macedo, H., Nkwasa, A., Tang, T., Kaushal, S. S., Kumar, R., van Griensven, A., Bouwman,

L., Mosley, L. M. (2023): Global river water quality under climate change and hydroclimatic extremes. Nat. Rev. Earth Environ. 1–16. https://doi.org/10.1038/s43017-023-00472-3

Varga, A., Velísková, Y. (2021): Assessment of time course of water and air temperature in the locality of the Turček reservoir during its operation in the period 2005–2019. Acta Hydrol. Slovaca 22, 304–312. https://doi.org/10.31577/ahs-2021-0022.02.0034

Varga, A., Velísková, Y., Sokáč, M., Sočuvka, V., Mikula, P. (2023): Analysis of seasonal changes of thermal stratification in reservoir for drinking water supply (Slovakia, Turček reservoir). Acta Hydrol. Slovaca 24, 33–42. https://doi.org/10.31577/ahs-2023-0024.01.0005

Webb, B. W., Hannah, D. M., Moore, R. D., Brown, L. E., Nobilis, F. (2008): Recent advances in stream and river temperature research. Hydrol. Process. 22, 902–918. https://doi.org/10.1002/hyp.6994

Ing. Zbyněk Bajtek, PhD (*corresponding author, e-mail: bajtek@uh.savba.sk)
RNDr. Pavla Pekárová, DrSc.
RNDr. Pavol Miklánek, CSc.
Institute of Hydrology SAS
Dúbravská cesta č. 9
841 04 Bratislava
Slovak Republic

Ing. Katarína Jeneiová, PhD.
Slovak Hydrometeorological Institute
Jeséniova 17
833 15 Bratislava
Slovak Republic

DOI: 10.31577/ahs-2023-0024.02.0023

ACTA HYDROLOGICA SLOVACA

Volume 24, No. 2, 2023, 205 – 213

Analyzing fire-induced water repellency and runoff in forest soil from beech forest: A controlled laboratory experiment

Peter ŠURDA*, Justína VITKOVÁ, Anton ZVALA, Ľubomír LICHNER

Forest fires are a common ecological disturbance affecting soil properties and hydrological processes. In this study, we investigated the impact of fire on surface runoff and soil water repellency (SWR) in beech forest through a laboratory experiment. Our main goals were to quantify the severity of SWR caused by low-intensity fires (simulated at 300°C in a muffle furnace) using contact angle measurements with an optical goniometer and to analyze the relationship between heat-induced alterations in SWR and subsequent surface runoff generated by a rainfall simulator in laboratory conditions. The secondary goal of this study was to propose an innovative laboratory approach as an alternative for fire experiments in real forest environments.

We collected six monoliths, each with a forest soil surface layer measuring 20 cm x 15 cm x 10 cm, from the Zvolen-Budča site. These monoliths were heated at 300°C for 20 minutes in a muffle furnace to simulate the impact of low-intensity wildfires. Subsequently, the burnt monoliths and the Control were exposed to artificial rain from a rainfall simulator, and surface runoff was measured.

The results showed a significant increase in surface runoff from the burnt monoliths compared to the Control, indicating the impact of fire-induced changes in soil structure and SWR. Additionally, contact angle measurements using an optical goniometer showed increased SWR in the burnt disturbed samples.

The findings of our study underscore the significance of the interplay between fire-induced alterations in SWR and surface runoff. They offer valuable insights into the post-fire hydrological responses and erosion risks in forest ecosystems. These insights could help develop effective strategies to mitigate the environmental impacts of forest fires.

KEY WORDS: forest fires, soil hydrophobicity, surface runoff, contact angle

Introduction

Forest wildfires have the potential to cause significant disruptions and changes to the ecosystem. Soil properties can experience short-term, long-term, or permanent fire-induced changes, depending chiefly on the type of property, severity and frequency of fires, and post-fire climatic conditions (Certini, 2005; Derafshi, 2022).

Many studies have suggested that surface runoff and overland flow increase with an increase in soil water repellency (SWR) (Keizer et al., 2005; Gomi et al., 2008; Miyata et al., 2010; Valeron and Meixner, 2010; Ferreira et al., 2016). A majority of these studies focused on the impact of forest fires. Fires induce SWR due to the combustion of organic matter, producing waxy substances that coat soil particles (DeBano, 2000). The type and density of forest vegetation, organic carbon content, and soil properties play crucial roles in altering SWR (Arcenegui et al., 2007; Mataix-Solera et al., 2008; Negri et al., 2021). Notably, high temperatures, between 175 and 270°C, increase the formation of organic carbon coatings responsible for SWR, while temperatures between 270°C and 400°C destroy hydrophobic substances, suppressing SWR (Dekker et al., 1998; Doerr et al., 2004; Varela et al., 2005; Wu et al., 2020). The intensity of the fire and soil characteristics, such as moisture and particle-size distribution, primarily influences the depth of the water-repellent (WR) front in the soil. However, regardless of the severity of the fire and soil features, the depth of the WR front rarely exceeds 6-8 cm (Huffman et al. 2001).

Fires can decrease soil infiltration capacity relative to unburned areas (DeBano, 2000; Doerr and Moody, 2004; Shakesby and Doerr, 2006; Larsen et al., 2009; Ebel and Moody, 2017; Zvala, 2022; Hološ, 2023). The study by Robichaud (2000) found that the hydraulic conductivity of soil under *Pseudotsuga menziesii* and *Pinus contorta* was reduced by 40% after a fire. Similarly, Everett et al. (1995) found that water drop penetration time to soil increased significantly from instantaneous to over 270 seconds following slash burning in a mixed forest dominated by *P. contorta*.

The combination of wildfire-induced changes to soil and vegetation often results in increased runoff and erosion,

driven in many cases by infiltration-excess overland flow (Benavides-Solorio and MacDonald, 2001; Moody and Ebel, 2014). Runoff behaves in a threshold manner, meaning that a certain amount of rainfall is needed to initiate it. When the rainfall rate becomes greater than the infiltration rate, excess water accumulates on the soil surface in depressions, forming puddles. Runoff begins once the surface storage is fully occupied and the puddles overflow (Horton, 1933). The rate of runoff depends on various factors, including soil surface conditions such as micro-topography, depressions, stone cover, water repellency, and surface hydraulic conditions.

When trying to simulate natural fires, soil samples are often heated in laboratory muffle furnaces. However, using a muffle furnace can result in significant differences from natural fires since the samples are heated from all sides instead of just the soil surface (Brucker et al., 2022). A muffle furnace experiment conducted by Martínez et al. (2022) confirmed that the hydraulic conductivity (both saturated and unsaturated) of sandy loam soil increased with temperature while the organic matter content of the soil decreased. Negri et al., 2021 found that SWR was maximized at 200°C during the muffle furnace heating experiment and dramatically lost above this temperature in loamy sand from beech forest, regardless of the SWR displayed by samples at lower temperatures.

Rainfall events that cause runoff are challenging to study due to their unpredictable nature. In order to recreate scenarios under semi-controlled conditions, rainfall simulators are often used, as they are considered to be reliable (Zhang et al., 1997). However, these studies have limitations such as their small scale, the differences between simulated and natural rainfall (Lascelles et al., 2000), and high experimental costs. In a review of rainfall simulation techniques, many authors highlighted these issues associated with different approaches and concluded that there is no ideal rainfall simulator.

Understanding the dynamics of SWR induced by fires in forest ecosystems is crucial for assessing the environmental impact of forest fires. As vital components of terrestrial ecosystems, forests are vulnerable to wildfires that can significantly alter their hydrological processes. Fire-induced SWR can lead to increased surface runoff, erosion, and altered nutrient cycling. These changes have far-reaching implications, including potential threats to water quality, ecosystem health, and human settlements downstream. Conducting experiments to study fire-induced SWR in natural forest settings is challenging due to the unpredictable nature of wildfires and safety concerns. Therefore, developing innovative laboratory approaches is essential. Controlled laboratory experiments offer a safe environment to simulate fire-induced SWR accurately. These laboratory approaches allow for precise control of variables, enabling systematic investigations into the effects of different fire intensities, soil types, and vegetation cover. Moreover, they facilitate the development of predictive models to assess the potential impact of forest fires on hydrological processes under various scenarios. Through these experiments, scientists can identify effective mitigation strategies, enhance ecosystem resilience, and inform land management practices to minimize the adverse consequences of fire-induced SWR and increased runoff.

The main goals of our research were: 1. to quantify the severity of SWR induced by the low-intensity fires, simulated at 300°C in a muffle furnace, utilizing contact angle measurements with an optical goniometer; 2. to analyze the relationship between heat-induced alterations in SWR and subsequent surface runoff, generated by rainfall simulator in laboratory condition. The secondary goal of this study was to develop a novel laboratory approach specifically designed to address the challenges associated with conducting fire experiments in real forest environments. Recognizing the limitations of conducting field experiments due to safety concerns and uncontrollable variables, our aim was to create a replicable and controlled laboratory methodology.

We hypothesized a significant increase in SWR in the soil samples subjected to heating compared to the control group, indicating the presence of hydrophobic substances due to heat exposure. Furthermore, we anticipate that there will be a direct and positive correlation between the heat-induced alterations in SWR and the subsequent increase in surface runoff.

Material and methods

Study site

Soil samples (monoliths) were taken from the study site at Budča village, 6 km southwest of the district town of Zvolen, on the right bank of the Hron River, where the Kremnica Mountains meet the Štiavnica Mountains. The study site (48° 34' 55.2468" N, 19° 3' 15.5592" E; 410 m a. s. l.) is an eastern slope logging site, representing the habitat of the transition from beech to oak-hornbeam forest, covered mainly with scattered European Beech, Common Nettle, Bushgrass and Bugleweed (Fig. 1).

The region has a mildly warm climate. Average annual air temperature ranges from -6.5°C in January to 20.5°C in July, depending on altitude. Average annual rainfall ranges from 530 to 600 mm. The geological bedrock consists of heterogeneous volcanic products, andesite agglomerates and tuffs (Bačíková, 2015). The soils of the site are classified as Cambisols and have a silt loam texture (WRB, 2015). The basic physical and chemical characteristics of the disturbed soil samples are presented in Table 1.

The study site was chosen due to its significant slope, with an average of 14 degrees, which increases the likelihood of induced runoff after disturbances such as wildfires. The site is located in a logging area, making it more susceptible to wildfires. Furthermore, the site has a diverse habitat ranging from beech to oak-hornbeam forest, which allows for an examination of the variability in soil responses across different plant species. The presence of residues on the forest floor acts as potential fuel during wildfires, aggravating the impact of fire on the soil. Additionally, the site has experienced previous runoff events, indicating a history of water movement that has likely altered soil properties.

Table 1. Characteristics of the topsoil horizon (0–10 cm) of the study site near Budča (Cox = organic carbon content; CA= contact angle). The results are presented as arithmetic mean and standard deviation (SD)

	Sand [%]	Silt [%]	Clay [%]	Cox [%]	Humus [%]	CA [°]
	mean (SD)	mean (SD)	mean (SD)	mean (SD)	mean (SD)	mean (SD)
Zvolen-Budča	20.72 (1.54)	67.11 (1.08)	12.17 (0.46)	2.10 (0.19)	3.62 (0.33)	16.41 (2.40)

Fig. 1. Study site in September 2023: a) vegetation cover; b) detail of forest floor biomass.

Soil sampling and heating experiment

Soil sampling was conducted in September 2023. We carefully extracted six soil monoliths with forest floor biomass at the study site, measuring 20 cm x 15 cm x 10 cm, using a spade and shovels to disturb the soil structure as little as possible. We placed the soil monoliths in crates and secured them against displacement. In the laboratory, we left the monoliths air-dried in the crates for seven days.

After reaching equilibrium, the monoliths were placed in aluminium containers and weighed. Half of the monoliths were heated in a muffle furnace (LAC, s.r.o., Židlochovice, Czech Republic; Type: LE 15/11) (Fig. 2) at a temperature of 300°C for 20 min. After a given time, we pulled the samples out of the furnace and allowed them to cool to room temperature.

Measurement of soil water repellency

The severity of SWR was estimated by the sessile drop method. This involved placing a water drop on the soil sample's surface and analyzing the static contact angle (CA) by reviewing image recordings taken with the optical goniometer OCA 11 (DataPhysics Instruments GmbH, Filderstadt, Germany). The procedure described by Bachmann et al. (2000) was used to prepare the samples, which involved covering a glass slide with double-sided adhesive tape and pressing soil particles onto the tape for several seconds. The slide was shaken carefully to remove any unglued soil particles, and then a 5 µL drop of deionized water was placed on the sample surface using a 0.91 mm syringe needle. After 1 s when mechanical disruption of the surface was complete after drop placement, CA was evaluated by analyzing the shape of the drop (ellipsoid approximation) and fitting tangents on both sides of the drop using dpiMAX version 1.51.90.75 software (DataPhysics Instruments GmbH, Filderstadt, Germany) according to Goebel et al. (2013). CA of each drop was determined as an arithmetic mean of the CA values on the left and right sides of the drop. The following classes of the severity of SWR can be distinguished: non-water-repellent soil (wettable) ($CA < 40°$), slightly ($40° \leq CA < 90°$), moderately ($90° \leq CA < 110°$), strongly and very strongly ($110° \leq CA < 130°$), and extremely ($CA \geq 130°$)

water repellent soil (Papierowska et al., 2018). CA was estimated with five repetitions for each monolith.

Laboratory runoff experiment

Surface runoff measurements were made using a portable rainfall simulator (Royal Eijkelkamp, Giesbeek, Netherlands) placed on a structure designed for this measurement with an inclined monolith and a space in front for catching runoff (Fig. 2). The runoff area of the rainfall simulator was limited to the surface of prepared monoliths (191 cm^2), and runoff water was captured at the lowest point. The sprinkler unit of the simulator is equipped with 49 glass capillary tubes, each 0.6 mm in diameter and 10 mm in length–only 15 of the capillary tubes were intended to produce simulated rain over the defined runoff area. The soil monoliths were prepared to match the intended area on which the 15 capillaries were designed to drip. This step involved the careful trimming of each monolith using a trimmer to gently remove excess material from the edges of the monoliths. Distilled water was used to simulate rain, with drops weighing 0.106 g falling from an average height of 0.4 m onto the soil monolith surface. Rainfall simulations were conducted on three burned and three unburned monoliths. After the installation of the monoliths, the slope of the drainage area was measured with a digital spirit level (Robert Bosch GmbH, Gerlingen, Germany; Type: GLM50C). A total of 6 rainfall simulations (one simulation on each monolith), with a duration of 4 minutes, were performed. Rainfall intensity, set by the height of the aeration tube (8 cm), varied between 4.28 mm min^{-1} and 4.48 mm min^{-1} (Table 2), with an average value of 4.4 mm min^{-1}.

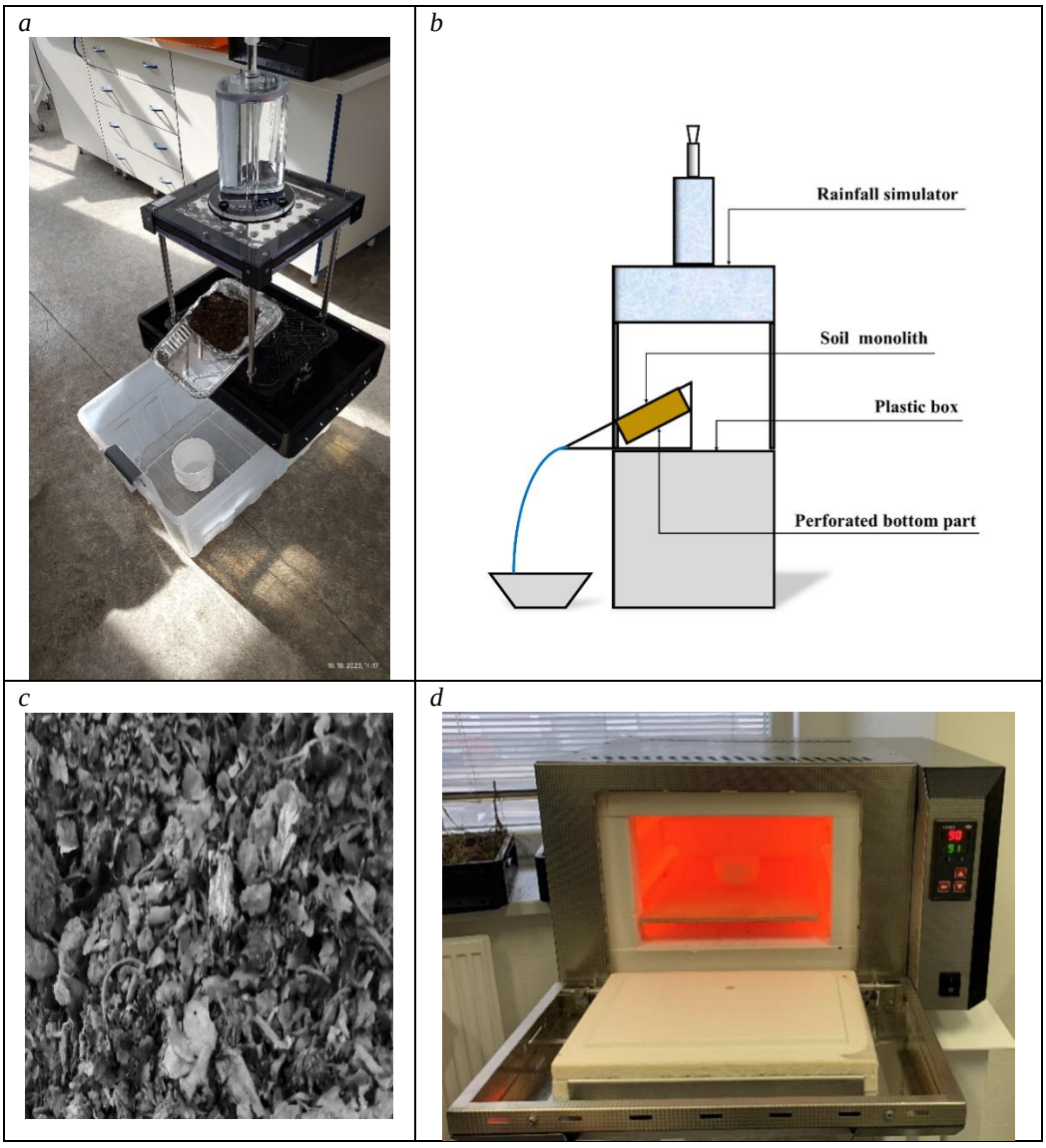

Fig. 2. A laboratory design of rainfall simulator with an inclined monolith: (a) photo and (b) simplified sketch. The burned surface of the monolith (c) and heated muffle furnace (d).

Table 2. Rainfall simulation parameters for the experiment (rainfall intensity i_r, total rainfall, H_r) and volumetric moisture content w prior to the experiments and the slope of the runoff plots.

Parameter	Minimum	Maximum	Mean	SD
i_r [mm min^{-1}]	4.28	4.48	4.4	0.09
H_r [mm]	17.12	17.92	17.6	0.35
w [% vol.]	1.3	3.4	2.2	0.51
slope [°]	15.9	19	17.3	1.28

The statistical analysis of rainfall simulation parameters, slope, and soil moisture content showed no significant differences between the burned and unburned monoliths. This uniformity indicates that the experimental conditions were consistent. It is important to note that any differences in measured runoff can be attributed to changes that occurred specifically after the heating process.

Surface runoff from the prepared monoliths was assessed using the surface runoff coefficient (C_r), defined as the proportion of simulated rainfall that is transformed to direct surface runoff (Miyata et al., 2007), and the surface runoff generation time (T_r), defined as the time for the first drop of generated runoff to flow into the prepared container.

Statistical analysis

Comparisons between the burned and unburned treatments (Control) have been performed by t-test. A t-test is a statistical test used to compare the means of two groups. It was used in hypothesis testing to determine whether any treatment has an effect on the population of Control. The null hypothesis (H0) is that the true difference between the Control and burned treatment group means is zero. The alternate hypothesis (Ha) is that the true difference differs from zero. The statistical significance of the analysis was defined at $P < 0.05$. All statistical analyses were performed using the NCSS statistical software (NCSS 12 Statistical Software, 2018).

Results and discussion

The results of our laboratory experiment showed that evident changes occurred in various parameters after heating monoliths from the deciduous forest. Before heating, the contact angle (CA) ranged from a minimum of 14.74° to a maximum of 19.85°, with an average of 16.41°. After heating, the contact angle substantially increased, ranging from 61.84° to 89.91°, with an average of 79.26°. This increase, on average by 62.85°, signifies a remarkable enhancement in soil water repellency following the heating process, confirmed by a significant increase in CA values after heating (Fig. 3a). In our previous studies (Šurda et al., 2023; Hološ et al., 2022), we observed the increase in CA in sandy soil with the heating temperature in an interval from 50°C to 300°C. Also, Samburova et al. (2021) found that sand samples treated with fire emissions showed increased contact angle (CA) between 78° and 87°, while the untreated sand samples showed CA = 48°. Negri et al. (2021) found that with growing temperatures, the Alpine soil samples displayed extremely different wettable behaviour, with or without fire-induced SWR build-up. This happened mainly concerning the content and composition of soil organic material. Carrà et al. (2021) found a moderate SWR in loamy sand soil in chestnut forests and a strong SWR in both pine and oak forests after prescribed fire.

Similarly, the surface runoff coefficient (C_r) displayed notable variations. Before heating, the coefficient ranged from 0.40 to 0.49, with an average of 0.45. Post-heating, the coefficient increased significantly, ranging from 0.57 to 0.73, with an average of 0.63. The increase, on average by 0.18, indicates a higher tendency for surface runoff generation after the heating process, proved by a significant increase in C_r values after heating (Fig. 3b). Previous research proved a strong correlation between fire-induced SWR and increased runoff in various soils. Leighton-Boyce et al. (2007) found that runoff caused by SWR in Eucalyptus plantations with loamy sand and sandy soils increased 16 times. Müller et al. (2018) proved that SWR governed runoff in sandy loam Andosol. Carrà et al. (2021) observed increased runoff in the window of disturbance after fire in loamy sand from oak, chestnut and pine forests. González-Pelayo et al. (2010) observed that surface runoff values in shrubland areas with sandy loam soil treated with low-intensity prescribed fire were 22-fold the values measured in untreated sites. Morales et al. (2000) found an 18-fold increase in runoff one year after the fire in the litosols and rendzins with sandy texture at altitudes above 2500 m a.s.l.

Surface runoff generation time (T_r) also exhibited distinct changes. Before heating, the time ranged from 47 seconds to 52 seconds, with an average of 49.3 seconds. After heating, the range decreased from 25 seconds to 26 seconds, with an average of 25.7 seconds. This reduction, averaging 23.6 seconds, signifies a faster initiation of runoff after the soil is heated, confirmed by a significant decrease in T_r values after heating (Fig. 4a). Müller et al. (2018) observed that the short lag time for runoff initiation, in accordance with the increase in runoff, indicated infiltration excess as the process which is generating runoff.

Furthermore, surface runoff total (H_r) demonstrated significant alterations. Before heating, the total runoff ranged from 5.69 mm to 8.36 mm, averaging 7.02 mm. After heating, the range increased from 10.02 mm to 13.01 mm, averaging 11.28 mm. The change, averaging 4.26 mm, highlights a substantial increase in runoff volume following the heating process, demonstrating

a significant increase in Hr values after heating (Fig. 4b). When analyzing the results, we further focused on exploring the relationship between C_r (surface runoff coefficient) and CA (static contact angle) based on a dataset consisting of six observations. Our analysis revealed a robust correlation between these two parameters, with a correlation coefficient of 0.92; we derived a regression equation to represent this relationship quantitatively: C_r = 0.3977 + 0.0031 CA (Fig. 5a). Furthermore, we found a significant R^2 value of 0.8464, which demonstrates that approximately 84.64% of the variation in the surface runoff coefficient (C_r) can be attributed to variations in static contact angle. (CA). This indicates a strong relationship between these two

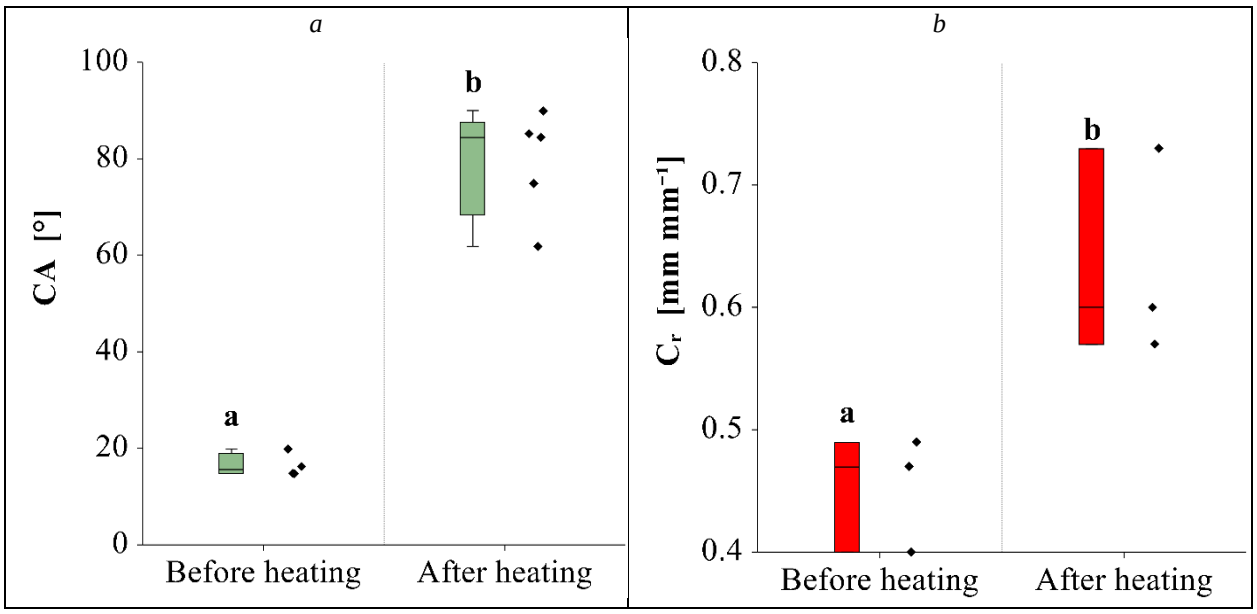

Fig. 3. The measured values of (a) static contact angle (CA) and (b) surface runoff coefficient (C_r). The plot displays individual measurements as points. The whiskers extend to a distance of 1.5 times the interquartile range from the edges of the box. Box plots represented by different letters are significantly different at a 0.05 significance level.

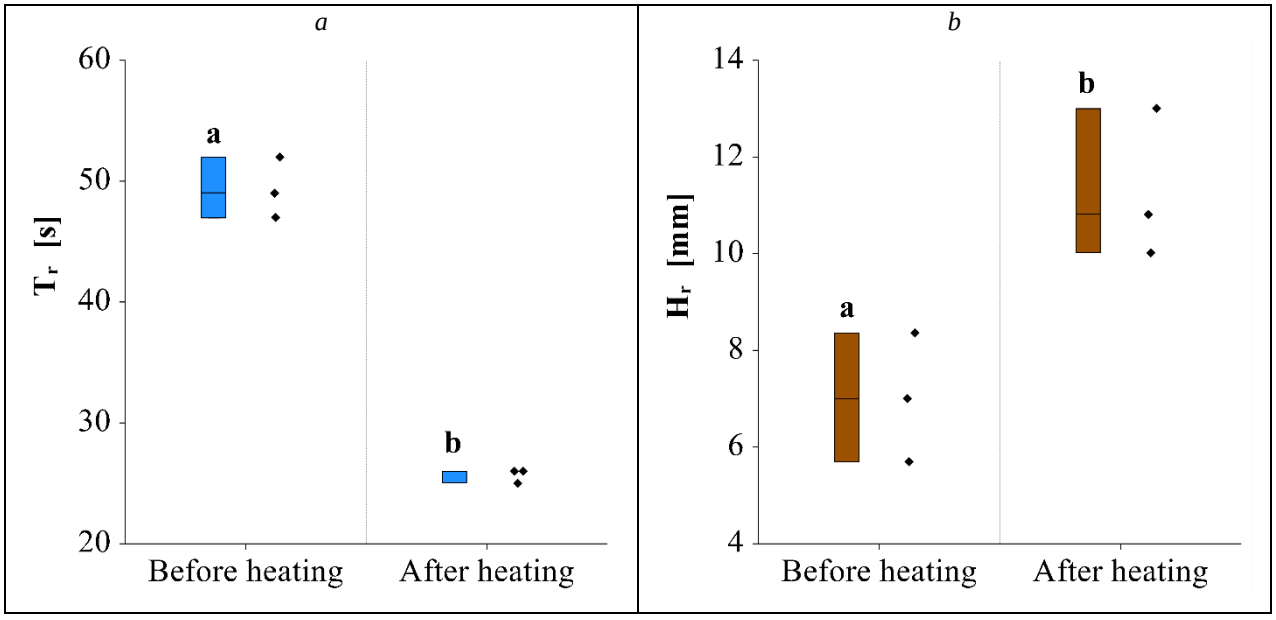

Fig. 4. The measured values of (a) surface runoff generation time (T_r) and (b) surface runoff total (H_r). The plot displays individual measurements as points. The whiskers extend to a distance of 1.5 times the interquartile range from the edges of the box. Box plots represented by different letters are significantly different at a 0.05 significance level.

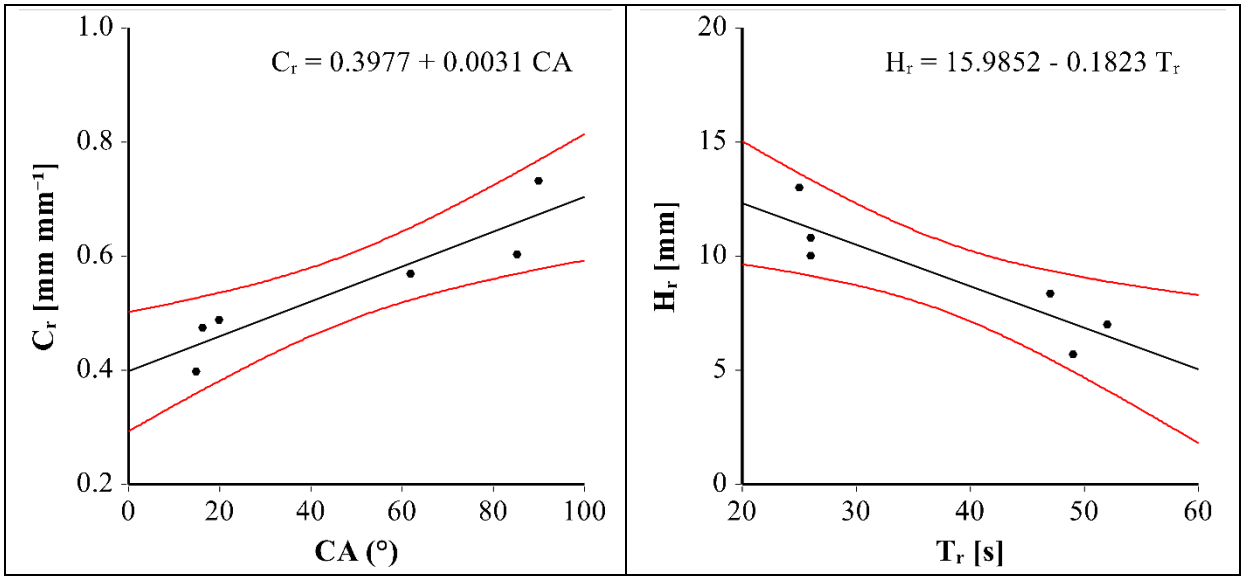

Fig. 5. The derived regression lines and equations of (a) the relationship between surface runoff coefficient (C_r) and static contact angle (CA) and (b) the relationship between simulated precipitation total (H_r) and surface runoff generation time (T_r). The black line displays the regression line, and the red lines represent the confidence limits (the upper and lower boundaries of a confidence interval of the mean at a specific value of X).

variables. The relationship between H_r (simulated precipitation total) and T_r (surface runoff generation time) was investigated using a dataset consisting of 6 observations. The regression equation representing this relationship was derived as follows: H_r = 15.9852 - 0.1823 T_r (Fig. 5b). The R^2 value, which measures the proportion of the variation in Hr explained by variations in T_r, was 0.7983. Our analysis further revealed a strong correlation between H_r and T_r, with a correlation coefficient of -0.89. This negative correlation suggests a robust inverse relationship.

Conclusion

Our study investigated the effects of heat-induced soil water repellency (SWR) on surface runoff through controlled laboratory experiments. We confirmed the hypothesis predicting increased SWR and subsequent surface runoff after heating. Significant changes were observed following soil heating at 300°C. These included a substantial increase in SWR, as indicated by higher contact angle (CA) values; a notable rise in the surface runoff coefficient (C_r), demonstrating a higher tendency for runoff generation; a faster initiation of runoff, as evidenced by reduced surface runoff generation time (T_r); and a considerable increase in total runoff volume (H_r). Moreover, our analysis revealed strong correlations between variables. The relationship between C_r and CA was robust (correlation coefficient = 0.92), leading to the derivation of a regression equation (C_r = 0.3977 + 0.0031 CA). Similarly, the inverse relationship between H_r and T_r was well-established (correlation coefficient = -0.89), represented by the regression equation (H_r = 15.9852 - 0.1823 T_r).

The proposed methodology offers an effective alternative to field experiments by simulating fire-induced SWR and subsequent runoff under controlled conditions. This approach overcomes the limitations of safety concerns and uncontrollable variables associated with working in natural forest environments. Using this method, we can increase the safety and replicability of experiments.

In summary, our findings highlight the impact of heat-induced SWR on surface runoff patterns. These results provide valuable insights for hydrological modelling and environmental management. It emphasizes the importance of considering SWR effects in predicting post-fire runoff processes.

Acknowledgement

This work was supported by Scientific Grant Agency No. VEGA 2/0150/20 and EIG CONCERT-Japan No. EIG JC2019-074.

References

Arcenegui, V., Mataix-Solera, J., Guerrero, C., Zornoza, R., Mayoral, A.M., Morales, J. (2007): Factors Controlling the Water Repellency Induced by Fire in Calcareous Mediterranean Forest Soils. European Journal of Soil Science, vol. 58, 1254–1259.

Bachmann, J., Horton, R., van der Ploeg, R. R., Woche, S. (2000): Modified sessile drop method for assessing initial soil-water contact angle of sandy soil. Soil Sci. Soc. Am. J., 64, 564–567.

Bačíková, Z. (2015): Život v Budči. Obec Budča, 1st ed., 23–35.

Benavides-Solorio, J., MacDonald, L. H. (2001): Post-fire runoff and erosion from simulated rainfall on small plots, Colorado Front Range. Hydrological Processes, 15(15), 2931–2952. https://doi.org/10.1002/hyp.383

Brucker, C. P., Livneh, B., Minear, J. T., Rosario-Ortiz, F. L. (2022): A review of simulation experiment techniques used to analyze wildfire effects on water quality and supply. Environ. Sci. Process. Impacts, 24, 1110; https://doi.org/10.1039/D2EM00045H.

Carrà, B. G., Bombino, G., Denisi, P., Plaza-Àlvarez, P. A., Lucas-Borja, M. E., Zema, D. A. (2021): Water Infiltration after Prescribed Fire and Soil Mulching with Fern in Mediterranean Forests. Hydrology, 8, 95.

Certini, G. (2005): Effects of Fire on Properties of Forest Soils: A Review. Ecologia, vol. 143, no. 1, 1–10.

DeBano, L. F. (2000): The role of fire and soil heating on water repellency in wildland environments: A review. Journal of Hydrology, 231–232, 195–206. https://doi.org/10.1016/S0022-1694(00)00194-3

Derafshi, M., Matin, N., Hassani, A. (2022): A short review on polycyclic aromatic hydrocarbon contamination. Acta Horticulturae et Regiotecturae, vol. 25, no. 2, 174–180. https://doi.org/10.2478/ahr-2022-0021

Dekker, L. W., Ritsema, C. J., Oostindie, K., Boersma, O. H. (1998): Effect of Drying Temperature on the Severity of Soil Water Repellency. Soil Science, vol. 163, no. 10, 780–796.

Doerr, S. H., Blake, W. H., Shakesby, R. A., Stagnitti, F., Vuurens, S. H., Humphreys, G. S., Wallbrink, P. (2004): Heating Effects on Water Repellency in Australian Eucalypt Forest Soils and their Value in Estimating Wildfire Soil Temperatures. International Journal of Wildland Fire, vol. 13, no. 2, 157–163.

Doerr, S. H., Moody, J. A. (2004): Hydrological effects of soil water repellency: On spatial and temporal uncertainties. Hydrological Processes, 18(4), 829–832. https://doi.org/10.1002/hyp.5518

Ebel, B. A., Moody, J. A. (2017): Synthesis of soil-hydraulic properties and infiltration timescales in wildfire-affected soils. Hydrological Processes, 31(2), 324–340. https://doi.org/10.1002/hyp.10998

Everett, R. L., Java-Sharpe, B. J., Scherer, G. R., Wilt, F. M., Ottmar, R. D. (1995): Co-occurrence of hydrophobicity and allelopathy in sand pits under burned slash. Soil Sci Soc Am J, 59:1176–1183

Ferreira, R. V., Serpa, D., Cerqueira, M. A., Keizer, J. J. (2016): Short-time phosphorus losses by overland flow in burnt pine and eucalypt plantations in north-central Portugal: a study at micro-plot scale. Sci. Total Environ. 551, 631–639.

Goebel, M. O., Woche, S. K., Abraham, P. M., Schaumann, G. E., Bachmann, J. (2013): Water repellency enhances the deposition of negatively charged hydrophilic colloids in a water-saturated sand matrix. Colloids Surf. A Physicochem. Eng. Asp., 431, 150–160.

Gomi, T., Sidle, R. C., Ueno, M., Miyata, S., Kosugi, K. I. (2008): Characteristics of overland flow generation on steep forested hillslopes of central Japan. J. Hydrol. 361 (3–4), 275–290.

González-Pelayo, O., Andreu, V., Gimeno-García, E., Campo, J., Rubio, J. L. (2010): Rainfall influence on plot-scale runoff and soil loss from repeated burning in a Mediterranean-shrub ecosystem, Valencia, Spain. Geomorphology, 118, 3–4, 444–452.

Hološ, S., Šurda, P., Lichner, Ľ., Zvala, A., Píš, V. (2022): Fire-induced changes in soil properties depend on age and type of forests. Journal of Hydrology and Hydromechanics, 70, 4, 442–449. https://doi.org/10.2478/johh-2022-0034

Hološ, S., Zvala, A., Šurda, P., Lichner, Ľ. (2023): Fire induced water repellency in the forest soil covered with different types of forest floor biomass. Acta Hydrologica Slovaca, 24, 1, 151–158. https://doi.org/10.31577/ahs-2023-0024.01.0017

Horton, H. E. (1933): The role of infiltration in the hydrologic cycle. Trans. Am. Geophys. Union 14, 446–460.

Huffman, E. L., MacDonald, L. H., Stednick, J. D. (2001): Strength and persistence of fire-induced soil hydrophobicity under ponderosa and lodgepole pine, Colorado Front Range. Hydrol Process, 15:2877–2892

Keizer, J. J., Coelho, C. O. A., Shakesby, R. A., Domingues, C. S. P., Malvar, M. C., Perez, I. M. B., Matias, M. J. S., Ferreira, A. J. D. (2005): The role of soil water repellency in overland flow generation in pine and eucalypt forest stands in coastal Portugal. Aust. J. Soil Res. 43 (3), 337–349.

Lascelles, B., Favis-Mortlock, D. T., Parsons, A. J., Guerra, A. J. T. (2000): Spatial and temporal variation in two rainfall simulators: implications for spatially explicit rainfall simulation experiments. Earth Surf. Process. Landf. 25, 709–721.

Larsen, I. J., MacDonald, L. H., Brown, E., Rough, D., Welsh, M. J., Pietraszek, J. H., Libohova, Z., de Dios Benavides-Solorio, J., Schaffrath, K. (2009): Causes of post-fire runoff and erosion: Water repellency, cover, or soil sealing? Soil Science Society of America Journal, 73, 4, 1393–1407. https://doi.org/10.2136/sssaj2007.0432

Leighton-Boyce, G., Doerr, S. H., Shakesby, R. A., Walsh, R. P. D. (2007): Quantifying the impact of soil water repellency on overland flow generation and erosion: a new approach using rainfall simulation and wetting agent on in situ soil. Hydrol. Process. 21, 2337–2345.

Martínez, S. I., Contreras, C. P., Acevedo, S. E., Bonilla, C. A. (2022): Unveiling soil temperature reached during a wildfire event using ex-post chemical and hydraulic soil analysis. Sci. Total Environ., 822, 153654; https://doi.org/10.1016/j.scitotenv.2022.153654.

Mataix-Solera, J., Arcenegui, V., Guerrero, C., Jordán, M. M., Dlapa, P., Tessler, N., Wittenberg, L. (2008): Can Terra Rossa Become Water Repellent by Burning? A Laboratory Approach. Geoderma, vol. 147, 178–184

Miyata, S., Kosugi, K., Gomi, T., Onda, Y., Mizuyama, T. (2007): Surface runoff as affected by soil water repellency in a japanese cypress forest. Hydrol. Process. 21, 2365–2376. https://doi.org/10.1002/hyp.6749

Miyata, S., Kosugi, K., Nishi, Y., Gomi, T., Sidle, R. C., Mizuyama, T. (2010): Spatial pattern of infiltration rate and its effect on hydrological processes in a small headwater catchment. Hydrol. Process. 24, 535–549.

Moody, J. A., Ebel, B. A. (2014): Infiltration and runoff generation processes in fire-affected soils. Hydrological Processes, 28(9), 3432–3453. https://doi.org/10.1002/hyp.9857

Morales, H. A., Návar, J., Domınguez, P. A. (2000): The effect of prescribed burning on surface runoff in a pine forest stand of Chihuahua, Mexico. Forest Ecology and Management, 137, 1–3, 199–207. https://doi.org/10.1016/S0378-1127(99)00328-X

Müller, K., Mason, K., Strozzi, A.G., Simpson, R., Komatsu, T., Kawamoto, K., Clothier, B. (2018): Runoff and nutrient lossfrom a water-repellent soil. Geoderma, 322, 28–37.

Negri, S., Stanchi, S., Celi, L., Bonifacio, E. (2021): Simulating Wildfires with Lab-heating Experiments: Drivers and Mechanisms of Water Repellency in Alpine Soils. Geoderma, vol. 402, 115357.

NCSS 12 Statistical Software. Statistical Software; N.C.S.S., L.L.C.: Kaysville, UT, USA, 2018. Available online: https://www.ncss.com/software/ncss/

Papierowska, E., Matysiak, W., Szatyłowicz, J., Debaene, G., Urbanek, E., Kalisz, B., Łachacz, A. (2018): Compatibility of methods used for soil water repellency determination for organic and organo-mineral soils. Geoderma, 314, 221–231.

Robichaud, P. R. (2000): Fire effects on infiltration rates after prescribed fire in Northern Rocky Mountain forests, USA. J Hydrol, 231:220–229

Samburova, V., Shillito, R. M., Berli, M., Khlystov, A. Y., Moosmüller, H. (2021): Effect of biomass-burning emissions on soil water repellency: A pilot laboratory study. Fire, 4, 24.

Shakesby, R. A., Doerr, S. H. (2006): Wildfire as a hydrological and geomorphological agent. Earth-Science Reviews, 74(3–4), 269–307. https://doi.org/ 10.1016/j.earscirev.2005.10.006

Šurda, P., Lichner, Ľ., Iovino, M., Hološ, S., Zvala, A. (2023): The Effect of Heating on Properties of Sandy Soils. Land, 12, 1752. https://doi.org/10.3390/land12091752

Valeron, B., Meixner, T. (2010): Overland flow generation in chaparral ecosystems: temporal and spatial variability. Hydrol. Process. 24, 65–75.

Varela, M. E., Benito, E., de Blas, E. (2005): Impact of Wildfires on Surface Water Repellency in Soils of Northwest Spain, Hydrological Processes, vol. 19, no. 18, 3649–3657.

WRB, (2015): World Reference Base for Soil Resources 2014. Update 2015. World Soil Resources Reports No. 106; FAO: Rome, Italy, 2015; 192p.

Wu, Y., Zhang, N., Slater, G., Waddington, J. M., de Lannoy, Ch.-F. (2020): Hydrophobicity of Peat Soils: Characterization of Organic Compound Changes Associated with Heat-induced Water Repellency. Science of The Total Environment, vol. 714, 136444.

Zhang, X. C., Norton, L. D., Hickman, M. (1997): Rain pattern and soil moisture content effects on atrazine and metolachlor losses in runoff. J. Environ. Qual. 26, 1539–1547.

Zvala, A., Šurda, P., Hološ, S. (2022): The effect of different fire temperatures on the water repellency parameters of forest sandy soil under different types of vegetation. Acta Hydrologica Slovaca, 23, 1, 140–146. https://doi.org/10.31577/ahs-2022-0023.01.0015

Ing. Peter Šurda, PhD. (*corresponding author, e-mail: surda@uh.savba.sk)
Ing. Justína Vitková, PhD.
Ing. Ľubomír Lichner, DrSc.
Mgr. Anton Zvala, PhD.
Institute of Hydrology SAS
Dúbravská cesta 9
84104 Bratislava
Slovak Republic

DOI: 10.31577/ahs-2023-0024.02.0024

ACTA HYDROLOGICA SLOVACA

Volume 24, No. 2, 2023, 214 – 220

A CNN Bidirectional LSTM framework for predicting monsoon rainfall in India

Rajaprasad SVS*, Rambabu MUKKAMALA

Rainfall prediction has evolved as a paramount research significance in recent times due to its complexities and ongoing demand such as water resource planning and management. Agriculture is a major source of employment in India, as well as a substantial contributor to gross domestic product, and crop output is dependent on the monsoon season. Rainfall prediction is useful to authorities for water storage and timely release to increase crop productivity. The current study proposes a Deep Neural Network (DNN) based hybrid model using a combination of convolutional neural network bi-directional long short-term memory (CNN BiLSTM) to predict monthly rain fall during monsoon seasons. The DNN models were used to analyze the average monthly rainfall data collected across the country from 1871 to 2019 during the monsoon seasons. Furthermore, the hybrid model's results were compared to the Bidirectional LSTM (BiLSTM) architecture. In predicting rainfall in India, the proposed hybrid model framework has been found to be more accurate than the BiLSTM. The findings of the study suggest that a DNN frame work can be successfully adopted for time series analysis in water resource management and related domains to reduce the associated risks.

KEY WORDS: rainfall, prediction, DNN, CNN-BiLSTM, monsoon

Introduction

Rainfall prediction is crucial in Indian civilization, and it plays a significant part in human life. Rainfall water management boosts productivity in agriculture in developing countries, especially India. Rainfall prediction is critical because fluctuations in rainfall can have severe consequences, such as crop and property damage; hence, a better prediction tool is useful for early warning, which can reduce risks. Rainfall prediction is a complex situation due to unreliable climate parameters. Accurate rainfall prediction is vital for countries like India, whose economy is primarily based on agriculture. The parameters that have a direct impact on the amount of rainfall include temperature, relative humidity, pressure, and evaporation (Liyew and Melese, 2021). Rainfall prediction has recently received the greatest scholarly significance due to its complex and continual application in flood prediction. As a way to minimize damage, studies have explored and suggested rainfall prediction approaches in order to prepare for any type of situation (Barrera-Animas et al., 2022). As a result, several techniques for predicting rainfall have evolved in order to ensure efficient and precise results.

To predict rainfall, statistical approaches such as basic regression analysis, exponential smoothing, and autoregressive integrated moving average (ARIMA) are often used. Because environmental information is non-linear; multiple research studies indicate that these methods are still ineffective for predicting rainfall, but a few studies using these methods have proven to be effective (Shrivastava et al., 2012; Farajzadeh et al., 2014). In the past studies have been carried out employing empirical approaches to predict rainfall; however, the complexity of rainfall, such as its non-linearity, makes it difficult to predict (Wu and Chau, 2013). However, the statistical models used involve substantial computational capacity and can be time-consuming with few outcomes. As a result, the researchers' emphasis is focused on applying artificial neural networks for accurately predicting rainfall. The spatial and temporal heterogeneity of rainfalls influences prediction results, and recurrent Neural Networks (RNNs) are the best tool for addressing these issues (Hossain et al., 2020). Conversely, a drawback of the RNN framework is its limited capacity to understand in predicting the long-term time series data. To address this issue, a long short-term memory (LSTM) network came into existence, consisting of memory cells that govern the transfer of information between the different cells (Greff et al., 2016). When supervised machine learning (ML) approaches are integrated with fuzzy logic, the results outperform conventional approaches in rainfall prediction (Rahman et al., 2022). LSTM framework implementation is a relatively technically advanced process, it is a proven for accurate prediction of rainfall (Billah et al., 2022). Although empirical models can predict rainfall, ANN models outperformed

due to their computing capability and precision.
Based on the significance of LSTM architecture in rainfall prediction, the paper proposes two LSTM-based architectures; Bidirectional LSTM and CNN Bidirectional LSTM, which have been used to predict monthly rainfall during the monsoon seasons across India. To assess the performance of the DNN algorithms, the evaluation indicators mean absolute error (MAE), mean absolute percentage error (MAPE), root-mean-squared error (RMSE), and R square (R^2) have been adopted (Zhang et al., 2015). The study used all India monthly rainfall time series data relating to pre, post and monsoon periods from 1871 to 2019, and the model parameters are evaluated and compared.

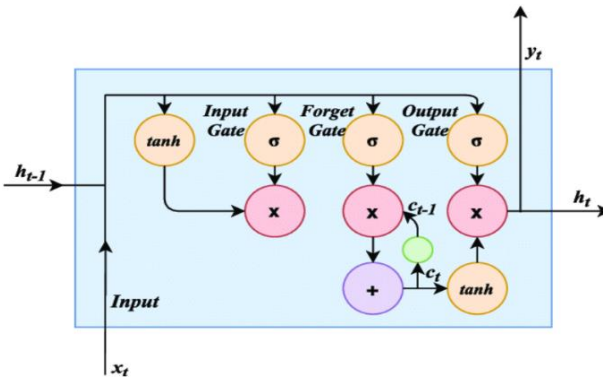

Fig. 1. LSTM block diagram.

Material and methods

The study aimed to evaluate the performance DNN algorithms. The LSTM architecture was exhaustively discussed in order to better understand the architectures of the Bidirectional and CNN-Bidirectional LSTM models despite the fact that the LSTM model was not employed in data analysis. The main feature of the analysis is to develop a hybrid model based on CNN. This section illustrates in detail the structure of deep learning(DL) networks adopted in the analysis. DNN were used to investigate the effectiveness of the model parameters on the prediction of all India rainfall during the monsoon seasons.

Rainfall data collection

In India, the yearly rainfall contribution is 97.9% from March to December and 2.1% during the winter months. The monsoon seasons are divided into three types: pre-monsoon, southwest monsoon, and post-monsoon. The data corresponding to three monsoon seasons from 1871 to 2019 are included for analysis in this study. For the period mentioned, all-India average monthly rainfall values were calculated by weighing each of the 30 sub-divisional rainfalls with their corresponding area as a weight (Kothawale and Rajeevan, 2017). To eliminate outliers and its marginal annual rainfall contribution, the winter rainfall data was not considered. The Indian Meteorological Department's (IMD) data from 1871 to 2019 were utilized to train and validate BiLSTM and CNN BiLSTM architectures.

LSTM Model

LSTM networks are a type of recurrent neural network (RNN) that increases memory recall by remembering past data (Liu et al., 2022) and backpropagation is used to train the model, which is ideally suited to predicting time series with unpredictable time lags. The LSTM networks were explicitly developed to circumvent the long-term dependency issues and handle the vanishing gradient problem successfully, and the model is divided into three sections which perform a specific function as shown in Fig. 1.
The first section determines whether the data from the previous time step is relevant or can be ignored. In the second and final sections, the cell seeks to learn new information from the input and transfers the updated information from the current time step to the next time step respectively, and the LSTM cycle is viewed as a single-time step. These three sections of the LSTM unit are known as forget gate, input gate, and output gate. A memory cell in an LSTM network can be viewed as a layer of neurons in a typical feedforward neural network, with each neuron having a hidden layer and an ongoing state. These gates also solve the problem of vanishing gradient, which generally occurs in RNNs. As a result, it is widely used in a variety of applications in time series prediction (Huang, et al., 2022). The first section determines whether to retain or remove the information from the previous time step. Equation 1 depicts the forget gate. The activation value of forget gate f_t at time t is calculated using a sigmoid function. The f_t is then multiplied by the previous time step's cell condition.

$$f_t = \sigma\,(X_t * U_f + h_{t-1} * W_f) \quad (1)$$

where
X_t – input to the on-going time step,
U_f – weight related with the input,
h_{t-1} – hidden state of the preceding time step,
W_f – weight matrix related with the hidden state.

The second gate, the input gate, is used to evaluate the relevance of the new information carried by the input, and its equation is shown in Equation 2.

$$i_t = \sigma\,(X_t * U_i + h_{t-1} * W_i) \quad (2)$$

where
U_i – weight matrix of input,
W_i – weight matrix of input associated with hidden state.

The sigmoid function is then applied on top of this, resulting in the value of 'i' at time step t being between 0 and 1. Equation 3 is used to calculate the new information.

$$N_t = tanh\,((X_t * U_c + h_{t-1} * W_c) \quad (3)$$

The new information that has to be provided to the cell state is now a function of a hidden state at time step t-1

and input *x* at time step *t*. Tanh is the activation function, and the value of the new information runs from -1 to 1. If N_t is negative, information is subtracted from the cell state and added to the continuing state, and vice versa. The N_t, however, is not directly added to the cell state. Equation 4 depicts the modified cell state equation.

$$C_t = f_t * C_{t-1} + i_t * N_t \quad (4)$$

where
C_{t-1} – the cell state at the on-going time step.

The equation of the output gate is shown as Equation 5.

$$o_t = \sigma\,(X_t * U_o + h_{t-1} * W_o) \quad (5)$$

Equation 6 is used to compute the current hidden state using the output state 'o_t' and tanh of the updated cell state. As indicated in Equation 7, the hidden state is a function of long-term memory (C_t) and the current output, and the output of the current time step is determined by applying the SoftMax activation to hidden state ht. The predicted value is nothing but the maximum score in the output.

$$h_t = o_t * tanh\,(C_t) \quad (6)$$

$$Output = Softmax\,(h_t) \quad (7)$$

Finally, backpropagation is used to obtain the LSTM, which is then stored in memory blocks. Now, the LSTM can successfully familiarize the inputted time series data to produce a long-term memory function (Wang et al., 2021). In this model, the outputs of the cell are controlled by the gates. Fig. 2 depicts the architecture of a single LSTM cell (Metlek et al., 2021).

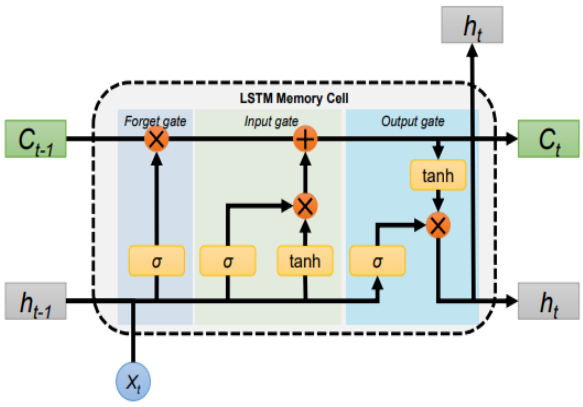

Fig. 2. Schematic diagram of the LSTM cell architecture.

BiLSTM Model

LSTM may receive long range information prior to the output time but cannot use reverse information. To greatly increase prediction accuracy, the forward and backward information of time series data should be completely considered in time series prediction. BiLSTM is made up of two LSTM's, one forward and one backward layer. In comparison to the regular LSTM's one-way-state transmission, BiLSTM evaluates data changes before and after data transmission and can make more full and detailed decisions based on past and future information (Zhuang and Cao, (2022). BiLSTM model performs forward and backward calculations as shown in the model structure in Fig. 3 and it depicts the two-way flow of time series information in the model, whereas data information flows vertically in only one direction from the input layer to the hidden layer to the output layer (Varghese et al., 2022). The purpose of using the LSTM twice makes the model to learn the model long-term dependencies and increase its accuracy (Metlek et al., 2021).

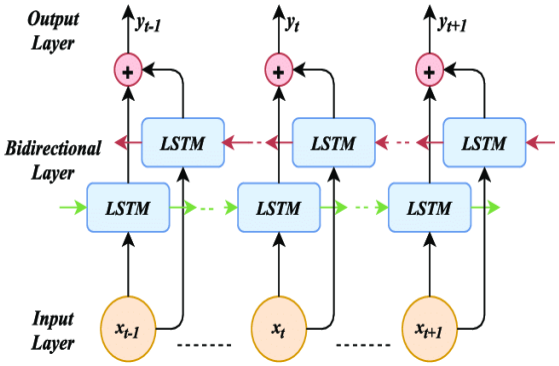

Fig. 3. Schematic diagram of BiLSTM structure.

CNN BiLSTM Model

The model combining CNN, BiLSTM and the connection layer proposed to predict the average monthly rainfall during the monsoon seasons across India is referred to as the CNN BiLSTM or hybrid model. The input of the hybrid model first enters the CNN layer, and after convolution calculation and max-pooling; a new feature matrix is generated. The feature matrix obtained from the CNN is used as the BiLSTM's input, and the BiLSTM's hidden output is obtained. The hidden output is routed through the connection layer, which is made up of a linear layer. The connection layer then returns the final results (Ullah et al., 2019; Metlek, 2023). Fig. 4 depicts the hybrid model architecture (Varghese et al., 2022).
The hybrid model describes how input and output interact. The recursive multi-step forecasting approach is used to create the univariate time series forecasting model. The univariate time series must be modified to suit the CNN input and output BiLSTMs because the hybrid model employs supervised learning. Assuming a univariate time series sample $y^{(1)}$, $y^{(2)}$.,. $Y^{(n)}$ with lag, the predicted value of $y^{(\tau+1)}$) can be obtained using the preceding steps. The one-dimensional vector is then rebuilt into a $(\tau + 1)$ dimensional matrix. Equation 8 shows how to generate the reconstructed sample matrix, Θ.

$$\Theta = [Y^{(1)}, Y^{(2)}, \ldots, Y^{(\tau)}, Y^{(\tau+1)}] \quad (8)$$

where
$Y^{(1)} = [y^{(1)}, y^{(2)}, \ldots, y^{(\tau)}, y^{(\tau+1)}]$ - a column vector with lag τ.

Then, the input to the hybrid model is a matrix X consisting of the previous τ column vectors $[Y^{(1)}, Y^{(2)}, \ldots, Y^{(\tau)}]$, and the output is the (τ + 1) as shown in Equation (8). When the forecasting reaches step τ + 1, the input vector already contains all of the predicted values, implying that the extrapolation is complete (Chen and Fu, 2023). The hybrid model training process to predict the average monthly rainfall during the monsoon seasons is as follows:
Step 1: Clean up the data by removing unnecessary items, serializing time data, and dividing the training and testing sets.
Step 2: Input the pre-processed time series data into the hybrid model for training.
Step 3: Feed the training data into the trained model to predict.
Step 4: Using the formulas, restore the predicted data.
Step 5: Plot a graph that compares the actual and expected rainfall values, and use the actual and predicted values to evaluate the model's prediction power.

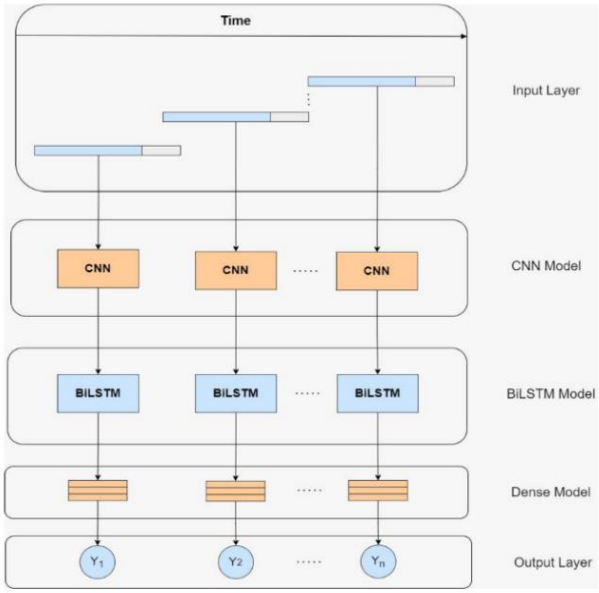

Fig. 4. Hybrid model architecture.

Results and discussion

Data preprocessing

In the present study, data refer to the year 1871 to 2019 for pre-monsoon, south west monsoon and post monsoon seasons was considered for analysis. The rainfall data relating to the winter months was excluded. The dataset consists of 1472 monthly average of all India rainfall data of three monsoon seasons. To maintain high data quality, the authors removed the outliers and standardized the data format and there are no null data points present. Data points were normalized between 0 and 1 using the MinMax scaler before splitting the data set for training and testing. Out of 1472 data points, 1030 (70%) and 442 (30%) were used to train and test the dataset to assess the models' predictive capability. Finally, five evaluation metrics namely; MAE, MAPE, RMSE and R^2 were used to check the model's predictive capability.

Parameters and the Experimental Models

In this study, the results of the hybrid model were compared to the evaluation metrics of BiLSTM model. The model and training parameters of two models are kept the same for comparison purposes. The Adam optimizer is used to calculate the adaptive parameter learning rate based on the mean of the first and second moments of the gradient. Several experiments were carried out to determine the best possible architectural configuration by varying model parameters (viz. number of hidden layers, number of filters, kernel size, pooling size, and dropout percentage) and optimizing several hyperparameters (viz. learning rate, batch size, number of epochs, and loss functions). The learning rate is 0.0001, and MAE is used as the loss function. The forecasting model was developed using a value of 12 preceding monthly rainfall instances (Deepak et al., 2019). It only measures the mean modulus length of the predicted value error, disregarding direction, and is more robust to outliers. The batch size and the number of epochs is 32 and 250 respectively with early stopping. Table 1 displays the hybrid model's parameter settings.

Table 1. Parameter settings of hybrid model

Parameters	Value
Conv1D(filters)	16
Conv1D kernel_size	2
Conv1D activation function	LeakyReLU
MaxPooling1D pool_size	1
BiLSTM units	32
BiSLSTM activation function	Tanh
Dense units	1

The average monthly rainfall data during the monsoon seasons after preprocessing are put into the BiLSTM, and hybrid models for training. The test dataset is used for prediction after completing the training. The plot of the hybrid model relating to the actual and predicted values in the last 1000 months are shown in Fig. 5. The learning curve of the hybrid model in prediction of average monthly rainfall is shown in Fig. 6. The learning curves are plotted to check whether the train or validation datasets are appropriately representative of the domain area. The learning curve shows that the model fit is good, with a training and validation loss reducing to a stability

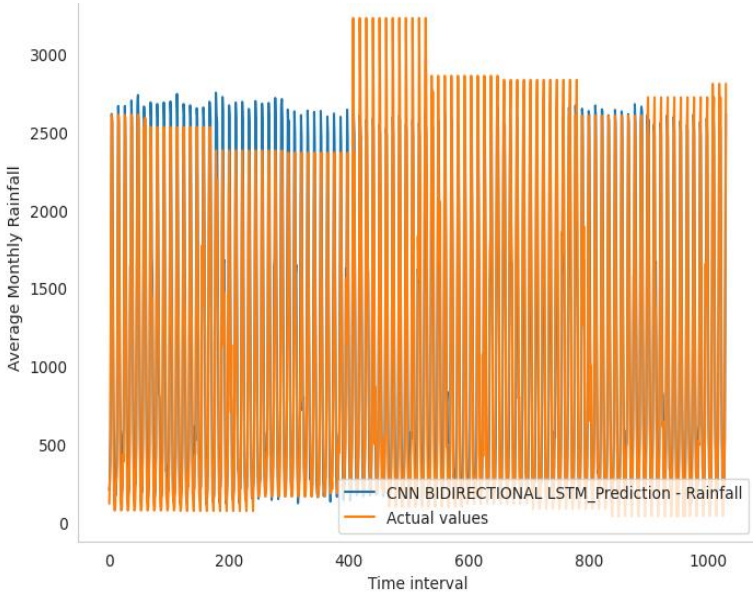

Fig. 5. Hybrid model – Actual vs predicted value of GHI.

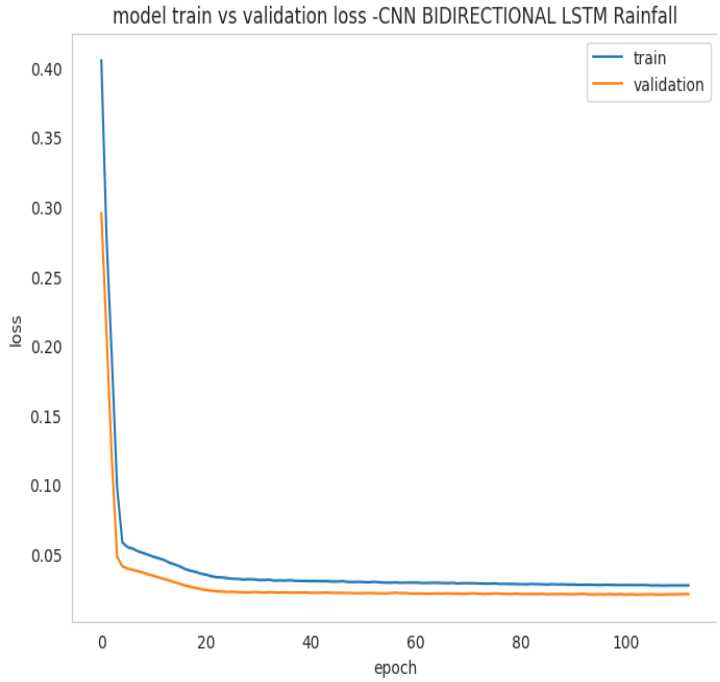

Fig. 6. Hybrid model learning curve (Model training vs validation loss of Rainfall).

point with a marginal difference between the two final loss values.

The most important evaluation parameters MAE, MAPE, RMSE, and R^2 are utilized in the analysis to compare the model results. These four parameters are used to assess the difference between predicted and actual rainfall, and their values are shown in Table 2. When compared to the Bidirectional LSTM model, the hybrid model has a higher R^2 score. The hybrid model's MAE, MAPE, and RMSE scores are significantly lower, showing that the model's predictive power is accurate.

To construct a hybrid model, the LSTM and BiLSTM prediction data are integrated with CNN for feature extraction, and more significant extended features are learned. The R^2 score of the hybrid model is 0.9485,which is greater than the R^2 scores of the BiLSTM model and it shows that the model

Table 2. Model evaluation parameters of rainfall

Model	MAE	MAPE	RMSE	R^2
BiLSTM	178.908	41.225	249.255	0.9243
Hybrid model	189.568	47.257	256.586	0.9485

outperformed the empirical and DL models in terms of predicting time-series data (Varghese et al., 2022). The LSTM model outperformed the RNN in forecasting average monthly yearly rainfall in India from 1871 to 2016 (Deepak et al., 2019) with a correlation coefficient of 0.960, whereas the hybrid model in the current study obtained a correlation coefficient of 0.974. A combination of a one-dimensional Convolutional Neural Network and a Multi-Layer Perceptron neural network proved to be a better model for predicting daily rainfall by considering nine variables that are closely associated with daily rainfall variation with a coefficient of correlation ranging from 0.41 to 0.76 (Mislan et al., 2015). The hybrid model has the best degree of fit based on the evaluation parameters between the predicted and actual values. The Extreme Gradient Boost gradient descent machine learning approach predicts rainfall in Bahir Dar, Ethiopia more accurately than the random forest algorithm and Multi-Layer Perceptron neural network with low MAE and RMSE scores (Liyew and Melese, 2021). Backpropagation Neural Network demonstrated better results for predicting rainfall in Tenggarong, East Kalimantan, Indonesia, with the lowest mean squared error when the hyperparameters were varied (Mislan et al., 2015). According to previous studies, the hybrid model was not applied for rainfall analysis, and the model findings in the present research are substantially improved. Recent approaches in predicting the rainfall using hybrid models of LSTM-Networks will be investigated. Recently developed architectures for time series data prediction will be studied using hybrid LSTM models (Altan et al., 2021), and the present study effectively analyzed the rainfall data using a CNN-BiLSTM hybrid model.

The learning curve of the hybrid model shows that the model fit is good with no overfitting or underfitting. The accuracy of the models used was validated against the actual rainfall, resulting in an average absolute percent error value of less than 1%. Compared to the BiLSTM model, the results of the hybrid model show that the improvement in the predictive capability and the predicted values are closely following the trend of the original dataset. The proposed model can be trained and used with the other parameters of the meteorological data that have an impact on the rainfall. The hybrid model can be applied to regression and time series data via a one-dimensional filter as in the proposed model. As a result, the proposed hybrid model can be applied in many fields such as forecasting of meteorological, health care, and environmental datasets in the long term.

Conclusion

The study aims to model India's average monthly rainfall during the monsoon seasons. The BiLSTM model was used for this purpose and in addition to this model, a hybrid model is developed and proposed. The hybrid model R^2 scores provided better results for predicting rainfall. The results reveal that the hybrid model outperforms the BiLSTM deep learning neural networks in terms of prediction. The evaluation parameters of the models used were verified using the actual rainfall and the MAPE of the proposed model was less than 1%. The coefficient of correlation is closer to one which confirms the robustness of the model in predicting rainfall. The proposed model fit is good as it falls between an overfit and an underfit model. The proposed hybrid model can be applied to model the meteorological parameters that influence rainfall. The limitation of the study is parameters which are influencing the monthly rain were not considered. The study can be extended in the future by developing a multivariate CNN-BiLSTM architecture by considering the variables that have a direct impact on rainfall. Furthermore, a comprehensive evaluation of the inclusion of the variables influencing rainfall should be investigated to increase the effectiveness of prediction models.

Acknowledgement

We acknowledge the data utilized from Research Report No. RR-138 ESSO/IITM/STCVP/SR/02(2017)/189, Monthly, Seasonal and Annual Rainfall Time Series for All-India, Homogeneous Regions and Meteorological Subdivisions: 1871-2016, Indian Institute of Tropical Meteorology (IITM), India and also Open Government Data(OGD) platform, India (https://data.gov.in/catalog /rainfall-india).

References

Altan, A., Karasu, S., Zio, E. (2021): A new hybrid model for wind speed forecasting combining long short-term memory neural network, decomposition methods and grey wolf optimizer. Applied Soft Computing, vol.100, 106996.

Barrera-Animas, A. Y., Lukumon, O. O., Muhammad, B., Taofeek, D. A., Juan, M. D., Lukman, A. A. (2022): Rainfall prediction: A comparative analysis of modern machine learning algorithms for time-series forecasting. Machine Learning with Applications, vol. 7, no. 100204, 1–20.

Billah, M., Adnan, Md. N., Akhond, M. R., Ema, R. R., Hossain, Md. A., Md. G. S. (2022): Rainfall prediction system for Bangladesh using long short-term memory. Open Computer Science, vol. 12, no. 1, 323–331.

Chen, Y., Fu, Z. (2023): Multi-Step Ahead Forecasting of the Energy Consumed by the Residential and Commercial Sectors in the United States Based on a Hybrid CNN-BiLSTM Model. Sustainability, vol. 15, no.3, 1–21.

Deepak, K., Anshuman, S., Pijush, S., Rishi Kumar, J. (2019): Forecasting monthly precipitation using sequential modelling. Hydrological Sciences Journal, vol.64, no. 6, 690–700.

Farajzadeh, J., Fard, A. F., Lotfi, S. (2014): Modeling of monthly rainfall and runoff of Urmia lake basin using feed-forward neural network and time series analysis model. Water Resources and Industry, vol. 7–8, 38–48.

Greff, K., Srivastava, R. K., Koutník, J., Steunebrink, B. R., Schmidhuber, J. (2016): LSTM: A search space odyssey. IEEE Transactions on Neural Networks and Learning Systems, vol.28, no.10, 2222–2232.

Hossain, I., Rasel, H., Imteaz, M. A., Mekanik, F. (2020): Long-term seasonal rainfall forecasting using linear and non-linear modelling approaches: A case study for western Australia. Meteorology and Atmospheric Physics, vol.132, no.1, 131–141.

Huang, X., Li, Q., Tai, Y., Chen, Z., Liu, J., Shi, J., Liu, W. (2022): Time series forecasting for hourly photovoltaic power using conditional generative adversarial network and Bi-LSTM. Energy, vol. 246, 123403.

Kothawale, D. R., Rajeevan, M. (2017): Research Report No. RR-138 ESSO/IITM/STCVP/SR/02(2017)/189, Monthly, Seasonal and Annual Rainfall Time Series for All-India, Homogeneous Regions and Meteorological Subdivisions: 1871-2016, Indian Institute of Tropical Meteorology (IITM), 1–169.

Liu, Y., Meenakshi, V., Karthikeyan, L., Maroušek, J., Krishnamoorthy, N. R., Sekar, M., Xia, C. (2022): Machine learning based predictive modelling of micro gas turbine engine fueled with microalgae blends on using LSTM networks: An experimental approach. Fuel, vol. 322, 1–8.

Liyew, C. M., Melese, H. A. (2021): Machine learning techniques to predict daily rainfall amount. J Big Data, vol. 8, no. 153, 1–11.

Metlek, S., Kayaalp, K., Basyigit, I. B., Genc, A., Dogan, H. (2021): The dielectric properties prediction of the vegetation depending on the moisture content using the deep neural network model. International Journal of RF and Microwave Computer-Aided Engineering, vol.31, no.1, 1–10.

Metlek, S. (2023): A new proposal for the prediction of an aircraft engine fuel consumption: a novel CNN-BiLSTM deep neural network model. Aircraft Engineering and Aerospace Technology, vol. 95, no.5, 838–848.

Mislan, H., Sigit, H., Sumaryono, M. A. (2015): Rainfall Monthly Prediction Based on Artificial Neural Network: A Case Study in Tenggarong Station, East Kalimantan – Indonesia. Procedia Computer Science, vol. 59, 142–151.

Rahman, A. U., Abbas, S., Gollapalli, M., Ahmed, R., Aftab, S., Ahmad, M., Khan, M. A., Mosavi, A. (2022): Rainfall Prediction System Using Machine Learning Fusion for Smart Cities. Sensors, vol.22, no. 3504, 1–15.

Shrivastava, G., Karmakar, S., Kowar, M. K. (2012): Application of Artificial Neural Networks in Weather Forecasting: A Comprehensive Literature Review. International Journal of Computer Applications, vol. 51, 17–29.

Ullah, F. U. M., Ullah, A., Haq, I. U., Rho, S., Baik, S. W. (2019): Short-term prediction of residential power energy consumption via CNN and multi-layer bi-directional LSTM networks. IEEE Access, vol. 8, 123369-123380.

Varghese, J., Anshuman, M., Sowmaye, T., Shruti, M., Sandeepkumar, S., Sachi, N. M. (2022): A hybrid deep learning framework with CNN and Bi – directional LSTM for store item demand forecasting. Computers and Electrical Engineering, vol.103, 1–14.

Wang, H., Wang, J., Cao, L., Li, Y., Sun, Q., Wang, J. (2021): A stock closing price prediction model based on CNN BiSLSTM. Complexity, 1–12.

Wu, C., Chau, K.W. (2013): Prediction of rainfall time series using modular soft computing methods. Engineering Applications of Artificial Intelligence, vol.26, no.3, 997–1007.

Zhang, J., Florita, A., Hodge, B. M., Lu, S., Hamann, H. F., Banunarayanan, V., Brockway, A. M. (2015): A suite of metrics for assessing the performance of solar power forecasting. Solar Energy, vol.111, 157–175.

Zhuang, W., Cao, Y. (2022): Short-Term Traffic Flow Prediction Based on CNN-BILSTM with Multicomponent Information. Applied Sciences, vol. 12, no.17, 1–15.

Dr. Rajaprasad Svs, Ph.D (*corresponding author, e-mail: rajaprasad@nicmar.ac.in)
Rambabu Mukkamala, M.Tech
National Institute of Construction Management and Research (NICMAR)
Hyderabad
India

DOI: 10.31577/ahs-2023-0024.02.0025

ACTA HYDROLOGICA SLOVACA

Volume 24, No. 2, 2023, 221 – 231

Comparison of meteorological drought over two normal periods

Dana PAVELKOVÁ*, Branislav KANDRA, Andrej TALL, Helena HLAVATÁ, Milan GOMBOŠ

The frequency of extreme meteorological events, including drought, has risen in the last years. This is, among, due to climatic changes occurring in the atmosphere. These extremes have been monitored also on the East Slovakian Lowland. Dry periods are defined as periods of water scarcity in their various forms. In order to quantify changes in the climate at a particular location, it is useful to compare the climatic characteristics monitored over two normal periods. The basic assumption of this work is that Earth's climate has been warming and therefore the drought incidence has been increasing. The aim of this work is to quantify differences in the climate at a particular location over two consecutive normal periods. The two normal periods (NP) are the years 1961–1990 (NP1) and 1991–2020 (NP2). Compared atmospheric elements were monitored at the meteorological station of SHMÚ (Slovak Hydrometeorological Institute) in Milhostov, which is in the central part of the East Slovakian Lowland. Normal periods were analysed in terms of precipitation, temperature, potential evapotranspiration, and selected drought indices. The analysis has shown that the normal period of 1991–2020 (NP2) is both annually and monthly drier than the period of 1961–1990 (NP1), with a significant increase in temperatures and potential evapotranspiration.

KEY WORDS: drought index, normal period, meteorological elements

Introduction

Changes in the atmosphere have caused an increase in the frequency of extreme hydrological events (Raikes et al., 2019; Trnka et al., 2016; Climate atlas of Slovakia, 2015; Rodný and Šurda, 2010). In Slovakia, this is manifested in prolonged rainless periods and a higher frequency of extreme precipitation in terms of intensity and abundance. It is useful to compare the changes in atmospheric elements in two different normal periods for the quantification of climate change in the investigated locality. These normal periods allow the comparison of both atmospheric and hydrometeorological elements in different regions and periods. Representative hydrological and atmospheric elements are, in general, calculated from the normal period. The length of the normal period is at least 30 years. It is a common problem to obtain an uninterrupted series of measurements over 30 years (Bonacci et al., 2023; Pinheiro and Blanco, 2021). World Meteorological Organization (WMO, 1935) has specified that for the worldwide comparison of data, three reference normal periods will be used: periods between 1901–1930, 1931–1960 and 1961–1990. WMO recommended that standard 30-years long reference periods should be updated every decade so that they reflect climate change. WMO congress (WMO, 2021) suggested that new 30-years long standard reference period from 1991to 2020 is set.

The studies of drought need consistent analysis method. The first step in drought analysis is to define the term drought. This is not an easy task, as the impact and form of drought are different in different climatic regions. What is considered drought in the tropical forest, is not considered drought in deserts. Originally, there was only one, very general definition of drought, saying: “Basic characteristic of drought is the decrease in water availability over specified period on a specific area”. Beran and Rodier (1985) and Yevjevich (1967) believe that this absence of an accurate and objective definition of the term drought was the fundamental obstacle to scientific investigation of the phenomenon in the past. At present, drought is considered a state when water availability from water sources is lower than the statistical needs of water in the concerned area. In this sense, it is perceived as the discrepancy between natural water sources and social needs for water supply. Currently, the widespread definition of drought (especially in the US) is that a drought is a period of unusually dry weather that is long enough for a lack of water to cause a hydrological imbalance in the affected area American Meteorological Society (2019).

Drought can have a severe impact on the environment, economy, and human society. By reducing the agricultural yield, it can threaten food security (Haigh et al., 2022a; 2022b; Pecho, 2016) of people. Dry or

damaged vegetation affects the quality of soils, increases fire risks (Hološ et al., 2022; Li et al., 2022) and provokes the death of animals and changes in biodiversity and ecosystems. A decrease in water availability and water quality may provoke social tension and bring about a struggle between different social groups for access to water sources (Brázdil et al., 2016). Based on this, drought can be of several types: meteorological (Gomboš and Pavelková, 2009), hydrological (Almikaeel et al., 2023), soil and socio-economic. At this point, it is needed to say that the timing of phases of drought are different, depending on the drought type (Wilhite and Glantz, 1985).

The work assumes that Earth's climate has been warming and therefore the drought incidence has been increasing (Wilhite, 2016). The aim of this work is to quantify differences in the local climate over two consecutive normal periods – the period between the years 1961–1990 and 1991–2020. Compared atmospheric elements were monitored at the meteorological station of SHMÚ (Slovak Hydrometeorological Institute) in Milhostov, which is in the central part of the East Slovakian Lowland. Normal periods were analysed in terms of precipitation, temperature, potential evapotranspiration, and selected drought indices. Quantification of the climate change is necessary for forecasting future development and the proposal of measures to eliminate drought impact on the environment.

Methodology

Data for the study were obtained from the meteorological station in Milhostov which is located in the central part of the East Slovakian Lowland (48° 40′ 11″; 21° 44′ 18″). This station has monitored meteorological data from the area since 1960. It is situated in the locality which, from the climatic point of view, lies in the transitional area between oceanic and continental climate. The local climate is mainly warm and semi-humid with cold winters. Great temporal variability of the weather and all the meteorological elements is typical of the climate in the area. Air masses swiftly change throughout the year, regardless of season, and cyclonic activity is highly developed (Kveták, 1983a; 1983b; Markovič et al., 2021).

This work compares the data from two consecutive normal periods 1961–1990 and 1991–2020 (Mikulová et al., 2008). Database for the analysis contains annual precipitation totals, long-term average monthly precipitation totals, average annual air temperatures and average annual and monthly potential evapotranspiration totals. Precipitation, temperature and evaporation are key balance characteristics of hydrological processes in the system of atmosphere – plant cover – unsaturated zone – groundwater (Faško et al., 2000; Hlavatá and Tomková, 2015). Evaporation in this work is represented by potential evapotranspiration (Novák, 1995). It contains the energy balance of the environment and the conditions for water vapour transport to the atmosphere.

Apart from the abovementioned hydrometeorological elements, selected drought indices have been used for comparing the two normal periods. Drought indices are used as a substitute for complex climatic functions (Mukherjee et al., 2018) in the monitoring and quantification of drought. They enable the quantification of climatic anomalies in terms of their severity, duration and incidence (Choudhary et al., 2023). They can convey, in an understandable way, important information on the severity of drought event (Tsakiris et al., 2007; Soľáková et al., 2022). Drought indices are used in the investigation, in the decision-making processes as well as in the proposal of adaptive measures. The indices are not universal and thus it is usually necessary to use more than one index at a time (Morid et al. 2006; Čimo et al., 2008; Jarošová and Igaz, 2018).

For the analysis of the normal periods, simple indices commonly used in the past were applied: Vysocky index, Climatic indicator of irrigation, Hydrothermal coefficient of Selyaninov, Lang`s rain factor, Drought index and Palmer drought severity index (PDSI). All but PDSI are simple indices. Their calculation is based on precipitation, temperatures and potential evapotranspiration. The formulas for the calculation of the indices and the classification tables for evaluating the calculated values are described below.

Vysocky index (V_i)

$$V_i = \frac{P_r}{ET_{pot}} \quad (1)$$

where
P_r – precipitation total for the evaluated period,
ET_{pot} – potential evapotranspiration total for the evaluated period.

Table 1. Evaluating scale for Vysocky index

0–1	Evapotranspiration predominates
1	Precipitation equal to evapotranspiration
>1	Precipitation predominate

Climatic indicator of irrigation (K_z)

$$K_z = ET_{pot} - P_r \quad (2)$$

where
ET_{pot} – potential evapotranspiration total for the evaluated period,
P_r – precipitation total for the evaluated period.

Table 2. Evaluating scale for Climatic indicator of irrigation

>0	Evapotransporation predominates
0	Precipitation equal to evapotranspiration
<0	Precipitation predominates

Hydrothermal coefficient of Selyaninov (K_{HT}) (Jůva, 1959)

$$K_{HT} = \frac{\sum H_Z}{0.1 \sum t_{10}} \quad (3)$$

where
$\sum H_Z$ – precipitation total for the evaluated period [mm],
$\sum t_{10}$ – sum of average daily temperatures (t >10°C) for the evaluated period [°C].

Table 3. Evaluating scale for Hydrothermal coefficient of Selyaninov

<0.30	Catastrophic drought
0.31–0.50	Drought
0.51–0.99	Water shortage
1.00	Precipitation equal to evapotranspiration
1.01–2.00	Sufficient water
>2.00	Water excess

Lang´s rain factor (f)

$$f = \frac{P_r}{T_p} \quad (4)$$

where
P_r – precipitation annual total [mm],
T_p – average annual air temperature [°C].

Table 4. Evaluating scale for Lang´s rain factor

20–40	Arid climate area
40–60	Intermediate climate area
>60	Humid climate area

Drought index (S_i) (Klementová, 1990)

$$S_i = \frac{\Delta t_i}{\sigma_t} - \frac{\Delta z_i}{\sigma_z} \quad (5)$$

where

$$\Delta t_i = t_i - \bar{t} \qquad \Delta z_i = z_i - \bar{z}$$

$$\bar{t} = \frac{1}{n}\sum_{i=1}^{n} t_i \qquad \bar{z} = \frac{1}{n}\sum_{i=1}^{n} z_i$$

$$\sigma_t = \sqrt{\frac{1}{n}\sum_{i=1}^{n}(t_i - \bar{t})^2}$$

$$\sigma_z = \sqrt{\frac{1}{n}\sum_{i=1}^{n}(z - \bar{z})^2}$$

Δt – deviation of the average monthly temperature from the long-term monthly average [°C],
Δz – deviation of the average monthly precipitation total from the long-term monthly average [mm],
n – range of the statistical file (number of evaluated years (1961–2020)),
σ_t, σ_z – standard deviations (of average monthly temperature and monthly precipitation totals),
t_i – average monthly air temperature [°C] in the i-th year,
z_i – monthly precipitation total [mm] in the i-th year,
$\bar{t}$ – long-term average air temperature of the relevant month [°C],
$\bar{z}$ – average monthly precipitation [mm].

Table 5. Scale for evaluating the values of Drought index

>2	Very arid area
1–2	Arid area
0–1	Moderately arid area
0–(-1)	Moderately humid area
(-1)–(-2)	Humid area
<-2	Very humid area

Palmer drought severity index (PDSI)

The last evaluated drought index is Palmer Drought Severity Index (PDSI). This index is used for drought quantification of a large area with variable pedological and climatic conditions (Palmer, 1965; Litschmann et al., 2002). It is used mainly in the US. Its relatively high complexity in terms of calculation is compensated by its versatility. Input variables for calculating PDSI are precipitation, potential evapotranspiration (monthly totals) and the value of available water capacity. For calculating ET_{pot} the formula (6) is used. It is necessary that various meteorological parameters are known: air temperature, duration of sunshine, water vapour pressure and wind speed. Algorithm for PDSI calculation for

Table 6. Evaluation scale for Palmer drought severity index

>4.00	Extreme wet spell
3.00–3.99	Severe wet spell
2.00–2.99	Moderate wet spell
1.00–1.99	Mild wet spell
0.50–0.99	Developing wet spell
-0.49–0.49	Normal
-0.50– -0.99	Developing drought
-1.00– -1.99	Mild drought
-1.99– -2.99	Moderate drought
-2.99– -3.99	Severe drought
<-4.00	Extreme drought

the purposes of this study was created at SHMI in Michalovce on the basis of the original Palmer methodology using the programming language Visual Basic for Application (VBA).

For calculating these indicators, daily meteorological parameters such as air temperature, precipitation, duration of sunshine, water vapour pressure and wind speed were used. Meteorological parameters were obtained from Slovak Hydrometeorological Institute in Košice from the meteorological station in Milhostov for period of 1961–2020.

Potential evapotranspiration (ET_{pot}) is calculated by the formula (Allen et al., 1998):

$$ET_{pot} = \frac{0.408\,\Delta\,(R_n - G) + \gamma \frac{900}{T+273}\,u_2\,(e_s - e_a)}{\Delta + \gamma\,(1 + 0.34\,u_2)} \quad (6)$$

where

ET_{pot} – reference evapotranspiration [mm day^{-1}],
R_n – radiation balance of the crop surface [MJ m^{-2} day^{-1}],
G – heat flow in the soil [MJ.m^{-2} day^{-1}],
T – average daily air temperature at a height of 2 m [°C],
u_2 – average daily wind speed at a height of 2 m [m s^{-1}],
e_s – saturated water vapor pressure [kPa],
e_a – current water vapor pressure [kPa],
Δ – derivative of saturated water vapor pressure [kPa C^{-1}],
γ – psychrometric constant [kPa °C^{-1}].

Results and discussion

Table 7 describes the characteristics of descriptive statistics for the average annual air temperatures, annual precipitation totals and annual ET_{pot} totals for the normal periods of 1961–1990 and 1991–2020. It is obvious that, in comparison to the previous normal period of 1961–1990 (NP1), the normal period of 1991–2020 (NP2) is warmer by 1°C on average. Its average annual precipitation total is higher by 5.8% and average annual potential evapotranspiration is higher by 11.9%. The difference between average annual ET_{pot} and average annual precipitation total raised from 24% in NP1 to 31% in NP2. Variability of the evaluated parameters in NP2 is slightly higher compared to NP1, however, when related to the average, it is the same. Statistical distribution of the evaluated parameters is skewed to the left, in NP2 it is skewed to the right.

Fig. 1 illustrates the development of average annual temperatures in both normal periods. There was a significant increase in temperatures in NP2. Warming is visible also in long-term average monthly temperatures in Fig. 2. In summer, this is most striking in July and August and in winter in January.

Annual precipitation totals and their linear trends are shown in Fig. 3. From Fig. 3 and Table 7 it is obvious that NP2 has more abundant precipitation with slightly increasing linear trend in comparison to NP1. Regarding long-term average monthly precipitation totals shown in Fig. 4, their increase in NP2 is most evident in May, Jun, July and September. In other half of the year, the increase is most significant in October and a bit less in February. In other months, long-term average monthly precipitation totals in NP1 exceed precipitation in NP2.

The course of annual potential evapotranspiration totals and their trends is shown in Fig. 5. The course of the trends in the normal periods are analogous to the course of temperature trends. In NP2, there is a rising trend in the potential evapotranspiration totals in comparison to NP1. In terms of average monthly ET_{pot} total (Fig. 6), there is a significant increase between April and September. In winter and autumn, the changes were negligible.

Table 7. Descriptive statistics for the average annual air temperatures, annual precipitation totals and annual ET_{pot} totals at Milhostov meteorological station in the normal periods 1961–1990 and 1991–2020

	average annual air temperature		annual precipitation total		annual Et_{pot} total	
	1961–1990	1991–2020	1961–1990	1991–2020	1961–1990	1991–2020
Mean	9.0	10.0	546.9	578.4	678.0	758.6
Standard Error	0.1	0.1	16.7	17.6	8.4	9.2
Median	9.0	10.0	546.3	562.5	675.2	750.9
Standard Deviation	0.6	0.7	91.6	96.4	45.8	50.6
Sample Variance	0.4	0.6	8389.8	9284.4	2096.5	2560.4
Kurtosis	-0.5	-0.8	-0.3	2.6	-0.8	-0.7
Skewness	-0.2	0.2	-0.1	1.2	0.1	0.2
Range	2.2	2.6	364.7	453.7	166.5	192.4
Minimum	7.8	8.7	351.9	438.1	596.2	667.0
Maximum	10.0	11.4	716.6	891.8	762.7	859.4
Sum	268.9	300.7	16405.9	17351.0	20339.6	22759.5
Count	30	30	30	30	30	30
Confidence Level (95.0%)	0.2	0.3	34.2	36.0	17.1	18.9

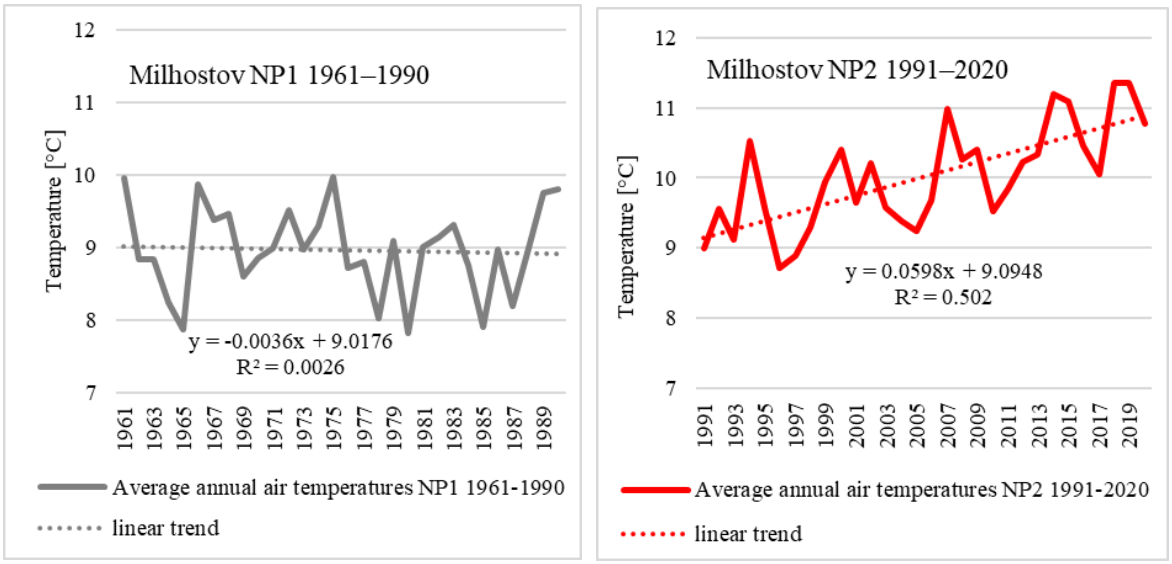

Fig. 1. Average annual air temperatures and their trends at Milhostov meteorological station in the normal periods of NP1 1961–1990 and NP2 1991–2020.

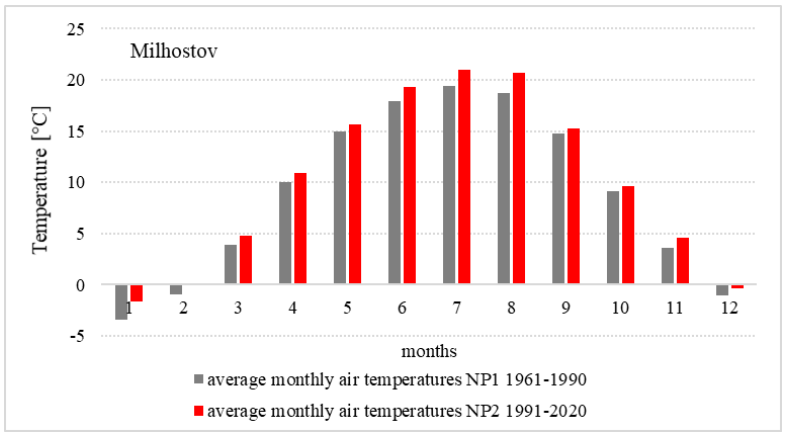

Fig. 2. Comparison of long-term average monthly air temperatures at Milhostov meteorological station between the two normal periods NP1 1961–1990 and NP2 1991–2020.

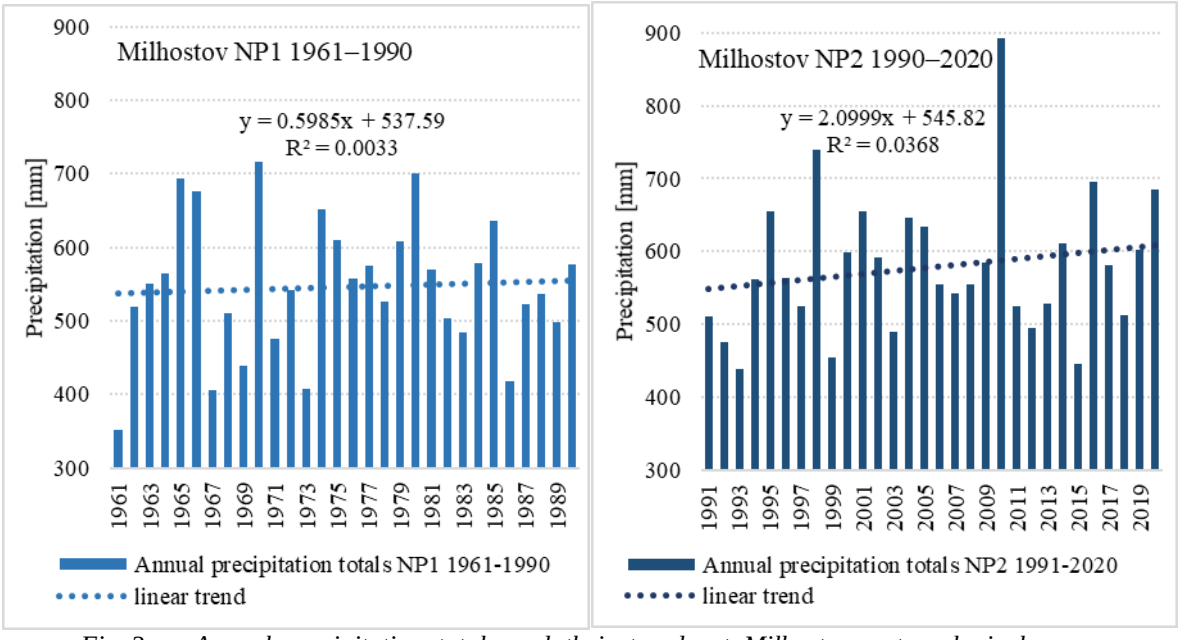

Fig. 3. Annual precipitation totals and their trends at Milhostov meteorological station in the normal period of NP1 1961–1990 and NP2 1991–2020.

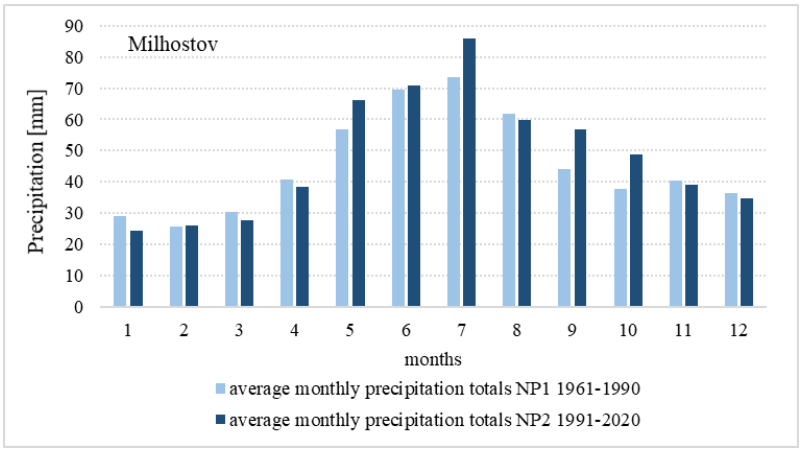

Fig. 4. Long-term average monthly precipitation totals and long-term average precipitation totals at Milhostov meteorological station in the normal periods of NP1 1961–1990 and NP2 1991–2020.

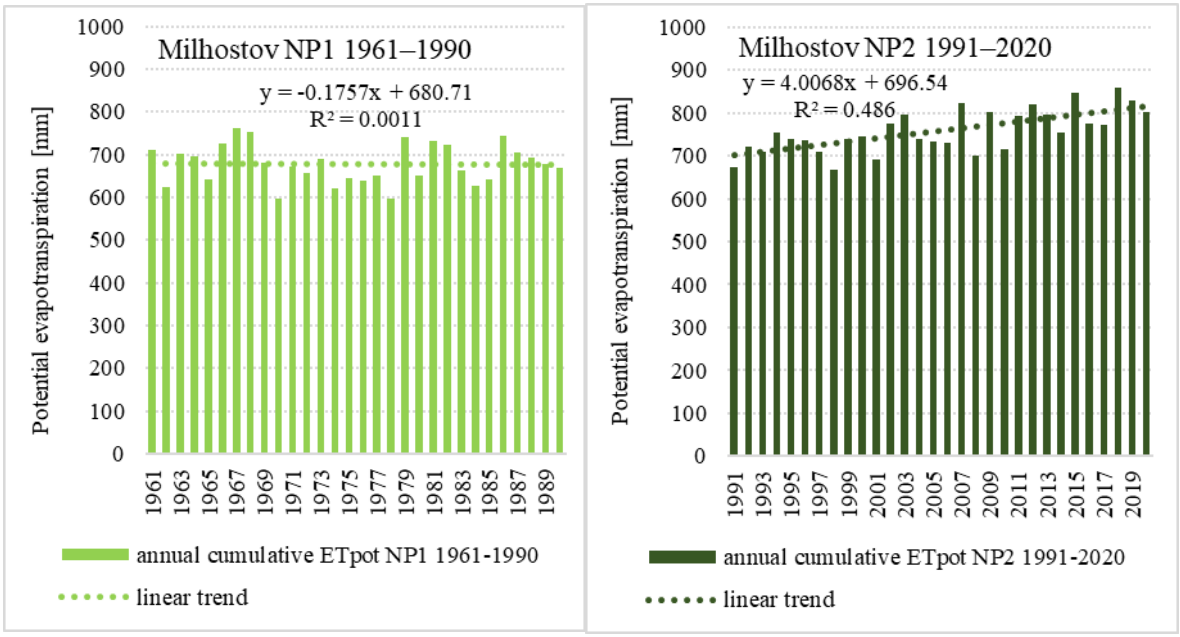

Fig. 5. Trend analysis of the annual cumulated values of potential evapotranspiration (ET_{pot}) at Milhostov meteorological station in the normal periods of NP1 1961–1990 and NP2 1991–2020.

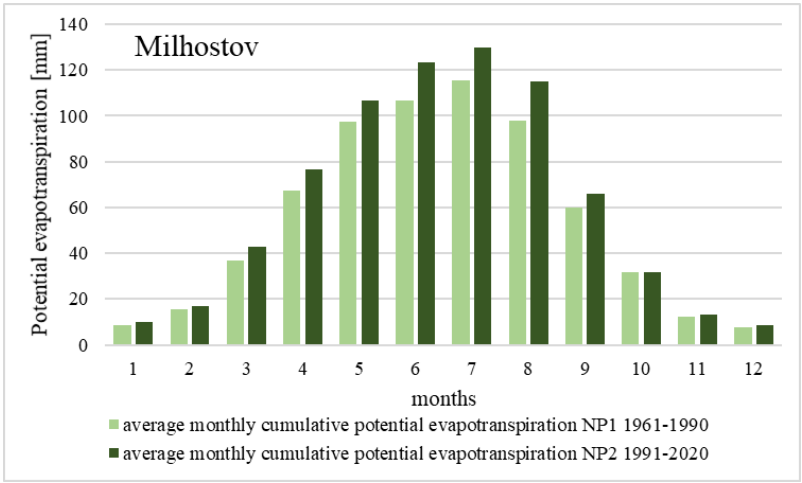

Fig. 6. Long-term average monthly cumulated potential evapotranspiration (ET_{pot}) at Milhostov meteorological station in the normal periods of NP1 1961–1990 and NP2 1991–2020.

Fig. 7 shows courses and trends of Vysocky index in the evaluated normal periods. It is clear, that in both periods potential evaporation exceeds precipitation while there is no significant trend shift. In NP1, 4 years were identified (1965, 1970, 1974 and 1980) in which precipitation exceeded ET_{pot}. In NP2 such situation occurred in two years (1998 and 2010).

The same is manifested in Fig. 8 which represents Climatic indicator of irrigation. In both normal periods, the same years were identified in which precipitation exceeded ET_{pot}.

The course of the hydrothermal coefficient, shown in Fig. 9, mostly moves within the interval 1.01–2.00. This is defined as water sufficiency. Although the values of hydrothermal coefficient in NP2 approach the lower boundary of the interval, they do not drop further. The years in which water sufficiency is most marked and the years in which precipitation exceeded potential evapotranspiration, are identical.

The analysis of Lang`s rain factor (Fig. 10) shows that in NP1 the prevailing values belong in the interval for humid climate area and the prevailing values in NP2 belong in the interval for intermediate climate area. The results obtained from data at Milhostov station were compared to the results from obtained from data at eight meteorological stations in the western part of Slovakia (Jarošová and Igaz, 2018). The station in Piešťany gave very similar results to those from Milhostov.

Fig. 11 shows the drought indices and their linear trends. NP1 gave a flat, slightly decreasing trend. Most values

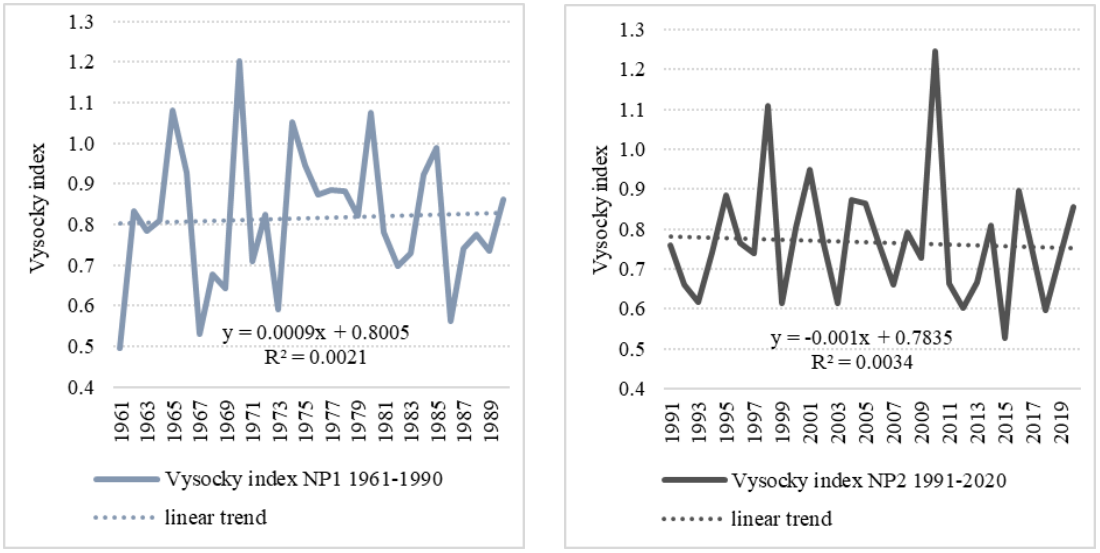

Fig. 7. Course of Vysocky index at Milhostov meteorological station in the evaluated normal periods NP1 1961–1990 and NP2 1991–2020.

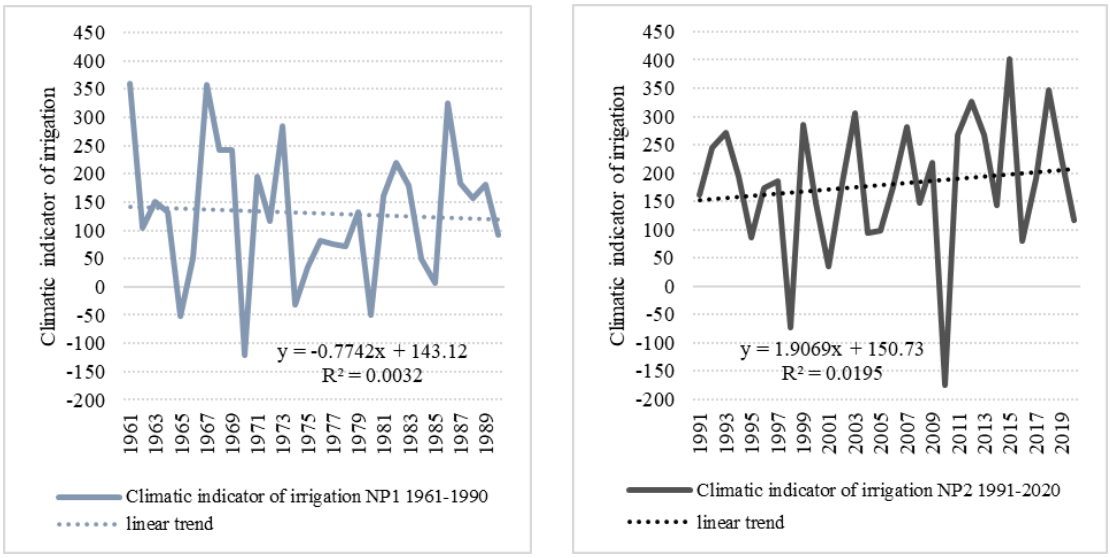

Fig. 8. Course of Climatic indicator of irrigation at Milhostov meteorological station in the evaluated normal periods NP1 1961–1990 and NP2 1991–2020.

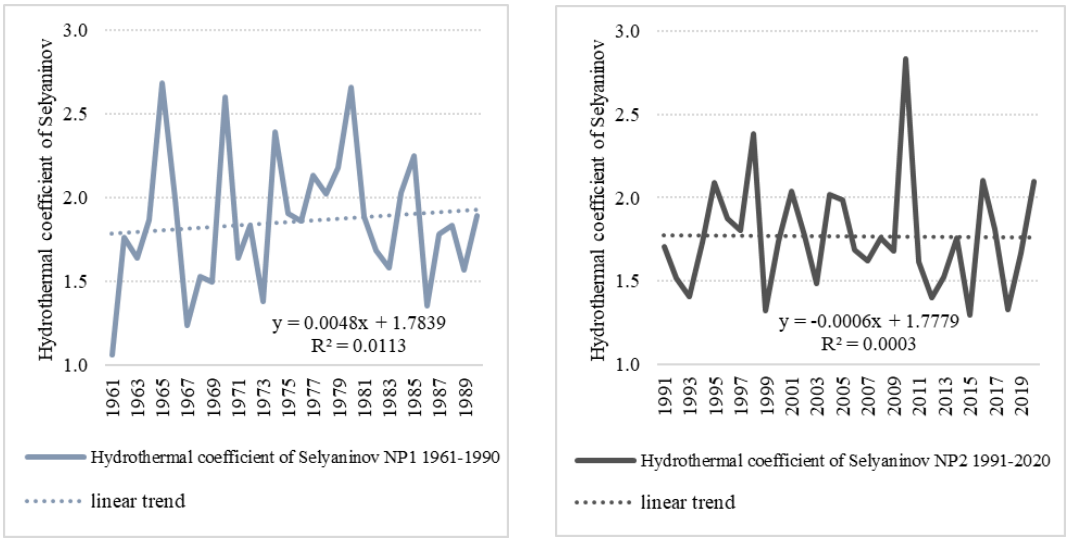

Fig. 9. Course of Hydrothermal coefficient of Selyaninov at Milhostov meteorological station in the evaluated normal periods NP1 1961–1990 and NP2 1991–2020.

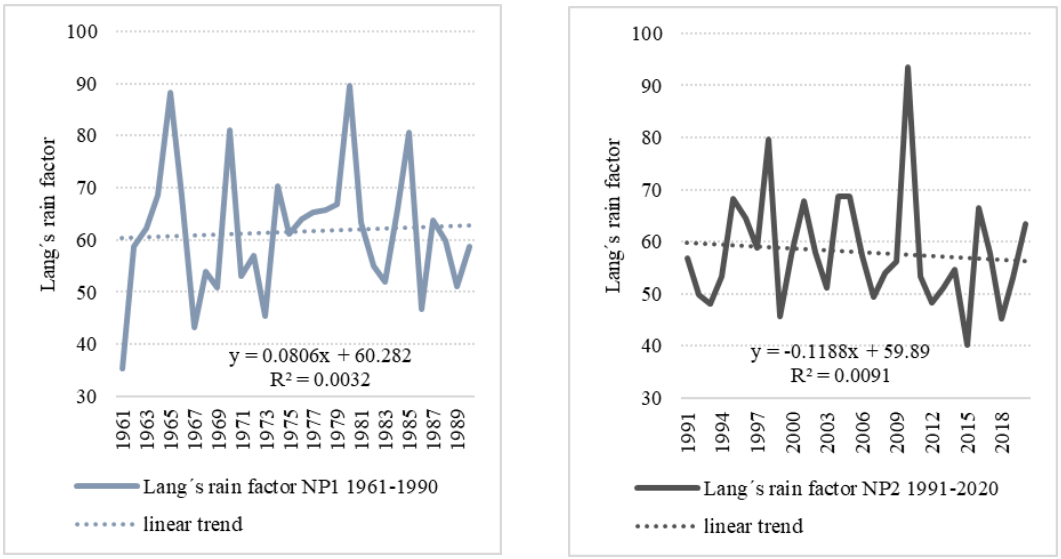

Fig. 10. Course of Lang´s rain factor at Milhostov meteorological station in the evaluated normal periods NP1 1961–1990 and NP2 1991–2020.

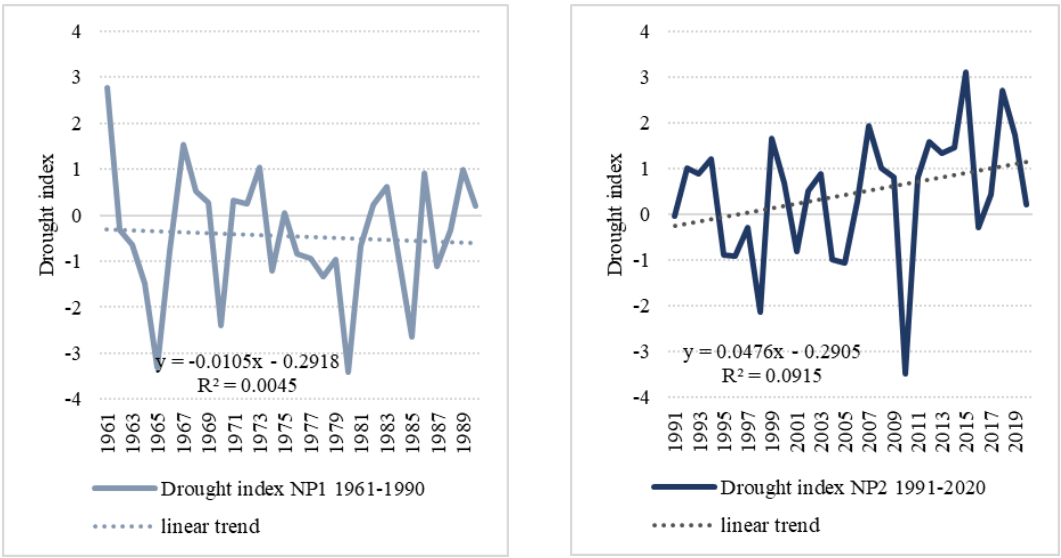

Fig. 11. Course of the Drought index at Milhostov meteorological station in the evaluated normal periods NP1 1961–1990 and NP2 1991–2020.

belong to the interval for moderately humid area and moderately arid area. In NP2, the values are similar, however, the trend is rising towards the values for arid areas. Extremely wet years are identical to those identified by previous analyses.

Fig. 12 shows the courses of PDSI. It is obvious that in NP2, there is a moderate trend towards drought. Dry years occurred mainly in the last years of NP2. Extremely dry years were identified in 1968, 2015 and 2019. Extremely wet years are identical to those identified by previous analyses, i.e., 1965, 1970, 1974, 1980, 1998 and 2010.

Table 8 represents a complex evaluation of both normal periods by drought indices and their trends. Overall results in all indices show that NP2 is drier than NP1.

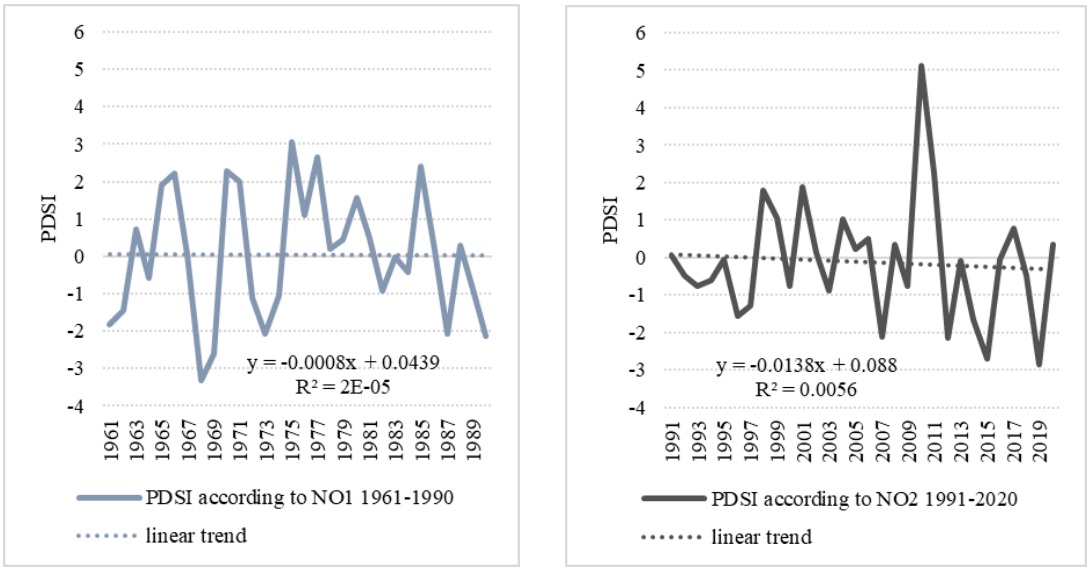

Fig. 12. Course of Palmer drought severity index at Milhostov meteorological station in the evaluated normal periods NP1 1961–1990 and NP2 1991–2020.

Table 8. Analysis of normal periods NP1 1961–1990 and NP2 1991–2020 as to drought indices and their trends at Milhostov meteorological station

Drought indicator	trend	NP1 1961–1990				trend	NP2 1991–2020				NP2 versus NP1
		description	avg	st. dev.	C_v		description	avg	st. dev.	C_v	
Vysocky index	slightly increasing	in most years evaporation predominates	**0.81**	0.17	0.21	slightly decreasing	in most years evaporation predomina-tes	**0.77**	0.15	0.20	**drier**
Climatic indicator of irrigation	slightly increasing	in most years evaporation predominates	**131.12**	119.75	0.91	increasing	in most years evaporation predomina-tes	**180.28**	120.27	0.67	**drier**
Hydrothermal coefficient of Selyaninov	increasing	sufficient water	**1.86**	0.40	0.21	decreasing	tends to normal /sufficient water	**1.77**	0.33	0.19	**drier**
Lang´s rain factor	increasing	intermediate / wet	**61.53**	12.50	0.20	slightly increasing	tends to drying	**58.05**	10.95	0.19	**drier**
Drought index	decreasing	dry / wet	**-0.45**	1.38	-3.03	increasing	tends to drying	**0.45**	1.39	3.10	**drier**
PDSI	slightly decreasing	tends to drying	**0.26**	2.27	8.73	slightly decreasing	tends to drying	**0.15**	2.19	14.60	**drier**

C_v – coefficient of variation

Conclusion

In the past years, the incidence of dry periods on the East Slovakian Lowland has increased. Dry periods are periods in which water availability from other water sources is below the statistical need for water in drought-stricken areas. From the social point of view, drought is understood as a period with stable, uncommonly dry weather, which is long enough for the lack of water to damage plant cover and cause serious problems in water supply. The magnitude of drought regarding its impact on the countryside depends on its duration, degree of moisture deficit and the size of affected area. In this sense, one of possible causes of drought are climatic changes. The work is based on the assumption that Earth's climate has been warming and therefore the drought incidence has been increasing. The aim of this work is to quantify differences in the climate at a particular location over two consecutive normal periods. For the purpose of the work, the normal periods defined are NP1 between the years 1961 and 1990 and NP2 between the years 1991 and 2020. Analysed meteorological parameters were measured at Milhostov meteorological station, which is in the central part of East Slovakian Lowland. The normal periods were analysed in terms of precipitation, temperature, potential evapotranspiration and selected drought indices. For the analysis of the normal periods, simple indices commonly used in the past were applied: Vysocky index, Climatic indicator of irrigation, Hydrothermal coefficient of Selyaninov, Lang`s rain factor, Drought index and Palmer drought severity index. All but PDSI are simple indices. Their calculation is based on precipitation, temperatures and potential evapotranspiration. The analysis of normal periods identified significant changes in temperatures and potential evapotranspiration. In NP2, the values of these parameters were annually and monthly higher. The linear trends of these parameters have the rising tendency. Contrary to this, the linear trends of annual precipitation totals were flat. The analysis of the normal periods in terms of the values and linear trends of drought indices shows that NP2 is drier than NP1. The trends in NP2 are approaching the drought limits.

Acknowledgement

This study was supported by the grant from the Slovak Academy of Sciences (project VEGA No. 2/0044/20). The authors thank the agency for its research support.

References

Allen, R. G., Pereira, L. S., Raes, D., Smith, M. (1998): Crop evapotranspiration - Guidelines for computing crop water requirements: FAO Irrigation and drainage paper 56. Rome: FAO, 1998. 301 p.

Almikaeel, W., Almeida, L. C., Čubanová, L., Šoltész, A., Mydla, J., Barolová, D. (2023): Understanding the impact of drought on Topľa River discharge seasonality Acta Hydrologica Slovaca, vol. 24, issue 1, 63–72

American Meteorological Society (2019): Glossary of Meteorology, http://glossary.ametsoc.org/.

Beran, M., Rodier, J. A. (1985): Hydrological aspects of drought. In: Studies and reports in hydrology, č. 39, 1985, 269–275. UNESCO-WMO, Paris, France.

Bonacci, O., Bonacci, D., Roje-Bonacci, T., Vrsalović, A. (2023): Proposal of a new method for drought analysis. Journal of Hydrology and Hydromechanics, vol.71, no.1, 2023, 100–110. https://doi.org/10.2478/johh-2022-0030

Brázdil, R., Raška, P., Trnka, M., Zahradníček, P., Valasek, H., Dobrovolny, P., Řezníčková, L., Tremi, P., Stachoň, Z. (2016): The Central European drought of 1947: causes and consequences, with particular reference to the Czech Lands. Clim Res 70: 161–178

Choudhary, A., Mahato, S., Roy, P. S., Pandey, D. N., Joshi, P. K. (2023): Analyzing the long-term variability and trend of aridity in India using non-parametric approach. Stoch Environ Res Risk Assess (2023). https://doi.org/10.1007/s00477-023-02483-4

Čimo, J., Igaz, D., Bárek, V. (2008): Bioklimatologické aspekty hodnocení procesů v krajině. Mikulov 9.–11. 9. 2008, ISBN 978-80-86690-55-1

Faško, P., Lapin, M., Šťastný, P. (2000): Maximum Daily Precipitation Totals in Slovakia in 1951–2000 Period. In: National climate Program of the Slovak Republic, vol. 9, 2000, 107–119.

Gomboš, M., Pavelková, D. (2009): Analýza meteorologického sucha v centrálnej časti východoslovenskej nížiny. Acta Hydrologica Slovaca, ISSN 1335-6291, 2009, roč. 10, č. 1, 69–74.

Haigh, T. R., Otkin, J. A., Woloszyn, M., Todey, D., Felkley, C. (2022a): Meeting the Drought Information Needs of Midwest Perennial Specialty Crop Producers. J. Appl. Meteor. Climatol., 61, 839–855, https://doi.org/10.1175/JAMC-D-21-0105.1.

Haigh, T., Wickham, E., Hamlin, S., Knutson, C. (2022b): Planning Strategies and Barriers to Achieving Local Drought Preparedness, Journal of the American Planning Association, DOI: 10.1080/01944363.2022.2071324

Hlavatá, H., Tomková, M. (2015): Analýza vývoja teploty vzduchu na stanici Michalovce v zimnom období počas rokov 1961 –2014. Acta Hydrologica Slovaca, ÚH SAV Bratislava, 2015, č.2, 153–159. (in Slovak)

Hološ, S., Šurda, P., Lichner, Ľ., Zvala, A., Píš, V. (2022): Fire-induced changes in soil properties depend on age and type of forests. Journal of Hydrology and Hydromechanics, vol. 70, no. 4, 2022, 442–449. https://doi.org/10.2478/johh-2022-0034

Jarošová, M., Igaz, D., (2018): Identifikácia výskytu sucha podľa rozličných indexov na staniciach západného Slovenska, Meteorologický časopis, 20, 2017, 73–82. (in Slovak)

Jůva, K. (1959): Závlaha půdy, Praha, SZN, s. 597. (in Czech)

Klementová, E. (1990): Hodnotenie vybraných oblastí indexom sucha. In: ZS VÚ II-5-6/0301.4, Bratislava KHM SvF 1990, 23 s. (in Slovak)

Klimatický atlas Slovenska. (2015): Climate atlas of Slovakia. Banská Bystrica: Slovenský hydrometeorologický ústav, 228 s. (in Slovak)

Kveták, Š. (1983b): Niektoré vzťahy medzi klimatickými prvkami vo vybraných lokalitách na Slovensku. Bratislava, ALFA 1983. 264 s. (in Slovak)

Kveták, Š. (1983a): Príspevok ku kontinentalite podnebia na Slovensku. Bratislava, ALFA 1983. 220 s. (in Slovak)

Li, T., Jeřábek, J., Winkler, J., Vaverková, M. D., Zumr, D. (2022): Effects of prescribed fire on topsoil properties: a small-scale straw burning experiment. Journal of Hydrology and Hydromechanics, vol. 70, no. 4, 2022,

450–461. https://doi.org/10.2478/johh-2022-0032
Litschmann, T., Klementová, E., Rožnovský, J. (2002): Vyhodnocení period sucha v časových řadách pražského Klementina a Hurbanova pomocí PDSI. XIV. Česko-slovenská bioklimatologická konference, Lednice na Moravě 2.–4. září 2002, ISBN 80-85813-99-8, 280–289. (in Czech)
Markovič, L., Faško, P., Pecho, J. (2021): Climatology of the extreme heavy precipitation events in Slovakia in the 1951–2020 period. In Acta Hydrologica Slovaca, vol. 22, no.2, pp. 294-303. 2644-6291 (printed until 2018). DOI: https://doi.org/10.31577/ahs-2021-0022.02.0033
Mikulová, K., Faško, P., Bochníček, O., Ondruška, P., Čepčeková, E., Šťastný, P., Pecho, J. (2008): Klimatické normály 1961–1990 meteorologických prvkov teploty vzduchu a atmosférických zrážok. Záverečná správa výskumnej úlohy. (in Slovak)
Morid, S., Smakhtin, V. U., Moghaddasi, M. (2006): Comparison of seven meteorological indices for drought monitoring in Iran. Int J Climatol 26: 971–985
Mukherjee, S., Mishra, A., Trenberth, K. E. (2018): Climate Change and Drought: a Perspective on Drought Indices. Curr Clim Change Rep 4, 145–163. https://doi.org/ 10.1007/s40641-018-0098-x
Novák, V. (1995): Výpočet potenciálnej evapotranspirácie homogénnych povrchov. In: Vyparovanie vody v prírode a metódy jeho určovania, 1995, 211–214. (in Slovak)
Palmer, W. C. (1965): Meteorological drought. In: Research Paper č. 45, 201–232. U.S. Department of Commerc Berau, Washington, D. C.
Pecho, J. (2016): Extrémne počasie, zmeny klímy a potravinová bezpečnosť, 2016, http://climatemap. blogspot.sk/ (in Slovak)
Pinheiro, G. E., Blanco, C. J. C. (2021): Daily rainfall estimates considering seasonality from a MODWT-ANN hybrid model. Journal of Hydrology and Hydromechanics, vol.69, no.1, 2021, 13–28. https://doi.org/10.2478/johh-2020-0043
Raikes, J., Smith, T. F., Jacobson, C., Baldwin, C. (2019): Pre-disaster planning and preparedness for floods and droughts: A systematic review. International Journal of Disaster Risk Reduction 38, 101207:101207, https://doi.org/10.1016/j.ijdrr.2019.101207
Rodný, M., Šurda, P. (2010): Stanovenie indexov meteorologického sucha a ich spojitosť s vodným režimom pôdy lokality Báč na Žitnom ostrove. In: Hydrologické dny 2010, 2010 Hradec Králové, ISBN 978-80-86690-84-1, Praha: Nakladatelství Český hydro-meteorologický ústav, 109–116. (in Slovak)
Soľáková, T., Zeleňáková, M., Mikita, V., Hlavatá, H., Simonová, D., Abd-Elhamid, H. (2022): Assessment of meteorological and hydrological drought using drought indices: SPI and SSI in eastern Slovakia. Acta Hydrologica Slovaca, vol. 23, issue 2, 267–272
Trnka, M., Balek, J., Šťepánek, P., Zahradníček, P., Mozny, M., Eitzinger, J., Zalud, Z. Formayer, H., Turna, M., Nejedlik, P., Semeradova, D., Hlavinka. P., Brázdil, R. (2016): Drought trends over part of Central Europe between 1961 and 2014. Clim Res 70: 143–160
Tsakiris, G., Pangalou, D., Vangelis, H. (2007): Regional Drought Assessment Based on the Reconnaissance Drought Index (RDI). Water Resour Manage 21, 821–833. https://doi.org/10.1007/s11269-006-9105-4
Wilhite, D. A., Glantz, M. H. (1985): Understanding the drought phenomenon: the role of definitions. Water Int 10: 111−120
Wilhite, D. A. (2016): Introduction: Managing drought risk in a changing climate. Climate Research 70:99, https://doi.org/10.3354/cr01430
WMO (1935): World Meteorological Organization (wmo.int), (1935)
WMO (2021): Updated 30-year reference period reflects changing climate https://public.wmo.int/en/media/news/ updated-30-year-reference-period-reflects-changing-climate, (2021).
Yevjevich, V. (1967): An objective approach to definition and investigations of continental hydrologic droughts. In: Hydrology papers, 1967, no. 23, Colorado State University, Fort Collins, USA.

Ing. Dana Pavelková, PhD. (*corresponding author, e-mail: pavelkova@uh.savba.sk)
Ing. Branislav Kandra, PhD.
RNDr. Andrej Tall, PhD.
Ing. Milan Gomboš, CSc.
Institute of Hydrology SAS
Dúbravská cesta 9
841 04 Bratislava
Slovak Republic

Ing. Helena Hlavatá, PhD.
Slovak Hydrometeorological Institute
Regional Office Košice
Ďumbierska 26
041 17 Košice
Slovak Republic

DOI: 10.31577/ahs-2023-0024.02.0026

ACTA HYDROLOGICA SLOVACA

Volume 24, No. 2, 2023, 232 – 241

Challenges in selecting the new reference period for long-term hydrological characteristics in Slovakia

Lotta BLAŠKOVIČOVÁ*, Katarína JENEIOVÁ, Katarína KOTRÍKOVÁ, Ľubica LOVÁSOVÁ, Katarína MELOVÁ, Soňa LIOVÁ

Establishment of a new reference period is an ongoing topic in Slovakia as the currently used reference period is 1961–2000. This contribution focuses on the assessment of spatial and temporal changes in the mean long-term yearly discharges and long-term mean monthly discharges at 140 water-gauging stations. The years 2021 and 2022 have been further evaluated at selected 13 water-gauging stations to assess the possible impacts of using different reference periods (1991–2020, 1981–2020, 1971–2020 and 1961–2000) on the water management. The analyses have confirmed that there are significant changes between long-term values, especially for the period 1991–2020 compared with the reference period 1961–2000, with the highest negative changes in monthly discharges being in April and highest positive changes being in January. Evaluation of mean monthly and annual discharges in 2021 and 2022 for 13 selected water-gauging stations, according to the four above mentioned reference periods, has identified changes especially in set categories of monthly discharges. The same average monthly but also annual flows in one station have fallen into different assessment categories, in several cases. For annual flows the changes have manifested in 6 water-gauging stations in the year 2021 and 2 stations in the year 2022. The number of stations with changes in categories between different reference periods used for particular months have varied from 2 to 8 water-gauging stations in 2021 (62 cases for the whole year) and from 2 to 6 water-gauging stations in 2022 (40 cases for the whole year). The highest number of changes for both years were detected in June (14) and August and December (11). The selection of the reference period can therefore lead into different set of applied water management rules.

KEY WORDS: reference period, design values, mean monthly discharges, annual discharges

Introduction

As the climate change effects are becoming more pronounced, an understanding of spatial and temporal distribution of water resources is crucial for adaptation, management and mitigation of the effects of extreme hydrological situations.

Until the end of 2020, the most current and widely used standard reference period for calculating climate normal was the 30-year period 1981–2010. Recently the World Meteorological Organisation (WMO, 2020) recommends a 30-year period 1991–2020 for the purpose of the comparison of the hydrological and climatic characteristics. However, for the purposes of historical comparison and climate change monitoring, WMO recommends the 1961–1990 period for the computation and tracking global climate anomalies relative to a fixed and common reference period.

In the water management of Slovakia, the reference period 1961–2000 is currently valid in decision-making and hydrological regime evaluation (Šipikalová, 2005). However, various changes of hydrological regime were described in recent studies (Pekárová et al., 2017; Fendeková et al., 2018; Ďurigová and Hlavčová, 2020; Halmová et al., 2022; Poórová et al., 2023). Establishment of a new reference period is a sensitive topic, as the hydrological design values based on this reference period, are a vital part of many decision-making processes (e.g., flood protection, hydrological drought management, water use permits, etc.). Therefore a significant change in these limit values can start a cascade effect of changes in the water management, where the societal and economical effects are yet to be addressed.

This contribution focuses on the assessment of spatial and temporal changes in the mean long-term yearly discharges and long-term mean monthly discharges for the purpose of the establishment of a new reference period in Slovakia. The recent years 2021 and 2022 have been evaluated in comparison with selected reference periods 1991–2020, 1981–2020, 1971–2020 and 1961–2000, at selected water gauging stations to assess the possible impacts on the water management.

Material and methods

In Slovakia, the currently used 40-year long reference period (1961–2000) was preceded by a 50-year reference period 1931–1980 and the 30-year period 1931–1960. Therefore, we have focused on the comparison of 30-, 40- and 50-year long periods (1991–2020, 1981–2020, 1971–2020) with the reference period 1961–2000.

For the analysis, we have selected 140 mainly near natural water-gauging stations (WS) (WS with affected regime by the human influence are marked in the results, if relevant), with sufficiently long observation period (covering all analysed periods) (Fig. 1). WS are representing the main sub-basins in Slovakia: Morava (Slovak part only), Danube, Váh (assessed separately for sub-catchments with different regimes: Váh, Nitra and Malý Dunaj), Hron, Ipeľ, Slaná, Bodva, Hornád, Bodrog and Poprad (including Dunajec).

The long-term mean discharges and mean monthly discharges were computed for all three above-mentioned periods and compared with the long-term values of currently used reference period 1961–2000. We have used the hydrological years, i.e. from November to October.

The long-term values of all 4 periods have been also used for the classification of mean yearly discharges and mean monthly discharges for 2021 and 2022 in 13 selected WS in Váh sub-catchment, to see the differences in results by using different reference periods (Fig. 1).

Results

Mean long-term discharges (Q_a)

The % deviations of the mean long-term discharges (ΔQ_a [%]) for selected periods, from the values of the reference period, have differed in individual sub-catchments of Slovakia. However, the stations with the decrease of Q_a in all three periods (1971–2020, 1981–2020, 1991–2020) were prevailing compared with $Q_{a,1961\text{-}2000}$. Positive deviations have been observed mostly in the sub-basin of Poprad and Dunajec, as well as in the upper parts of sub-basins Váh and Hornád (Fig. 2). Comparing the changes in the three periods from

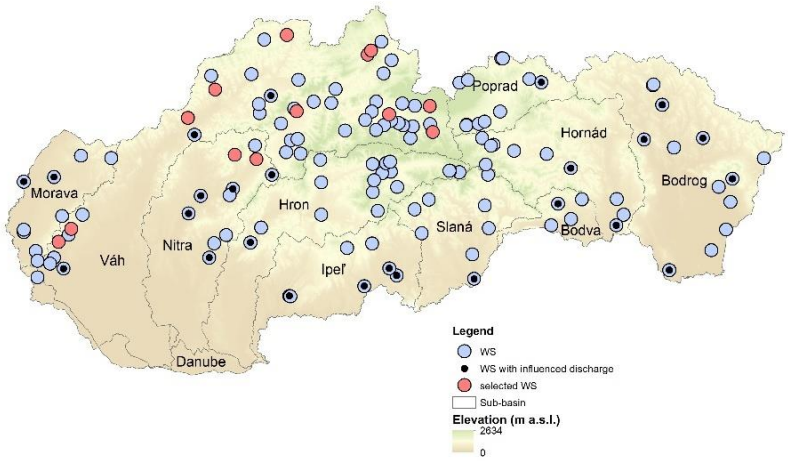

Fig. 1. Location of WS used in analysis, with marked WS with influenced discharge and selected 13 stations used for further analysis.

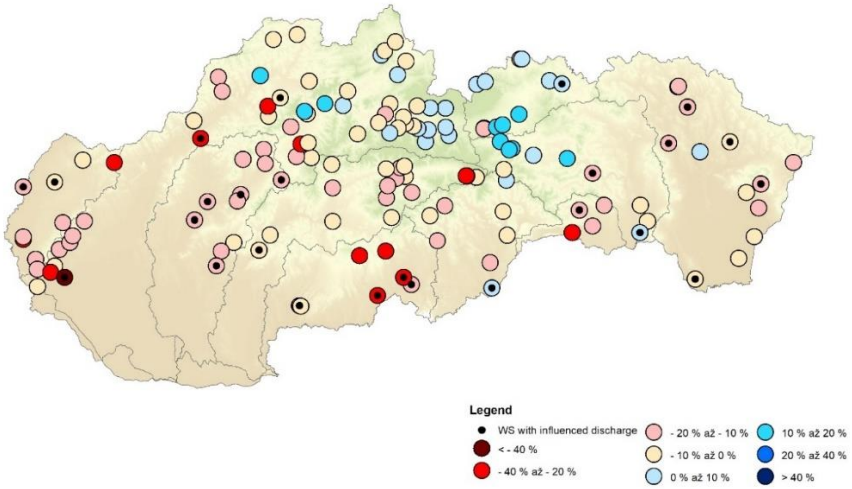

Fig. 2. Deviations [%] of mean long-term discharges for period 1991–2020 compared with reference period 1961–2000.

the period 1971–2020 to 1981–2020 toward period 1991–2020, the extremality of deviations of Q_a is in many cases increasing, both in positive and negative values. According to the average values of ΔQ_a [%] for individual sub-basins, most negative values for period 1991–2020 have been shown in sub-basins Bodva (-19.0%), Ipeľ (-17.8%), Morava (-14.9%) and sub-catchments of lower part of Váh sub-basin: Malý Dunaj (16.8%) and Nitra (-14.5%).

This can be seen also in the average values of ΔQ_a [%] for Slovakia. The values of average deviations are negative for all three evaluated periods, with higher magnitudes in two later periods ($\Delta Q_{a,1971\text{-}2020}$: -5.1%, $\Delta Q_{a,1981\text{-}2020}$: -7.9%, $\Delta Q_{a,1991\text{-}2020}$: -7.3%); in medians the changes are even higher (-5.2%; -8.4%; -8.6%). However, these values do not adequately describe the situation, as in all three periods the deviations in the individual sub-basins and water-gauging stations vary considerably both in positive and negative directions (Fig. 3) (minimum -34.9 % (Hosťovce – Bodva, sub-basin Bodva, period 1981-2020), maximum +19.5 % (Kežmarok – Ľubica, sub-basin Poprad and Dunajec, period 1991–2020).

Mean monthly discharges (Q_{ma})

The variability of the deviations of the mean long-term monthly discharges ΔQ_{ma} [%] in all three periods is much wider than for Q_a. The mean values of the deviations vary in the particular months, with largest magnitudes for most months in the period 1991–2020 and less for the period 1971–2020. The most extreme average deviations can be seen in April (negative deviation: -14.9%) and in January (positive deviation: +6.1%), both for period 1991–2020 (Table 1).

Extreme values for individual WS vary from -59.4% (August, 1991–2020, WS in sub-catchment of Malý Dunaj in Váh sub-basin) to +103.5% (September, 1991–2020, WS in Morava sub-basin).

Looking at the boxplot of the deviations for period 1991–2020 (Fig. 4), we can state, that the months with prevailing WS with negative deviations are December, April, May, June, July, August and October, while months with prevailing WS with positive deviations are November, January, February and September. March is the month with the least changes in Q_{ma} on average.

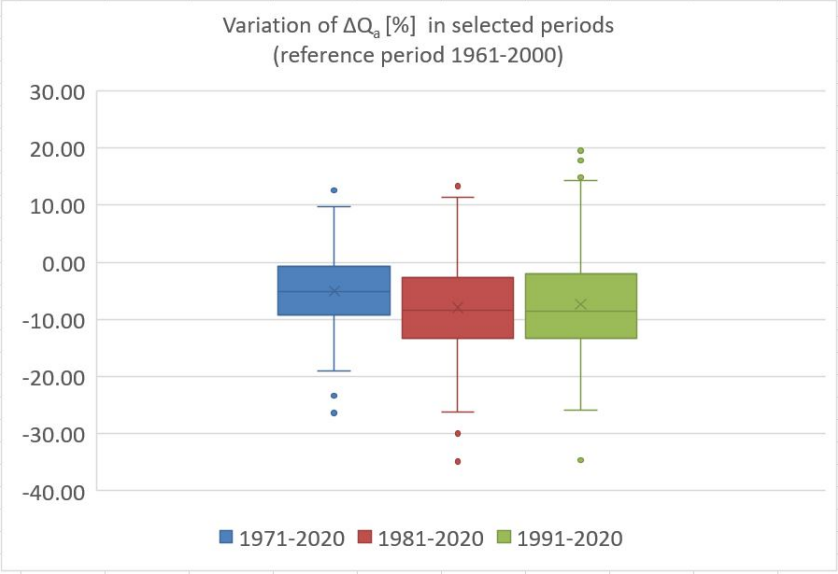

Fig. 3. Variations of ΔQ_a [%] of periods 1971–2020, 1981–2020 and 1991–2020 compared with reference period 1961–2000.

Table 1. Average deviations of mean long-term monthly discharges in the periods 1971–2020, 1981–2020 and 1991–2020 from the values of the reference period 1961–2000

ΔQ_{ma} [%] = $(Q_{ma,obd} - Q_{ma,ref})*100/Q_{ma,ref}$ - average for SR

Period	11	12	1	2	3	4	5	6	7	8	9	10	Q_a
1971–2020	-4.7	-4.3	5.5	1.7	-3.4	-13.1	-4.6	-8.2	-6.8	-4.4	1.6	-1.5	-5.1
1981–2020	-5.6	-9.9	3.3	-3.4	-2.8	-14.6	-7.9	-9.8	-10.4	-7.8	1.4	-12.5	-7.9
1991–2020	0.1	-9.3	6.1	2.0	-1.8	-14.9	-13.9	-13.8	-6.5	-5.4	3.8	-7.1	-7.3

The results show, that the month with the most negative changes of $Q_{ma,1991-2020}$, in the terms of frequency of the occurrence of negative deviations from the reference period among the WS, is April. This is clearly visible also on Fig. 5.

The negative deviations in this month are present in the majority of the WS, with the exception of several WS in the north of Slovakia (High Tatras region), in the upper parts of the sub-basins of Poprad and Váh. The negative deviations with higher magnitudes occur mostly in southern half of the Slovak territory. Assessing the individual sub-basins, the worst situation in terms of negative deviations in prevailing number of WS and the magnitudes of the deviations for April, is in sub-basins of Morava, Ipeľ, Bodva, and Nitra and Malý Dunaj (sub-catchments of Váh). The average of deviations in these sub-basins are as follows: -30.1% (Malý Dunaj), -29.1% (Bodva), -27.7% (Ipeľ), -22.5% (Morava), -19.5% (Nitra). The situation is similar in May.

Positive changes have been observed mostly in January, and also in September. The higher magnitudes of ΔQ_{ma} [%] in January can be seen mainly in the mountainous areas (Fig. 6). This is connected with the phenomena of the earlier snowmelt at the beginning of the year, as one of the consequences of the climate change. In the Poprad River basin (High Tatras region), the higher positive magnitudes of ΔQ_{ma} [%] are shifted to February.

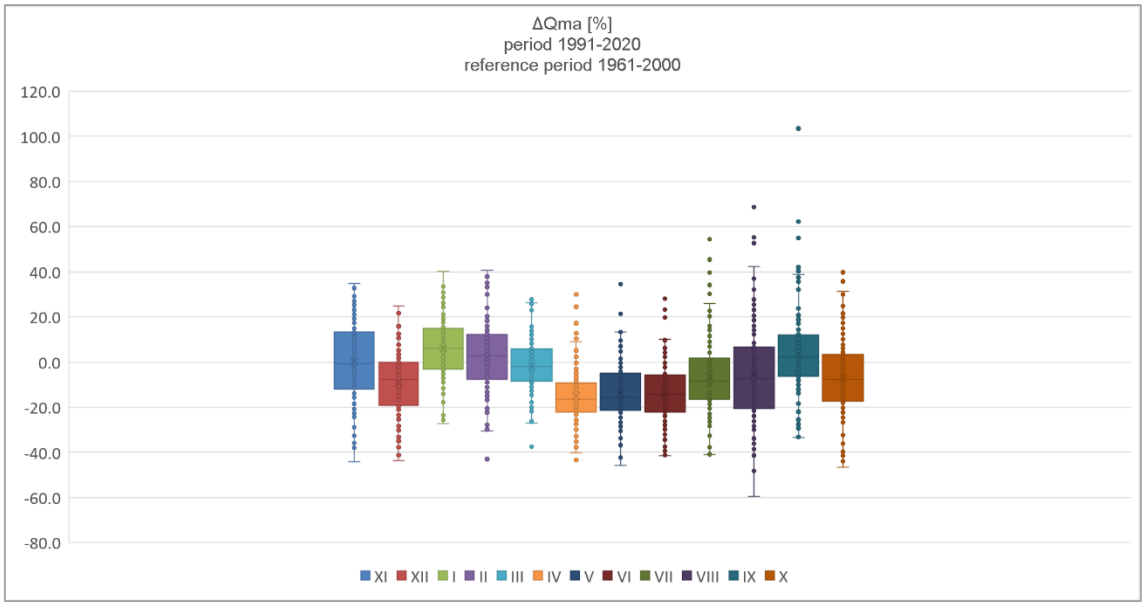

Fig. 4. ΔQ_{ma} [%] of period 1991–2020 compared with reference period 1961–2000.

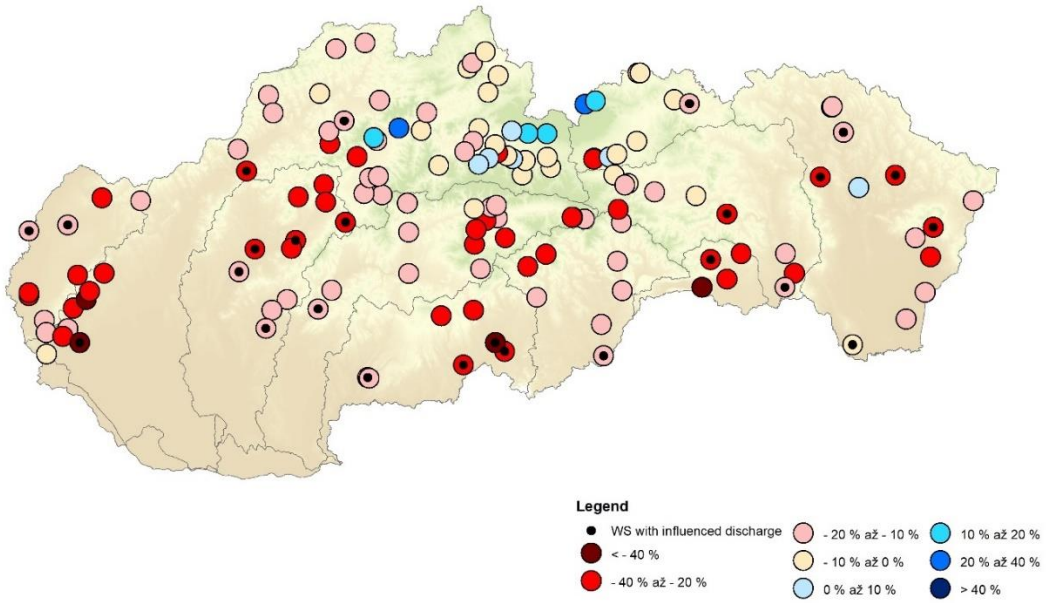

Fig. 5. ΔQ_{ma} [%] in April for period 1991–2020 compared with reference period 1961–2000.

Situation in the individual sub-basins

The situation vary between particular sub-basins, and also among WS inside individual sub-basins. Especially for larger sub-basins, the deviations in WS can vary significantly, according to different hydrogeological and morphological conditions in upper and lower parts of the basins. In the sub-basins, where the most significant negative deviations of Q_a have been identified, the prevailing number of the months of the year is with negative values of ΔQ_{ma} [%] as well. This can be seen on Table 2, where the median values of ΔQ_{ma} [%] for individual sub-basins are listed. The Nitra sub-catchment is the only one, where the medians of ΔQ_{ma} [%] are negative in all months of the year, with greatest magnitudes in December (-25.1%) and then in April, May, June, and August (around -20%). The other sub-basins with more or equal than 10 months of the year with negative medians of ΔQ_{ma} [%] are Morava, Bodva, Ipeľ and sub-catchment Malý Dunaj.

The highest magnitudes of negative deviations (median values for sub-basin) have been identified in Ipeľ sub-basin (-33.2% in May for period 1991–2020) (Fig. 7). There are visible increases of the magnitudes of median deviations among the three consecutive periods in April and May. However, comparing the values of medians of ΔQ_{ma} for all three periods we can see the changes in months August and September, where the negligible values (less than 1%) in period 1971–2020 were replaced by negative values in period 1981–2020 (-4.0%, -7.9%), and then by positive values in period 1991–2020 (+10.1%; +3.0%).

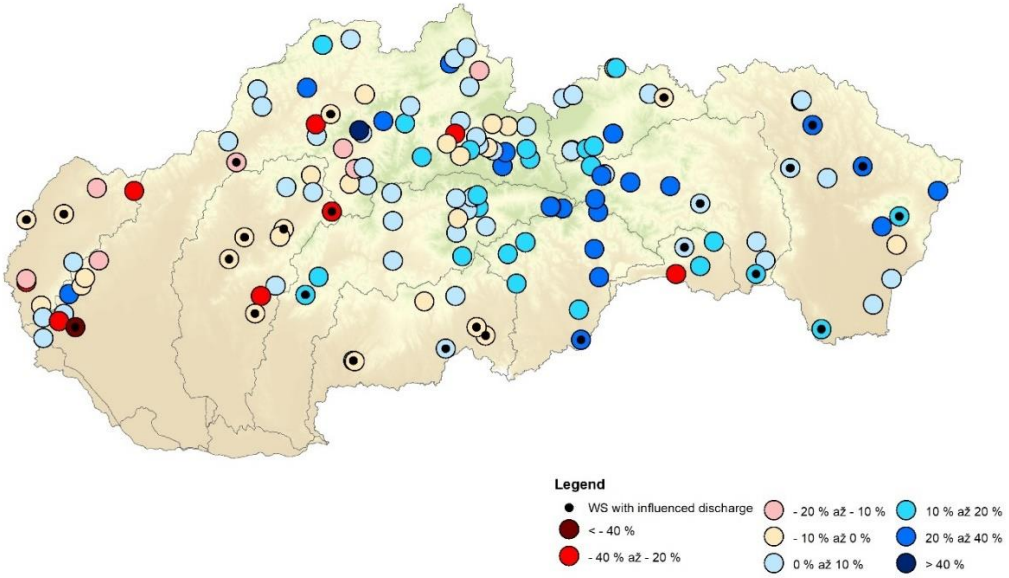

Fig. 6. ΔQ_{ma} [%] in January for period 1991–2020 compared with reference period 1961–2000.

Table 2. ΔQ_{ma} [%] for period 1991–2020 vs reference period 1961–2000 – median values for sub-basins

ΔQ_{ma} [%] = $(Q_{ma,1991-2020} - Q_{ma,1961-2000})*100/Q_{ma,1961-2000}$ - median													
Sub-basin	11	12	1	2	3	4	5	6	7	8	9	10	Q_a
P	18.6	-3.2	6.6	13.9	6.2	-0.4	5.1	0.9	11.6	-2.9	13.6	10.2	5.2
M	-4.7	-23.2	-9.9	-15.8	-3.4	-20.7	-18.5	-22.9	-18.1	-21.2	8.1	9.9	-13.8
D	-4.2	-10.5	6.6	-6.1	3.9	-12.1	-14.2	-14.1	-13.1	-8.0	24.2	3.0	-6.8
V	6.1	-9.8	3.9	7.9	3.8	-9.9	-11.9	-15.1	-3.7	-9.4	1.0	-3.2	-4.1
N	-9.6	-25.1	-6.1	-10.1	-9.7	-20.2	-19.8	-20.5	-16.6	-20.0	-2.8	-5.3	-13.6
MD	-15.7	-15.9	-3.0	-11.3	-3.4	-29.1	-25.3	-16.9	-22.3	-20.3	9.0	8.9	-14.3
R	-4.6	-4.1	9.3	2.3	-1.5	-17.3	-24.2	-20.9	-6.4	6.3	-0.6	-17.1	-9.7
I	-21.7	-13.6	-0.6	-12.7	-17.9	-28.8	-33.2	-12.9	-8.6	10.1	3.0	-24.6	-21.0
S	-2.2	0.5	21.7	1.6	-5.6	-17.1	-19.2	-4.6	-7.7	16.0	8.5	-18.2	-7.9
A	-13.2	-12.2	11.2	-15.0	-8.6	-26.9	-22.4	-9.8	-19.3	-15.7	-16.6	-21.5	-15.4
H	18.3	13.3	13.1	9.3	4.6	-15.0	-7.9	-2.3	21.6	21.3	19.1	2.1	5.0
B	3.4	-8.0	13.2	7.3	-7.3	-19.0	-7.8	-14.2	-23.7	-17.3	-17.6	-17.2	-9.7

LEGEND of sub-basins/sub-catchments: P-Poprad, M-Morava, D-Danube, V-Váh, N-Nitra, MD-Malý Dunaj, R-Hron, I-Ipeľ, S-Slaná, A-Bodva, H-Hornád, B-Bodrog

The sub-basin with most positive changes in Q_{ma} identified is Poprad (including Dunajec), Fig. 8. The highest positive medians of ΔQ_{ma} can be seen in November, February and September, however, positive deviations are also in January, May, July and October. In December we can see the change of the positive value in the period 1971-2020 (+2.2%), small negative magnitude in period 1981-2020 (-0.5%) to negative deviation -3.2%. Other months with negative medians of ΔQ_{ma} are April and August, however in April there is visible decreasing of the negative magnitude towards the third period (-7.1%; -5.5%; -0.4%). This is the opposite trend in April compared to most of the other sub-basins. Another change from negative value to positive shows in June, however the magnitudes are not significant.

Danube River itself presents a different hydrological regime than the rest of Slovak streams, as the majority of the waters of this significantly bigger river does not originate from Slovak territory. However, we have noticed changes also on this river (Fig. 9). Negative changes we can see in the deviations of Q_a in all 3 periods (-2.3%; -1.8%; -2.4%). Negative changes in Q_{ma} are visible in months December and April to August, with highest magnitude in July (-8.3%; -11.7%; -13.3%). Positive deviations have been identified in November, January, March, September and October, being highest in January (+8.3%; +11.1%; +9.6%).

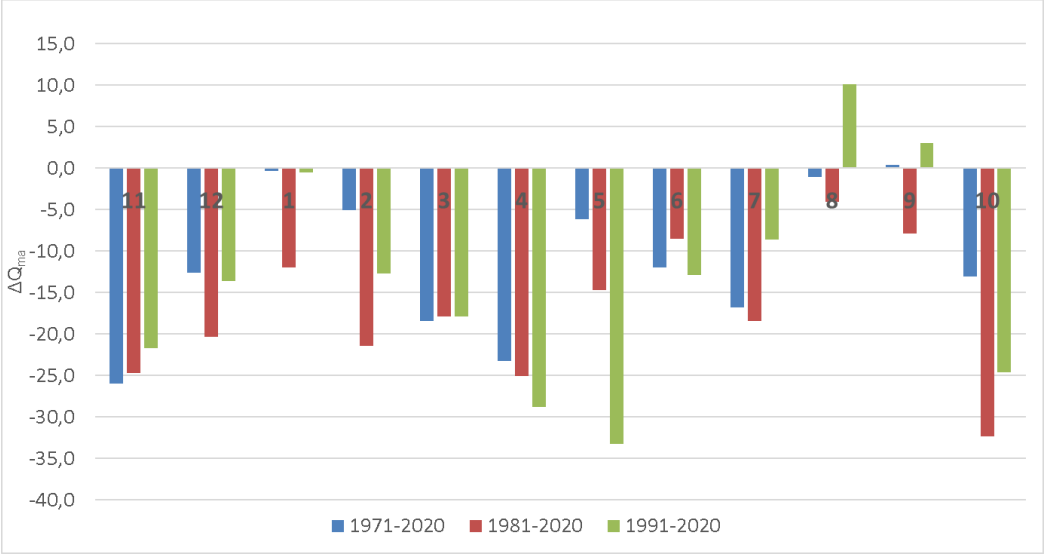

Fig. 7. Median values of ΔQ_{ma} for periods 1971–2020, 1981–2020 and 1991–2020 compared with reference period 1961–2000, sub-basin Ipeľ.

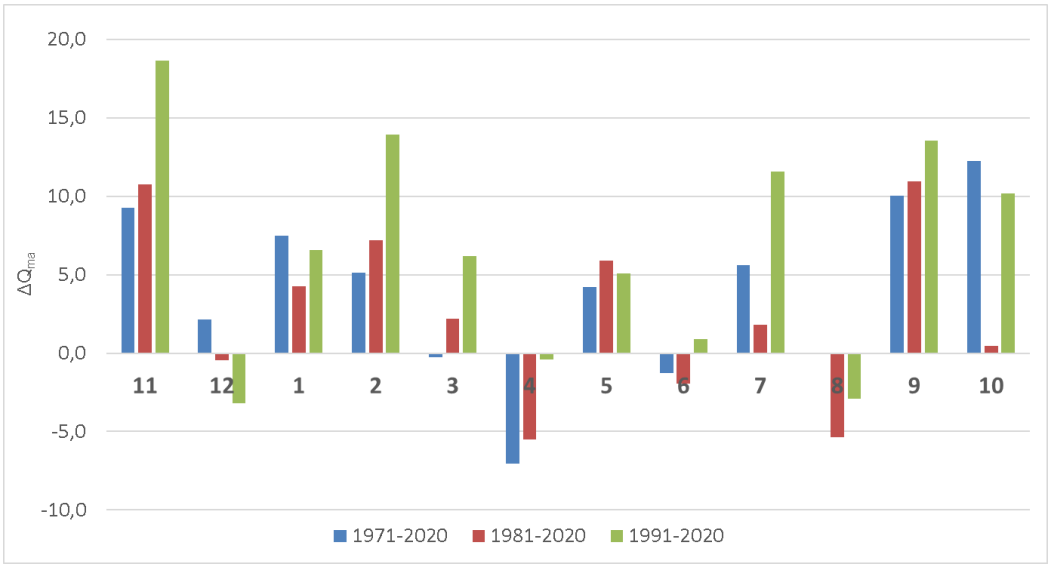

Fig. 8. Median values of ΔQ_{ma} for periods 1971–2020, 1981–2020 and 1991–2020 compared with reference period 1961–2000, sub-basin Poprad.

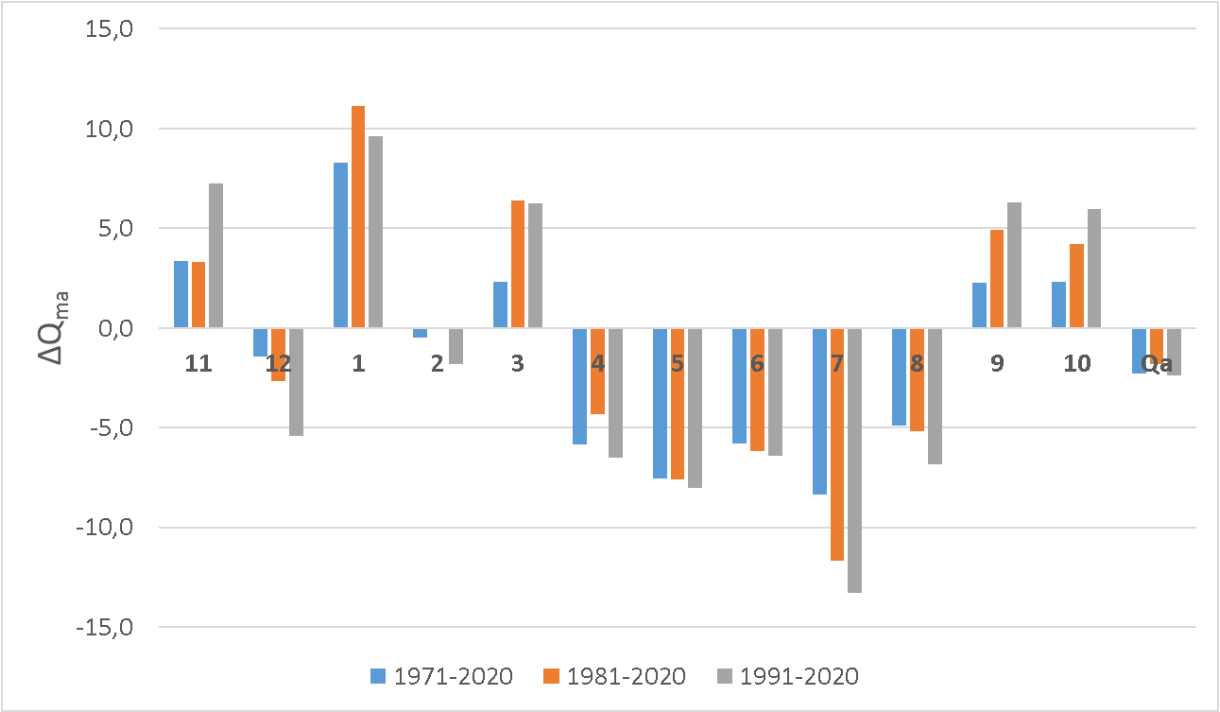

Fig. 9. ΔQ_{ma} and ΔQ_a for periods 1971–2020, 1981–2020 and 1991–2020 compared with reference period 1961–2000, WS Bratislava – Danube.

Assessment of the selected WS in 2021 and 2022

We have evaluated mean monthly discharges (Q_m) and mean yearly discharges (Q_r) in 13 selected WS in the sub-basins of Váh River basin (including sub-catchments Malý Dunaj and Nitra) for calendar years 2021 and 2022. These years have been chosen as two hydrologically different years (2021 being normal and 2022 being dry in average runoff in Slovakia). The values of Q_r and Q_{ma} have been assessed according to four reference periods: 1961–2000, 1971–2020, 1981–2020 and 1991–2020.

The Q_r values (Table 3) in the evaluated WS in 2021 ranged from normal, subnormal to dry year categories. Q_r in two WS (Dohňany – Biela Voda, Horné Sŕnie - Vlára) in the middle part of the Váh sub-basin were assessed as dry year when comparing Q_r with the long-term values of Q_a for reference period 1961–2000, for other reference periods, the Q_r in these WS was assessed as subnormal. In three WS (Pezinok – Blatina, Píla - Gidra, Nedožery - Nitra) in the lower part of the sub-basin and in one WS in the upper part of sub-basin (Čierny Váh - Ipoltica), a difference in a placement into a category was detected, when Q_r values were evaluated according to reference period 1961–2000 (subnormal year) and reference periods 1981–2020 and 1991–2020 (in one case also 1971–2020) (normal year). The assessment in six WS (Podbanské - Belá, Liptovský Mikuláš - Váh, Lokca - Biela Orava, Oravská Jasenica - Veselianka, Martin - Turiec, Čadca - Kysuca) was in the same categories for all reference periods (normal/subnormal years).

The Q_r values in 2022 were at the level of the normal, subnormal, dry and very dry year categories, while the values of Q_r in dry to very dry year categories were classified in WSs mainly in the lower half of the Váh sub-basin, including WS on Kysuca. Changes of categories within one WS according to different reference periods were manifested only in two WS (Martin - Turiec, Liešťany - Nitrica).

The assessment of Q_m has shown bigger differences between categories related to particular reference periods. The number of stations with changes in categories between different reference periods used for particular months vary from two to eight WS in 2021 (62 cases for the whole year) and from two to six in 2022 (40 cases for the whole year). The months with highest number of such cases for both years is June (14) and August and December (11). Generally, more cases were in the less dry year 2021. The example of difference in years for the month July, which was dry for both evaluated years, is shown in Table 4; however, it was more significantly dry in 2022. There is one case in 2021 in WS in lower part of the Váh sub-basin (Pezinok - Blatina) where, according to the reference period used, there are 3 categories of the assessment of the month: from dry (ref. period 1961–2000), significantly sub-normal (ref. periods 1981–2020 and 1991–2020) to sub-normal month (ref. period1971-2020). There are changes in categories in seven WSs (Podbanské - Belá, Martin - Turiec, Čadca - Kysuca, Dohňany - Biela Voda, Nedožery - Nitra, Liešťany - Nitrica, Pezinok - Blatina) in 2021, but only two cases (Nedožery - Nitra, Liešťany - Nitrica) in 2022.

Less number of changes in categories was found in January (four cases for both years), March (6) and

September (5). January was relatively wet in both years in the majority of WS and we can see quite uniform results for individual WSs (two cases of the changes in categories per year) (Table 5).

The most extreme deviations of % values of Q_m evaluated according to reference periods 1971–2020, 1981–2020 and 1991–2020, from the values of reference period 1961–2020, have been identified as follows: the negative deviations with highest magnitudes occurred mostly in January and February (about -50%, mainly in the upper part of the sub-basin), the positive deviations appeared mainly in the lower half of the sub-basin (up to +129% in 2021). Comparing the three reference periods, the most extreme values of % deviations have been identified in the period 1991–2020.

Table 3. Assessment of Q_r in 2021 and 2022 according to four reference periods

WS	Čierny Váh - Ipoltica	Podbanské - Belá	L. Mikuláš - Váh	Lokca - Biela Orava	Or. Jasenica - Veselianka	Martin - Turiec	Čadca - Kysuca	Dohňany - Biela Voda	Horné Srnie - Vlára	Nedožery - Nitra	Liešťany - Nitrica	Pezinok - Blatina	Píla - Gidra
ref. period	2021												
1961–2000	89.8	99.3	99.0	82.8	75.8	91.4	79.0	69.7	69.3	82.7	96.0	84.4	81.2
1971–2020	90.0	97.0	100.0	81.3	76.3	94.2	81.5	75.4	72.4	89.5	104.4	101.8	88.4
1981–2020	92.4	98.6	102.0	83.0	78.3	95.4	83.0	77.2	72.7	91.7	107.8	102.2	90.3
1991–2020	88.4	96.4	99.4	80.4	79.0	93.6	83.6	79.7	74.2	94.1	109.4	95.2	90.9
	2022												
1961–2000	67.8	92.8	78.9	98.9	85.5	68.7	65.9	45.3	36.8	53.9	61.8	16.0	25.5
1971–2020	67.9	90.7	79.7	97.2	86.1	70.8	67.9	49.0	38.5	58.3	67.2	19.3	27.8
1981–2020	69.8	92.2	81.3	99.1	88.3	71.7	69.2	50.2	38.6	59.7	69.4	19.4	28.4
1991–2020	66.7	90.1	79.2	96.1	89.1	70.3	69.7	51.8	39.4	61.3	70.4	18.0	28.5

LEGEND

$Q_r / Q_{a,ref}$ [%]	Category of the year
0 – 40	very dry
40 – 70	dry
70 – 90	sub-normal
90 – 110	normal
110 – 130	above normal
130 – 160	wet
> 160	very wet

Table 4. Assessment of $Q_{m,VII}$ in 2021 and 2022 according to 4 reference periods

WS	Čierny Váh - Ipoltica	Podbanské - Belá	L. Mikuláš - Váh	Lokca - Biela Orava	Or. Jasenica - Veselianka	Martin - Turiec	Čadca - Kysuca	Dohňany - Biela Voda	Horné Srnie - Vlára	Nedožery - Nitra	Liešťany - Nitrica	Pezinok - Blatina	Píla - Gidra
ref. period	2021												
1961–2000	56.4	56.6	63.7	31.3	20.2	56.9	17.9	19.4	23.4	78.4	129.7	39.5	40.4
1971–2020	53.9	57.5	64.1	34.0	22.5	61.4	21.1	23.7	27.6	92.0	151.8	60.7	48.1
1981–2020	55.0	61.4	65.9	35.4	23.4	61.2	22.4	26.5	30.0	96.6	160.4	57.9	50.3
1991–2020	50.4	60.0	62.2	33.4	22.2	58.3	21.2	26.8	28.0	97.9	155.5	47.0	47.3
	2022												
1961–2000	33.3	40.4	35.5	22.1	21.5	36.5	21.3	11.6	7.0	38.6	39.1	3.4	16.1
1971–2020	31.8	41.0	35.7	24.0	24.0	39.4	25.0	14.2	8.2	45.3	45.8	5.2	19.1
1981–2020	32.4	43.8	36.7	25.0	24.9	39.2	26.5	15.8	9.0	47.6	48.4	5.0	20.0
1991–2020	29.7	42.8	34.6	23.6	23.7	37.4	25.1	16.0	8.3	48.2	46.9	4.1	18.8

LEGEND

$Q_m / Q_{ma,ref}$ [%]	Category of the month
0 – 20	extremely dry
20 – 40	dry
40 – 60	significantly sub-normal
60 – 80	sub-normal
80 – 120	normal
120 – 160	above normal
160 – 200	significantly above normal
> 200	extremely wet

Table 5. Assessment of $Q_{m,I}$ in 2021 and 2022 according to 4 reference periods

WS	Čierny Váh - Ipoltica	Podbanské - Belá	L. Mikuláš - Váh	Lokca - Biela Orava	Or. Jasenica - Veselianka	Martin - Turiec	Čadca - Kysuca	Dohňany - Biela Voda	Horné Sŕnie - Vlára	Nedožery - Nitra	Liešťany - Nitrica	Pezinok - Blatina	Píla - Gidra
ref. period	2021												
1961–2000	125.9	117.3	131.4	108.2	80.6	182.6	113.4	132.8	182.9	152.4	187.0	252.9	188.5
1971–2020	116.0	114.0	122.9	91.7	72.4	166.6	101.5	122.0	174.5	148.0	181.3	229.4	185.7
1981–2020	116.7	113.0	124.2	92.3	73.1	169.1	104.6	123.2	176.4	148.3	184.3	223.1	186.2
1991–2020	109.1	111.8	120.4	88.9	74.4	166.4	105.2	131.7	179.3	150.6	182.4	200.9	193.0
	2022												
1961–2000	96.0	169.5	138.7	278.2	204.6	115.2	163.7	87.2	65.7	87.2	78.8	37.2	36.5
1971–2020	88.5	164.8	129.7	235.8	183.9	105.2	146.6	80.1	62.7	84.7	76.4	33.8	36.0
1981–2020	89.0	163.3	131.1	237.5	185.7	106.7	151.1	80.9	63.3	84.8	77.7	32.8	36.1
1991–2020	83.2	161.5	127.1	228.6	189.0	105.0	151.8	86.5	64.4	86.2	76.8	29.6	37.4

LEGEND

$Q_m / Q_{ma,ref}$ [%]	Category of the month
0 – 20	extremely dry
20 – 40	dry
40 – 60	significantly sub-normal
60 – 80	sub-normal
80 – 120	normal
120 – 160	above normal
160 – 200	significantly above normal
> 200	extremely wet

Discussion and conclusion

The comparison of the long-term values of Q_a and Q_{ma} for periods 1971–2020, 1981–2020 and 1991–2020 with the currently valid reference period in Slovakia (1961–2000) has been made in selected water-gauging stations. The results are in line with the findings of previous national studies (Blaškovičová et al., 2019, 2020; Poórová et al., 2018), which have focused on the analyses of the changes in runoff in last decades. These studies have pointed to the fact, that the differences in the runoff distribution throughout the year as well as other changes in hydrological characteristics (long-term values, extreme discharges connected with floods and droughts, their frequency and duration, etc.), is attributed mostly to the climate change, and are becoming more significant. The changes in discharge in Slovak streams, according to the results of this article, show the decrease of long-term values in most parts of Slovakia. The increase of Q_a has been identified in the northern part of Slovak territory, in Poprad and Dunajec sub-basin and the upper parts of sub-basins Váh and Hornád. Among the three evaluated periods, these changes are more pronounced in the period 1991–2020, than for periods 1971–2020 and 1981–2020. This logically follows from the fact, that the period 1971–2020 overlaps with the reference period 1961–2000 to a much greater extent than the last considered one. The 30-year period 1991–2020 is more influenced by the 20-year period after 2000 with significantly increased manifestations of the effects of climate change in hydrological regime of Slovak streams. Similarly, the changes in the runoff distribution in the year are most significant for the period 1991–2020 in the majority of the evaluated WS. The changes in Q_{ma} are showing the positive deviations in average in January, February and September; for the rest of the months we can see the negative deviations in average, being most important in April.

The comparison of the three periods of different length (50-, 40- and 30-years) is connected with the general problem of the recommended length of the reference period in hydrology. This follows from the long-term regime of flow fluctuations and its rules. Kašpárek (2000) in Czech region, with similar climatic conditions as Slovakia, does not recommend extending the primary period over 50 years, as far as they are considered to be stationary. It is more appropriate to limit the length of the data series to 40 - 50 years, to reduce the possible errors corresponding to long-term fluctuations in precipitation. Pekárová et al. (2003) identified 28-year cycle in the large rivers of Europe and World. This points to the possible suitability of using a 30-year period, especially if the aim is to provide the basis for proposals for solutions and measures in the sense of a forecast for the future, not an evaluation of a long-term regime. The results in Poórová et al. (2023) indicated as well, that the use of the 30-year long period 1991–2020 is probably suitable, especially for mutual comparison between climatic and hydrological characteristics for climate change research.

The period 1991–2020 is the one recommended by WMO as the reference period for current assessment of hydrological situation, to be comparable with climatic assessment based on the same reference period. However, for long-term comparison as well as climate change assessment, there is the recommendation to use the period 1961–1990. This is quite close to the period 1961–2000, currently valid as reference period for

surface water hydrology in Slovakia. It is therefore important to consider for what purpose which reference period is used. On the example of the assessment of Q_r and Q_m in selected WSs in the Váh sub-basin for the years 2021 and 2022 according to different reference periods, it can be seen that the same average monthly but also annual flows in one station can fall into different assessment categories. This is especially important in the periods of low flows, when the water use needs to be carefully managed to provide the necessary balance between the requirements of the users and the ecological status of waters. The differences in evaluated categories can thus lead into different set of applied water management rules.

This study covers only one part of the evaluation, focused on long-term values analyses. More detailed analyses (the assessment of the data series of monthly discharges, yearly discharge analyses are partially published in Poórová et al., 2023, daily and extreme discharges, long term trends, precipitation, etc.) are needed to fully support the selection of the new reference period (or more of them for specific purposes) used for the water management and decision making needs.

Acknowledgement

This work was supported by the Slovak Research and Development Agency under the Contract no. APVV-20-0374.

References

Blaškovičová L. (Ed.) (2019): Hodnotenie hydrologického sucha, časť 2: Hodnotenie zmien a trendov mesačných a ročných prietokov, čiastková správa. 64 s. SHMÚ, ISBN 978-80-99929-14-3. (in Slovak)

Blaškovičová L. (Ed.) (2020): Hodnotenie hydrologického sucha, časť 3: Hodnotenie M-denných prietokov a neprietokových charakteristík, čiastková správa. 92 s. SHMÚ, ISBN 978-80-99929-26-6. (in Slovak)

Ďurigová, M., Hlavčová, K. (2020): The detection of changes in the upper Váh river basin according to a decadal analysis. Acta Hydrologica Slovaca, 21, 1, 39–47; DOI: https://doi.org/10.31577/ahs-2020-0021.01.0005.

Fendeková, M., Gauster, T., Labudová, L., Vrablíková, D., Danáčová, Z., Fendek, M., Pekárová, P. (2018): Analysing 21st century meteorological and hydrological drought events in Slovakia. Journal of Hydrology and Hydromechanics, 66, 4, 393–403.

Halmová, D., Pekárová, P., Podolinská, J., Jeneiová, K. (2022): The assessment of changes in the long-term water balance in the Krupinica River basin for the period 1931–2020. Acta Hydrologica Slovaca, 23, 1, 21–31; DOI: https://doi.org/10.31577/ahs-2022-0023.01.0003.

Kašpárek, L. (2000): Vliv kolísaní klimatu na postup výpočtu návrhových hydrologických dat, Hydrologické dny 2000, Plzeň, Zborník konferencie. (in Czech)

Pekárová, P., Miklánek, P., Pekár, J. (2003): Spatial and temporal runoff oscillation analysis of the main rivers of the world during the 19th – 20th centuries. Journal of Hydrology, 274, 1–4, 62–79, https://doi.org/10.1016/S0022-1694(02)00397-9.

Pekárová, P., Miklánek, P., Pekár, J., Pramuk, B. (2017): Identifikácia zmien režimu denných prietokov slovenských riek II. časť: Porovnanie dvoch období [Identification of the Slovak rivers daily discharge regime changes. Part II.: Comparison of the two periods]. Acta Hydrologica Slovaca, 18, 2, 183–192; ISSN 2644-4690. (in Slovak)

Poórova, J. (Ed.) (2018): Hodnotenie hydrologického sucha, časť 1: Hodnotenie vodnosti roka a zmien rozdelenia odtoku v roku, čiastková správa, 110 s, SHMÚ, ISBN 978-80-99929-09-9. (in Slovak)

Poórová, J., Jeneiová, K., Blaškovičová, L., Danáčová, Z., Kotríková, K., Melová, K., Paľušová, Z. (2023): Effects of the Time Period Length on the Determination of Long-Term Mean Annual Discharge. Hydrology, 10, 88. https://doi.org/10.3390/hydrology10040088.

Šipikalová, H. (Ed.) (2005): Spracovanie hydrologických charakteristík - Koordinácia, Záverečná správa čiastkovej výskumno-vývojovej úlohy 3030-05, SHMÚ. (in Slovak)

WMO (2020): Statement on the term Hydrological Normal, Hydrological Coordination Panel. Available online: https://community.wmo.int/activity-areas/hydrology-and-water-resources/hydrological-coordination-panel (accessed on 27.1.2023).

Ing. Lotta Blaškovičová, PhD. (*corresponding author, e-mail: lotta.blaskovicova@shmu.sk)
Ing. Katarína Jeneiová, PhD.
Ing. Katarína Kotríková, PhD.
Ing. Ľubica Lovásová
Mgr. Katarína Melová, PhD.
Slovak Hydrometeorological Institute
Jeséniova 17, 833 15 Bratislava
Slovak Republic

Ing. Soňa Liová
Slovak Hydrometeorological Institute
Bôrická cesta 103, 011 13 Žilina
Slovak Republic

DOI: 10.31577/ahs-2023-0024.02.0027

ACTA HYDROLOGICA SLOVACA

Volume 24, No. 2, 2023, 242 – 253

Case study: Assessment of radar-based and ground precipitation data during the flood situation in May 2021 in the Upper Hron River basin in Slovakia

Kateřina HRUŠKOVÁ*, Hana HLAVÁČIKOVÁ

Precipitation is a major factor influencing the results of rainfall-runoff modelling. Errors in precipitation propagate to other phases of water quantity and quality analysis. In the field of operational hydrology, the primary focus is on simulated and predicted discharges. This paper provides a comprehensive analysis of radar-estimated precipitation in comparison with precipitation obtained from rain gauge stations during the monthly period when flooding occurred in the Upper Hron River basin in central Slovakia. The precipitation is analysed from the point of view of its further use in the HBV hydrological model applied for hydrological forecasts in the operational hydrological service of the SHMU. Even though, there are high correlation coefficients between measured and radar precipitation, the underestimation of radar precipitation was investigated, with a clear west-east trend. The radar product generally recorded more hours of rain. Low intensities up to 3 mm hr^{-1} prevailed, while precipitation with higher intensities (above 5 mm hr^{-1}) was detected less frequently compared to ground data. Hydrological evaluation of radar precipitation has shown that bias correction methods applied to precipitation data prior to input to the model can enhance subsequent discharge simulation. The improvement was observed mainly in upstream subbasines, especially in the Čierny Hron subbasin. The NSE was calculated at 0.915. The error in peak flow was also reduced, but the underestimation of the maximum discharge was still observed. The assessment included one month's data, therefore more site-specific situations would need to be analysed for more general conclusions.

KEY WORDS: precipitation uncertainty, hydrological forecasts, HBV model

Introduction

In mid-May 2021, we observed a flood situation that affected most of the river basins on the Slovak territory. At the gauging stations in the Upper Hron River basin up to the Banská Bystrica outlet, we recorded the exceedance of the 1st to 3rd degree of alert levels. The causal precipitation was associated with the passage of several cold fronts, which crossed the territory of Slovakia from the west between 12 and 17 May. Intense convective precipitation predominated during the first days, followed by continuous precipitation. Rainfall activity was highest during the day on 17 May. Most of the total rainfall amount fell in 12 hours between 6:00 and 18:00 CEST. Basin precipitation ranged from 25 mm in the Hron River head area to 45 mm in the western direction. There was 55 to 70 mm of rainfall in the surroundings of Banská Bystrica and exceptionally more on the windward slopes of the Kremnické and Starohorské hills (Hrušková et al., 2021).

The water level on the Hron River at the outlet of Banská Bystrica exceeded the 3rd degree of alert level at midnight on 18 May. The peak discharge occurred in the morning of 18 May and has reached the value of 5-year flood discharge. The most significant peak discharges, 10-year flood discharges, were evaluated at the water gauging stations on the right-hand tributaries the Jasenianský Creek and the Bystrica River. The risk of flooding in Banská Bystrica was not based on the value of the peak runoff, but rather on the construction of flood defences. The May flood is also described in Pekárová et al. (2022). They focused on the reconstruction of the flood wave caused by the breach of the stone dam in Rudno nad Hronom.

During the flood, the Department of Hydrological Forecasts and Warnings (DHFW) of the Slovak Hydrometeorological Institute (SHMU) issued model forecasts updated four times a day. Deterministic forecasts were made using the well-known conceptual semi-distributed rainfall-runoff model HBV (Bergström, 1992). The course of the flood suggested that the model predictions underestimated reality. The predicted onset of the flood was slower and the peak flow lower. This was confirmed by a post-flood feedback evaluation of model performance during the flood. As Vlasák and Krejčí (2021) state, the understanding why hydrological forecasts differ from observations is key to making successful deterministic and probabilistic forecasts.

The DHFW regularly evaluates model performance in both simulation and forecast mode at selected gauging stations (Hlaváčiková et al., 2023). The paper summarises the results of the evaluation of observed precipitation used as climatological forcing data in the HBV model. Climatological forcing data determine the initial conditions of the model prior to the forecast run.

In forecast mode, the hydrological model, calibrated using historical data and simulating runoff with actual meteorological forcing, is run forward in time with the input data provided by the meteorological forecast. The way the hydrological model simulates extreme runoff phases has a strong influence on its ability to set the initial conditions before the hydrological forecast (Hrušková and Hlaváčiková, 2022). It is therefore important that the model describes them as accurately as possible. WMO (2011) states that errors in the initial conditions determine extremely large errors and forecasting uncertainty in the case of rainfall-runoff models. As it further explaines, the soil moisture content at the beginning of an event can change the predicted runoff by an order of magnitude.

The most commonly used sources of precipitation data for hydrological modelling are rain gauges and meteorological radars. Meteorological radars provide real-time, spatially distributed precipitation estimates. Conventional rain gauge data are spatially limited to the exact location and often considered to be true observations at ground level compared to precipitation estimated from other data sources (McMillan et al., 2011). The HBV model is designed to easily incorporate rain gauge precipitation data. The weights are used to convert the point measurement to an area (basin) value (SMHI, 2014).

Precipitation measured at a single point is considered to be the most accurate source of information, but it is characterised by a high degree of spatial variability. The areal average is often poorly represented by point measurements, especially in cases where rain gauges are sparsely distributed or outside the area of interest (Starks and Moriasi, 2009; Tobin and Bennett, 2009; Price et al., 2014). Since mid-May 2019, the DHFW uses radar precipitation estimates merged with rain gauge data (hereafter referred to as "qPrec") as actual meteorological forcing data input to the rainfall-runoff forecasting process (Méri et al., 2021). Radar precipitation estimates are implemented by calculating the mean areal precipitation over the basin (basin precipitation).

It is a generally known fact that precipitations input in hydrological models contain a large source of uncertainty and has a critical effect on the accuracy of hydrological model predictions (McMillan et al., 2011).

Reason is that there is a limited number of available ground based observations and the high spatio-temporal variability of this characteristic (Kavetski et al., 2006). Bardossy et al. (2022) documented that up to 50% of the hydrological model error in their study can be attributed to precipitation uncertainty. In adition, in mountaineous regions the error can be even higher because of the orographic effect (McMillan et al., 2011; Sleziak et al., 2023).

The quality of the precipitation input has an impact on the runoff processes simulation. Without accurate measurements or estimates of precipitation, hydrological modelling cannot be effective. When modelling hydrological processes, precipitation affects several internal state variables of the model, e.g. soil moisture, evapotranspiration, snow or groundwater flow (Bingeman et al., 2006). As such it influences the initial conditions prior to hydrological forecast run. Thus, through the initial conditions, the radar precipitation influences the final hydrological forecast.

The objective of the study was to evaluate the differences between measured and radar-estimated precipitation at selected rain gauge stations in the Upper Hron River basin during flood situation in May 2021 and to assess the influence of qPrec basin averages on model performance. We used the same setup of the HBV model, including parameters, as is used as standard in the hydrological forecasting process at SHMU. Precipitation analysis from an operational hydrology point of view is valuable to better understand the behavior of the calibrated model, especially during flood situations. On the other hand, it provides feedback to the SHMU Department of Remote Sensing to improve its qPrec product.

Materials and methods

Study area

The Upper Hron River basin was selected as the area of interest for our case study (Fig. 1). The catchment area up to the Banská Bystrica outlet is 1766 km^2. The catchment is characterised by a west-east orientation with a high altitude range from 334 m to 2024 m a.s.l.

Processing of ground and radar data

The study uses hourly rainfall data from 16 automatic weather (AWS) and precipitation (APS) stations located in the Upper Hron River basin (Table 1). The exception is the data from Chopok AWS because of only 6-hourly time step of manually measured precipitation data for SYNOP (surface synoptic observations) message. Chopok AWS is a high mountain weather station located on the ridge of the Low Tatras in extreme climatological conditions with strong wind effects and also icing phenomena in winter.

For our analysis, we also used radar rainfall estimates at rain gauge stations from the qPrec software, which is continuously developed and improved by the SHMU Department of Remote Sensing. As Meri at al. (2021) explains, the qPrec software for quantitative precipitation estimation was developed in an iterative approach. Each upgrade or modification of the software (e.g. the incorporation of an additional quality index, new input field, and modified algorithm) was validated against the 24-hour precipitation amount from the network of about 600 climatological and pluviometric stations of the SHMU.

Fig. 2 shows an example of 24-hour precipitation as

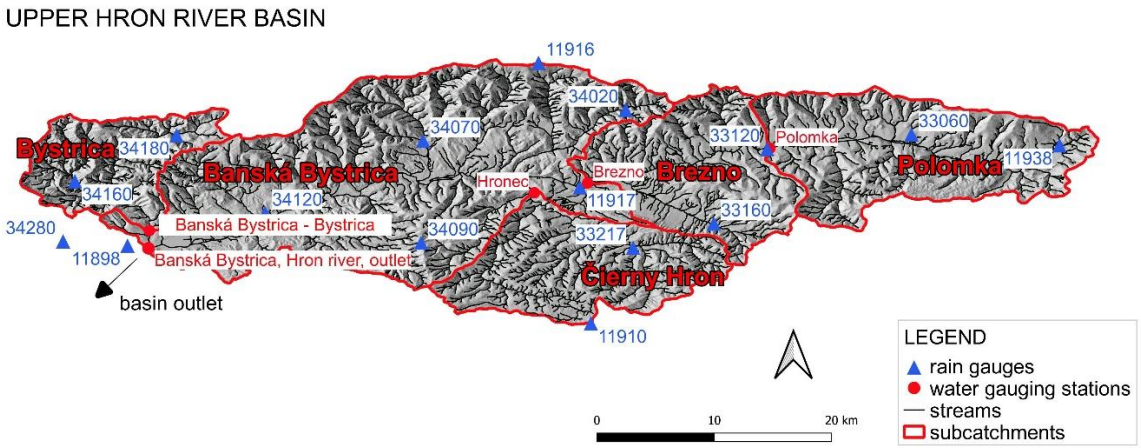

Fig. 1. Map of the Upper Hron River basin study site with main subcatchments, location of rain gauges and water gauging stations.

Table 1. Automatic weather and precipitation stations located in the Upper Hron River basin

	ID	Name	Type	Longitude	Latitude	Altitude [m a.s.l.]
1.	11898	Banská Bystrica	AWS	19.11528	48.73333	427
2.	11910	Lom nad Rimavicou	AWS	19.64917	48.64389	1018
3.	11916	Chopok	AWS	19.58889	48.94333	2002
4.	11917	Brezno	AWS	19.63652	48.80035	487
5.	11938	Telgárt	AWS	20.18920	48.84860	906
6.	33060	Pohorelá	APS	20.01858	48.86111	747
7.	33120	Polomka	APS	19.85234	48.84426	605
8.	33160	Pohronská Polhora	APS	19.79083	48.75861	619
9.	33217	Čierny Balog-Dobroč	APS	19.69787	48.73096	570
10.	34020	Jarabá	APS	19.68929	48.88937	892
11.	34070	Jasenie	APS	19.45593	48.85387	538
12.	34090	Chata pod Hrbom	APS	19.45358	48.73662	1079
13.	34120	Slovenská Ľupča	APS	19.27372	48.77084	389
14.	34160	Dolný Harmanec	APS	19.05461	48.80738	481
15.	34180	Motyčky	APS	19.17182	48.86018	678
16.	34280	Králiky	APS	19.04101	48.73818	627

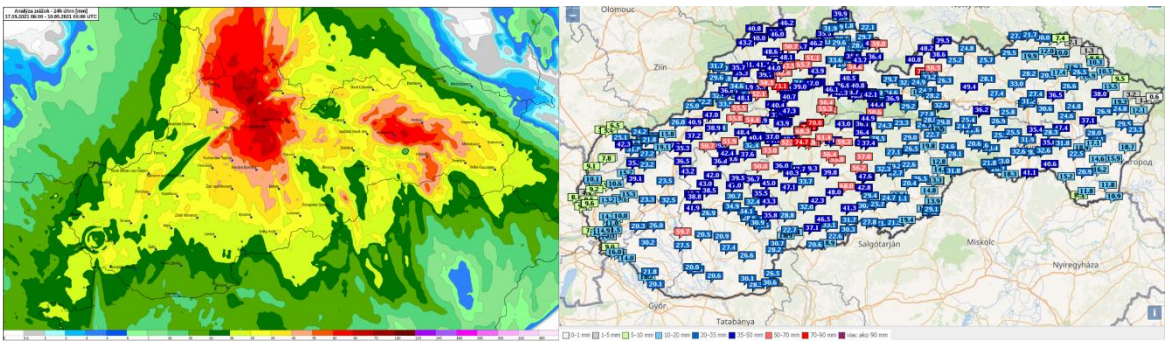

Fig. 2. 24-hour precipitation totals from automatic rain gauge stations until 18. 5. 2021 04:00 UTC (LEFT) and spatial analysis of 24-hour precipitation based on radar estimates until 18. 5. 2021 06:00 UTC (RIGHT).

measured by automatic rain gauge stations (until 18. 5. 2021 04:00 UTC) and based on radar estimates (until 18. 5. 2021 06:00 UTC).

Statistical evaluation

The ground data were compared to hourly radar-based precipitation estimates. Using paired hourly data, Pearson's correlation coefficient was applied to measure the degree of linear relationship between radar based and observed precipitation. Percent bias (PBias) was used to investigate the tendency of the radar based precipitation to over- or underestimate the measured data.

$$PBias = \frac{P_{radar} - P_{meas}}{P_{meas}} * 100 \quad (1)$$

where

P_{radar} –monthly precipitation based on radar estimates [mm],

P_{meas} – monthly measured precipitation at rain gauge station [mm].

The hourly intensities were divided into several intervals (0.1–1, 1–3, 3–5, 5–7, 7–9, 9–11, 11–15, >15mm) and frequency analysis was performed. For this purpose, all hourly values for which both data types reported zero precipitation (less than 0.1 mm) were neglected.

To show the distribution of the numerical data and their skewness, the data were presented in a box plots using the five-number summary of a data set – including the minimum score, first (lower) quartile, median, third (upper) quartile, and maximum score.

Hydrological modelling

The next step was to try to answer the question of how to use the results of precipitation analysis in operational hydrological modelling. The hydrological model used to achieve our goal was the HBV rainfall-runoff model, with the same settings as those regularly used by the DHFW for the discharge forecasting process.

Five forecasting gauging stations naturally define five subbasines in the Upper Hron River basin, which are summarised in the Table 2 and shown in Fig. 1. Upstream subbasines are connected to downstream ones and the simulated discharge flows downstream to the basin outlet on the Hron River in Banská Bystrica. This means that the rainfall runoff process is simulated in three upstream subbasins (Polomka, Hronec, Bystrica), while in the remaining two subbasines it is combined with a single flood routing (Brezno, Banská Bystrica).

The HBV model contains subroutines for snow accumulation and melt, soil moisture accounting procedure, routines for runoff generation and routing. Detailed information on the model structure and parameters can be found in the literature (Bergström, 1992; SMHI, 2014).

The HBV model is a continuous semi-distributed rainfall runoff model that solves water balance at each computational time step. Catchments are divided into sub-catchments, elevation zones of 100 m each, and vegetation zones (as forest or field). Basin averages of radar-based precipitation estimates and air temperature, both at a hourly time step, are used as input data to the model. Radar-based precipitation estimates based on measurements from four Slovak meteorological radars are operational from May 2016.

Continuous basin mean series of the radar-based precipitation product for the model calibration (qPrec) have been available since June 2016. The calibration itself covered the period from August 2016 to December 2020. The results of the model calibration are summarised in the Table 3 below. The table includes the performance evaluation by Nash-Sutcliffe Efficiency (Nash and Sutcliffe, 1970; Moriasi et al, 2007) and the parameter values for each subbasin. Calibrated model outputs are used as a benchmark for the next analysis.

For each sub-basin, some rain gauge stations were selected to calculate the correction factor to adjust the rainfall estimates. A quantitative relationship between monthly measured and estimated radar precipitation was calculated for each rain gauge station. The basin-averaged ratio was used to correct original hourly radar data (qPrec), which was then used as the adjusted basin precipitation input to the hydrological model. Monthly values were used to smooth out extremes in precipitation data contained in a short time step (high value of hourly intensities) and to find a long term basin value of the correction factor. Fig. 3 shows an overview of the rain gauges used in the analyses for particular subcatchment.

Model parameters were not changed when simulating, they were the same as in the benchmark setup. The results of the simulation, hourly discharges to five outlets, were assessed by Nash-Sutcliffe Efficiency (NSE) and compared to the benchmark. Several output variables were also evaluated. Soil moisture storage, upper and lower zone filling describe initial conditions at the beginning of the discharge forecasting process. To assess the accuracy of the peak flow, the percentage error in peak flow in percentages (PE) was used (Cheng et al., 2017):

Table 2. The overview of the subbasins allocated in the Upper Hron River basin

	Subbasin					Upper Hron River basin
	Polomka	Brezno	Čierny Hron	Bystrica	Banská Bystrica	
River	Hron	Hron	Čierny Hron	Bystrica	Hron	Hron
Outlet	Polomka	Brezno	Hronec	Banská Bystrica	Banská Bystrica	Banská Bystrica
Area [km^2]	329.54	252.54	239.41	160.46	784.53	1766.48

Table 3. Parameter values followed by Nash-Sutcliffe efficiency for sub-basins in the Upper Hron River basin, valid for the calibration period August 2016 to December 2020. Detailed description of the parameters can be found in Bergström, 1992 or SMHI, 2014

Parameter	Unit	Polomka	Brezno	Čierny Hron	Bystrica	Banská Bystrica
rfcf	-	0.930	0.950	0.938	0.943	0.874
sfcf	-	1.480	1.480	1.400	1.400	1.700
cfmax	mm °C^{-1} day^{-1}	4.200	4.250	3.597	5.000	5.000
tt	°C	-0.229	0.000	-0.105	-1.029	2.000
dttm	°C	0.360	0.025	0.285	-0.230	-2.000
fc	mm	95.000	82.000	142.115	204.000	174.747
lp	-	1.000	0.550	0.841	0.913	1.000
beta	-	2.300	3.500	4.000	2.943	4.000
cflux	mm day^{-1}	1.870	1.500	0.000	0.905	0.010
ecorr	-	1.050	0.726	0.959	0.700	0.713
k4	day^{-1}	0.025	0.012	0.072	0.025	0.002
perc	mm day^{-1}	2.000	1.250	4.203	4.950	0.013
khq	day^{-1}	0.099	0.120	0.177	0.110	0.066
alfa	-	0.950	0.950	0.634	0.929	1.500
maxbaz	day	0.090	0.000	0.000	0.000	0.000
NSE	-	0.847	0.945	0.806	0.906	0.815

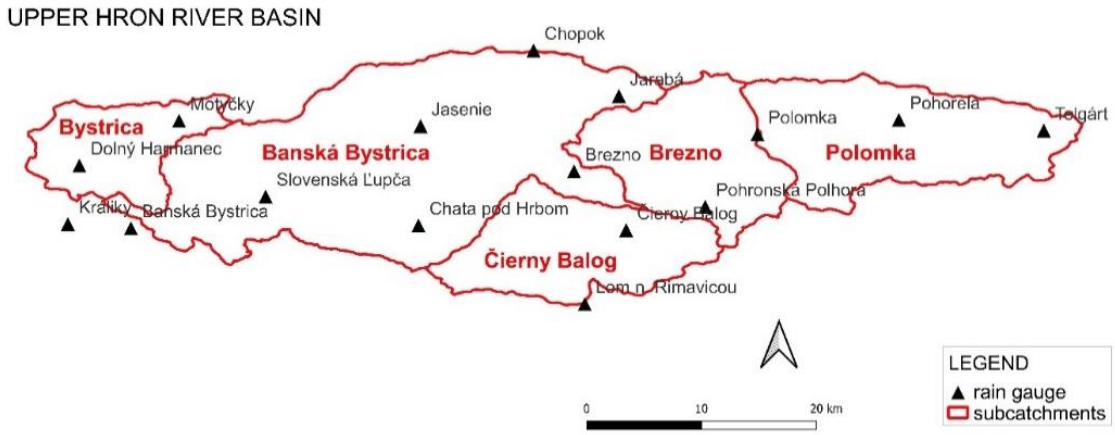

Fig. 3. The overview of rain gauge stations within the subcatchments.

$$PE = \frac{Q_{max} - Q'_{max}}{Q_{max}} * 100 \qquad (2)$$

where
Q_{max} –the observed peak value [m^3 s^{-1}],
Q'_{max} –the simulated peak value [m^3 s^{-1}].

Results and discussion

Comparison of radar-based and ground precipitation data

Radar-based and ground precipitation data show strong relationship described by Pearson's correlation coefficient (Fig. 4). The values range from 0.745 (Chopok AWS) to 0.937 (Jasenie APS). The lowest value is influenced by six-hourly timestep of analysed data. The second lowest value is 0.847 for Pohronská Polhora APS. Higher correlation coefficients were calculated in the western part of the basin, where higher monthly precipitation totals and also higher underestimation are observed. Detailed analysis showed that the pairwise differences in hourly data were systematically biased in the western part of the basin, while in the eastern part the same differences were randomly spreaded. This resulted in comparable monthly totals from both precipitation sources in the eastern part, but with a slightly lower correlation. Similar findings are presented in the publication of Sleziak et al. (2023). As they indicate, high values of the correlation coefficients may suggest that although the radar-based precipitation are underestimated compared to measured precipitation, but the underestimation at individual sites is in analysed situation relatively stable.

The west-easterly orientation of the basin influenced the amount of measured precipitation. The prevailing synoptic situation brought more precipitation to

the western part of the basin. Monthly precipitation sums decrease towards the east. Monthly radar estimates show the same but a more moderate trend. According to the trend lines in Fig. 5, the differences between the corresponding measured and estimated monthly data decrease in the west-east direction. The compared monthly values at Polomka (33120) and Pohorelá (33060) were almost identical. The lowest monthly precipitation sums based on radar estimates were observed at stations in the southern part of the basin – Lom nad Rimavicou (11910), Čierny Balog (33217) and Pohronská Polhora (33160).

Rain gauge stations in the northern part of the basin recorded more precipitation than stations in the southern part. In addition, the southern stations show larger deviations from radar estimates than the northern stations. This includes the southern station of Chata pod Hrbom (34090; 1079 m a.s.l.) too, which is not shown in the Fig. 6. The southern rain gauge stations, which are at a higher altitude, mostly showed lower precipitation totals for May 2021 than the station (Brezno AWS, 11917) in the Hron valley.

Our work did not find that the underestimation of radar precipitation was related to elevation, as was the case of Sleziak et al. (2023) shown in the mountain basin analyses. However, it must be said that we only analysed one month of data for a specific hydrologic situation, and more site-specific situations would need to be analysed for more general conclusions.

The greatest differences between measured and radar-estimated precipitation was found for the stations located in the west and decreased towards the east (Fig. 7). The radar-based precipitation underestimates measured monthly precipitation totals by 6 to 40%, with the exception of two rain gauge stations. Polomka (33120) and Pohorelá (33060) show a positive deviation of 0.25% and 3.62%, 0.33 mm and 4.39 mm respectively. The underestimation of 29 to 40% was found at Králiky APS (34280) and at the southern rain gauge stations Chata pod Hrbom (34090), Lom nad Rimavicou AWS (11910), Čierny Balog APS (33217) and Pohronská Polhora APS (33160). Králiky APS (34280) is the westernmost rain gauge station in the basin.

The analysis of the hourly data using scatter plots (Fig. 8) show a systematic underestimation of radar-based precipitation in comparison with ground measurements. For higher rainfall intensities, which are critical for correct peak flow simulations, the underestimation is most pronounced. Although the amount of precipitation estimated by the radar is clearly underestimated, the timing of the radar-based precipitation events is in good agreement with the measured data, as is shown in the example in Fig. 9.

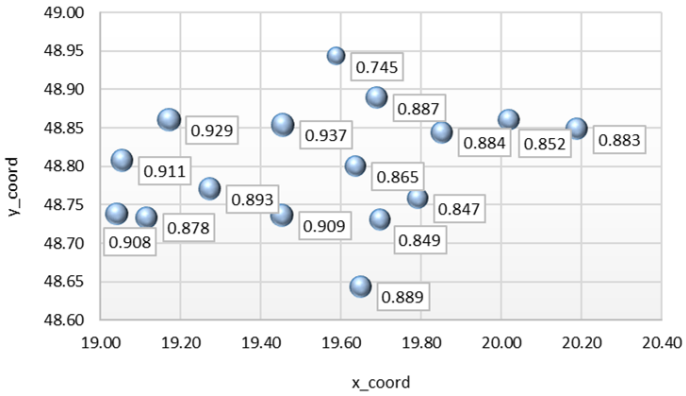

Fig. 4. Spatial variability of Pearson's correlation coefficients [-] between radar-based and ground precipitation data at selected precipitation stations in May 2021.

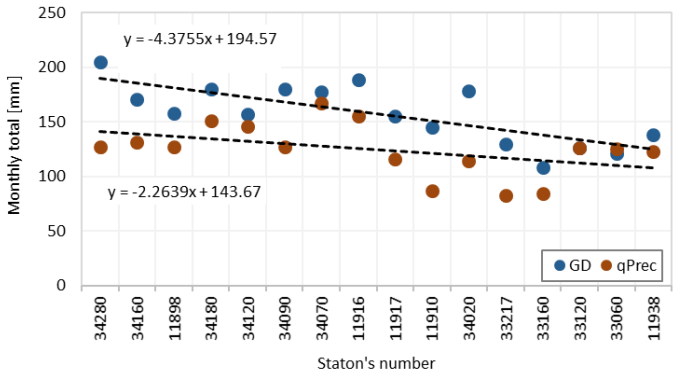

Fig. 5. Measured and radar-estimated monthly precipitation totals in the west-east direction (precipitation stations are ordered by longitude). GD is measured ground data and qPrec radar based estimates of precipitation at a rain gauge station.

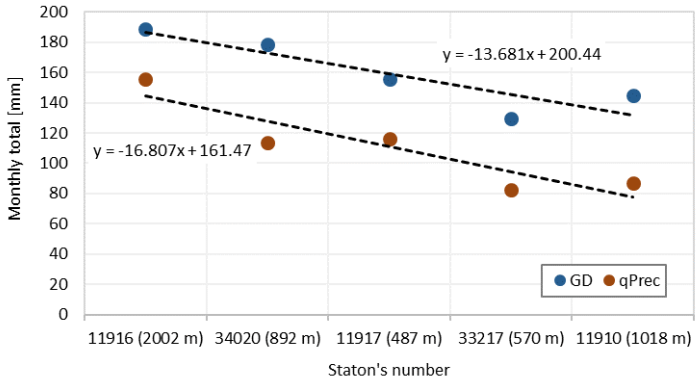

Fig. 6. Monthly precipitation values derived from radar estimates compared to data from precipitation stations (ID) in north-south crossection. The numbers in brackets indicate the altitude of the rain gauge stations. GD is measured ground data and qPrec radar based estimates of precipitation at a rain gauge station.

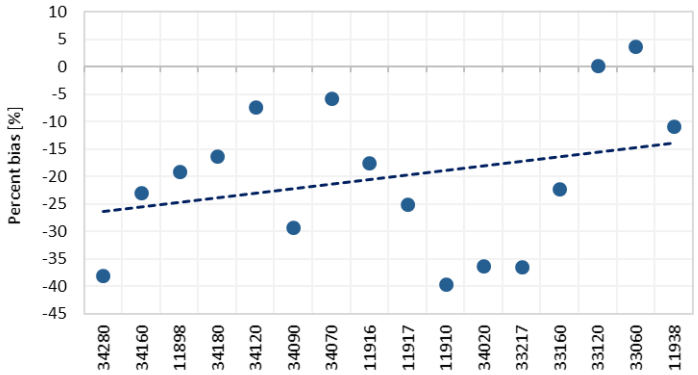

Fig. 7. Percent bias values at raingauge stations in the Upper Hron River basin in May 2021. Minus signs indicate that the radar-based precipitation underestimates the observed precipitation. The rain gauge stations are arranged according to their longitude from west to east.

A comparison of hourly rainfall intensities showed that the radar detected more hours with rain. In only one case (34020, Jarabá APS), the total number of hours with rain was higher compared to the radar data. The radar-based precipitation with lower intensities (up to 3 mm hr^{-1}) was assessed much more frequently. On the other hand, radar-based precipitation with higher intensities (above 5 mm hr^{-1}) was detected less frequently than in the case of the observed precipitation (Fig. 10). These results suggest a negative bias towards higher radar estimated precipitation intensities.

Result indicates that the mountainous relief of Slovakia has a significant influence on radar estimates of precipitation. For a basin surrounded by mountains, such as the Upper Hron River basin, the mountains form a natural barrier that affects any measurement of meteorological radar because of beam-blockage and beam height above the terrain (Méri et al, 2021; Sleziak et al, 2023).

The results in Fig. 11 show that the radar-based hourly precipitation was systematically underestimated (lower median, upper quartile and maximum values compared to measured data). Similar results were reported by Sleziak et al. (2023) for the mountain catchment in the Western Tatra Mountains. Visual interpretation of the interquartile range of each box plot indicates a higher concentration of radar data around the median, which means that the radar data are more clustered and show less time variability than measured data.

Hydrological modelling results

The subbasin means of the ratios between monthly measured and radar estimated precipitation at selected rain gauge stations are given in the Fig. 12. The specific values range from 1.028 to 1.617. The lowest value was calculated for the Polomka subbasin. This confirms the results of the previous analysis that the monthly totals of the hourly radar based data in the eastern part of the Upper Hron River basin correspond reasonably well to the measured precipitation. The highest mean value shows that the greatest underestimation of measured precipitation was observed at rain gauge stations in the Čierny Hron subbasin. Using the calculated basin-averaged ratio, the original hourly radar data (qPrec) were modified and used as the adjusted basin precipitation input to the HBV hydrological model.

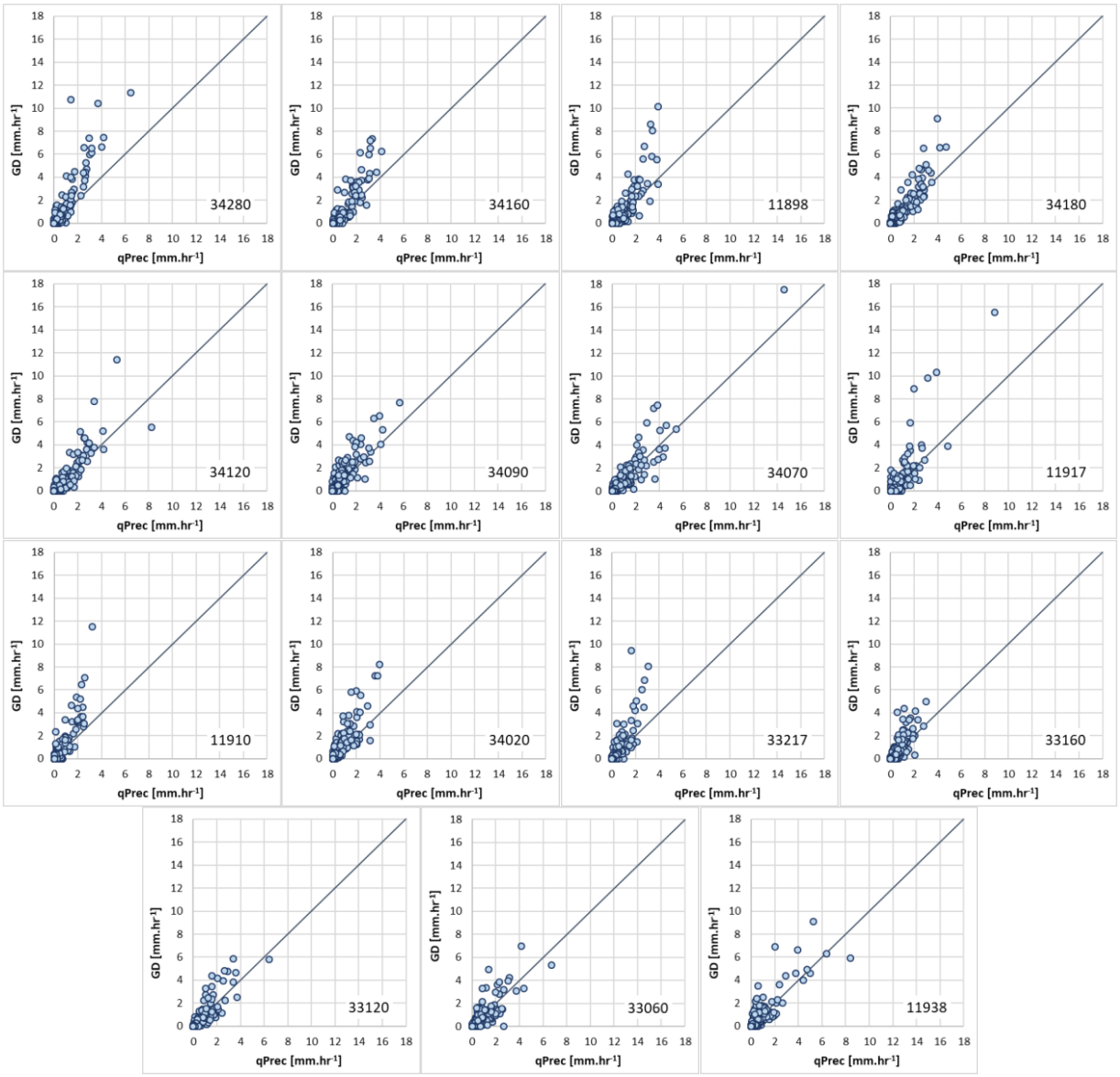

Fig. 8. Scatter plots of measured (GD) and radar estimated (qPrec) hourly precipitation at raingauge stations in the Upper Hron River basin in May 2021 (the station ID is in the bottom right corner). The diagonal line corresponds to the identity line.

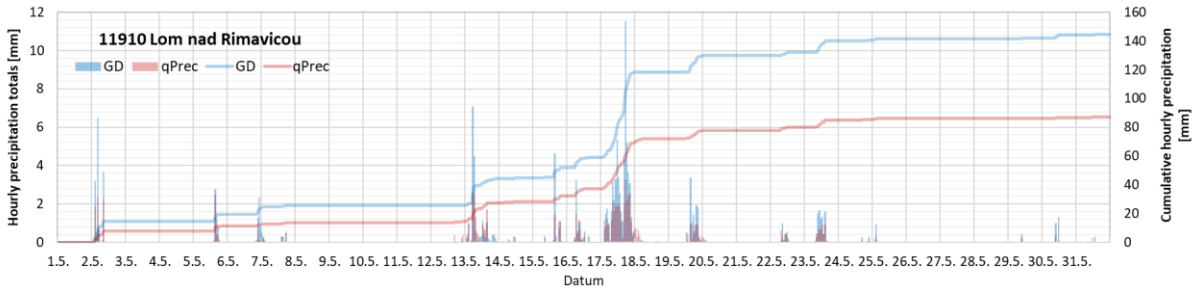

Fig. 9. Measured (GD) and radar estimated (qPrec) hourly precipitation totals and cumulative hourly precipitation at selected raingauge station in the Upper Hron River basin in May 2021.

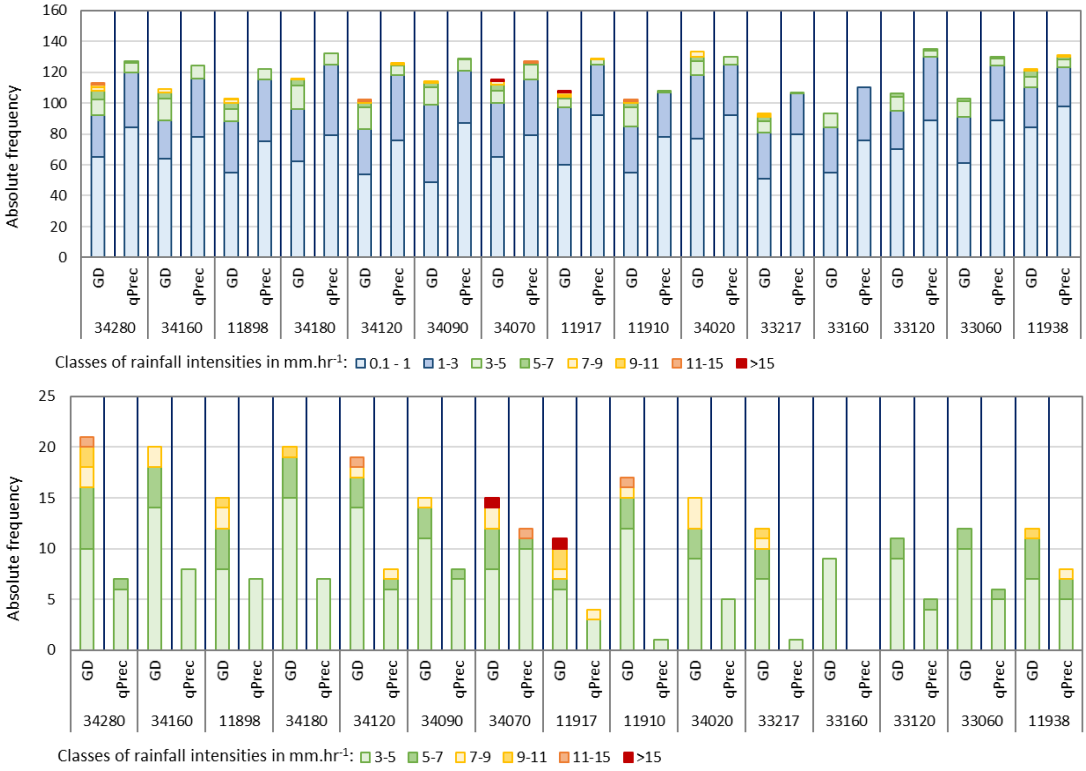

Fig. 10. Absolute frequency of measured (GD) and radar estimated (qPrec) hourly rainfall intensities higher than 0.1 mm hr^{-1} (up) and 3 mm hr^{-1} (down) at selected rain gauge stations in May 2021.

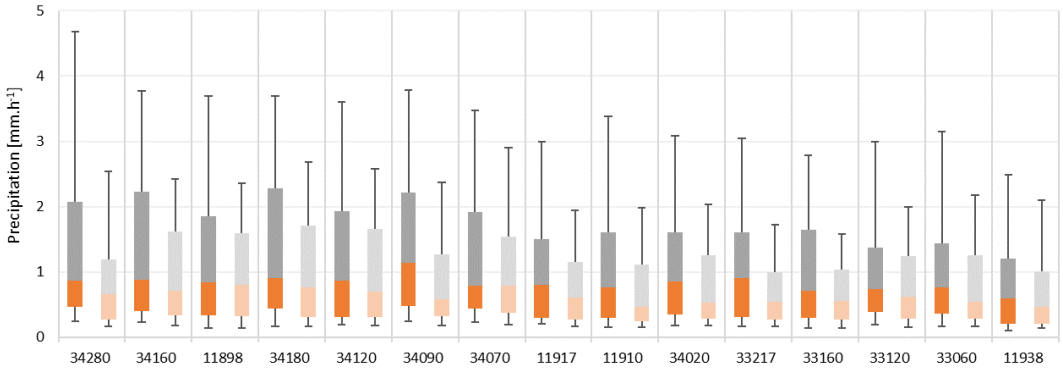

Fig. 11. Boxplots of measured and radar-based precipitation in hourly time step at selected rain gauge stations in the Upper Hron River basin in May 2021; the whiskers represent percentiles 10 and 90, the boxes are the upper and lower quartiles and the center line shows medians.

During the simulation, model parameters were not changed. They remained the same as those used in the benchmark run. Table below shows the values of the NSE for the benchmark run as well as for the run with the modified precipitation inputs in each subbasin. In all subbasines, the benchmark underestimated the observed discharges. According to NSE (Table 4), the statistically best values were obtained in the Bystrica and Banská Bystrica subbasines. The weakest benchmark result was detected in the Čierny Hron subbasin. The simulated discharge significantly underestimated the observed one.

The simulation with modified precipitation input showed the greatest improvement in the Čierny Hron subbasin. The simulated discharge corresponds to the observed runoff more closely compared to the benchmark (Fig. 13). This also confirms the high value of NSE (Table 4), although the observed peak flow is still underestimated.

In four of the five subbasines, the simulations with modified precipitation input improved model performance. According to the NSE value, the decrease

in model efficiency occurred in the Banská Bystrica subbasin. In the benchmark simulation, there was an underestimation of the peak flow by almost 27%. A 15% overestimation of the peak flow was calculated in the simulation with modified precipitation input. This means, that in this case the runoff generation in the subbasin Banská Bystrica, which is the most downstream subbasin, is more influenced by upstream inflows than by rainfall runoff processes in the subbasin itself. At the same time, it can be seen that the model calibration to some extent corrects errors or biases in the precipitation data through parameter adjustment.

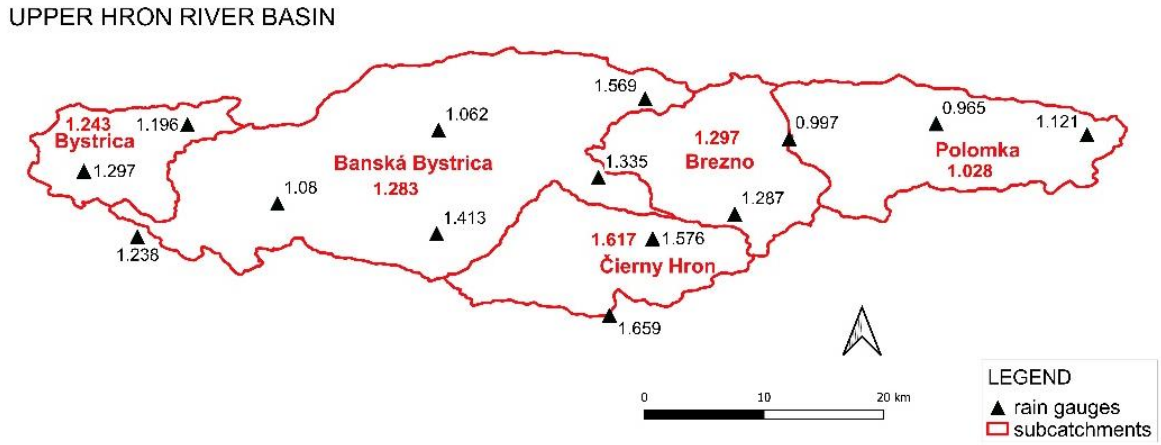

Fig. 12. The ratios between monthly sums of measured and radar estimated precipitation at selected rain gauge stations and mean subbasin values used to adjust hourly precipitation estimates (qPrec) input to the hydrological model.

Table 4. Values of NSE [-] and errors in peak flow PE [%] for benchmark simulations (qPrec) and simulations with modified precipitation input (qPrec_M) for individual subbasins in May 2021. A positive sign of PE indicates an underestimated and a negative sign an overestimated simulated peak flow compared to observed data

	Statistical criteria	Subbasins				
		Polomka	Brezno	Čierny Hron	Bystrica	Banská Bystrica
Benchmark (qPrec)	NSE	0.655	0.777	0.098	0.827	0.917
	PE	24.439	31.639	74.277	25.527	26.629
Modified (qPrec_M)	NSE	0.693	0.904	0.915	0.869	0.763
	PE	21.600	5.973	30.796	-9.384	-15.374

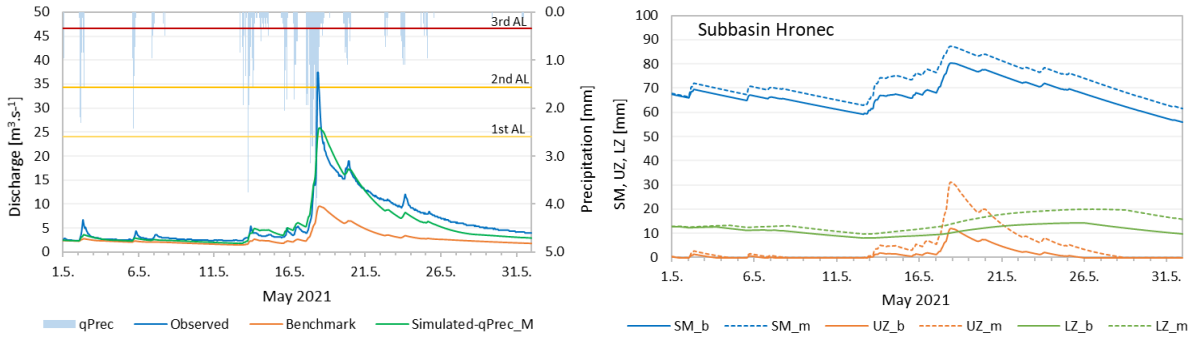

Fig. 13. The hydrograph of observed and simulated discharges at selected outlet in May 2021 (LEFT). "Benchmark" is simulated with radar estimates qPrec, "Simulated-qPrec_M" using modified precipitation input. The 1st to 3rd alert levels (AL) are also marked. Simulated soil moisture (SM), upper (UZ) and lower (LZ) zone storage at selected outlet in May 2021 (RIGHT). Outputs from the benchmark run (_b) are shown as a single lines, dashed lines correspond to outputs from the model run with modified precipitation input (_m).

Conclusion

For SHMU Department of Hydrological Forecasts and Warnings, radar-based precipitation estimates from qPrec software are the primary source of precipitation data used as climatological forcing data in hydrological modelling and forecasting. The grid outputs with 1 km resolution and hourly time step are converted to subbasin averages, which are then used as input to the semi-distributed HBV model.

In our case study, we focused on the flood event that affected the Upper Hron River basin in May 2021. We compared measured precipitation at selected automatic rain gauge stations with radar-based estimates at a location of the ground measurement. There are high correlation coefficients between measured and radar-estimated precipitation data. However, the underestimation of radar precipitation was found at both monthly and hourly time steps, with a clear west-east trend. Negative percent bias decreased towards the eastern part of the Upper Hron River basin. An analysis of the hourly rainfall intensities showed that the radar product recorded more hours with rain in general, but low intensities up to 3 mm hr^{-1} prevailed. On the other side, radar-based precipitation with higher intensities (above 5 mm hr^{-1}) was detected with less frequency than in the case of ground data.

Radar-based precipitation estimates are usually verified by ground measurements. An effective way to evaluate the performance of such data is to verify them using a hydrological model, particularly with a focus on extreme runoff situations. Basin averages from qPrec were fed into the HBV model. The model setup (including parameters) was the same as that operationally used by the SHMU hydrological forecasting service. Simulated and measured discharges were evaluated for five subbasines defined in the Upper Hron River basin. According to statistical criteria, a really poor discharge simulation with qPrec as input was detected for the Čierny Hron subbasin. The NSE for the flood event was close to zero. All discharge simulations underestimated peak flows, mostly in the range of 24–32%. In the case of the Čierny Hron subbasin the underestimation reached 74%. Using the basin-averaged ratio between monthly measured and radar precipitation at selected rain gauge stations, the original hourly radar data (qPrec) were modified and used as the modified basin precipitation input to the HBV model. The simulation with corrected precipitation showed improvement in four upstream subbasines, the greatest being in the Čierny Hron subbasin. The NSE was calculated at 0.915. Errors in peak flow were also reduced, but the underestimation was still observed at most outlets. For the Banská Bystrica subbasin, which is the most downstream and the largest subbasin, the runoff simulation with modified qPrec input resulted in worse model performance than in the case where the original qPrec data were used. The NSE decreased and the error in peak flow indicated an overestimation of maximum discharge. In terms of hydrological forecasting, this means that the runoff simulation and forecast at the Banská Bystrica outlet in May 2021 ware more influenced by the rainfall runoff processes in the upstream subbasins, than by the rainfall-runoff process in the subbasin itself.

In the future work, we would like to focus on how to implement the findings gained into the hydrological forecasting process. How to compensate the bias of the qPrec product prior to its input to the hydrological model? First of all, we need to carry out similar analyses so that we have knowledge about other river basins. The precipitation analysis carried out on a regular basis can help to understand the model performance in both simulation and forecast modes, especially during the floods. It must be said, we have only assessed one specific hydrological event using one month's data. More site-specific situations need to be analysed to make more general conclusions.

Acknowledgement

The Slovak Research and Development Agency under the Contract no. APVV-19-0340 supported this work.

References

Bárdossy, A., Kilsby, C., Birkinshaw, S., Wang, N., Anwar, F. (2022): Is Precipitation Responsible for the most Hydrological Model Uncertainty? Front. Water, 4, 836554. doi: 10.3389/frwa.2022.836554

Bergström, S. (1992): The HBV model - its structure and applications. Swedish Meteorological and Hydrological Institute, Norrköping, SMHI Reports Hydrology, RH No. 4, Norrköping, 32 p.

Bingeman, A. K., Kouwen, N., Soulis, E. D. (2006): Validation of the hydrological processes in a hydrological model. Journal of Hydrologic Engineering, 11(5), 451–463. doi: 10.1061/(ASCE)1084-0699(2006)11:5(451)

Hlaváčiková, H., Hrušková, K., Kopáčiková, E., Mikuličková, M., Zvolenský, M., Shenga, Z., Lešková, D. (2023): Different aspects of hydrological forecast assessment in Slovakia, EGU General Assembly 2023, Vienna, Austria, 24–28 Apr 2023, EGU23-7049. https://doi.org/10.5194/egusphere-egu23-7049.

Hrušková, K., Hlaváčiková, H. (2022): How to improve hydrological model forecast using precipitation data from small experimental basin. In: Book of Abstracts of the 18th Biennial Conference ERB 2022 Euromediterranean Network of Experimental and Representative Basins. Portoferraio, Elba Island, Italy, p. 37.

Hrušková, K., Halaj, M., Trstenský, T. (2021): Toky v povodí Hrona, Ipľa a Slanej v máji 2021. Povodňová správa. SHMÚ OHPaV, Bratislava, 25 s. ISSN-2729-918X (in Slovak only)

Cheng, K-S., Lien, Y-T., Wu, Y-C., Su, Y-F. (2017): On the criteria of model performance evaluation for real-time flood forecasting. Stoch Environ Res Risk Assess 31, 1123–1146. doi: 10.1007/s00477-016-1322-7

Kavetski, D., Kuczera, D., Franks, S. W. (2006): Bayesian analysis of input uncertainty in hydrological modeling: 1. Theory, Water Resources Research, 42, W03407. doi: 10.1029/2005WR004368

McMillan, H., Jackson, B., Clark, M., Kavetski, D., Woods, R. (2011): Rainfall uncertainty in hydrological modelling: An evaluation of multiplicative error models, Journal of

Hydrology, 400, 83–94. doi: 10.1016/j.jhydrol. 2011.01.026

Méri, L., Gaál, L., Bartok, J., Gažák, M., Gera, M., Jurašek, M., Kelemen, M. (2021): Improved radar composites and enhanced value of meteorological radar data using different quality indices. Sustainability, 13, 9, 5285. doi: 10.3390/su13095285

Moriasi, D. N., Arnold, J. G., van Liew, M. W., Bingner, R. L., Harmel, R. D., Veith, T. L. (2007): Model Evaluation Guidelines for Systematic Quantification of Accuracy in Watershed Simulations, Transactions of the ASABE, 50(3), 885–900. doi: 10.13031/2013.23153

Nash, J. E., Sutcliffe, J. V. (1970): River flow forecasting through conceptual models: Part 1. A discussion of principles. Journal of Hydrology, 10, 282–290.

Pekárová, P., Miklánek, P., Pekár, J., Podolinská, J. (2022): Post-flood analysis of the flood from the rupture of the stone dam in Rudno nad Hronom on May 17, 2021. Acta Hydrologica Slovaca, vol. 23, no. 1, 62–72. doi: 10.31577/ahs-2022-0023.01.0007

Price, K., Purucker, S. T., Kraemer, S. R., Babendreier, J. E., Knightes, C. D. (2014): Comparison of radar and gauge precipitation data in watershed models across varying spatial and temporal scales, Hydrological Proccesses, 28, 3505-3520. doi: 10.1002/hyp.9890

Sleziak, P., Jančo, M., Danko, M., Méri L., Holko, L. (2023): Accuracy of radar-estimated precipitation in a mountain catchment in Slovakia. Journal of Hydrology and Hydromechanics, 71(1), 111–122. doi: 10.2478/johh-2022-0037

SMHI (2014): Integrated Hydrological Modelling System, Manual, ver. 6.4, approved by B. Johansson, Dnr: 2013/ 299/2.10.1, SMHI, 140 p.

Starks, P. J., Moriasi, D. N. (2009): Spatial resolution effect of precipitation data on SWAT calibration and performance: Implications for CEAP. Transactions of the ASABE, 52(4), 1171–1180. doi: 10.13031/2013.27792

Tobin, K. J., Bennett, M. E. (2009): Using SWAT to model streamflow in two river basins with ground and satellite precipitation data. JAWRA Journal of the American Water Resources Association, 45: 253-271. doi: 10.1111/j.1752-1688.2008.00276.x

Vlasák, T., Krejčí, J. (2021): Statistical post-processing of short-term hydrological ensemble forecasts using the application of the dressing method. Acta Hydrologica Slovaca, vol. 22, no. 2, 276–283. doi: 10.31577/ahs-2021-0022.02.0031

World Meteorological Organization (WMO) (2011): Manual on flood forecasting and warning. WMO-No. 1072, WMO Geneva, 138 p. ISBN: 978-92-63-11072-5.

Mgr. Kateřina Hrušková, PhD. (*corresponding author, e-mail: katerina.hruskova@shmu.sk)
Ing. Hana Hlaváčiková, PhD.
Slovak Hydrometeorological Institute
Jeséniova 17
83315 Bratislava
Slovak Republic

DOI: 10.31577/ahs-2023-0024.02.0028

ACTA HYDROLOGICA SLOVACA

Volume 24, No. 2, 2023, 254 – 265

Interactions of natural and anthropogenic drivers and hydrological processes on local and regional scales: A review of main results of Slovak hydrology from 2019 to 2022

Ján SZOLGAY*, Pavol MIKLÁNEK, Roman VÝLETA

The need to increase understanding of the impacts of changing natural and anthropogenic drivers on hydrological processes on local and regional scales is an essential prerequisite for advancing hydrology and a precondition for solving water resources management tasks. Slovakia exhibits abundant spatial and temporal variability of hydrological processes complicating the generalisation of runoff regimes. Changing climate and recent extreme floods and droughts put additional pressure on improving the observing, monitoring, describing, and modelling of hydrological processes. This paper reviews the response of hydrologic research in Slovakia to these challenges published in international journals from 2019 to 2022. It continues the practice of publishing the review part of the Slovak National Reports to IUGG on behalf of the IAHS (Szolgay, 2003; 2007; 2011; 2015; 2019), which follows the custom of National IUGG Committees to prepare a Quadrennial Report for the IUGG General Assemblies containing comprehensive summaries of national activities in geodesy and geophysics (Szolgay, et al., 2023).

KEY WORDS: climate change, hydrological processes, runoff regimes, hydrological research, Slovakia

Introduction

It is internationally recognized that the need to increase understanding of the impacts of changing natural and anthropogenic drivers on hydrological processes on local and regional scales is an essential prerequisite not only for the advance of the science of hydrology but a necessary precondition for addressing practical water resources management problems (Blöschl et al., 2019; Blauhut et al., 2022; Dolejš et al., 2022). The abundance of spatial and temporal variability of climatic drivers and regional and local runoff generation controls in Slovakia (Lehotský et al., 2022; Lehotský and Boltižiar, 2022) results in various runoff regimes. That complicates the attempts to arrive at generalized descriptions of the genesis of particular types of regimes and events. The same applies to hydrological extremes, which generally exhibit specific patterns of regional and local hazards (Blöschl et al., 2019), complicating thereby the design of generally applicable mitigation schemes (Lun et al., 2021; van Loon et al., 2022). In this respect, understanding the local, catchment and regional scale of hydrological processes became imperative in addressing science and practical water resources management questions. Specifying ecosystem services (Kaletová et al., 2019; Pastor et al., 2022) requires studying fundamental drivers that alter patterns and processes across spatial and temporal dimensions in catchments and streams (Allen et al., 2020). New data sources (such as remote sensing (Kuban et al., 2022), radar meteorology (Nechaj et al., 2019; Méri et al., 2021), Lidar measurements (Vorobyeva et al., 2019) experiments on hillslopes, and tracer studies have offered unique opportunities to develop and compare different models of the same type (e.g., distributed) or different types of models (e.g., distributed vs lumped, process-based vs conceptual) on a local and regional basis. The confrontation of catchment experiments with results from catchment modelling has become popular in recent years in the region (Szolgay et al., 2020). This report continues the tradition of the Slovak National Reports to the International Union of Geodesy and Geophysics (IUGG) on behalf of the International Association of Hydrological Sciences (IAHS), (see Szolgay, 2003; 2007; 2011; 2015; 2019). It contains the part of the 2019 – 2022 report which reviews the response of hydrologic research in Slovakia from 2019 to 2022 to these challenges (Szolgay et al., 2023). The main research focuses are referenced in the bibliography of selected research papers with a short description of the paper.

Soil-water-plant-atmosphere interactions on point and plot scales

The need to develop an increased understanding of the erosion and transport processes on the plot and catchment scales under the specific physiographic conditions of Slovakia was stressed. Research on water

and material transport in the soil-water-plant-atmosphere system has been partly focused on quantifying the water balance components in the unsaturated zone of soils in natural, agricultural and forested catchment ecosystems. Field research was conducted, and methodological aspects of modelling were tested and verified under lowland conditions and in forested experimental mountainous catchments. Estimation of the components of the water balance (including water content of the snowpack), the interpretation of infiltration, evaporation, transpiration, capillary inflow and the seepage of water into lower horizons using monitoring and mathematical modelling resulted in an advanced quantitative analysis of the elements of the water balance equation. The spatial and temporal variability of the soil's hydraulic conductivity were also studied. Soil water repellency was studied at several sites on actual natural soils. Laboratory and field research on the shrinking and swelling processes in heavy soils was focused on the East Slovakian Lowland.

Botyanszká et al. (2022) investigated the effect of the microplastics in silty loam soil on selected soil properties and the growth of radishes. Still, the measured values of the soil characteristics have not shown significant changes. Czachor et al. (2020) investigated how sample geometry affects the water retention curve by simulation and experimental proof. A 3D virtual network was numerically constructed from particles of various sizes, and the drainage process was simulated. The resulting moisture retention curves suggested that the sample geometry affects the drainage. Dulovičová et al. (2022) assessed the hydraulic conductivities from 14 empirical formulas. They developed a simple method to estimate hydraulic conductivities for clayey sand sediments using sediment samples extracted from irrigation canals in Žitný Ostrov, Southern Slovakia. Gluba et al. (2021) studied the effect of fine-size-fractionated sunflower husk biochar on water retention properties of sandy arable soil and explained the water retention effects as the interplay between the dose, the size of biochar particles, and the porous properties of biochar fractions. Gomboš et al. (2021) studied the winter water refill of the soil profile of heavy clay soils, lighter clay-loam-silty soils and the lightest loam soils from three localities of East Slovakian Lowland. The soil water storage, vertical scatter of soil profile moisture volume, temporal and spatial moisture regime changes and soil water availability for plant cover during the 2015 extreme drought period were analysed.

Gomboš et al. (2022) presented results of theoretical approaches and experimental measurements of the settling rate of soil microparticles from laser diffraction measurements on soil samples taken in the East Slovakian Lowland. The results were compared with the results calculated by the Stokes equation. Hlaváčiková et al. (2019a) presented results of quantification of the number of macropores, their relative volume and the ratio of water infiltrating through the macropores for five study sites with stony soils located in a mountain catchment of northern Slovakia. Hlaváčiková et al. (2019b) investigated the effect of two types of biochars on the water retention of clay, loamy soil and silica sand. Despite the positive effect on soil water retention, a statistically significant increase in available water capacity was identified only in the loam soil.

Jančo et al. (2021) investigated the effect of mature spruce forests on canopy interception in subalpine conditions during three growing seasons. Throughfall and gross precipitation measurements were carried out at an elevation of 1,420 m a.s.l. in the Western Tatra Mountains and evaluated with respect to the interception process during the growing season from May to October 2018–2020. Kidron et al. (2022) reviewed mechanisms for biocrust-modulated runoff generation concerning mechanisms for runoff generation due to water repellency, pore-clogging, soil texture and structural features, including surface roughness. Oravcová and Vido (2022) aimed to evaluate the risk of drought from a meteorological point of view and the subsequent response in soil hydrology throughout the hydrological years 2015 and 2016 in beech forests in Central Slovakia. The drought lasted longer in deeper layers and retreated only after long-lasting rainfall. Sudden heavy rainfall has proven ineffective at moistening the entire soil profile, impacting only the upper few centimetres while the main root zone suffers from water shortage. Rončák et al. (2021) analysed and statistically confirmed the relationship between the computed daily values of the effective precipitation index and the measured moisture content of the topsoil of a research site near Nitra, Slovakia. Sándor et al. (2021) considered the impact of climate, soil properties and grassland cover on soil water repellency. They showed an area of land is more likely to be water-repellent if it has a sandy soil texture and a high frequency of prolonged drought events. To study the separate and combined effects of soil texture, climate, and grassland cover type, four sites from different climatic and soil regions were selected in Italy, Hungary, United Kingdom and Slovakia.

Tall et al. (2019) studied the influence of soil texture on the course of volume changes of soil on 172 soil samples with different textures collected from 11 sites in the Eastern Slovak Lowland. These were used to measure dependencies between soil volume changes and soil moisture changes under laboratory conditions. Ten mathematical models were created to estimate the relationship between volume changes of soil and soil moisture content and texture. Tall et al. (2019) and Tall and Pavelková (2020) dealt with the development and comparison of individual soil water balance components in two different soil profiles from the Easter-Slovakian-Lowland using two lysimeters filled monolithically with sandy soil profile and silty-loam soil maintaining a constant groundwater level of 1 m below ground. The level was maintained in both soil profiles. Under the same meteorological conditions, all differences in the development of water balance components were caused only by the differences in soil profiles. The actual evapotranspiration and water flow at the bottom of the soil profiles were compared. Under the specific conditions of this experiment, it was shown that the silty-loam soil profile was more prone to drought than the sandy soil profile.

Catchment scale surface, subsurface and groundwater flow processes and mathematical modelling of runoff and water quality

With a particular interest in surface, subsurface and groundwater runoff, runoff components were estimated by experimental research, mathematical rainfall-runoff models, water balance studies, and runoff separation methods. Tracer techniques were used to study water movement in the soil and bedrock and the mean transit times in catchments. Modelling was used to estimate the relationship between surface waters and groundwater in the weathered zone of stony soils, where rapid runoff and the reaction of groundwater were studied. Remote sensing was used when describing the spatial distribution components of the hydrological cycle in mountainous catchments. The overall trends in the spatial and temporal distributions of snow density, height and water equivalent in several mountainous catchments were analysed. Snowmelt components hydrologic models used both energy-based and temperature-index approaches in general. The validation of snow models using satellite images was tested.

Cisty et al. (2021a) presented a study dealing with the similarity of catchments, which may be utilised in estimating river flows in catchments without flow measurements. A penalisation method of evaluating similarity was proposed, which helps to identify hydrological similarity, i.e., finding the most similar catchment to a given catchment in the rainfall-runoff process. Kaya et al. (2021) studied the capabilities of soft computing techniques for estimating daily evapotranspiration in Košice. Daily solar radiation, relative humidity, air temperature, and wind speed were the meteorological variables considered in different combinations of multilayer perceptron MLP, support vector regression, and multilinear regression models and are compared with each other and with the Hargreaves-Samani, Ritchie, and Turc empirical equations. Model results showed that the MLP model performed better than the other soft computing techniques. Kuban et al. (2022) investigated the effects of satellite soil moisture data on the parametrisation of topsoil and root zone soil moisture in a conceptual hydrological model in those catchments, which in the validation of the dual-layer conceptual semi-distributed model showed improvement in the runoff simulation efficiency compared to the single objective runoff calibration. The runoff simulation efficiency of three multi-objective calibration approaches was separately considered. Inferences about the specific location and the physiographic properties of the catchments where the inclusion of ASCAT data proved beneficial were made. Lukasová et al. (2019) and Lukasová et al. (2020) investigated the potential of phenological metrics from moderate resolution remotely sensed data to monitor the altitudinal variations in phenological phases of European beech and phenological response to drought. Phenological metrics were derived from the NDVI annual trajectories fitted with a double sigmoid logistic function. Ground observations of phenological phases from twelve beech stands along the altitudinal gradient were employed. The effect of altitude was evaluated through differences in local climatic conditions, especially temperature and precipitation, from the last 30 years in 12 study stands. The approach presented in this paper contributes to a more explicit understanding of satellite data-based beech phenology along the altitudinal gradient. It will be useful for determining the optimal distribution range of European beech under changing climate conditions in hydrological modelling.

Mačejná et al. (2021) hydro-bio-chemical balance of total mercury at former cinnabar mining locality. The most important fluxes of total mercury in two small forested catchment areas with different anthropogenic loads in the Kremnické vrchy Mountains. The study highlighted the importance of forest areas to the biogeochemical cycle of Hg and the influence of areas close to cinnabar mining, even inactive ones. Mezei et al. (2019) combined yearly Landsat-derived bark beetle infestation spots from 2006 to 2014 and meteorological data to identify the susceptibility of forest stands to beetle infestation. Digital elevation model-derived potential radiation loads predicted beetle infestation, especially in the peak phase of the beetle epidemic. indicating that bark beetles prefer sites with higher insolation during outbreaks. Solar radiation, easily determined from the DEM, better identified beetle infestations than commonly used meteorological variables and can be used in hydrological models in beetle infestation prediction sub-models.

Tátošová et al. (2021) evaluated the extent of changes in land use in Nitra from 1954 to 2017. The growth of areas with minimal infiltration capacity in the Slovak University of Agriculture area was identified. The possibilities of using rainwater and its accumulation in the monitored area were discussed. Varga and Velísková (2021) assessed the time course of water and air temperature in the locality of the Turček reservoir during its operation from 2005–2019. The analysis confirmed that it is impossible to determine a significant trend despite the rise in annual air temperature during the study period.

Experimental research in snow hydrology has a long tradition in Slovakia. Systematic measurements resulted in a large database of field measurements which started in 1960 in the Low Tatra Mountains and were later extended to the West Tatra Mountains by the Institute of Hydrology of the Slovak Academy of Sciences (Holko et al., 2021). The snow regime of forested sites received particular attention (Bartík et al., 2019). The estimation of snow redistribution by the wind was also outlined, and the spatial and temporal variations of snow water equivalent and the water balance were also documented (Holko et al., 2021). The impact of the changing climate on the snow water using isotopic data, trend and attribution analyses were studied (Holko et al., 2020b). Snow accumulation and melt modelling were practically oriented recently (Holko et al., 2022). Ways were explored how to constrain the parameters of the snowmelt components of an HBV-type model and improve its performance (Sleziak et al., 2020). Studies focusing on the distribution of snow cover in the forests and ski slopes in Central Slovakia were also conducted, and implications for ecosystem services

were defined (Mikloš et al., 2020a; Mikloš et al., 2020b).

Erosion, sediment transport, river morphology and hydro-ecology

Qualitative and quantitative investigations of the effect of river morphology on ichthyological fauna in both natural and regulated segments of selected rivers were conducted (e.g., fish species composition, species diversity, the abundance and biomass of particular species, the mean individual weight and the ichthyomass were monitored during the spring and autumn seasons, etc.). Factors affecting fish population density were also specified. In a natural stream segment, the number of species, the diversity of species and equitability indices were higher than in regulated ones. Several projects focused on studying river and floodplain processes (flow regime, development of river channels and floodplains, sediment transport) using numerical and physical models to analyse the impacts of human interventions on the river's environmental quality and the adjacent areas. Morphologically stable and environmentally sensitive river training measures were also sought to support creating a natural range of instream and bankside habitats for fisheries, flora and fauna and to protect the wetland ecosystems.

Cisty et al. (2021b) set out options for modelling suspended sediment concentrations for ungauged periods on the Danube River profile in Bratislava. Regression using least absolute selection and shrinkage operator, support vector regression and deep learning neural network were compared using various data sources. A significant increase in the precision of modelling suspended sediment concentrations over the standard rating curve method was achieved. Hlavčová et al. (2019) estimated the effectiveness of crop management on sediment transport on hilly agricultural land in the Myjava region. Field experiments with a rainfall simulator on experimental plots estimated surface runoff and the mass of sediments transported and were used to parameterise the SMODERP physically-based hydrological model. The hydrological modelling of the surface runoff on the selected slope profile quantified the protective effect of various soil covers on reducing surface runoff and sediment transport. Honek et al. (2020) estimated and compared sedimentation rates in small reservoirs by three empirical models (USLE, RUSLE and USPED) applied to two small catchments taking advantage of real measured and modelled sedimentation during 2012 and 2017. The study emphasised the importance of the R-factor value, which quantifies the ability of precipitation to cause soil erosion and is a key component of the above-mentioned empirical models. The authors identified the correlation ($R > 0.7$) between observed sedimentation, the R-factor, and precipitation, and concluded that the supposed rise of precipitation in Central Europe due to climate change will lead to an increase in the levels of stored sediment in reservoirs. The USPED model was recommended to estimate the modelling of the siltation rate in small reservoir maintenance projects.

Kaletová et al. (2019), Kaletova et al. (2021), and Pastor et al. (2022) considered the temporal flow variability of non-perennial rivers and the relevance of intermittent rivers in an agricultural landscape in assessing their ecosystem service provision for three different hydrological phases: flowing conditions, isolated pools, and dry streambeds. They also discussed the spatial variability of flow regimes. Kidová et al. (2021) evaluated the impact of river training works on the braided-wandering Belá River in the Slovakian Carpathians. Decreasing geodiversity in managed river reaches, a rapid increase in flow velocity during an extreme flood in trained river reaches, and increasing erosive force in the channel zone was confirmed.

Lehotský et al. (2022) reconstructed the history of the Danube Plain (Podunajská rovina), the largest fluvial system in Slovakia. They showed that in the past, the territory of the Danube Plain has operated as a dynamic fluvial system (inland delta) with its anastomosing, migrating, meandering and braided river channel patterns and the development of several fluvial terraces, levees, abandoned channels and aeolian landforms. Okhravi et al. (2022) addressed the problem of flow resistance in lowland rivers impacted by distributed aquatic vegetation by hypothesising that a fixed value for the bed roughness coefficient in lowland rivers (mostly sand-bed rivers) is deemed practically questionable in 45 cross-sections in four lowland streams. They showed that bed forms and aquatic vegetation were significant sources of boundary resistance in lowland rivers. The study ended with two new flow resistance predictors, which connected the dimensionless unit discharge to flow resistance factors, Darcy-Weisbach and Manning coefficients.

Rodríguez-González et al. (2022) stressed the role of Riparian zones as the paragon of transitional ecosystems, providing critical habitat and ecosystem services that are especially threatened by global change. Following consultation with experts, they identified ten key challenges which must be addressed for riparian vegetation science and management improvement. Using a sediment cascade approach, Rusnák et al. (2020) studied channel and cut-bluff failure connectivity in the braided-wandering Belá River. A terrestrial laser scanning time series was generated by systematically monitoring the cut-bluff slope surface. Volume changes were estimated, and the conceptualisation model of coupling of cut-bluff slope based on spatial and temporal analyses of channel hydrology, a gravity-conditioned transformation of matter and detailed sediment budget calculations was developed. Rusnák et al. (2019) monitored a chute cutoff in the meander bend, the avulsion channel evolution and river morphology changes using UAV photogrammetry on the gravel bed of the Ondava River in Outer Western Carpathians after the 2010 flood events. The mechanism of evolution and post-cutoff avulsion channel adjustment using photogrammetry and field survey was described. Sokáč et al. (2019) presented new approaches to simulating 1D substance transport and tested them on tracer experiments in three small streams in Slovakia with dead zones. Evaluation of the proposed methods, based on different probability distributions, confirmed that they

approximate the measured concentrations significantly better than those based upon the commonly used Gaussian distribution.

Štefunková et al. (2020) evaluated a methodology to assess the influence of hydraulic characteristics on habitat quality from the Riverine Habitat Simulation model, which represents the quality of the aquatic habitat by the weighted usable area using brown trout as the bioindicator. The influence of flow velocity and water depth as basic abiotic characteristics that determine the ratio of the suitability of the instream habitat on the objective evaluation of the habitat quality was targeted. Three methods for assessing the habitat quality were tested. Štefunková et al. (2021) evaluated the relationship between abiotic flow characteristics and habitat quality in mountain streams of Slovakia, which was assessed using the Instream Flow Incremental Methodology (IFIM), which uses bioindication. Brown trout was selected as a bioindicator because of its sensitivity to morphological changes, and its occurrence in sufficient reference reaches. Fifty-nine reference reaches of fifty-two mountain and piedmont streams in Slovakia were analysed. Valent et al. (2019) performed a joint sedimentation-flood retention assessment of a small water reservoir in Slovakia. They presented an analysis of changes in the retention capacity over eight years based on a detailed reservoir bathymetry conducted using an acoustic Doppler current profiler. The possibility of strengthening the reservoir's role in flood protection was also investigated.

Pekárová et al. (2020) analysed the long-term development of runoff and nitrates nitrogen concentrations in the Parná River at Horné Orešany water gauge station during the period 1991–2018. Discharges in the Parná River decreased slightly; nitrate concentrations markedly decreased in this river basin. The relation between discharge and nitrate concentration was used to derive exponential empirical relations for estimating the nitrate-nitrogen concentrations in the stream based on mean daily discharge. Siman and Velísková (2020) presented results of the comparison of yearly total nitrogen emissions and the contribution of different emission pathways on these emissions into surface streams for three river catchments in Slovakia territory with a contrasting proportion of agricultural land to the total area of the river catchment using the numerical MONERIS model. Results indicated that in river catchments with a higher proportion of agricultural land, higher contribution of nitrogen emission was carried out mainly via groundwater (especially in lowland) and agricultural erosion and drainage systems.

Groundwater

The quantitative aspects of groundwater formation and regimes were studied regionally. Research is also oriented towards the influence of human activities on the natural groundwater regime and surface-groundwater interactions. Research on the impact of human activities on the recharging groundwater amounts and water quality under different hydrologic conditions was conducted. Numerical groundwater models were used to analyse, predict and control groundwater levels at several water structures in Slovakia. The conditions under which technical measures could improve groundwater regimes, even in extreme hydrologic conditions, were also sought. Abd-Elaty et al. (2019) contributed to groundwater protection techniques based on changing boundary conditions, installing a cut-off wall and using linings for polluted drains. They presented a possible way forward to treat contaminated stream networks. It was concluded that technical measures could improve the groundwater regime. Abd-Elaty et al. (2020) presented simulation-based solutions for reducing soil and groundwater contamination from fertilisers in arid and semi-arid regions by installing drainage networks, which can decrease the groundwater and soil contamination from nonpoint contamination. Baroková et al. (2020) assessed the impact of cut-off walls on the regime of groundwater levels during extreme hydrological conditions in the broader area for both steady and unsteady scenarios. Červeňanská et al. (2021) reconstructed in a case study concerning the May and June 2010 flood the groundwater level rise in the Žitný ostrov region and established the basis for the construction of flood hazard maps and flood risk management plans. Pekárová et al. (2022) aimed to analyse and model the groundwater temperature at the water table in different regions of Slovakia by a simple groundwater temperature model based on a one-dimensional differential Fourier heat conduction equation. It can estimate future groundwater temperature trends using regional air temperature projections for different greenhouse gas emission scenarios. Šoltész et al. (2020) presented a hydraulic assessment of groundwater flow in the area affected by the realisation of the hydraulic gate on a river branch. A 3D mathematical model was created to simulate groundwater flow by changing boundary conditions of surface water flows during flood periods.

Hydrological extremes

Recent extreme events in Europe have also stimulated public discussion on the issue of whether the frequency and severity of these have been increasing in Europe and Slovakia and if such changes could be attributed to anthropogenic influence. Large floods and droughts occurred in some regions of Central Europe also during the period covered by this report. That increased interest in the flood and drought formation in catchments from various areas of Slovakia. Statistical analysis was used to study past extreme events. Knowledge of the genesis of extreme precipitation and floods and data on rare events was needed to develop regional generalizations of the flood and drought regime. Several extreme events were individually investigated, and the formation of these in ungauged basins was reconstructed using data from at-site hydrological surveillance and available data from the hydrological and meteorological network, together with radar and satellite data. An assessment of the historical extremes floods in several rivers

complemented characteristics of measured and historical extreme flows. The various risks associated with flooding and droughts were characterized.

Almikaeel et al. (2022b) used a machine to learn hydrological drought forecasting. The assessment of hydrological drought was carried out by indexing dry, normal, and wet hydrological situations. Artificial neural networks and support vector machine models were applied to predict the hydrological drought based on daily average discharges. Bačová Mitková et al. (2021) stressed the need to harmonize design flood assessment methods along long international rivers in the example of the Danube River. Using the Log-Pearson type III distribution, the regionalization of the Log-Pearson type III distribution skew parameter, they also analysed the effect of the inclusion and exclusion of the historical extremes. Bartok et al. (2022b) applied a novel approach in using machine learning-based fog nowcasting for aviation. Various machine learning algorithms (support vector machine, decision trees, k-nearest neighbours) were adopted to predict fog with visibility below 300 m for a lead time of 30 min. Beyond the standard meteorological variables as predictors, the forecast models also used information on visibility obtained through remote camera observations. These were also applied by Bartok et al. (2022a) to assess visibility conditions.

Blöschl et al. (2019) and Blöschl et al. (2020), with the participation of Slovak hydrologists, analysed a comprehensive dataset of flood observations in Europe. They showed that the changing climate has increased river flood discharges in some regions of Europe but decreased in others. They also showed that the past three decades were among the most flood-rich periods in Europe in the past 500 years. The flood changes were broadly consistent with climate model projections for the next century, suggesting that climate-driven changes are already happening. This period differs from other past flood-rich periods in terms of its extent, air temperatures and flood seasonality. The results support calls for considering climate change in flood risk management. The same dataset was used by Lun et al. (2021) to provide a performance baseline for more local flood studies by assessing the estimation accuracy of regional multiple linear regression models for estimating flood moments in ungauged basins.

Čubanová et al. (2019), Šoltész et al. (2021), Mydla et al. (2021), Šoltész et al. (2022), and Čubanová et al. (2022) proposed several management solutions for mitigating flood and drought risk in smaller municipalities based on hydrological-hydraulic assessment. Markovič et al. (2021) investigated extreme heavy precipitation events in the Slovak Republic in the period 1951–2020 in terms of their spatial and temporal distribution. The goal was to create a dynamic-climatological analysis of atmospheric circulation patterns that can eventually lead to extreme multi-day precipitation events. Onderka and Pecho (2021) evaluated the sensitivity of total rainfall kinetic energy, 15-min peak intensities, and total event depth concerning pre-event atmospheric conditions in the northern part of the Pannonian Plain. The analyses revealed strong responsiveness of rainfall kinetic energy and 15-minute peak rainfall intensities to dew point temperature.

Solín and Rusnák (2020) presented a methodological approach to preliminary flood risk assessment conceptually based on the regional typing and integrated flood risk assessment. The basic spatial unit was defined as the municipality district. The flood risk potential index was determined as aggregating the flood hazard and flood consequences. Šurda et al. (2020) aimed to determine the monthly values of the meteorological drought indices of the Nitra region in 2014–2018 and to analyse their sensitivity based on comparing the determined droughts frequency. Vojtek et al. (2022) mapped and assessed the riverine flood potential in municipalities of Slovakia using vector-based spatial multi-criteria analysis and geographic information systems. The flood potential index in municipalities was computed based on eight flood factors, and sensitivity analysis using the modelling approaches was proposed.

Raška et al. (2022) focused on the empirical evidence of the effects of nature-based solutions in flood risk mitigation across various fragmented settings, and their implementation faces a series of institutional barriers. A community expert perspective was used to identify barriers and their cascading and compound interactions. A comprehensive set of 17 barriers affecting the implementation of 12 groups in both urban and rural settings in five European regional environmental domains were identified, and avenues for further research, connecting hydrology and soil science, on the one hand, and land use planning, social geography and economics, on the other suggested. Solín (2019) and Solín and Sládeková Madajová (2019) identified regional types of flood hazards in mountainous regions resulting from the physiographic characteristics. It has been shown that the soil texture permeability and the forest cover are the basin attributes that influence the spatial variability of flood hazards. Based on their combination, several physical geographic classes were created. A framework of integrated flood risk assessment was taken into account.

Vojtek et al. (2019) reported a sensitivity analysis of flood inundation mapping in small and ungauged basins using the event-based approach for small and ungauged basins and a one-dimensional in terms of simulated flood area and volume to different combinations of input parameters. Hydrologic modelling results highlighted the great variety of design peak discharges, which strongly influence the modelled area and volume. Vojtek et al. (2021) identified areas with different levels of riverine flood potential in the Nitra River basin using multi-criteria evaluation, hierarchical analytical process, geographic information systems, and seven flood conditioning factors. Zeleňáková et al. (2019) presented a case study of flow modelling focusing on the open channel of the Slatvinec stream running through the north-east Slovakian village of Kružlov for identifying flood risk areas in the village. Cost analysis for evaluating flood damage to property supplemented the modelling.

Runoff fluctuations and anthropogenic impacts on hydrological processes

Time series of precipitation, air temperature and runoff were analysed in several studies to detect and attribute climate change signals using statistical methods. The long-term variability of extremes of Slovak rivers, as well as rivers in the temperate zone of the Northern Hemisphere, were also analysed. The analysis detected a time shift in the occurrence of runoff extremes in the regions studied. Studies of groundwater runoff changes in different geological conditions in the last four decades showed a decrease in groundwater runoff in most of the assessed catchments in Slovakia. Studies of spring yields in the karstic areas of Slovakia showed decreasing trends in almost all the evaluated cases. Local and regional hydrological droughts and the water balance of the sensitive regions, such as agricultural land and wetlands, were studied, too. Intermittency was observed recently in several rivers, and the phenomenon started to be explored. Several RCM and GCM-based climate change scenarios were used, and the construction of physically plausible downscaled scenarios of daily, monthly and annual time series for air temperature, precipitation and air humidity was also attempted. Attempts to design scenarios of extreme short-term precipitation totals began. According to these scenarios, a significant increase in air temperature, small changes in long-term precipitation totals, and a remarkable rise in short-term precipitation extremes are expected in Slovakia in the warm half-years. On the other hand, more frequent and extended periods of drought may occur, mainly in the Slovak lowlands, because higher precipitation and a warmer climate in winter will significantly affect the winter runoff and snow regime on most of the territory of Slovakia. Therefore, the whole territory of Slovakia could become more vulnerable to drought in the summer and autumn.

Almikaeel et al. (2022a) investigated flow rate fluctuations in two different streams in Slovakia to investigate the low and peak flow periods and to identify the trends in monthly and annual mean flows for both rivers. Analysing daily mean discharge data from two different types of streams has required using a robust normalisation approach to verify the comparability between the chosen streams. Blaškovičová et al. (2022a) and Blaškovičová et al. (2022b) focused on the assessment of river drought in Slovakia. Low-flow characteristics and their changes in the 2001–2015 period compared with the 1961–2000 reference period were evaluated with two methods at selected representative water-gauging stations. The results show significant changes in the compared periods. Differences in individual regions of Slovakia were also described.

Csáki et al. (2020) described a multi-model climatic water balance prediction in the Zala River Basin using a modified Budyko framework. The research included validating models and predictions of the main components of the water balance (evapotranspiration and runoff) and using precipitation and temperature results of 12 regional climate model simulations. The mean annual evapotranspiration rate is expected to increase slightly during the 21st century, and for runoff, a substantial decrease can be anticipated. Danáčová et al. (2021) studied the occurrence of areal droughts from 2011 to 2020 in Slovakia based on the data from 164 water gauging stations. The mean monthly discharges were compared with the long-term mean monthly discharges for the baseline period 1961–2000. Trend detection analysis of the mean monthly discharges in 1961–2020 was conducted. The months of April, June, July, August and October were detected as the months with the highest occurrence of mean monthly discharges below 40% of the long–term mean monthly discharges for the reference period.

Halmová et al. (2022) evaluated changes in the hydrological balance of the Krupinica River for the entire 90-year period of observations and three 30-year subperiods. Changes in water resources in the river basin over the three mentioned time subperiods were analysed, and a simple regression relationship between runoff, precipitation and the air temperature was derived to estimate the future development of the annual runoff from the basin. Holko et al. (2020a) Analysed changes in the hydrological cycle of a pristine alpine mountain catchment by isotopic data, trend and attribution analyses. δ18O in precipitation has remained constantly higher since 2014, which might be related to greater evaporation in the region of origin of the air masses bringing precipitation to the studied part of Central Europe. The seasonality of δ18O became less pronounced since 2014. Linear regressions between the drivers and supposedly changed data series explained only about 31% to 36% of the variability.

Lukasová et al. (2021) dealt with regional and altitudinal aspects of summer heatwave intensification in the Western Carpathians for various elevations. The percentile threshold-based calculation of heatwaves was used, which, compared to those using absolute thresholds, allows for revealing the possible threats of climate warming extremes at the range of altitudes. The greatest intensification of heatwaves was evident, particularly in the last decade. Minďaš et al. (2020) evaluated the long-term changes in the chemical composition of precipitation in the mountain forests of Slovakia in a forty-one-year period (1987 to 2018). Two stations with long-term measurements of precipitation quality were selected, all basic chemical components were analysed, and changes in the individual components were statistically evaluated. The results showed significant declining trends for almost all components, which can significantly affect element cycles in mountain forest ecosystems.

Onderka et al. (2020) evaluated the efficiency and reliability of water harvesting systems in dependence on the local climate in Slovakia using 84 rainfall records from climatologically distinct regions. A considerable spatial and seasonal variability has been observed in the statistics of rainfall events. Inter-event times decrease with elevation, whereas event volume and annual incidence of rainfall events increase with elevation. The applicability of the derived rainfall statistics was illustrated by simulations for a typical residential house using the analytical probabilistic approach. Empirical

relationships between tank size and site elevation have been developed to estimate tank sizes for ungauged locations. The simulations show that rain barrels in the southern parts of Slovakia require larger storage capacities than those located in the mountainous regions. The presented annual and seasonal estimates of rainfall characteristics are published for the first time.

Škvareninová et al. (2022) stressed that the onset and duration of phenological events are key indicators of the ecological impact of climate change on vegetation. During 1987–2016, they analysed the occurrence and intensity of frosts during May. Results indicate that recent climate change caused the beginning of flowering to start significantly earlier; thus, the risk of late frost damage to flowers is highly probable, particularly at 160, 300 and 500 m a.s.l., where the flowering and frosts co-occur. Decreased risk of frost damage was found at 400 and 700 m a.s.l., Vido and Nalevanková (2020) stressed that the West Carpathian region forms a transitional zone for drought patterns, which are complicated because of the geomorphologically complicated landscape and analysed drought occurrence and trends indices at available climatological stations of the Slovak Hydrometeorological Institute in the upper Hron region within the 1984–2014 period. They found that drought incidence decreased with increasing altitude, and increasing air temperature increased the difference in drought trends between lowlands and mountains. Abrupt changes in the time series of drought indices, which could indicate some signals of changing atmospheric circulation patterns, were not revealed.

Conclusion

Changing climate, recent extreme events and the requirements of implementing the European Water Framework Directive have stimulated public and scientific discussion in Slovakia on improving observing, monitoring and modelling hydrological processes describing these (Szolgay et al., 2020). This report reviewed the response of hydrologic research in Slovakia to the challenges of global hydrologic research between 2019 and 2022. It follows previous reports from 1999, 2004, 2007, 2011 and 2015, and 2019. It summarizes the results and outcomes of the leading research programs in hydrology in Slovakia. The short review and the selected annotated bibliography on hydrological research in Slovakia showed how research reflected the need to investigate the effects of changing natural drivers and new societal pressures on water resources and hydrological processes.

Recent extreme flood and drought events in Slovakia, along with indications of a changing climate, have sparked debate in the scientific community and among the general public about whether the frequency and severity of these events have been rising, how much of these changes may be attributable to human activity, and how best to observe, track, and model the processes that describe them. A thorough understanding of the effects of changing land use and management practices on runoff processes in general and those of extremes in particular, is still desperately needed, despite the substantial amount of research that has been done to explore the primary sources of natural drivers and societal pressures of hydrological phenomena in Slovakia.

It was challenging to come up with generalized explanations of the genesis of particular types of hydrological regimes and events because of Slovakia's rich spatial and temporal heterogeneity of climatic drivers, regional and local control conditions, and the variety of active flow processes during specific seasons and events. This also holds true for particular local and regional hazards of extremes. In this regard, answering scientific and real-world water resource management issues still requires a regional grasp of watershed hydrological dynamics and their modeling. Opportunities provided by new data sources, based on the most recent advancements in radar meteorology, hillslope experiments, and catchment tracer investigations, will allow hydrologists in Slovakia to compare various models on a local and regional scale. Improved process representations in both stochastic and deterministic models in various hydrological settings will be made possible by the additional data sources, which will also make predictions in ungauged basins more trustworthy. It will become crucial to compare the findings of catchment modeling with those of catchment experiments.

Acknowledgement

This work was supported by the Slovak Research and Development Agency under Contract No. APVV 19-0340, No. APVV 20-0374 and by the VEGA Grant Agency Project No. VEGA 1/0577/23.

References

Abd-Elaty, I., Zelenakova, M., Straface, S., Vranayova, Z., Abu-hashim, M. (2019): Integrated Modelling for Groundwater Contamination from Polluted Streams Using New Protection Process Techniques. Water 11 (11), 2321.

Abd-Elaty, I., Pugliese, L., Zelenakova, M., Mesaros, P., Shinawi, A. E. (2020): Simulation-Based Solutions Reducing Soil and Groundwater Contamination from Fertilizers in Arid and Semi-Arid Regions: Case Study the Eastern Nile Delta, Egypt. International journal of environmental research and public health 17 (24), 9373.

Allen, D. C., Datry, T., Boersma, K. S., Bogan, M. T., Boulton, A. J., Bruno, D., Busch, M. H., Costigan, K. H., Dodds, W. K., Fritz, K. M., Godsey, S. E., Jones, J. B., Kaletova, T., Kampf, S. K., Mims, M. C., Neeson, T. M., Olden, J. D., Pastor, A. V., Poff, N. L., Ruddell, B. L., Ruhi, A., Singer, G., Vezza, P., Ward, A. S., Zimmer, M. (2020): River ecosystem conceptual models and non-perennial rivers: A critical review. WIREs Water 7 (5), 1–5.

Almikaeel, W., Čubanová, L., Šoltész, A. (2022a): Comparison of mean daily discharge data for under-mountain and highland-lowland types of rivers. Acta Hydrologica Slovaca 23 (1), 73–81.

Almikaeel, W., Čubanová, L., Šoltész, A. (2022b): Hydrological Drought Forecasting Using Machine Learning—Gidra River Case Study. Water 14 (3), 387.

Bačová Mitková, V., Pekárová, P., Halmová, D., Miklánek, P. (2021): The Use of a Uniform Technique for Harmonization and Generalization in Assessing the Flood

Discharge Frequencies of Long Return Period Floods in the Danube River Basin. Water 13 (10), 1337.

Baroková, D., Červeňanská, M., Šoltész, A. (2020): Assessment of the impact of proposed cut-off walls on ground-water level regime during extreme hydrological conditions. Acta Hydrologica Slovaca 21 (1), 113–122.

Bartík, M., Holko, L., Jančo, M., Škvarenina, J., Danko, M., Kostka, Z. (2019): Influence of Mountain Spruce Forest Dieback on Snow Accumulation and Melt. Journal of Hydrology and Hydromechanics 67 (1), 59–69.

Bartok, J., Ivica, L., Gaál, L., Bartoková, I., Kelemen, M. (2022a): A Novel Camera-Based Approach to Increase the Quality, Objectivity and Efficiency of Aeronautical Meteorological Observations. Applied Sciences 12 (6), 2925.

Bartok, J., Šišan, P., Ivica, L., Bartoková, I., Malkin Ondík, I., Gaál, L. (2022b): Machine Learning-Based Fog Nowcasting for Aviation with the Aid of Camera Observations. Atmosphere 13 (10), 1684.

Blaškovičová, L., Jeneiová, K., Melová, K., Poórová, J., Liová, S., Slivková, K., Síčová, B. (2022a): Changes in Selected Low-Flow Characteristics in the 2001–2015 Period Compared to the 1961–2000 Reference Period in Slovakia. Climate 10 (6), 81.

Blaškovičová, L., Melová, K., Liová, S., Podolinská, J., Síčová, B., Groholʼ, M. (2022b): The drought characteristics and their changes in selected water-gauging stations in Slovakia in the period 2001–2020 compared to the reference period 1961–2000. Acta Hydrologica Slovaca 23 (1), 10–20.

Blauhut, V., Stoelzle, M., Ahopelto, L., Brunner, M. I., Teutschbein, C., Wendt, D. E., Akstinas, V., Bakke, S. J., Barker, L. J., Bartošová, L., Briede, A., Cammalleri, C., Kalin, K. C., De Stefano, L., Fendeková, M., Finger, D. C., …, Willems, P., Živković, N. (2022): Lessons from the 2018–2019 European droughts: a collective need for unifying drought risk management, Nat. Hazards Earth Syst. Sci., 22, 2201–2217, https://doi.org/10.5194/nhess-22-2201-2022.

Blöschl, G., Hall, J., Viglione, A., Perdigão, R.A.P., Parajka, J., …, Zaimi, K., Živković, N. (2019): Changing climate both increases and decreases European river floods. Nature 573 (7772), 108–111.

Blöschl, G., Kiss, A., Viglione, A., Barriendos, M., Böhm, O., …, Waser, J., Wetter, O. (2020): Current European flood-rich period exceptional compared with past 500 years. Nature 583 (7817), 560–566.

Botyanszká, L., Šurda, P., Vitková, J., Lichner, Ľ., Igaz, D. (2022): Effect of microplastics on silty loam soil properties and radish growth. Journal of Hydrology and Hydromechanics 70 (3), 321–329.

Červeňanská, M., Baroková, D., Šoltész, A. (2021): Rye Island, 2010: Impact of the flooding on the groundwater level. Pollack Periodica 16 (3), 70–75.

Cisty, M., Povazanova, B., Aleksic, M. (2021a): Evaluation of Catchments' Similarity by Penalization in the Context of Engineering Tasks—A Case Study of Four Slovakian Catchments. Water 13 (20), 2894.

Cisty, M., Soldanova, V., Cyprich, F., Holubova, K., Simor, V. (2021b): Suspended sediment modelling with hydrological and climate input data. Journal of Hydroinformatics 23 (1), 192–210.

Csáki, P., Gyimóthy, K., Kalicz, P., Szolgay, J., Zagyvai-Kiss, K.A., Gribovszki, Z. (2020): Multi-model climatic water balance prediction in the Zala River Basin (Hungary) based on a modified Budyko framework. Journal of Hydrology and Hydromechanics 68 (2), 200–210.

Čubanová, L., Šoltész, A., Janík, A. (2019): Hydrological-hydraulic assessment of proposed flood protection measures. Pollack Periodica 14 (3), 97–108.

Čubanová, L., Šoltész, A., Mydla, J. (2022): Analysis of droughts due to the operation of water structures: Gidra river case study. Pollack 17 (1), 111–116.

Czachor, H., Rajkai, K., Lichner, L., Jozefaciuk, G. (2020): Sample geometry affects water retention curve: Simulation and experimental proves. Journal of Hydrology 588, 125131.

Danáčová, Z., Jeneiová, K., Blaškovičová, L. (2021): Hydrological situation on Slovak rivers from the point of view of hydrological drought assessment in the period 2011– 2020. Acta Hydrologica Slovaca 22 (2), 230–236.

Dolejš, M., Raška, P., Kohnová, S., Schinke, R., Warachowska, W., Thaler, T., Kočický, D. (2022): On the right track of flood planning policy? Land uptake in Central-European floodplains (1990–2018). Landscape and Urban Planning 228, 104560.

Dulovičová, R., Ovcharovichova, J., Velísková, Y. (2022): Statistical method for a hydraulic conductivity estimate using empirical formulas. J Appl Eng Science 20 (2), 455–463.

Gluba, Ł., Rafalska-Przysucha, A., Szewczak, K., Łukowski, M., Szlązak, R., Vitková, J., Kobyłecki, R., Bis, Z., Wichliński, M., Zarzycki, R., Kacprzak, A., Usowicz, B. (2021): Effect of Fine Size-Fractionated Sunflower Husk Biochar on Water Retention Properties of Arable Sandy Soil. Materials 14 (6).

Gomboš, M., Tall, A., Kandra, B., Pavelková, D. (2021): Influence of soil type on statistical characteristics and graphical results interpretation of the water storage distribution monitoring along the vertical of the soil profile. Acta Hydrologica Slovaca 22 (1), 97–105.

Gomboš, M., Tall, A., Pavelková, D., Kandra, B. (2022): Determination of sedimentation speed of soil micro-particles from laser diffraction measurements. Acta Hydrologica Slovaca 23 (1), 147–154.

Halmová, D., Pekárová, P., Podolinská, J., Jeneiová, K. (2022): The assessment of changes in the long-term water balance in the Krupinica River basin for the period 1931–2020. Acta Hydrologica Slovaca 23 (1), 21–31.

Hlaváčiková, H., Holko, L., Danko, M., Novák, V. (2019a): Estimation of macropore flow characteristics in stony soils of a small mountain catchment. Journal of Hydrology 574, 1176–1187.

Hlaváčiková, H., Novák, V., Kameyama, K., Brezianska, K., Rodný, M., Vitková, J. (2019b): Two types of biochars: one made from sugarcane bagasse, other one produced from paper fiber sludge and grain husks and their effects on water retention of a clay, a loamy soil and a silica sand. Soil Water Res. 14 (2), 67–75.

Hlavčová, K., Danáčová, M., Kohnová, S., Szolgay, J., Valent, P., Výleta, R. (2019): Estimating the effectiveness of crop management on reducing flood risk and sediment transport on hilly agricultural land – A Myjava case study, Slovakia. CATENA 172, 678–690.

Holko, L., Danko, M., Sleziak, P. (2020a): Analysis of changes in hydrological cycle of a pristine mountain catchment. 2. Isotopic data, trend and attribution analyses. Journal of Hydrology and Hydromechanics 68 (2), 192–199.

Holko, L., Sleziak, P., Danko, M., Bičárová, S., Pociask-Karteczka, J. (2020b): Analysis of changes in hydrological cycle of a pristine mountain catchment. 1. Water balance components and snow cover. Journal of Hydrology and Hydromechanics 68 (2), 180–191.

Holko, L., Danko, M., Sleziak, P. (2021): Snowmelt characteristics in a pristine mountain catchment of the Jalovecký Creek, Slovakia, over the last three decades. Hydrological Processes 35 (4).

Holko, L., Danko, M., Jančo, M., Sleziak, P. (2022): Empirical models to calculate the snow water equivalent in the high mountain catchments of the Western Carpathians. Acta Hydrologica Slovaca 23 (2), 241–248.

Honek, D., Michalková, M. Š., Smetanová, A., Sočuvka, V., Velísková, Y., Karásek, P., Konečná, J., Németová, Z., Danáčová, M. (2020): Estimating sedimentation rates in small reservoirs – Suitable approaches for local municipalities in central Europe. Journal of environmental management 261, 109958.

Jančo, M., Mezei, P., Kvas, A., Danko, M., Sleziak, P., Minďáš, J., Škvarenina, J. (2021): Effect of mature spruce forest on canopy interception in subalpine conditions during three growing seasons. Journal of Hydrology and Hydromechanics 69 (4), 436–446.

Kaletova, T., Rodriguez-Lozano, P., Berger, E., Filipa Filipe, A., Logar, I., Helena Alves, M., Calleja, E. J., Jorda-Capdevila, D. (2021): Considering temporal flow variability of non-perennial rivers in assessing ecosystem service provision. Ecosystem Services 52, 101368.

Kaletová, T., Loures, L., Castanho, R. A., Aydin, E., Da Gama, J. T., Loures, A., Truchy, A. (2019): Relevance of Intermittent Rivers and Streams in Agricultural Landscape and Their Impact on Provided Ecosystem Services-A Mediterranean Case Study. International journal of environmental research and public health 16 (15).

Kaya, Y. Z., Zelenakova, M., Üneş, F., Demirci, M., Hlavata, H., Mesaros, P. (2021): Estimation of daily evapotranspiration in Košice City (Slovakia) using several soft computing techniques. Theor Appl Climatol 144 (1-2), 287–298.

Kidová, A., Radecki-Pawlik, A., Rusnák, M., Plesiński, K. (2021): Hydromorphological evaluation of the river training impact on a multi-thread river system (Belá River, Carpathians, Slovakia). Scientific reports 11 (1), 6289.

Kidron, G. J., Lichner, L., Fischer, T., Starinsky, A., Or, D. (2022): Mechanisms for biocrust-modulated runoff generation – A review. Earth-Science Reviews 231, 104100.

Kuban, M., Parajka, J., Tong, R., Greimeister-Pfeil, I., Vreugdenhil, M., Szolgay, J., Kohnova, S., Hlavcova, K., Sleziak, P., Brziak, A. (2022): The effects of satellite soil moisture data on the parametrization of topsoil and root zone soil moisture in a conceptual hydrological model. Journal of Hydrology and Hydromechanics 70 (3), 295–307.

Lehotský, M., Boltižiar, M. (Eds.) (2022): Landscapes and Landforms of Slovakia. World Geomorphological Landscapes. Springer International Publishing, Cham.

Lehotský, M., Maglay, J., Prochádzka, J., Rusnák, M. (2022): Inland Delta and Its Two Large Rivers: Danube Plain, the Danube and Váh Rivers, in: Lehotský, M., Boltižiar, M. (Eds.), Landscapes and Landforms of Slovakia. World Geomorphological Landscapes. Springer International Publishing, Cham, pp. 235–253.

Lukasová, V., Bucha, T., Škvareninová, J., Škvarenina, J. (2019): Validation and Application of European Beech Phenological Metrics Derived from MODIS Data along an Altitudinal Gradient. Forests 10 (1), 60.

Lukasová, V., Škvareninová, J., Bičárová, S., Sitárová, Z., Hlavatá, H., Borsányi, P., Škvarenina, J. (2021): Regional and altitudinal aspects in summer heatwave intensification in the Western Carpathians. Theor Appl Climatol 146 (3–4), 1111–1125.

Lukasová, V., Vido, J., Škvareninová, J., Bičárová, S., Hlavatá, H., Borsányi, P., Škvarenina, J. (2020): Autumn Phenological Response of European Beech to Summer Drought and Heat. Water 12 (9), 2610.

Lun, D., Viglione, A., Bertola, M., Komma, J., Parajka, J., Valent, P., Blöschl, G. (2021): Characteristics and process controls of statistical flood moments in Europe – a data-based analysis. Hydrol. Earth Syst. Sci. 25 (10), 5535–5560.

Mačejná, Ľ., Zacharová, A., Ollerová, H., Škvareninová, J., Škvarenina, J. (2021): Hydrobiochemical balance of total mercury in a forest catchment area at former cinnabar mining locality. Journal of Hydrology and Hydromechanics 69 (2), 209–219.

Markovič, L., Faško, P., Pecho, J. (2021): Climatology of the extreme heavy precipitation events in Slovakia in the 1951–2020 period. Acta Hydrologica Slovaca 22 (2), 294–303.

Méri, L., Gaál, L., Bartok, J., Gažák, M., Gera, M., Jurašek, M., Kelemen, M. (2021): Improved Radar Composites and Enhanced Value of Meteorological Radar Data Using Different Quality Indices. Sustainability 13 (9), 5285.

Mezei, P., Potterf, M., Škvarenina, J., Rasmussen, J. G., Jakuš, R. (2019): Potential Solar Radiation as a Driver for Bark Beetle Infestation on a Landscape Scale. Forests 10 (7), 604.

Mikloš, M., Igaz, D., Šinka, K., Škvareninová, J., Jančo, M., Vyskot, I., Škvarenina, J. (2020a): Ski piste snow ablation versus potential infiltration (Veporic Unit, Western Carpathians). Journal of Hydrology and Hydromechanics 68 (1), 28–37.

Mikloš, M., Skvarenina, J., Jančo, M., Skvareninova, J. (2020b): Density of Seasonal Snow in the Mountainous Environment of Five Slovak Ski Centers. Water 12 (12), 3563.

Minďaš, J., Hanzelová, M., Škvareninová, J., Škvarenina, J., Ďurský, J., Tóthová, S. (2020): Long-Term Temporal Changes of Precipitation Quality in Slovak Mountain Forests. Water 12 (10), 2920.

Mydla, J., Šoltész, A., Orfánus, M. (2021): Measures for flood discharge transformation on the Ondava River. Pollack Periodica 16 (2), 56–60.

Nechaj, P., Gaál, L., Bartok, J., Vorobyeva, O., Gera, M., Kelemen, M., Polishchuk, V. (2019): Monitoring of Low-Level Wind Shear by Ground-based 3D Lidar for Increased Flight Safety, Protection of Human Lives and Health. International journal of environmental research and public health 16 (22).

Okhravi, S., Schügerl, R., Velísková, Y. (2022): Flow Resistance in Lowland Rivers Impacted by Distributed Aquatic Vegetation. Water Resour Manage 36 (7), 2257–2273.

Onderka, M., Pecho, J. (2021): Sensitivity of selected summertime rainfall characteristics to pre-event atmospheric and near-surface conditions. Atmospheric Research 259, 105671.

Onderka, M., Pecho, J., Nejedlík, P. (2020): On how rainfall characteristics affect the sizing of rain barrels in Slovakia. Journal of Hydrology: Regional Studies 32, 100747.

Oravcová, Z., Vido, J. (2022): Understanding the Complexity of Drought within the Soil Profile in Beech Ecosystems on Their Lower Altitudinal Limit in Slovakia. Water 14 (9), 1338.

Pastor, A.V., Tzoraki, O., Bruno, D., Kaletová, T., …, Tsani, S., Jorda-Capdevila, D. (2022): Rethinking ecosystem service indicators for their application to intermittent rivers. Ecological Indicators 137, 108693.

Pekárová, P., Miklánek, P., Pekár, J., Danáčová, Z. (2020): Long-term development of discharge and nitrate concentrations in the Little Carpathians headwaters. Acta Hydrologica Slovaca 21 (1), 48–55.

Pekárová, P., Tall, A., Pekár, J., Vitková, J., Miklánek, P. (2022): Groundwater Temperature Modelling at the Water

Table with a Simple Heat Conduction Model. Hydrology 9 (10), 185.

Raška, P., Bezak, N., Ferreira, C. S. S., Kalantari, Z., …, Slavíková, L., Hartmann, T. (2022): Identifying barriers for nature-based solutions in flood risk management: An interdisciplinary overview using expert community approach. Journal of environmental management 310, 114725.

Rodríguez-González, P. M., Abraham, E., Aguiar, F., Andreoli, A., …, Zlatanov, T., Dufour, S. (2022): Bringing the margin to the focus: 10 challenges for riparian vegetation science and management. WIREs Water 9 (5).

Rončák, P., Šurda, P., Vitková, J. (2021): Analysis of a Topsoil Moisture Regime Through an Effective Precipitation Index for the Locality of Nitra, Slovakia. Slovak Journal of Civil Engineering 29 (1), 9–14.

Rusnák, M., Kaňuk, J., Kidová, A., Šašak, J., Lehotský, M., Pöppl, R., Šupinský, J. (2020): Channel and cut-bluff failure connectivity in a river system: Case study of the braided-wandering Belá River, Western Carpathians, Slovakia. The Science of the total environment 733, 139409.

Rusnák, M., Sládek, J., Pacina, J., Kidová, A. (2019): Monitoring of avulsion channel evolution and river morphology changes using UAV photogrammetry: Case study of the gravel bed Ondava River in Outer Western Carpathians. Area 51 (3), 549–560.

Sándor, R., Iovino, M., Lichner, L., Alagna, V., Forster, D., Fraser, M., Kollár, J., Šurda, P., Nagy, V., Szabó, A., Fodor, N. (2021): Impact of climate, soil properties and grassland cover on soil water repellency. Geoderma 383, 114780.

Siman, C., Velísková, Y. (2020): Impact of different proportion of agricultural land in river catchments on nitrogen surface streams pollution. Acta Hydrologica Slovaca 21 (1), 56–64.

Škvareninová, J., Lukasová, V., Borsányi, P., Kvas, A., Vido, J., Štefková, J., Škvarenina, J. (2022): The effect of climate change on spring frosts and flowering of Crataegus laevigata – The indicator of the validity of the weather lore about "The Ice Saints". Ecological Indicators 145, 109688.

Sleziak, P., Szolgay, J., Hlavčová, K., Danko, M., Parajka, J. (2020): The effect of the snow weighting on the temporal stability of hydrologic model efficiency and parameters. Journal of Hydrology 583, 124639.

Sokáč, M., Velísková, Y., Gualtieri, C. (2019): Application of Asymmetrical Statistical Distributions for 1D Simulation of Solute Transport in Streams. Water 11 (10), 2145.

Solín, Ľ. (2019): Flood Hazard in a Mountainous Region of Slovakia, in: Negm, A.M., Zeleňáková, M. (Eds.), Water Resources in Slovakia: Part II, vol. 70. The Handbook of Environmental Chemistry. Springer International Publishing, Cham, pp. 147–172.

Solín, Ľ., Sládeková Madajová, M. (2019): Flood Risk of Municipalities in Upper Basins of Slovakia, in: Negm, A.M., Zeleňáková, M. (Eds.), Water Resources in Slovakia: Part II, vol. 70. The Handbook of Environmental Chemistry. Springer International Publishing, Cham, pp. 173–193.

Solín, Ľ., Rusnák, M. (2020): Preliminary flood risk assessment: Case study of systematic processing of available or readily derivable information. Water Environ. J. 34 (S1), 683–698.

Šoltész, A., Baroková, D., Shenga, Z.D., Červeňanská, M. (2020): Hydraulic Assessment of the Impacts of Gate Realization on Groundwater Regime. Pollack Periodica 15 (3), 162–171.

Šoltész, A., Zeleňáková, M., Čubanová, L., Šugareková, M., Abd-Elhamid, H. (2021): Environmental Impact Assessment and Hydraulic Modelling of Different Flood Protection Measures. Water 13 (6), 786.

Šoltész, A., Orfánus, M., Mydla, J. (2022): Design of detention spaces in the Ulička and Ublianka River catchment. Acta Hydrologica Slovaca 23 (2), 282–287.

Štefunková, Z., Macura, V., Škrinár, A., Majorošová, M., Doláková, G., Halaj, P., Petrová, T. (2020): Evaluation of the Methodology to Assess the Influence of Hydraulic Characteristics on Habitat Quality. Water 12 (4), 1131.

Štefunková, Z., Macura, V., Škrinár, A., Ivan, P., Čistý, M., Majorošová, M., Tyukosová, V. (2021): Relationship between Morphological Characteristics and Quality of Aquatic Habitat in Mountain Streams of Slovakia. Water 13 (2), 142.

Šurda, P., Justína, V., Peter, R. (2020): Regional Drought Assessment Based on the Meteorological Indices. Bulletin of The Georgian National Academy of Sciences, 14 (2), 6.

Szolgay, J. (2003): Hydrological processes and mathematical modelling. Contributions to Geophysics and Geodesy 33 (Special issue), 49–74.

Szolgay, J. (2007): Catchment and river processes: experimental research and mathematical modeling. Contributions to Geophysics and Geodesy 37 (Special issue), 69–95.

Szolgay, J. (2011): Soil-water-plant-atmosphere interactions on various scales. Contributions to Geophysics and Geodesy 41 (Special issue), 37–56.

Szolgay, J. (2015): Catchment and river processes: review of experimental research and mathematical modeling in hydrology in Slovakia from 2011 to 2014. Contributions to Geophysics and Geodesy 45 (Special issue), 39–55.

Szolgay, J. (2019): Catchment and river processes: review of field experiments and mathematical modeling in hydrology in Slovakia from 2015 to 2018. Contributions to Geophysics and Geodesy 49 (Special issue), 37–65.

Szolgay, J., Blöschl, G., Gribovszki, Z., Parajka, J. (2020): Hydrology of the Carpathian Basin: interactions of climatic drivers and hydrological processes on local and regional scales – HydroCarpath Research. Journal of Hydrology and Hydromechanics 68 (2), 128–133.

Szolgay, J., Miklánek, P., Výleta, R. (2023): Interactions of natural and anthropogenic drivers and hydrological processes on local and regional scales: review of main results of Slovak hydrology from 2019 to 2022 (Report to IAHS). In: Geodesy and Geophysics in Slovakia 2019 – 2022, Slovak National Report to IUGG. Report of the Slovak National IUGG Committee, https://iugg.org/members/national-committee-reports/, 139 p.

Tall, A., Kandra, B., Gomboš, M., Pavelková, D. (2019): The influence of soil texture on the course of volume changes of soil. Soil Water Res. 14 (2), 57–66.

Tall, A., Pavelková, D. (2020): Results of water balance measurements in a sandy and silty-loam soil profile using lysimeters. Journal of Water and Land Development 45 (IV-VI), 179–184.

Tátošová, L., Šinka, K., Novotná, B., Húska, D. (2021): Water in the City and Remote Sensing. Environ. Earth Ecol. 5 (1), 26–38.

Valent, P., Výleta, R., Danáčová, M. (2019): A Joint Sedimentation-Flood Retention Assessment of a Small Water Reservoir in Slovakia: A New Hope for Old Reservoirs? Geosciences 9 (4), 158.

van Loon, A. F., Rangecroft, S., Coxon, G., Werner, M., …, Zhang, M., van Lanen, H. A. J. (2022): Streamflow droughts aggravated by human activities despite management. Environ. Res. Lett. 17 (4), 44059.

Varga, A., Velísková, Y. (2021): Assessment of time course of water and air temperature in the locality of the Turček

reservoir during its operation in the period 2005–2019. Acta Hydrologica Slovaca 22 (2), 304–312.

Vido, J., Nalevanková, P. (2020): Drought in the Upper Hron Region (Slovakia) between the Years 1984–2014. Water 12 (10), 2887.

Vojtek, M., Petroselli, A., Vojteková, J., Asgharinia, S. (2019): Flood inundation mapping in small and ungauged basins: sensitivity analysis using the EBA4SUB and HEC-RAS modeling approach. Hydrology Research 50 (4), 1002–1019.

Vojtek, M., Vojteková, J., Pham, Q.B. (2021): GIS-Based Spatial and Multi-Criteria Assessment of Riverine Flood Potential: A Case Study of the Nitra River Basin, Slovakia. ISPRS International Journal of Geo-Information 10 (9), 578.

Vojtek, M., Janizadeh, S., Vojteková, J. (2022): Riverine flood potential assessment at municipal level in Slovakia. Journal of Hydrology: Regional Studies 42, 101170.

Vorobyeva, O., Nechaj, P., Gaál, L. (2019): Lidar-Based Detection of Dangerous Meteorological Phenomena at the Bratislava Airport. Transportation Research Procedia 43, 199–208.

Zeleňáková, M., Fijko, R., Labant, S., Weiss, E., Markovič, G., Weiss, R. (2019): Flood risk modelling of the Slatvinec stream in Kružlov village, Slovakia. Journal of Cleaner Production 212, 109–118.

Prof. Ing. Ján Szolgay, PhD. (*corresponding author, e-mail: jan.szolgay@stuba.sk)
Assoc. Prof. Ing. Roman Výleta, PhD.
Department of Land and Water Resources Management
Faculty of Civil Engineering
Slovak University of Technology in Bratislava
Radlinského 11
810 05 Bratislava
Slovak Republic

RNDr. Pavol Miklánek, CSc.
Institute of Hydrology SAS
Dúbravská cesta 9
841 04 Bratislava
Slovak Republic

DOI: 10.31577/ahs-2023-0024.02.0029

ACTA HYDROLOGICA SLOVACA

Volume 24, No. 2, 2023, 266 – 274

Assessment of the impact of the accuracy of the DMR on the calculation of soil erosion using the USLE and USLE-2D models

Tatiana KOHUTOVÁ, Matúš TOMAŠČÍK, Michaela DANÁČOVÁ*, Kamila HLAVČOVÁ

Slovakia has recorded a potentially significant increase in water erosion, especially after consolidating the plots of hundreds of hectares of agricultural area with monocultures of marketable crops. This is also due to large blocks of land being created on sloping sites. Due to its simplicity, the Universal Soil Loss Equation (USLE) is most commonly used to calculate potential soil erosion. This study compares the classical USLE and the USLE-2D methods, which consider the combined spatially variable slope length and steepness. The slope length is replaced in USLE-2D by the contributing area based on a raster digital model relief model. Data from Tulčík cadastre in east Slovakia demonstrates the results of water erosion on 26 plots used as agricultural areas. As expected, differences were found, which were further analysed concerning slope lengths and steepness. Comparing the grid size (1, 10 and 20 m) for the USLE-2D model showed that more significant differences were obtained for plots with a smaller area and a higher slope. It was confirmed that at a lower pixel resolution, the results are overestimated.

KEY WORDS: soil erosion, DMR, LS-factor, USLE, USLE-2D

Introduction

Over the past few decades, technological progress has dramatically increased the “human landscape" at the expense of the natural environment. The result is that the landscape is losing its biological and cultural richness. One area where it is possible to reduce the consequences of human activity on natural ecosystems is the rural landscape (Bonfanti et al., 1997). Humans have significantly changed the natural structure of the environment into an agricultural landscape, which differs from the original and natural layout in its character and diversity as well as the duration of continuous vegetation cover on the land throughout the years. The effective use of the landscape along with the morphological features of the relief affects the development of the soil degradation process (Morgan, 2005; Nosko et al. 2019).

Since humankind began agriculture, erosion by wind and water has been the main threat to soil. Soil erosion is a natural process. However, its acceleration is most often caused by human activity in the countryside, and this causes problems that must be solved (Podhrádzka, 2010; Petlušová et al., 2017). It was confirmed that by soil erosion there are transported soil sediment and nitrogen which contributes to surface water contamination (Siman and Velisková, 2020).

Therefore, the rural landscape has become the subject of our interest. Our top priority is to reduce the impact of water soil erosion caused by agricultural activity. Many mathematical models categorized as empirical, conceptual, physically based, or process-oriented are available to estimate soil erosion on different spatial and temporal scales (De Vente and Poesen, 2005; Morgan, 2005). Due to its relatively simple analysis of the data and parameters input, the Universal Soil Loss Equation (USLE) was developed to calculate the average annual soil loss from an area (Wischmeier and Smith, 1978). However, the application of process-based physical models (e.g., Erosion 3D, WEPP, or PESERA) does not necessarily result in lower degrees of uncertainty compared to more simply structured empirical models such as USLE-type algorithms (Alewel, et al., 2019). The accuracy of the data input and the methodologies used to compute each factor have a direct impact on the quality of the final computations (Michalopoulou et al., 2022; Semari and Korichi, 2023).

The main objective of the study was to assess the intensity of soil erosion on the parcels of the Tulčík Cadastre. The results of the study should determine the issue of how important the resolution of the digital model relief (DMR) input data in calculating the joint topographical LS factor (LS-factor) is. To answer this question, algorithms for calculating the LS-factor according to various authors were also tested. This topographical factor is key in calculating the average annual soil loss using USLE-2D. The second part of the article compares the values obtained by the USLE-2D

and the classic USLE methods. In the conclusion, the advantages and disadvantages of these methods of determining the average annual soil loss on plots of different sizes and slope ratios are evaluated.

Methodology and data

Study area

The study area is the cadastral territory of Tulčík, located in eastern Slovakia in the northern part of Prešov (Fig 1.) The foothills of the Čergov range extend into the cadastral territory. There are clay soil types on the land from the north part of the village. The type of soil on the land is clay. The area of the cadastral territory is 12.9 km^2, and more than 70% of the total area is agricultural land (Fig. 1). The altitude ranges from 264 to 560 m a.s.l., and the maximum slope is 59 percent.
The location of the Tulčík study area in Slovakia is presented in Fig. 1, and the DMR and the map of the slopes are shown in Fig. 2. The input data of land use and DMRs are a product of ZBGIS (provider: Geodetic and Cartographic Institute Bratislava – GKÚ Bratislava). The geospatial data was processed in the open-source QGIS (Quantum Geographic Information System).

The USLE model

One of the most widely used methods for estimating water erosion is the "Universal Soil Loss Equation", (USLE) empirical model (Wischmeier and Smith, 1978). This method is used in Slovakia, mainly due to its simplicity. The USLE is used for assessing the long-term average soil loss by water erosion from agricultural lands in a given type of climate zone. It considers the given type of soil with a particular slope and the length of the slope and a specific system of growing crops, cultivating soil, and applying anti-erosion measures. Intense short-term rain plays an important role in the method (Impact of Changes in Short-Term Rainfall, e.g., Földes et al. 2022). The equation cannot be used for a period shorter than one year and also not for calculating soil loss from an individual rainfall or runoff from melting snow.
The USLE model is used to calculate the erosion risk:

$$G = R.K.L.S.C.P \qquad (1)$$

where G is the average annual soil loss [t ha^{-1} year^{-1}]; R is the rain erosion efficiency factor, expressed as a function of the maximum 30 min intensity and kinetic rainfall energy [MJ ha^{-1} cm h^{-1}]; K is the soil erodibility factor expressed as a function of the topsoil's texture and structure, organic matter content, and permeability [t ha^{-1} year^{-1}]; L is the length factor expressing the effect of an uninterrupted length of slope on the amount of soil loss due to erosion [-]; S is the slope factor expressing the effect the steepness of the slope on the amount of soil loss due to erosion [-]; C is the factor of the protective influence of the vegetation cover, depending on the development of the vegetation and the agricultural technology used [-]; and P is the impact factor of any anti-erosion measures [-].
The quality of the resulting calculations is directly dependent on the accuracy of the R, K, C, and P factors input and the methods used to calculate the L and S factors.

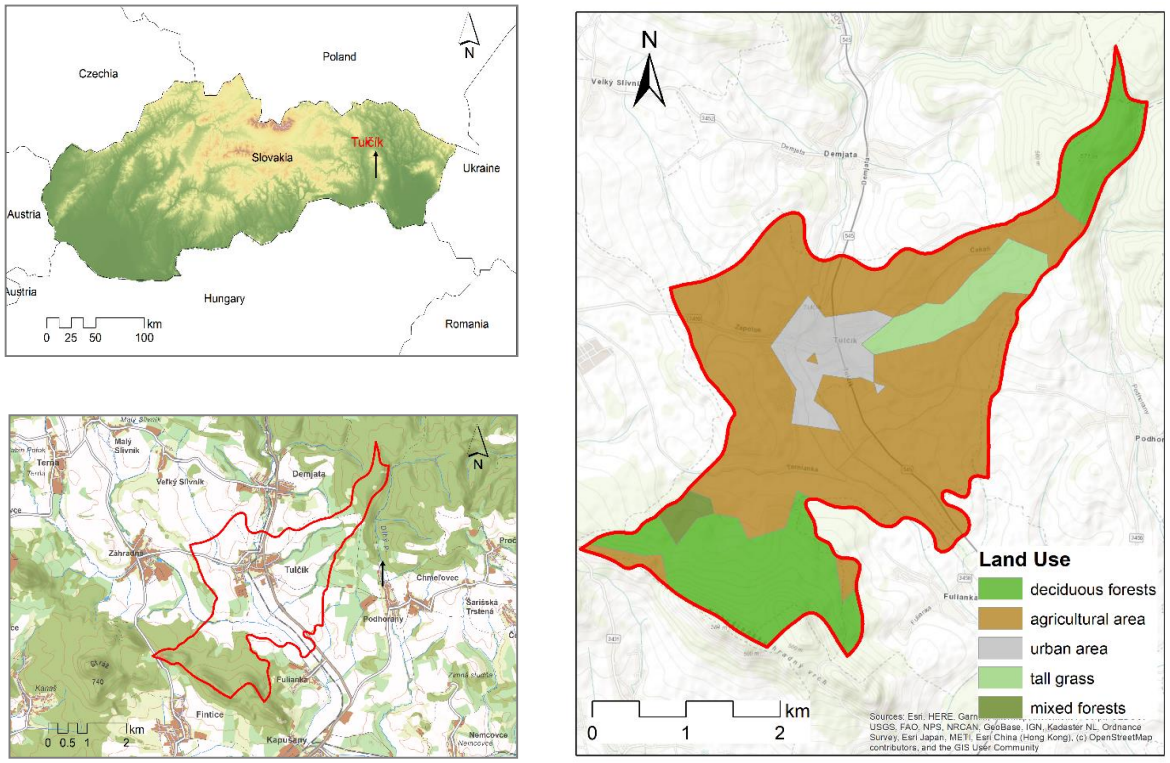

Fig. 1. Location of the Tulčík study area (Prešov region, Slovakia), sources: GKÚ Bratislava; Esri.

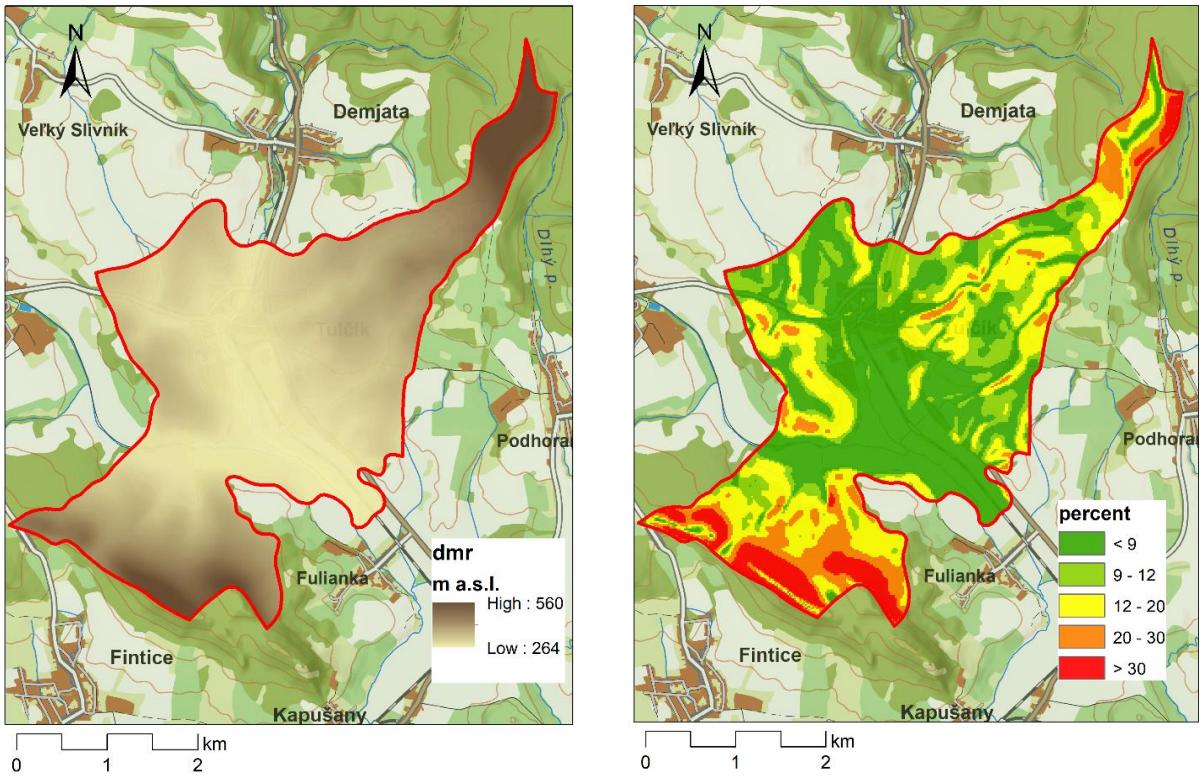

Fig. 2. Digital relief model (DMR) and the map of the slopes of the Tulčík study area (sources: GKÚ Bratislava; Esri).

Two of the most important parameters that affect soil loss are the slope (*S*) and the length of the slope (*L*), i.e., the length of the surface flow until it reaches a natural or artificial recipient.

USLE-2D model

The calculation of the risk of erosion by the USLE-2D model is based on the universal equation of the soil using the topographical factor (LS-factor). Specifically, the LS-factor is of great interest because of the variety of equations applied in the literature to calculate it and because these equations require the use of digital relief models.
The LS-factor is created from a digital model of the terrain and the layer of the land parcels distributing the area into partial surfaces.

LS – factor
We decided to compare the effect the topographic LS-factor (which will replace the *L* and *S* factors we calculated) will have on the resulting soil loss values. The LS-factor is calculated based on an algorithm using the formula:

$$LS = \sum_{j=1}^{N} \frac{S(i,j).\lambda(i,j)_{outlet}^{m+1} - S(i,j).\lambda(i,j)_{inlet}^{m+1}}{(\lambda(i,j)_{outlet} - \lambda(i,j)_{inlet}) \cdot 22.13^{m}} \quad (4)$$

where:
LS – topographic factor in USLE-2D for one plot,
$\sum_{j=1}^{N}$ – the sum of all cells from *i* to *j* for the plot,
$\lambda(i,j)_{outlet}$ – length of slope at the output for *i, j* cell [m],
$\lambda(i,j)_{inlet}$ – length of slope at the input for *i, j* cell [m],
$S(i,j)$ – slope factor for *i, j* cell,
m – slope length exponent.

The slope factor for the individual cells is expressed by algorithms according to several authors (Van Oost, Govers, 2000).

A) Relationship according to Wischmeier and Smith (1978):

$$S(i,j) = 65.41.\sin^2 \theta i,j + 4.56.\sin \theta i,j + 0.065 \quad (5)$$

B) The relationship according to McCool (1989), which is also used in RUSLE:

$$S(i,j) = 10.8.\sin \theta i,j + 0.03, \text{ where } \theta i,j \leq 9\% \quad (6)$$

$$S(i,j) = 16.8.\sin \theta i,j - 0.5, \text{ where } \theta i,j > 9\% \quad (7)$$

C) Govers' relationship was based on field data from 1991:

$$S(i,j) = (\tan \theta i,j \ / 0.09)1.45 \quad (8)$$

D) Nearing (1997) proposed a simple function for the slope factor:

$$S = -1.5 + \frac{17}{(1+e^{[2.3-6.1\sin(\Theta)]})} \quad (9)$$

Results and discussion

DMR and slope values

The property of the DMR was assessed using descriptive statistics (min, max, mean, standard deviation, range (min-max)); the values are summarized in Table 1. From the statistical analysis, the elevation values from each DMR examined have a substantial degree of similarity. The quality assessment should include the examination of the vertical accuracy. Ground control is considered the most accurate method and is, therefore, suitable for comparing DMR elevation values. This comparison is missing in the study as we did not have the available data. Comparing the DMR with different cell sizes may provide some important information regarding the accuracy of these elevation data (Polidori and Hage, 2020). In this study, the slope angle for each grid cell is calculated using a specific numerical method known as the Deterministic-8 method in ArcGIS. A comparison of both DMRs shows a high degree of divergence. The descriptive statistics for the slope values calculated are presented in Table 1.

It was confirmed that the maximum slope values for the DMR decreases with increases in the cell size, meaning that the higher the DMR resolution, the higher the maximum slope value calculated. The minimum slope value is zero for all the DMR data. The maximum slope value is noted in the southern and northern study DMR areas (DMR 1, grid size 1x1m); it is equal to approximately 87% (see Table 1). The standard deviation and mean of the slope values were compared for all DMR resolution. Results show minimal difference.

Comparison of the LS - factors

Different algorithms were used to examine the impact of the LS-factor on the soil loss results obtained by the USLE-2D model. The first one is based on the equation that was suggested by Wischmeier and Smith (W-S, equation 5); the second one uses the equation from the RUSLE model (McCool, equations 6 and 7); the third one is based on field data (Govers, equation 8); and the fourth one was suggested by Nearing (Nearing, equation 9). The descriptive statistics were calculated for the LS-factors for each DMR resolution (see Table 2).

The highest LS-factor values were obtained using the Govers method for all DMR resolutions. The lowest LS-factor values were obtained using to the W-S method (approximately 2 times lower than the Govers method). This study shows that the higher the resolution of the DMR data, the higher the maximum LS values, except for the W-S based method. This observation also applies to the mean values. The following figure shows the difference between the calculated mean values of LS-factors using all of the approaches examined (Fig. 3).

It can by seen that the LS values (mean) from the DMR 20 (grid size: 20x20m), DMR 10 (grid size: 10x10m), are much higher than the DMR 1 (grid size: 1x1m) for all the algorithms (Fig. 3). The lowest mean LS for the DMR 20 is calculated from the W-S, while the highest mean

Table 1. The descriptive statistics of the DMR files and the slope values [%] in the study area

	DMR 20 (grid size 20m)	DMR 10 (grid size 10m)	DMR 1 (grid size 1m)	Slope 20 [%]	Slope 10 [%]	Slope 1 [%]
MIN	264.8	265	261.8	0	0	0
MAX	560.5	574.7	581.0	58.95	71.8	87.2
MEAN	340.8	341.1	340.1	12.4	12.9	17.1
STD DEV.	70.2	70.5	70.0	9.15	9.9	15.1
RANGE	295.7	309.8	319.2	58.95	71.8	87.2

Table 2. The descriptive statistics of LS-factor for DMR with resolution pixel sizes of 1m, 10m and 20m

Method	LS - factor											
	W-S			McCool			Govers			Nearing		
	DMR 20 (20x20)	DMR 10 10x10)	DMR 1 (1x1)	DMR 20 (20x20)	DMR 10 (10x10)	DMR 1 (1x1)	DMR 20 (20x20)	DMR 10 (10x 10)	DMR1 (1x1)	DMR 20 (20x20)	DMR 10 (10x 10)	DMR 1 (1x1)
MIN	0	0	0	0	0	0	0	0	0	0	0	0
MAX	27	26	65	29	31	65	56	65	65	29	29	65
MEAN	1.469	1.411	0.402	1.583	1.522	0.383	**3.084**	**2.88**	**2.505**	1.519	1.458	0.383
STD DEV.	2.711	2.691	1.825	2.969	2.958	1.901	**5.964**	**2.834**	**4.207**	2.854	2.835	1.855
RANGE	27	26	65	29	31	65	56	65	65	29	29	65

value is calculated from Gover's approach.

The input data on the relief is very important for the USLE-2D method. When calculating the LS-factor, the resolution of the pixel with the altitude data plays a key role (Fijałkowska, 2021; Michalopoulou et al., 2022). A high resolution (1x1m) resulted in very low LS-factor values in this case. This is probably due to the overly complicated terrain for this type of process. Wang et al. (2020) studied the effect of the DMR resolution on the LS-factor by implementing two DMRs (5x5m and 30x30m grid size). This study highlighted the increase in the L factor and the decrease in the S factor with coarser DMR resolutions. Regarding the LS-factor, the results showed an increase in areas with a large relief and a decrease in smaller relief areas.

Annual Soil Loss Comparison – USLE-2D

The average annual soil loss of the study area was estimated by acquiring the USLE-2D and multiplying the rainfall erosivity factor (R), soil erodibility factor (K), slope length and steepness factor (LS-factor), cover management factor (C), and the anti-erosion measures factor (P).

The LS-factor was calculated based on Mc Cool's algorithm (equations (6), (7)). The soil erosion rates were estimated for three of the DMRs examined. The R-factor was calculated using the interpolation method according to Onderka and Pecho (2019). The background vector layer of the bonified soil-ecological unit's boundaries was used to calculate the *K*-factor. The value $P = 1$, which is often employed in practice was used. Only if there are no anti-erosion measures on the plots treated.

The results obtained based on DMR with a pixel resolution of 10 x 10m (range 0–79.3 t ha^{-1} year^{-1}, Fig. 4) and DMR with a pixel resolution of 20 x 20m (range 0 – 68.2 t ha^{-1} year^{-1}) were compared. The average annual soil loss was calculated on 45 plots of agricultural area. A soil loss value of more 4 t ha^{-1} year^{-1} (Act no. 220/2004) is marked in red in Fig. 4, where 11 plots are potentially at risk.

From the total number of 45 plots, we selected plots with

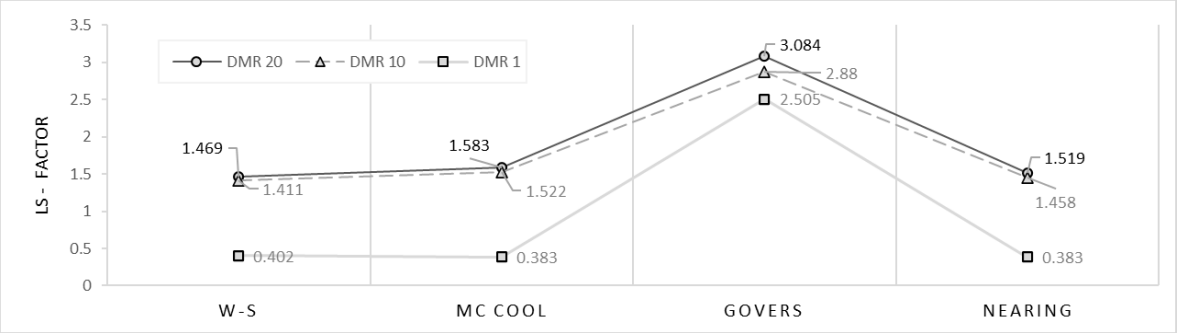

Fig. 3. LS factor values (average) obtained by all the methods for all the DMR resolutions (grid size: 1, 10, 20m).

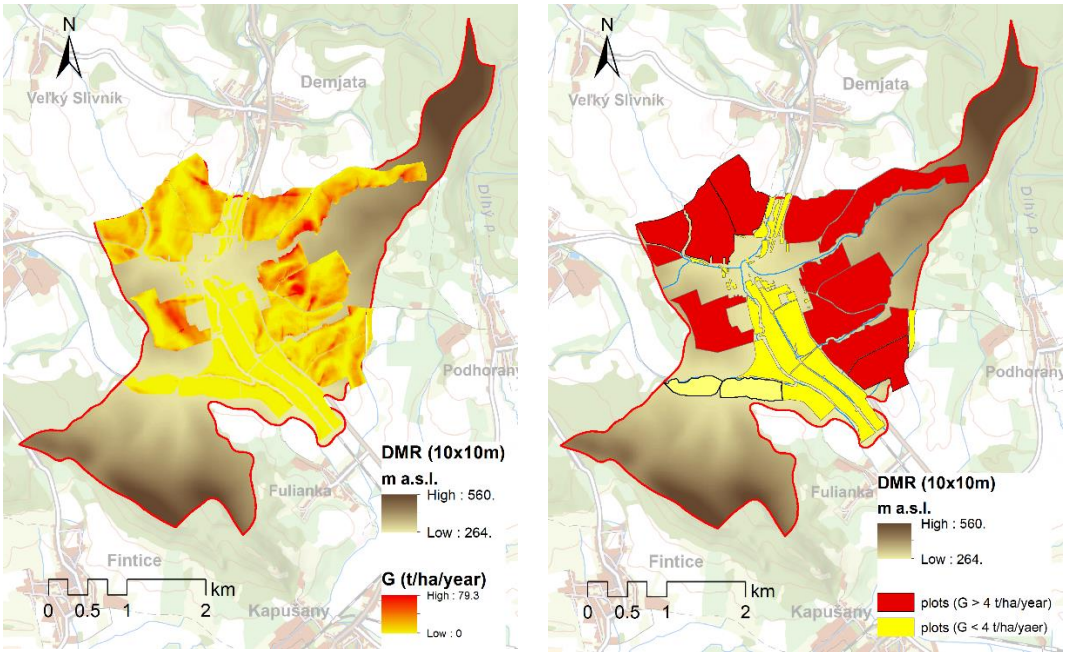

Fig. 4. Agriculture area (yellow plots) in the cadastral territory of Tulčík, on the right side are red plots with soil losses of more than 4 t ha^{-1} year^{-1} (USLE-2D model).

a greater length than 100 m. In the next part, the soil erosion values on 26 plots are compared.

For a direct comparison, the results of the average annual soil loss calculated for the DMR resolution (10m and 20m) are shown in Figure 5a. As can be seen, there are slight deviations throughout the range. The higher deviations were indicated at lower values of soil loss.

The descriptive statistics (box plot, Fig. 5b) of the relative values of the erosion loss show a significant median difference (for the 20x20m resolution, it is 4.6 t ha^{-1} year^{-1}; for the 10x10m resolution, the value is lower, i.e., 2.2 t ha^{-1} year^{-1}, and for the 1x1m resolution, it is 1.1 t ha^{-1} year^{-1}). The values of the 25th percentile or 75th (boundaries Q_1, Q_3), are very similar in case resolutions G10 (resolution 10x10m) and G20 (resolution 20x20m). The value of the average soil loss is 6.0 versus 5.5 t ha^{-1} year^{-1}.

Comparison of the USLE and USLE-2D methods

The difference between the USLE (classic method) and USLE-2D (resolution 10x10m) is evident. Both methods yield similar results in mapping relative erosion risks. However, there appear to be important differences in the absolute values. Although both methods provide identical slope values, the effect of flow convergence needs to be considered using the classic method.

In the case of the USLE method, the slopes and the lengths of the parcels were obtained manually from the map. Equations 2 and 3 were used to calculate the *L*-factor and *S*-factor. The values obtained of the annual soil loss ranged from 0.95 to 18.59 t ha^{-1} year^{-1}. Parcels with a soil loss value of more 4 t ha^{-1} year^{-1} are marked in red (Fig. 6). Twelve plots with a potential high threat of water erosion were identified.

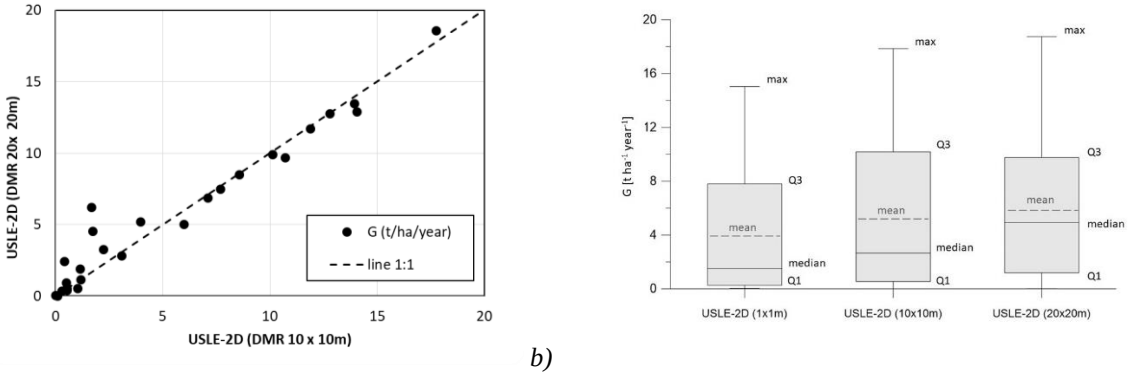

a) b)

Fig. 5. The impact of the accuracy of the DMR on the calculation of the annual soil erosion a) regression b) box plot.

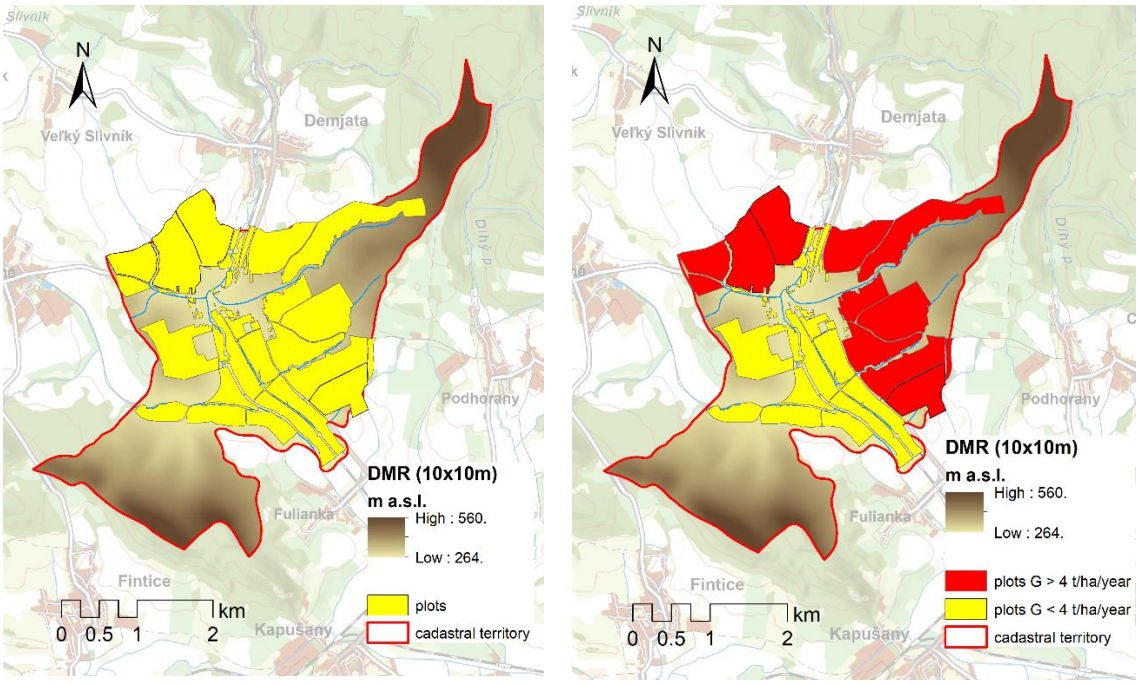

Fig. 6. Agricultural area (yellow plots) in the cadastral territory of Tulčík; on the right side are red plots with potential annual soil loss of more than 4 t ha^{-1} year^{-1} (USLE model).

We selected parcels (26) based on the slope lengths for a complex comparison of the soil erosion between USLE and USLE-2D. Table 3 shows the results of the annual soil erosion, and the assumed differences are demonstrated.

The soil loss results using the above methods are fairly consistent (see Table 3). The differences between the empirical methods are not significant (Fig. 7a). A total of 26 plots were evaluated, 50% of which exceeded the permissible soil loss value for medium-deep soils according to both methods.

During the evaluation, the impact of the slope of the plot (Fig. 7b) and the length of the slope (Fig. 7c) were directly analyzed. The values concerning the length, and the slope of the plot were taken from the manual determination for the calculation of USLE. The land area was obtained from a GIS environment. The steepness of the slope confirmed the high degree of sensitivity.

Both methods yield similar results in mapping relative erosion risks compared to the classical method. However, there appear to be significant differences in the absolute values. Although both methods provide similar slope values, the USLE method is needed to show an overestimation of the erosion risk clearly. According to USLE, only the overvalued plots had a low slope (up to 3%), a small area of up to 10 ha, and a slope length of up to 500m.

Figure 8 shows the specific values of the average annual soil loss for the 26 compared plots. Again, as is seen in the individual plots; the difference is fundamental in the USLE method (see plots 1–3, 15–17, 20, and 26).

Table 3. Comparison of soil erosion between USLE and USLE-2D (DMR with a pixel resolution of 10x10m), L_d is the length of the slope

Plot No.	L_d [m]	G – USLE [t ha^{-1} year^{-1}]	G – USLE-2D [t ha^{-1} year^{-1}]	Plot No.	L_d [m]	G – USLE [t ha^{-1} year^{-1}]	G – USLE-2D [t ha^{-1} year^{-1}]
1	663	**11.82**	**10.12**	14	768	**10.26**	**7.1**
2	384	**9.95**	**10.71**	15	611	**12.81**	**12.79**
3	780	**11.07**	**11.89**	16	410	**14.71**	**17.75**
4	232	0.75	0.53	17	627	**18.59**	**13.92**
5	488	1.96	1.011	18	538	**6.76**	5.97
6	231	1.93	1.16	19	545	3.74	3.94
7	128	1.90	0.41	20	872	**9.64**	**14.04**
8	156	1.51	0.53	21	282	2.58	3.06
9	219	1.62	0.49	22	169	2.52	1.12
10	1320	**4.99**	**7.68**	24	113	3.22	1.72
11	495	**7.29**	**8.55**	26	132	**4.64**	1.67
12	128	0.95	0.07	28	158	1.61	2.21
13	240	2.25	0.29	29	191	1.12	0.00

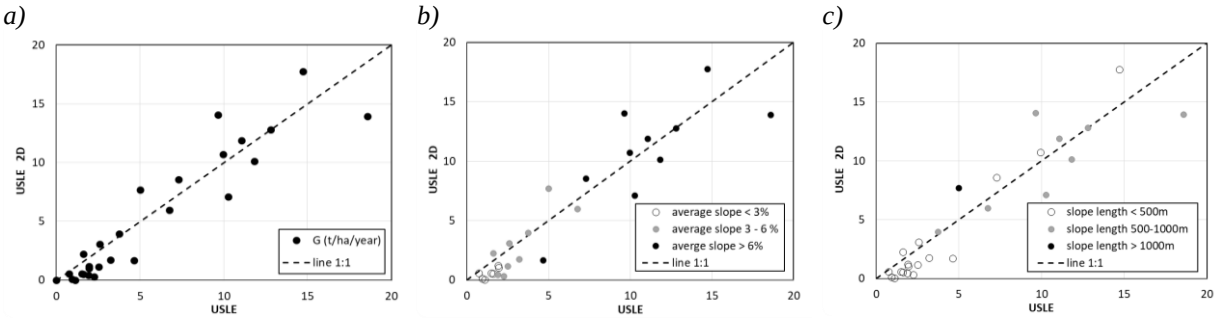

Fig. 7. Comparison of soil erosion G (t ha^{-1} year^{-1}) between the classic USLE and USLE-2D models (resolution 10x10 m), with the plots by b) average steepness of the slope c) slope length.

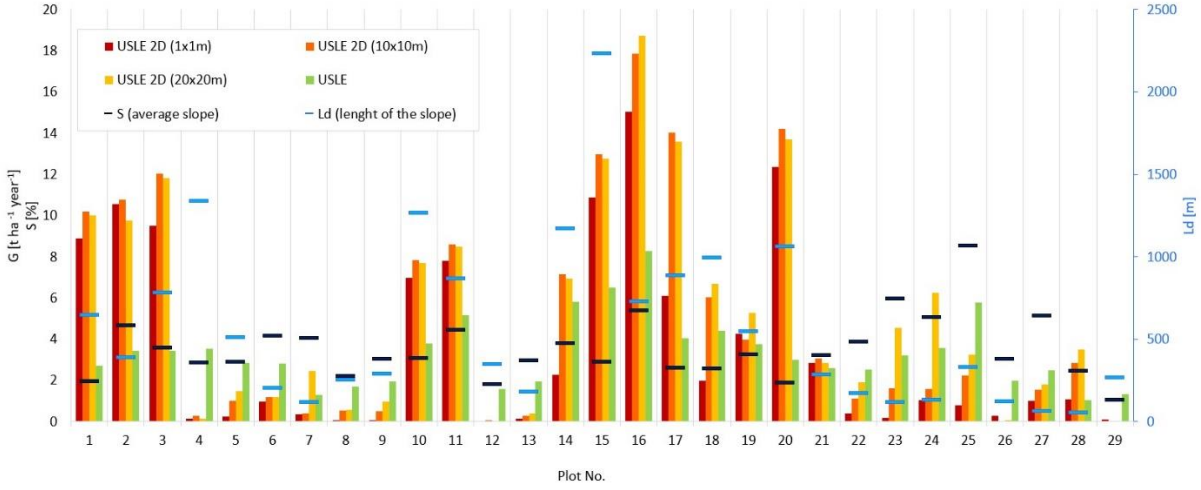

Fig. 8. Values of the annual average soil loss from 26 plots according to USLE and USLE-2D (resolution 1x1 m, 10x10 m, and 20x20 m DMR), the blue line is the length of the slope, and the black line is the average steepness of the slope.

Conclusion

In the cadastral territory of Tulčík, an estimate of the water erosion of the soil was made. Two simple models were used to calculate the soil loss, i.e., the USLE universal soil loss equation and the USLE 2D model with the LS-factor calculation algorithm, according to McCool (1978). The calculations were made in a GIS environment for the individual plots.

With the USLE method, the overestimation of the results was not confirmed, as pointed out by several authors. In this study, it was manifested on plots with a low intensity of erosion (up to 4 t ha^{-1} $year^{-1}$), which was the case only for plots with a small slope, short runoff length, and small plot size. A possible reason is the distinct fragmentation and shape of the individual plots' and the sensitivity of determining the runoff path using the classic USLE method. Both models are based on empirical and conceptual relationships, which may result in possible uncertainties concerning the results. During the evaluation, the impact of the slope of the plot, the length of the slope, and the plot's area were directly analyzed. The slope of the plot was the most pronounced. Comparing the grid size for the USLE-2D model showed that more significant differences were obtained for plots with a smaller area and a higher slope. It was confirmed that at a lower pixel resolution, the results are overestimated.

From the results obtained and a comparison of the LS-factor, it is advisable to consider using a detailed DMR with a resolution of 1x1m. Spatial data are available, but their applicability in fragmented and larger territories can be limited too (complicated for processes). It is advisable to supplement this study with further testing of other resolutions; it provides a useful reference for soil erosion study, particularly to develop model parameter assessment.

Acknowledgment

This work was supported by the Slovak Research and Development Agency under Contract No. APVV 19-0340, No. APVV 20-0374 and the VEGA Grant Agency No. VEGA 1/0782/21.

References

Alewell, Ch., Borrelli, P., Meusburger, K., Panagos, P. (2019): Using the USLE: Chances, challenges and limitations of soil erosion modelling, International Soil and Water Conservation Research, Vol. 7, Issue 3, 2019, 203–225, ISSN 2095-6339.

Bonfanti, P., Fregonese, A., Sigura. M. (1997): Landscape analysis in areas affected by land consolidation. Landscape and Urban Planning, Vol. 37, 91–98.

De Vente, J., Poesen, J. (2005): Predicting soil erosion and sediment yield at the basin scale: scale issues and semi-quantitative models. Earth-science reviews, 71(1-2), 95–125.

Desmet, P. J. J.; Govers, G. (1996): A GIS procedure for automatically calculating the USLE LS factor on topographically complex landscape units. Journal of soil and water conservation, 427–433.

Fijałkowska, A. (2021): Analysis of the Influence of DTM Source Data on the LS Factors of the Soil Water Erosion Model Values with the Use of GIS Technology. Remote Sens., 13, p. 678.

Földes, G., Labat, M. M., Kohnová, S., Hlavčová, K. (2022): Impact of Changes in Short-Term Rainfall on Design Floods: Case Study of the Hnilec River Basin, Slovak Journal of Civil Engineering, No. 1, Vol 30, 68–74.

McCool, D. K., Foster, G. R., Mutchler, C. K., Meyer L. D. (1989): „Revised Slope Length Factor for the Universal Soil Loss Equation." *Transactions of the ASAE* 32 (5): 1571–1576, http://dx.doi.org/10.13031/2013.31192.

Michalopoulou, M., Depountis, N., Nikolakopoulos, K., Boumpoulis, V. (2022): The Significance of Digital Elevation Models in the Calculation of LS Factor and Soil

Erosion. Land 2022, 11, 1592. https://doi.org/ 10.3390/land11091592

Morgan, R. P. C. (2005): Soil Erosion and Conservation; Wiley: New York, NY, USA, ISBN 9781405117814.

Nosko, R., Maliariková, M., Brziak, A., Kubáň, M. (2019): Formation of Gully Erosion in the Myjava Region, Slovak Journal of Civil Engineering, Vol. 27, No. 3, 63–72.

Onderka, M., Pecho, J. (2019): Update of the erosive rain factor in Slovakia using data from the period 1961–2009. Contributions to Geophysics and Geodesy, Vol. 49/3, 355–371.

Petlušová, V., Petluš, P., Hreško, J. (2017). The effect of land use changes on soil erosion in the areas of Ľubá and Belá (Hronská pahorkatina upland), Geographical Journal, 69, 3, 245–262.

Podhrázka, J. (2010): Soil and water protection measures in land adjustments. In: Rožnovský, J., Litschmann, T. (ed): Voda v krajině, Lednice, 2010, ISBN 978-80-86690-79-7.

Polidori, L., El Hage, M. (2020): Digital Elevation Model Quality Assessment Methods: A Critical Review. Remote Sens. 2020, 12, 3522.

Semari, K., Korichi, K. (2023): Water erosion mapping using several erosivity factors in the Macta Basin (North-West of Algeria), Acta Hydrologica Slovaca, Vol. 24, No. 1, 2023, 101–112.

Siman, C., Velisková Y. (2020): Impact of different proportion of agricultural land in river catchments on nitrogen surface streams pollution, Acta Hydrologica Slovaca, Vol. 21, No. 1, 2020, 56–64.

Van Oost, K., Govers, G. (2000): Usle2D Katholieke Universiteit Leuven Information provider: Physical and Regional Geography Research Group.

Wang, C., Shan, L., Liu, X., Yang, Q., Cruse, R. M., Liu, B., Li, R., Zhang, H., Pang, G. (2020): Impacts of Horizontal Resolution and Downscaling on the USLE LS Factor for Different Terrains. Int. Soil Water Conserv. Res. 2020, 8, 363–372.

Wischmeier, W. H., Smith, D. D. (1978): "Predicting rainfall erosion losses", Agricultural Handbook, no. 537, Washington D. C., U. S. Department of Agriculture, 58 p.

Ing. Tatiana Kohutová
Ing. Matúš Tomaščík
Assoc. Prof. Ing. Michaela Danáčová, PhD. (*corresponding author, e-mail: michaela.danacova@stuba.sk)
Prof. Ing. Kamila Hlavčová, Ph.D.
Department of Land and Water Resources Management
Faculty of Civil Engineering
Slovak University of Technology in Bratislava
Radlinského 11
810 05 Bratislava
Slovak Republic

DOI: 10.31577/ahs-2023-0024.02.0030

ACTA HYDROLOGICA SLOVACA

Volume 24, No. 2, 2023, 275 – 284

Numerical tests and sensitivity analysis of pollution source localisation tool applied on open channel system

Yvetta VELÍSKOVÁ*, Marek SOKÁČ, Maryam BARATI MOGHADDAM

This paper is focused on solving the inverse problem of pollution spreading in open channel system in order to find the location of pollutant sources. The goal was to propose localisation procedure, which should be operative and fast enough to enable quick interventions to prevent the spread of pollution. The proposed method, as well as the overall localisation procedure was numerically tested on a real sewer system data, which represents in this case an extensive open channel network structure with free surface flow. As part of the numerical tests of the model, a sensitivity analysis was also carried out. The sensitivity analysis was focused on the resulting localization error depending on concentration measurement errors. The numerical test results were successful and confirmed applicability of proposed localization tool in real conditions, the sensitivity analysis points to the influence of individual parameters on localization accuracy.

KEY WORDS: inverse problem, source localisation, pollution source, sensitivity analysis, numerical test

Introduction

Population growth and anthropogenic activities cause many management challenges (Novák, 2022), especially in secure disposal of water for various uses and protect water resources and environment from contamination, especially harmful substances such as emerging organic contaminants, heavy metals, biodegradable pollutants, micropollutants, pesticides, industrial chemicals, petroleum hydrocarbons and so on. Exposure to these contaminants cause serious health risks and environmental problems. Moreover, illegal discharges of high volumes of hazardous materials from industrial complexes may impair the function of the wastewater treatment plants, in case of pollution outflow in agricultural area or field can endanger the quality of the water body (Kováčová, 2023). In most cases the source of pollutant discharge is unknown and due to the complex factors and conditions in environment, it is often very difficult to identify the exact spill location. Hence, development of methods that are able to track down contaminant sources location can help in minimizing the adverse impacts as well as preventing future illegal spills.

Source identification is an inverse problem of the transport equation. From a mathematical point of view, contaminant source localization is an ill posed problem does not fulfil the well-posedness criteria of Hadamard (1923). Based on Hadamard's definition, a problem is well-posed if its solution is existent, unique and stable (that is the continuous dependence of the solution to input data). A problem which lacks any of these features is called an ill-posed problem. The ill-posedness feature of inverse source problem is generally originated from the fact that this problem is under-determined, because only limited observational data are available and the unknown source characteristics should be estimated in a number of instants which is much greater than available observed data. The second reason for the ill-posedness is a direct consequence of the irreversibility of dispersion phenomena, which gradually smooth the pollutant plume and decrease the amount of information that can be obtained from observations (Skaggs and Kabala 1998; Boano et al. 2005).

In the past decades, the problem of identifying unknown pollutant sources has attracted the attention of researchers around the world. Pollution source identification problem has been studied in different environments of watercourses, but this topic has not been addressed in watercourses networks or sewer networks (as limited case of watercourses network) properly. While identifying unknown pollutant sources is one of the essential measures in planning effective management strategies in urban areas. There are only few studies in the literature that dedicated to this topic. Banik et al. (2014) developed a toolkit library for SWMM5 to solve a pollution source identification problem in sewer networks. Their proposed methodology was able to identify the source location as well as its released

concentration, starting time and duration. However, their proposed method needs too much computational effort, especially in the case of large sewer networks, which makes it impractical to apply the method for real life situations. Later, in order to address the issue of excessive computational effort, Banik et al. (2015) presented a pre-screening procedure to apply before the source identification step. The proposed pre-screening procedure identifies a set of candidate nodes using the pollution matrix concept (Kessler, et al. 1998). Results showed that introducing the pre-screening procedure reduces in the required computational time significantly in large networks. It also improves the accuracy of the identification method. However, the effectiveness of the proposed pre-screening procedure is highly dependent to the placement arrangement of sensors. so, it is a factor that should be considered prior to using this method.

Shao et al. (2021) coupled Bayesian inference with SWMM and developed a stochastic source identification model to reconstruct the characteristics of an instantaneous pollutant discharge in sewer networks. Results showed that the performance of proposed method is highly dependent on walking step size, numbers of unknown source parameters and numbers of monitoring sites.

In this paper, we proposed a localization method and tool for identifying pollutant sources in open channel system which can be applied both at natural and urban catchments (watercourses network, sewer network).

Material and methods

Theoretical background

As it was mentioned above, localisation of unknown pollution sources is a challenging task in water resources management. The prevailing majority of existing simulation models is designed to simulate the pollution spreading in the water flow direction only. In current advancing monitoring technologies, a different task can occur: the monitored pollution time course in the cross-flow profile is known, but the pollution source is unknown. The solution of task defined such way is the source determination, which means the source localisation or determination of the pollution time course release parameters (start time, duration, concentration over time) or so-called source intensity function. Solution of such task is often called as solution of the inverse problem.

An inverse problem is the process of calculating the causal factors from a set of observations that produced them. Inverse problems are some of the most important mathematical problems in science and mathematics because they tell us about parameters that we cannot directly observe.

Methods for solving the inverse task related to the area of pollution transport in water environment was presented in the literature several times (Bagtzoglou and Atmadja, 2003; Cheng and Jia, 2010; El Badia and Hamdi, 2007; Ghane et al., 2016; Mazaheri et al., 2015; Telci and Aral, 2011; Wang et al., 2018). However, the research in this field is very often focused mainly on mathematical methods and tests (verification), applications in real conditions are very rare. The problems are mainly the computational demands of the inverse transport models, high uncertainty of the inverse task solution methods as well as the problems connected with the temporal and spatial data collection, sampling, sensitivity, accuracy.

The simplest way how to localize the pollution source is to deploy a number of sensors and to wait until a pollution spill occurs. The occurrence of the investigated pollution presence on particular sensors will determine the area with the pollution source.

Such approach on the other hand requires a large number of sensors and it is extensive time-consuming procedure (the user has to wait until next pollution spills occur, if even occur). Therefore, it is reasonable to develop a methodology for pollution source identification (even though with higher uncertainty) based on a single pollution spill event.

So far, no methods for the inverse task in sewer system were published, only for inverse task solutions in a river system (Ghane et al., 2016), which is hydraulically a similar task, but the main difference is the complexity and size of the area of interest (number of network nodes, branches).

The concept of well- and ill-posedness goes back to (Hadamard, 1923). However, the definition was given by (Courant and Hilbert, 1993). According to the definition, a mathematical problem is called well - posed (in the sense of (Hadamard, 1923) or properly posed or correctly posed if:

1. a solution of the problem exists in a given set of "admissible" solutions (existence condition),
2. the solution is unique (uniqueness condition),
3. the solution depends continuously on input data (stability condition).

If at least one of the three conditions fails, then the problem is called ill-posed (also improperly posed or incorrectly posed problem).

Typically, several approximate solutions can be found in real conditions (locations as well source intensity functions), which fits well with observed data. This is caused by the tree structure of the watercourses system, so the pollution can be transported from the unknown source to the observation point by different ways, whereas the transport time (dispersion process, dilution, time course transformation…) can be very similar, so the resulting concentration time course can be almost identical and by this way the unique solution of the inverse task cannot be ensured.

The source identifiability is closely connected with assumption of some information of the unknown source characteristics. The measured pollution concentration data over time (concentration time course) alone are insufficient source of data for solving the inverse task. Beside the known measured pollution time course, we have unknown the source location as well as the source intensity function. This makes the solution of the inverse task impossible (ill – posed task). To decrease the uncertainty degree of the task, we have to assume

some information about the pollution source. For example, in case of sewer network this could be the instantaneous pollution release, but more realistic would be some specific type of the pollution source intensity function, e.g. the inflow concentration time course. The total mass of the pollution can be estimated based on the measured data (measuring concentration and discharge). For task simplification we assume, that the pollution is conservative; this means, that the pollution is not a subject of chemical or biological degradation process during transport in water. However, for special pollution substances, such a volatile or fast reactive pollution types, this approach should be amended.

Assumptions

The inverse task solutions are usually connected with many unknown characteristics, as well as some methods of their solution require a large number of numerical simulations. Therefore, simplifying assumptions are often used, results of which are simple numerical models (e.g. analytical solutions of partial differential equations) that accelerate the numerical simulations and reduce the computing time required to solve the overall task.
For practical solution of an inverse problem the following assumptions are very often accepted:

1. the monitored substance is conservative,
2. the monitored substance will be not attached to the suspended particles, bed material or sediment, will not react with the other pollutants in water,
3. the monitored substance background concentration will be low (related to the concentration in substance source), or zero, eventually close to zero,
4. confluence points on the watercourses network change the monitored substance concentration, but do not change the concentration time course shape,
5. the monitored substance source is a simple one,
6. knowledge of the source intensity function,
7. the measuring intervals of the detection device will be sufficiently short,
8. the detection limit of the monitoring device - sensor will be sufficiently low,
9. various assumptions adopted in the hydraulic model of the sewer network, which includes:
   a) prismatic channel bed along a reach,
   b) the open channel network will have from the hydraulic point of view a simple tree structure, e.g. there will be no bifurcation (flow split-up) points, no looped circuits in the system structure, the flow path will be unique from each possible pollution point,
   c) there will be no objects (hydraulic obstacles, so called singularities) in the system network, which will completely disturb the pollution time course,
   d) the flow in the open channel system can be regarded as a steady and uniform one, at least during the substance transport from source to the observation point,
   e) it will be possible to determine discharges in each particular sections and related hydraulic and dispersion parameters,
   f) unpredictable and discontinuous pollutant inflows will not occur – e.g. large industrial discharges, varying in time, also flush flood discharges will not occur.

Methods for inverse task solution

There are several approaches to solve the inverse task. According (Barati Moghaddam et al., 2021) the methods can be categorized into three main groups:

1. optimisation methods,
2. stochastic (probabilistic) methods and
3. mathematics based methods and approaches.

The first ones – the optimisation approaches are based on the minimisation of the difference between simulated and observed contaminant concentrations at the observation points by using an optimization algorithm. As the optimisation algorithms can be used "classical" linear programming, least squares regression methods, as well as the "non-classical" methods like the genetic algorithms, artificial neural networks. This approach uses a numeric model for forward simulation and compares the output (modelled) data with the measured data. The numeric model can be an integrated model or an external model, linked through the above-mentioned optimisation procedure. Use of an external model can be very advantageous because of the complexity and reliability of the used model.
The stochastic (probabilistic) methods consider parameters to be random variables rather than fixed deterministic quantities. The major stumbling block to the use of probabilistic models is how to assess the statistical properties of unknown model parameters, considering that there is a large degree of uncertainty in their measured values. (Woodbury et al., 1998)
The last group of the methods solve the inverse problem using direct numerical or analytic methods. These methods are typically very complex and sophisticated, on the other hand less time consuming, more straightforward with more unique results (Barati Moghaddam et al., 2021).
Choosing the approach for the open channel or sewer systems, we focused our effort to the first group of inverse task solution methods, i.e. on optimisation methods.
Optimisation methods are very flexible and relatively easy to create the SW code, eventually the possibility of use of external flow and pollution transport models. Their disadvantage can be the lower level of mathematical apparatus, but regarding to the uncertainties in the whole localisation task it is not reasonable to use high sophisticated mathematic (numeric) methods, which in our opinion will not significantly increase the overall precision of the inverse task solution.
The next disadvantage of proposed method of solving the inverse problem is the necessity to realize a large number of numerical simulations, respectively long calculation time. This disadvantage, however, gradually disappears with the increase in computer technology performance and speed. Our proposed model performs the large number of simulations only once (creating

the unit pollutograms), eventually once for specific hydrologic situation. This procedure can be realised in advance, the localization procedure itself is then very quick.

Localisation tool principle and description

The proposed (and developed) localisation tool is based on model creation of so called "unit pollutograms", i.e. on creation of the substance concentration time course for each observation point and for each possible source point (i.e. all network points upstream the observation point). Unit pollutogram means, that the mass of the substance, instantaneous released in the source point is equal to one (arbitrary) unit; the mass of the substance flowing through the observation profile will be the same, i.e. equal to one unit. This modelling principle is very often used in hydraulic (hydrologic) modelling, whereas the unit pollutograms (hydrograms) are often referred as the response function.
The generated unit pollutograms are build up assuming the instantaneous pollution entry (source intensity function, in form of the Dirac impulse input). If a different source intensity function should be applied, the resulting modelled pollutogram in the observation point can be derived simply by the discretisation of the input function to the set of unit instantaneous pollution entries. The resulting (modelled) pollutogram can be simply derived by addition of particular unit pollutograms (response function), eventually multiplicated by the factor according the relative concentration ratio in the discretized source intensity function.
Real pollutogram in this sense means that this pollutogram contains absolute concentration values. This could be easily achieved by multiplying the unit pollutogram by the observed (monitored) mass of the substance, so the amount of the monitored and modelled substance will be equal. The localization procedure in the form of a flowchart is shown on Fig. 1.

Hydraulic model

Hydraulic model is a basic and crucial part of the overall localisation tool. The basic goal of the hydraulic model is to determine the hydraulic conditions in the open channel/sewer network, namely the hydraulic flow rates (discharges) and depending flow velocity for each part (branch) of the system. A basic condition is to have a database, which contains all structural data about the open channel network, e.g. diameters, slope, lengths, coordinates, topology information, etc.
The best option will be wide range monitoring of the necessary hydraulic parameters (velocity, flow rates), but of course, this is not possible, especially in case of wide and large network systems. Typically, nowadays the flow rate measuring devices are stationed only in few points, mainly at the end of a system part. Therefore, it is necessary to use a mathematical model, which will deliver information about the flow rates and other hydraulic parameters across the whole open channel network.

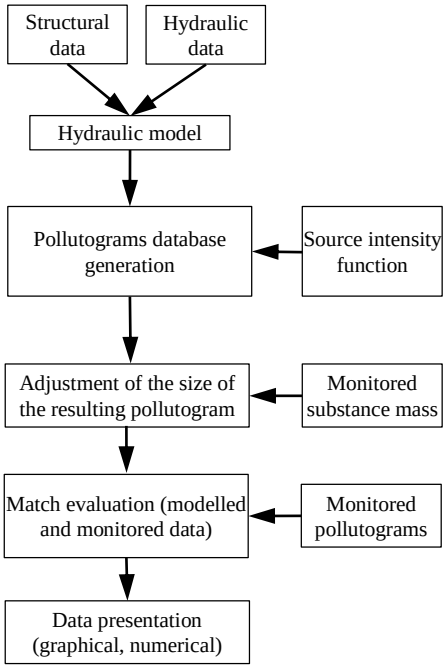

Fig. 1. Flowchart of the localisation tool.

The basic equation for the hydraulic model, used for calculation of the flow rate for specific cross-section of the sewer network is

$$Q_a \frac{N q_s}{86400} + \sum q_p \quad (1)$$

where Q_a is the average flow rate [l s^{-1}], N is the number of inhabitants, connected to the sewer system upstream of the investigated sewer network profile [-], q_s is the specific daily wastewater production per capita [l inh^{-1} day^{-1}], 86400 is the number of seconds per day [sec], the term $\sum q_p$ represents the sum of all point inflows into the sewer system upstream the investigated sewer network profile [l s^{-1}].
Anyway, from this point of view, any monitored information about the flow rates would be very useful. Because of this, implementation of flow in measuring (monitoring) devices (level, velocity sensors) is very welcomed and can significantly improve the localisation procedure precision.

Pollutant transport model

The modelling of the pollutant transport in open channel network consists of two basic and consecutive steps:
1. solution of the pollution transport in a single branch and,
2. confluence and mixing of the substance in junctions (sewer manholes).

For the pollution transport are in the model 5 various methods applied. All of used methods are based on the solution of the advection – dispersion equation (ADE), which describes the transport of solute in flowing water. To simplify an already rather complex task, we

used the one-dimensional form ADE. Such simplified ADE has a form (Fischer et al., 1979):

$$\frac{\partial Ac}{\partial t} + \frac{\partial Qc}{\partial x} - \frac{\partial}{\partial x}\left(AD_L \frac{\partial c}{\partial x}\right) = -AKc + C_s\, q \qquad (2)$$

where: c is a mass concentration [g l^{-1}]; D_L is the longitudinal dispersion coefficient [m^2 s^{-1}], A is a discharge area in a cross-section [m^2], Q is a discharge in a sewer [m^3 s^{-1}], K represents a rate of growth or decay of contaminant [s^{-1}], C_s is the concentration of a source, q is a discharge of a source, x is a distance [m].

For a faster response of the proposed localization tool and overall simplification of the procedure, analytical solutions of ADE were used for modelling the forward spread of pollution: Gauss (Fischer et al., 1979; Runkel and Broshears, 1991), Gumbel (Sokáč et al., 2018) and Generalised Extreme Value (GEV) distribution model (Sokáč et al., 2018).

As stated in the theoretical part, it can be assumed that "ideal" (immediate) mixing occurs at the points of confluence (watercourses confluences, manholes on the sewer network). This means that this will change the concentration of the pollutant due to mixing, but the shape of the time course of the concentration of the pollutant (pollutograms) will remain unchanged. Mathematically, mixing at confluence points can be expressed by the following equation (equation of ideal mixing):

$$c(t) = \frac{\sum_{i=1}^{i=N} Q_{i,t}\, c_{i,t}}{\sum_{i=1}^{i=N} Q_{i,t}} \qquad (3)$$

where the $c(t)$ is the concentration in time t [g l^{-1}], $Q_{i,t}$ is the flow rate [m^3 s^{-1}], inflowing in time t from the *i-th* inflow into the confluence point, $c_{i,t}$ is the pollutant concentration [mg l^{-1}] of this inflow in time t, N is the total number of inflow (connected watercourses / sewer branches).

It is obvious, that in case of confluence with one or more lateral inflows with zero pollutant concentration will the resulting (outflow) concentration abruptly decrease; the decrease rate is depending on the mutual ratio of discharges of particular inflows to the confluence node.

Pollutogram database generation

This part of the localisation tool generates the particular pollutograms for each point of the open channel system. The overall process proceeds as follows:

1. generation the substance input in specific point of the network,
2. modelling the pollutogram transformation (i.e. its advection and dispersion) along the adjacent (downstream) branch,
3. record the pollutogram into a database file(s),
4. the process in points 2 and 3 will repeat until the most downstream node of the open channel system is reached,
5. the process in points 1–4 is repeated for each point of the sewer network.

Such procedure will generate the transformed pollutograms between each pair of system nodes where a hydraulic connection between those two nodes.

The pollutograms database generation should be performed for various hydraulic conditions of watercourses system, i.e. for average, as well as for a wider range of flow rates between the minimal and maximal flow rates.

Pollutogram match evaluation – localisation procedure

The last step in the overall localisation procedure is the match evaluation between the modelled pollutograms (stored in the database) and measured pollutograms. This is realized through standard statistical tests, focused on the evaluation of the match of two time courses data series (pollutograms), namely the Root Mean Square Error (RMSE) and the Normalised Root Mean Square Error (NRMSE). The goal of this procedure is to assign to each node on the sewer network a probability, that the source we are looking for will be right at that point. The probability of the source occurrence in particular network points is determined within the value range from 0 to 1 (or 0 – 100%), whereas zero value means there is no possibility, that the source is located in this point; the value one means the highest probability of the source spill occurrence in this point.

It is necessary to known, in which point/location/profile of the open channel system was the substance pollutogram measured, i.e. to know the monitoring profile in the network. As potential pollutant sources are considered all network nodes, located upstream, all downstream nodes will be automatically assigned zero probability. The comparison procedure is performed with all network points located upstream and comparison results between the measured and modelled pollutograms (RMSE, NRMSE) are assigned to particular network points.

Localisation tool includes also option to exclude a part (branch) of the open channel system from the localisation procedure. This option can be used, if there another monitoring device, which does not register the presence of the monitored pollutant ("zero pollutogram") in that network part. This means, that the substance source will be definitely not located upstream of that monitoring device.

In order to compare two series of time (pollutograms), it is necessary first to put both time series on the same basis. In our localisation tool, the mass normalisation was used, i.e., in all cases the total tracer mass corresponds to one dimensionless unit; the time is not normalised. The dimensionless mass normalised concentration is defined:

$$c_d(t) = \frac{Q\, c(t)\, \Delta t}{\sum_{i=0}^{i=\infty} Q\, c_i\, \Delta t} \qquad (4)$$

where $c_d(t)$ is the dimensionless mass normalised concentration [-], c [t] is the substance concentration in time t [kg m^{-3}], Q is the flow rate [m^3 s^{-1}].

The measured and modelled pollutogram, normalised

such way can be subsequently subject of the statistical match evaluation, using the above-mentioned statistical methods (RMSE, NRMSE).

The resulting array (network nodes with assigned source location probability) is then sorted to present to the user the nodes with highest source occurrence probability. For better results presentation can be the result array also percentage normalised – the highest probability value can be regarded as 100% probability and the lowest value (typically close to zero or zero) as the 0 % probability. Such normalisation allows to use achieve a full-scale range of the results in graphical interpretation of the results. The normalised values are then assigned to each open channel system node and corresponding data (coordinates, source probability in normalised percentage) for the graphics are exported to a separate file. The graphical results presentation is currently implemented into the AutoCAD graphical software, where the source probability of particular nodes is shown by differentiated by various colour and size of the circles in corresponding open channel system nodes.

Numerical tests of the localisation tool

Since the tests and verification of the localization procedure is not easy in the real conditions of the watercourse system due to the difficulty of obtaining the input data, the localization tool was tested only on numerically generated cases of discharge of a pollutant in a fictitious, simplified sewer network, as a limit case of an open channel system. Input data were chosen on base of a dataset from a real sewer infrastructural database from a town in south-east part of Slovakia. The parameters of the infrastructural database are summarized in Table 1.

Tests were focused on the reliability and sensitivity of the localization tool to errors in the data obtained from possible sensors located in the field. This kind of test was performed to check the sensitivity on the localization method results on the accuracy of the measured data regarding obtained pollutograms. For this reason, we intentionally inserted random and systematic errors into the modelled data in the given range of percent (0%, 5% and 10%). For examples of the generated data with

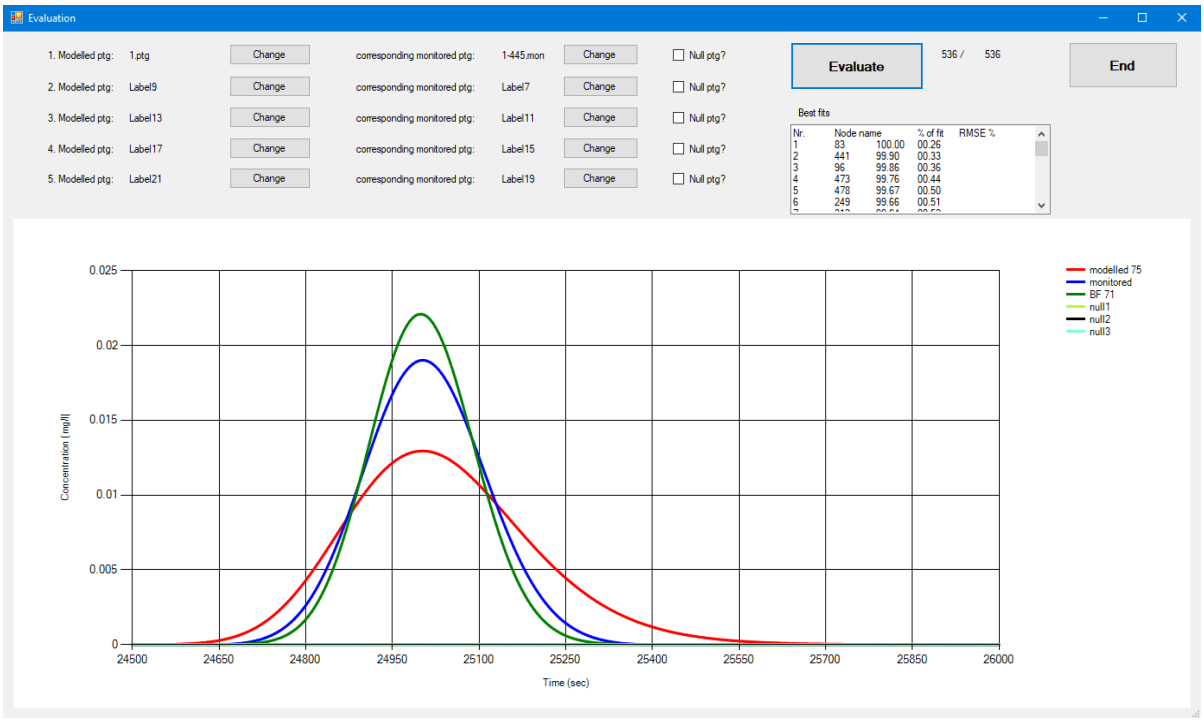

Fig. 2. Screenshot of the localisation SW procedure.

Table 1. Summary of sewer network parameters used for numerical test

Catchment	
Total catchment area	131.51 ha
Total impervious area	31.74 ha
Average runoff coefficient	0.241
Number of elementary sub-catchments	448
Min. node invert level	294.00 m a.s.l.
Max. node invert level	340.05 m a.s.l.
Sewer network	
Number of nodes (manholes)	562 (279*)
Number of sections (branches)	615 (261*)
Total sewer length	26 066 m (11 062*)

random and systematic error see Fig. 3 and Fig. 4. Such modified pollutogram was then used as input into the localization procedure as the basic input (instead of correct generated data). Such errors in the measured data can be caused not by the inaccuracy of the measuring devices, but also by the flow and concentration fluctuations.

Results and discussion

In our case of the sewer network (see Fig. 5), as the monitored manhole/profile was used the manhole Nr. 1 – the inlet manhole at the waste water treatment plant (WWTP). The tests were performed for pollutant inlet in the manhole Nr. 54 (see Fig. 5). The manhole Nr. 54 is 2622 m far from the WWTP (flow route on the sewer network). For the numerical test we used the initial (original) data, achieved by numerical modelling of the pollution spreading in the open channel system, namely for the manhole Nr. 54 (see Fig. 5). For the sensitivity analysis we apply on this dataset various (virtual) types of errors, as described later.

The initial test of the localisation procedure, using with zero error (0%, i.e. with the original data) selected the manhole Nr. 54 as the location with the highest probability of the source location. This was also a confirmation that the methodology is correct and the localization procedure was coded correctly.

However, this simple numeric test also showed other locations that had a high probability of locating the substance source in the interval chosen (90%). These locations in Fig. 5 are shown by the red colour of the points. As can be seen in this figure, there are several such locations on connected (side) open channels. For this reason, it is advisable to establish monitoring points upstream the connection of such channels to the main channel; this can in real cases confirm or exclude the inflow of pollution from a given direction by detection (or absence) of monitored substance.

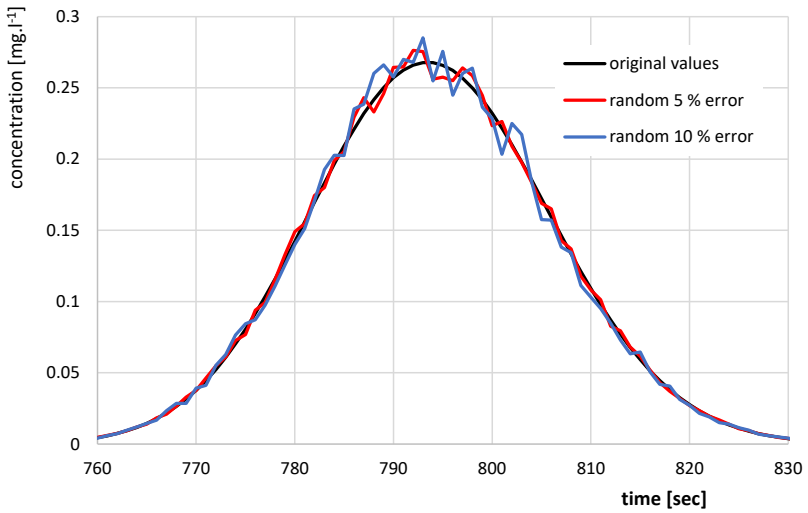

Fig. 3. Example of random error generation.

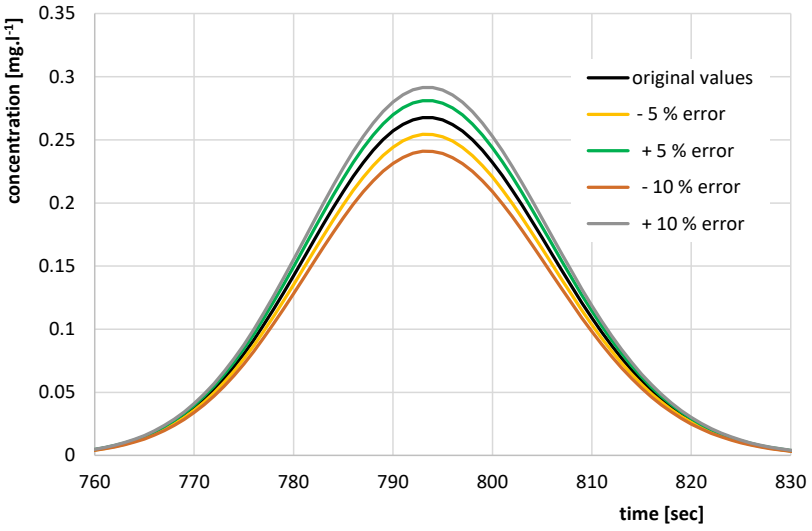

Fig. 4. Example of systematic error generation.

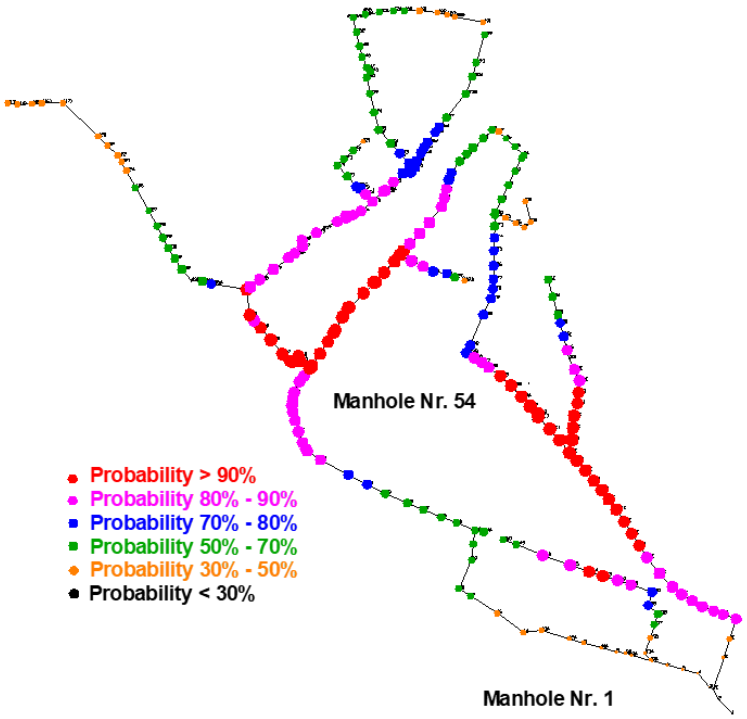

Fig. 5. Sewer network system used for tests, location probability results for zero error.

The tests with random errors (see Fig. 3) show, that small errors in measured values with ±5% does not significantly influence the accuracy of the localisation method. In opposite, larger errors in measured values (±10%) cause significantly higher localisation errors. Typically, the substance source dropped in the probability ranking by 34 up to 56 places in the highest probability ranking list, but the relative probability remains still very high (96.6–99.6%).

Analysing the data, we tried to suppress the random errors down applying the method of the moving average, using different number of the array members for the calculation of the moving average (3, 5 and 10 array members). This does not improve the results accuracy in any way, the accuracy was rather worse.

A second test was also performed, with simulated systematic error, i.e. the modelled data were modified by a systematic error of a certain percentage of the measured value (+5, 10% and –5, 10%, see the Fig. 4). The sensitivity test results that such error has almost no influence on the accuracy of the localisation procedure. Reason of this fact is probably the transformation of the pollutograms to the unitary form, which suppress the errors down.

Of course, the solution or prediction of the pollutant source location also depends on the accuracy of the all input data. There could be another data errors, which can cause large errors in the inverse problem solution, e.g. errors in the open channel physical definitions, their hydraulic data, flow regime (flow rates) etc. For this reason, it is necessary to approach the acquisition of this data with the highest possible degree of accuracy. At the same time, the authors recommend at least to verify the numerical model setup with a small number of tracer experiments in order to verify the parameters of the numerical model and to avoid large errors in the source localization solution.

Comparing our results with the similar studies is not easy, because of lack of relevant papers, dealing with the inverse- source localisation problem in extensive channel systems. The source localisation problem was studied by (Ghane et al., 2016) in the river network, where only few possible source localities were assumed, the study of (Telci and Aral, 2011) assumes 100 possible pollution source points. However, the last one study uses for the pollution point localisation training followed by a sequential elimination of the candidate spill locations which lead to the identification of potential spill locations.

Very similar work to our study was published by (Sonnenwald et al., 2023). The results of this study fully confirmed our assumption, that every point (possible pollution source) in the sewer network has its specific "fingerprint", which describes the possible concentration distributions observed at a monitoring location as a result of a pulse input at every upstream manhole. This inspiring study also states the fact that it is necessary to take into account the change of hydraulic parameters in the sewer network based on the time of day, or daily activity profile of residents (wastewater production).

Conclusion

In the paper we presented a solution of an inverse problem – the pollution source localisation in a system of open channel system. The proposed inverse problem solution method, as well as the overall localisation procedure was numerically tested on a simplified real

sewer system data, whereas part of the numerical tests was focused to the sensitivity analysis of the proposed method.

Numerical tests have confirmed the methodology correctness and the proper coding of the localization procedure. This was confirmed by the initial numeric test, which was performed with the initial (original) data, achieved by numerical modelling of the pollution spreading in the open channel system assuming as the pollution source the manhole Nr. 54. The initial test selects exactly this manhole as the node with the highest probability of the pollution source occurrence.

The sensitivity analysis was performed assuming two error types - random and systematic error. The first one occurs very often in open channels, particularly in sewer networks and is typically caused by probe (sensor) clogging. The sensitivity analysis results show, that this kind of error, especially when the random errors are bigger than 10%, significantly affects the results of the localisation procedure. Use of simply data filters (moving average) does not improve the results, so in this case maybe more advanced techniques shall be used, e.g. the Kalman filter (Chachuła et al. 2021)

The second error type – the systematic error can arise e.g. from incorrect calibration of the measuring device (probe), when the device shows a constant proportionally higher (or lower) value. The sensitivity analysis results of the proposed localisation procedure show, that in this case the input data inaccuracies has almost no influence on the localisation accuracy. The reason for this is the linear transformation of the measured data to the unitary form, which almost eliminates these errors.

Numerical tests confirmed the correctness of the methodology as well as the localization procedure itself. At the same time, however, they pointed out its weak points – random errors in measurements. Besides this type of errors, it is necessary in the next future to deal with other sources of random errors, such as the definitions of the physical properties of the network of open channels, their hydraulic parameters, eventually to perform a physical verification of the proposed model and methodology.

Acknowledgement

This study was supported by the grants from the Slovak Academy of Sciences (project VEGA No. 2/0085/20 with the title "Prediction of a point pollution source position in a watercourse network – a hydrodynamic approach") and by the H2020 EU funded project "SYSTEM", grant agreement No. 787128.

References

Bagtzoglou, A. C., Atmadja, J. (2003): Marching-jury backward beam equation and quasi-reversibility methods for hydrologic inversion: Application to contaminant plume spatial distribution recovery. Water Resour. Res. 39, 1–14. https://doi.org/10.1029/2001WR001021

Banik, B. K., Di Cristo, C., Leopardi, A. (2014): "SWMM5 toolkit development for pollution source identification in sewer systems." Procedia Engineering 89: 750–757. https://doi.org/10.1016/j.proeng.2014.11.503

Banik, B. K., Di Cristo, C., Leopardi, A. (2015): "A pre-screening procedure for pollution source identification in sewer systems." Procedia Engineering 119: 360–369. https://doi.org/10.1016/j.proeng.2015.08.896

Boano, F., Revelli, R. Ridolfi, L. (2005): Source identification in river pollution problems: A geostatistical approach. Water resources research, 41.

Chachuła, Krystian, Robert Nowak, and Fernando Solano. (2021): Pollution Source Localization in Wastewater Networks. Sensors 21, no. 3: 826. https://doi.org/10.3390/s21030826

Courant, R., Hilbert, D. (1993): Methoden der mathematischen Physik, Methoden der mathematischen Physik. Springer Berlin Heidelberg. https://doi.org/10.1007/978-3-642-58039-0

El Badia, A., Hamdi, A. (2007): Inverse source problem in an advection-dispersion-reaction system: Application to water pollution. Inverse Probl. 23, 2103–2120. https://doi.org/10.1088/0266-5611/23/5/017

Fischer, H.B., List, E.J., Koh, R.C.Y., Imberger, J., Brooks, N.H. (1979): Mixing in inland and coastal waters.

Ghane, A., Mazaheri, M., Mohammad Vali Samani, J. (2016): Location and release time identification of pollution point source in river networks based on the Backward Probability Method. J. Environ. Manage. 180, 164–171. https://doi.org/10.1016/j.jenvman.2016.05.015

Hadamard, J. (1923): Lectures on Cauchy's Problem in Linear Partial Differential Equations. New Haven: Yale University Press.

Skaggs, T. H., Kabala Z. J. (1994): Recovering the release history of a groundwater contaminant. Water Resour. Res, 30(1), 71–79.

Cheng, W. P., Jia, Y. (2010): Identification of contaminant point source in surface waters based on backward location probability density function method. Adv. Water Resour. 33, 397–410. https://doi.org/10.1016/j.advwatres.2010.01.004

Kessler, A., Ostfeld, A., Sinai, G., (1998): Detecting accidental contaminations in municipal water networks, J. Water Resour Plan and Manage. 124, 192–198.

Kováčová, V. (2023): Deterioration of water quality in aquatic system. Acta Hydrologica Slovaca, Vol. 24, No. 1, 2023, 141–150, https://doi: 10.31577/ahs-2023-0024.01.0016

Barati Moghaddam, M., Mazaheri, M., Mohammad Vali Samani, J. (2021): Inverse modeling of contaminant transport for pollution source identification in surface and groundwaters: a review. Groundwater for Sustainable Development, 15, 100651. https://doi.org/10.1016/J.GSD.2021.100651

Mazaheri, M., Mohammad Vali Samani, J., Samani, H. M. V. (2015): Mathematical Model for Pollution Source Identification in Rivers. Environ. Forensics 16, 310–321. https://doi.org/10.1080/15275922.2015.1059391

Novák, V. (2022): Global changes and hydrosphere, Acta Hydrologica Slovaca, Vol. 23, No. 1, 2022, 3–9, doi: 10.31577/ahs-2022-0023.01.0001

Runkel, R. L., Broshears, R. E. (1991): One-dimensional transport with inflow and storage (OTIS): A solute transport model for small streams. CADSWES-Center Adv. Decis. Support Water Environ. Syst. - Dep. Civ. Eng. - Univ. Color. 91.

Shao, Z., Xu, L., Chai, H., Yost, S. A., Zheng, Z., Wu, Z., He, Q. (2021): "A Bayesian-SWMM coupled stochastic model developed to reconstruct the complete profile of an unknown discharging incidence in sewer networks." Journal of Environmental Management 297: 113211.

Sokáč, M., Velísková, Y., Gualtieri, C. (2018): An approximate method for 1-D simulation of pollution transport in streams with dead zones. Journal of Hydrology and Hydromechanics 66, no.4 (2018): 437–447. https://doi.org/10.2478/johh-2018-0035

Sonnenwald, F., Shuttleworth, J., Bailey, O., Williams, M., Frankland, J., Rhead, B., Mark, O., Wade, M. J., Guymer, I. (2023): Quantifying Mixing in Sewer Networks for Source Localization. Journal of Environmental Engineering, 149(5): https://doi.org/10.1061/JOEEDU.EEENG-7134

Telci, I. T., Aral, M. M. (2011): Contaminant Source Location Identification in River Networks Using Water Quality Monitoring Systems for Exposure Analysis. Water Qual. Expo. Heal. 2, 205–218. https://doi.org/10.1007/s12403-011-0039-6

Wang, J., Zhao, J., Lei, X., Wang, H. (2018): New approach for point pollution source identification in rivers based on the backward probability method. Environ. Pollut. 241, 759–774. https://doi.org/10.1016/j.envpol.2018.05.093

Woodbury, A., Sudicky, E., Ulrych, T. J., Ludwig, R. (1998): Three-dimensional plume source reconstruction using minimum relative entropy inversion. J. Contam. Hydrol. 32, 131–158. https://doi.org/10.1016/S0169-7722(97)00088-0

Ing. Yvetta Velísková, PhD. (*corresponding author, e-mail: veliskova@uh.savba.sk)
Assoc. Prof. Ing. Marek Sokáč, PhD.
Institute of Hydrology SAS
Dúbravská cesta 9
841 04 Bratislava
Slovak Republic

Maryam Barati Moghaddam, PhD.
Department of Water Engineering and Management
Faculty of Agriculture
Tarbiat Modares University of Tehran
Irán

DOI: 10.31577/ahs-2023-0024.02.0031

ACTA HYDROLOGICA SLOVACA

Volume 24, No. 2, 2023, 285 – 293

Variability and trends of selected snow cover characteristics in the Tatra Mountains region in Slovakia 1981–2020

Lenka BALÁŽOVIČOVÁ*, Cyril SIMAN, Katarína MIKULOVÁ

Over the last decades, snow seasons in Europe were reported to become shorter with lower abundance of snow. However, at some stations situated above certain elevation, the amount of snow cover was found to be increasing. This is also the case of high mountains in Slovakia, where number of snow-related studies showed some differences related to the elevation. In this study we report on the trends of selected snow cover characteristics such as the number of days with snow cover (DSC) for 1, 10 and 20 cm depths, summed snow depths (SSD) and mean snow depths (MSD). The data used in this study were collected by the Slovak Hydrometeorological Institute (SHMI) at eight stations in the Tatra Mountains region during the 39 seasons 1981–2020 (01/07 to 30/06 the following year). Some increasing trends were observed for stations above 1100 m while stations below this elevation had generally decreasing estimates. The DSC for 1 cm ranged from 297 days at station elevated at 2635 m a.s.l. to 25 days for station at 640 m a.s.l. The MSD ranged from 100 to 7 cm on average for the whole period. Apart from global warming, other factors play role, and these can be complex in the mountainous regions making any trends more ambiguous to interpret.

KEY WORDS: snow cover, Western Carpathians, Tatra Mountains, climate change

Introduction

Snow cover is important climate characteristic and its amount and duration depend on various direct or indirect physical, geographic, vegetation, atmospheric or anthropogenic variables (Fiema, 2008). Based on satellite and station data, snow cover extent in the Northern Hemisphere has declined significantly over the past 90 years, with most reductions occurring since 1980 (EEA, 2021). The duration of snow seasons became shorter in Europe because of earlier snowmelt in spring and it is projected to decrease significantly by the end of this century, by over 100 days in some regions (EEA, 2023).

Studies of snow cover, its spatial and temporal variability and trends, are important in terms of climatological, hydrological or ecological processes (Holko et al., 2001, 2022; Brziak et al., 2021). Understanding of the long-term snow cover trends is key in relation to increasing air temperatures due to climate change (Falarz, 2004). Snow impacts the air by cooling, it reflects most of the radiation back into the atmosphere and thawing processes slow down rising temperatures during springtime in the northern hemisphere (Foster et al. 1983). In terms of water balance, it stores water that is later released during meltdown and supplies important moisture for new vegetation growth (Hríbik and Škvarenina, 2006). It also serves as an important insulant and protects plants from wind and deep-freezing temperatures (Elenberg, 1988; Hríbik and Škvarenina, 2006).

Long-term trends in snow cover were studied in Europe, for example in Poland (Falarz, 2002; Falarz, 2004), in Slovakia (Konček and Briedoň, 1964; Briedoň et al. 1974; Šamaj and Valovič 1988; Lapin and Faško 1996; Holko et al. 2009; Siman and Polčák, 2017), Switzerland (Beniston et al., 1994) or Estonia (Jaagus, 1997). Whole region of Eurasia was summarized by Clark et al. (1999), Bulygina et al. (2009) and of the whole of Northern Hemisphere by Brown (2000).

Considering climate change scenarios, increase in winter precipitation by 20% above 1100 m a.s.l. is expected in mountainous regions in Slovakia during this century (Lapin et al., 2007). A study by Holko et al. (2016) in Western Tatras showed that temperature increase was more pronounced in the colder season (December to March) and the number of snow-weak winters since 2010 was higher and snow cover duration shorter than in the decade before. Faško et al. (2020) in a 100-year study showed that from 1990s till recent there was a significant increase in mean values of air temperature and the decline in the amount of snow in Slovakia was most pronounced in the most recent decade 2011–2020.

First snow records in Tatras originated in the 16th century but these were only made on an occasional basis. First consistent scientific study on regular snow records was published by Konček and Briedoň (1964) in which

readings from 208 stations in Slovakia were presented during the 1921/22–1950/51 period. Changes in snow cover were later summarized by Chomicz and Kňazovický (1974). Briedoň et al. (1974) published a complex information on snow and other climate characteristics of Tatra Mountains. Snow conditions from 149 stations for the period 1920/21–1979/80 with some new statistical characteristics were reported by Šamaj and Valovič (1988). Snow cover in Low Tatras during the period 1921–1995 was examined by Faško et al. (1997) who observed that although daily sums of snow cover increased, the total number of days with snow was reduced at most stations.

Monthly snow characteristics and their correlation with mean monthly air temperature and precipitation values in the High and Low Tatras in Slovakia during the 1921–2006 period was analyzed by Lapin et al. (2007). Their study pointed out unequal snow conditions in the region influenced by air temperature, precipitation variability but also by altitude and local topographic conditions. During the 85-year period they showed an increase in air temperature by 1.2°C and a significant increase in winter precipitation. Siman and Slavková (2019) observed an increased number of days with snow cover of ≥ 20 cm in Tatras, and consequently increase in the sum and the average height of the snow cover. Increasing trend in snow cover was observed in altitudes around 2600 m a.s.l. and decline at stations located at about 1000 m a.s.l. on south and south-east slopes (Pribullová et al., 2009). Dynamics of snow cover in middle and high areas in Tatras were also studied by Vojtek (2010) and substantial work on snow variability in high mountains in Slovakia was undertaken by Holko (2000), Holko et al. (2001; 2005; 2011; 2021). Holko et al. (2005) observed snow depths in catchments in Tatras and Low Tatras during a 40-year period and found drop in duration of snow cover and snow water equivalent since 1980s at lower situated stations. Changes of snow cover in selected synoptical situations during 1966 to 1996 were studied in Polish Tatras by Fiema (2008) who showed that West and Northwest circulations have positive effect on snow cover duration and the amount of snow is related to the frequency of cyclonal situations.

The aim of this study is to examine temporal and spatial snow cover characteristics at eight selected stations in Tatra Mountains region in Slovakia during period 1981–2020. We analyse interannual variability and trends in characteristics of snow cover duration for stations above and below 1100 m, the summed and the mean depths of snow. We also establish and compare elevation gradients and temporal trends for selected snow characteristics and compare this data with another regional and international studies. The knowledge about duration and thickness of snow cover plays also curtail role in correction of cosmogenic exposure ages which attempt to date Quaternary landforms in mountain environments, like rock-slope failures and glacial moraines (e.g. Engel et al., 2015; Pánek et al., 2017; Makos et al., 2018; Zasadni et al., 2020).

Station network and methods

Eight stations operated by the Slovak Hydrometeorological Institute (SHMI) were chosen to evaluate snow cover parameters in Tatra Mountains, Low Tatras and surrounding areas such as Popradská and Liptovská basins, in Slovakia. Their main characteristics are summarized in Table 1.

Lowest mean annual temperature (-3.1°C) and the highest precipitation (1722 mm) occurs at Lomnický štít (Table 1). Mean annual temperature at Chopok (2005 m a.s.l.) is -0.4°C, in contrast with Liptovský Hrádok (640 m a.s.l.) 7.1°C. The highest mean summer precipitation was recorded at Skalnaté Pleso (1778 m a.s.l), closely followed by Tatranská Javorina (1013 m a.s.l), but the winter precipitation was most significant at Lomnický štít. The station with lowest precipitation is Poprad (613 mm per year). The differences are given mainly by elevation, slope orientation and prevailing winds.

For the eight stations, following snow cover characteristics for the period of 39 years – 1981/82 to 2019/20 seasons were analysed: (1) the number of days with snow cover (DSC) ≥1 cm, ≥10 cm, ≥20cm; (2) the summed snow depth (SSD) and (3) the mean snow depth (MSD).

Table 1. List of stations selected for the study, their elevation [m a.s.l.], orographic position and their mean air temperature and precipitation characteristic (1981–2020)

Code	Station		Elevation	Orography	MAT	MST	MWT	MAP	MSP	MWP
11874	Liptovský Hrádok	LHR	640	basin	7.1	16.7	-2.6	711	255	119
11916	Chopok	CHOP	2005	peak	-0.4	7.5	-7.7	1145	388	244
11930	Lomnický štít	LOM	2635	peak	-3.1	4.3	-10.1	1722	463	462
11931	Skalnaté Pleso	SKP	1778	hillside	2.5	10.1	-4.6	1424	562	218
11933	Štrbské Pleso	STR	1322	hillside	3.9	12.6	-4.4	1057	357	214
11934	Poprad	POP	693	basin	6.6	16.0	-3.0	613	247	79
11936	Tatranská Javorina	TAJ	1013	valley	4.4	12.9	-3.9	1364	551	191
11938	Telgárt	TEL	901	hillside	5.5	14.7	-3.6	872	321	125

Note: MAT – mean annual air temperature in °C, MST – mean summer air temperature (June–August), MWT – mean winter air temperature (December to February), MAP – mean annual precipitation totals in mm, MSP – mean summer rainfall (June–August), MWP – mean winter rainfall (December to February). Based on 1981–2020 data.

The mean depth of snow cover was calculated as the summed daily heights of snow cover divided by the number of days with snow cover (not the number of days of duration of snow cover). Summed snow depth was calculated as the sums of daily heights of snow cover. To include all the annual data, seasons were divided from 01/07 to 30/06 the following year.

The data were analysed for each snow attribute of the 1981/82–2019/20 period, as absolute values and by a coefficient of variation. Some correlations and trends were established, and some observations on the impact of snow depth or duration on elevation gradient were made and tested against some published work (e.g. Petrovič, 1972, Briedoň et al., 1974) in the studied region.

Results and discussion

Number of days with snow cover during winter months more or equal to 1, 10 and 20 cm are the basic characteristics of snow cover. The eight stations were divided according to their elevation into two groups: stations with elevations below 1100 m a.s.l. and stations situated above this elevation. Data of snow cover duration in days for each snow height interval and for each season (July to June) from 1981 to 2020 were plotted alongside their trendlines (Fig. 1). Also trends and coefficients of variability were compared, and overall changes established (Table 2).

Although some snow weak winters such as 1989/90, 1997/98, 2006/7 or 2010/11 alternate with snow rich winters such as 1995/96, 1999/2000 or 2007/08, some weaker trends can be observed in the number of days with characteristic snow cover. This trend appears to be decreasing for stations below 1100 m a.s.l. and steady or increasing for stations above this elevation. This was purposed as the effect of global warming, which is causing less solid precipitation at lower elevations, but more (solid) precipitation occurs at higher elevations (Holko et al. 2005).

With regards to the number of days with 1 cm snow cover, the steepest decrease was recorded at Tatranská Javorina (-0.836 days year^{-1}) which means this period could be shorter by about 8 days per decade. Poprad and Liptovský Hrádok would drop by about 6 days per decade. Maximum mean number of days with 1 cm snow cover occured at Lomnický štít (260 days) with the absolute maximum of 297 days in 1996/97 season and the minimum in Poprad (77 days) in 2006 with the absolute minimum in Liptovský Hrádok, recorded in the 2013/14 season.

Considering the mean number of days with 10 cm snow cover, the maximum was at Lomnický štít (236 days) and the minimum at Poprad (only 28 days). However, the highest estimated difference per decade is expected in

Table 2. Statistical summary and mean estimated decadal differences for number of days with characteristic snow cover at selected stations, based on data for the 1981/82–2019/20 period. Stations are ordered from highest to lowest elevation. SD stands for standard deviation

	LOM (2635)	CHOP (2005)	SKP (1778)	STR (1322)	TAJ (1013)	TEL (901)	POP (693)	LHR (640)
DAYS WITH 1 CM SNOW COVER								
Mean	259.51	198.59	171.56	158.74	145.10	103.62	76.74	80.97
SD	17.57	15.63	16.19	14.90	21.60	25.49	23.56	24.74
Minimum	223	169	134	123	86	54	38	25
Maximum	297	248	202	182	180	144	130	127
Trend	-0.451	-0.264	0.137	-0.332	-0.836	-0.453	-0.602	-0.632
Diff. per decade	-4.5	-2.6	1.4	-3.3	-8.4	-4.5	-6.0	-6.3
Pearsons coeff.	0.292	0.179	0.096	0.254	0.440	0.202	0.292	0.291
DAYS WITH 10 CM COVER								
Mean	235.56	173.77	138.95	139.28	116.41	64.49	28.36	36.87
SD	21.58	21.32	27.90	23.16	30.86	37.16	23.99	26.34
Minimum	188	97	49	74	37	4	0	0
Maximum	278	230	178	180	171	138	102	99
Trend	0.095	0.064	0.260	-0.001	-0.855	-0.145	-0.208	-0.802
Diff. per decade	0.9	0.6	2.6	-0.01	-8.5	-1.5	-2.1	-8.0
Pearsons coeff.	0.050	0.035	0.115	0.000	0.315	0.045	0.098	0.347
DAYS WITH 20 CM COVER								
Mean	218.97	158.87	104.36	121.69	95.03	40.54	10.85	16.10
SD	23.35	23.25	37.80	31.38	37.81	34.93	19.36	21.04
Minimum	168	56	10	47	6	0	0	0
Maximum	263	227	172	170	170	118	94	79
Trend	0.083	-0.034	0.313	0.122	-0.995	0.00	0.103	-0.305
Diff. per decade	0.8	-0.3	3.1	1.2	-10.0	0.0	1.0	-3.1
Pearsons coeff.	0.041	0.017	0.094	0.045	0.300	0.008	0.061	0.166

Tatranská Javorina and Liptovský Hrádok, both by about 8 days. During 1994/95 season, there was not a single day with snow cover of 10 cm and more recorded at Poprad station and in 1997/98 it was only one such day. In Liptovský Hrádok there were no days with 10 or more cm of snow during the 2013/14 season and during 2019/20 this was the case for both stations.

Similar trends have been observed for the number of days with snow cover of 20 cm and more. Mean maximum was understandably at Lomnický štít (219 days) and minimum at Poprad (11 days), with 11 seasons without this snow cover height at both Poprad and Liptovský Hrádok stations. Interestingly, the trend was most obvious at Tatranská Javorina suggesting possible 10 days drop of this snow cover per decade.

Despite the fact the trends were weak, it was interesting to see that they were decreasing for DSC/1 cm at 7 stations, with mean decrease -4.3 days per decade (± 2.9). For DSC/10 cm, the trend was increasing or steady at stations above 1100 m and decreasing for the rest. The mean was -2 days (±4.1). And the DSC/20 cm trend revealed interestingly insignificant difference, except Tatranská Javorina station, where it was -10 days per decade, causing mean difference to be -0.9 days.

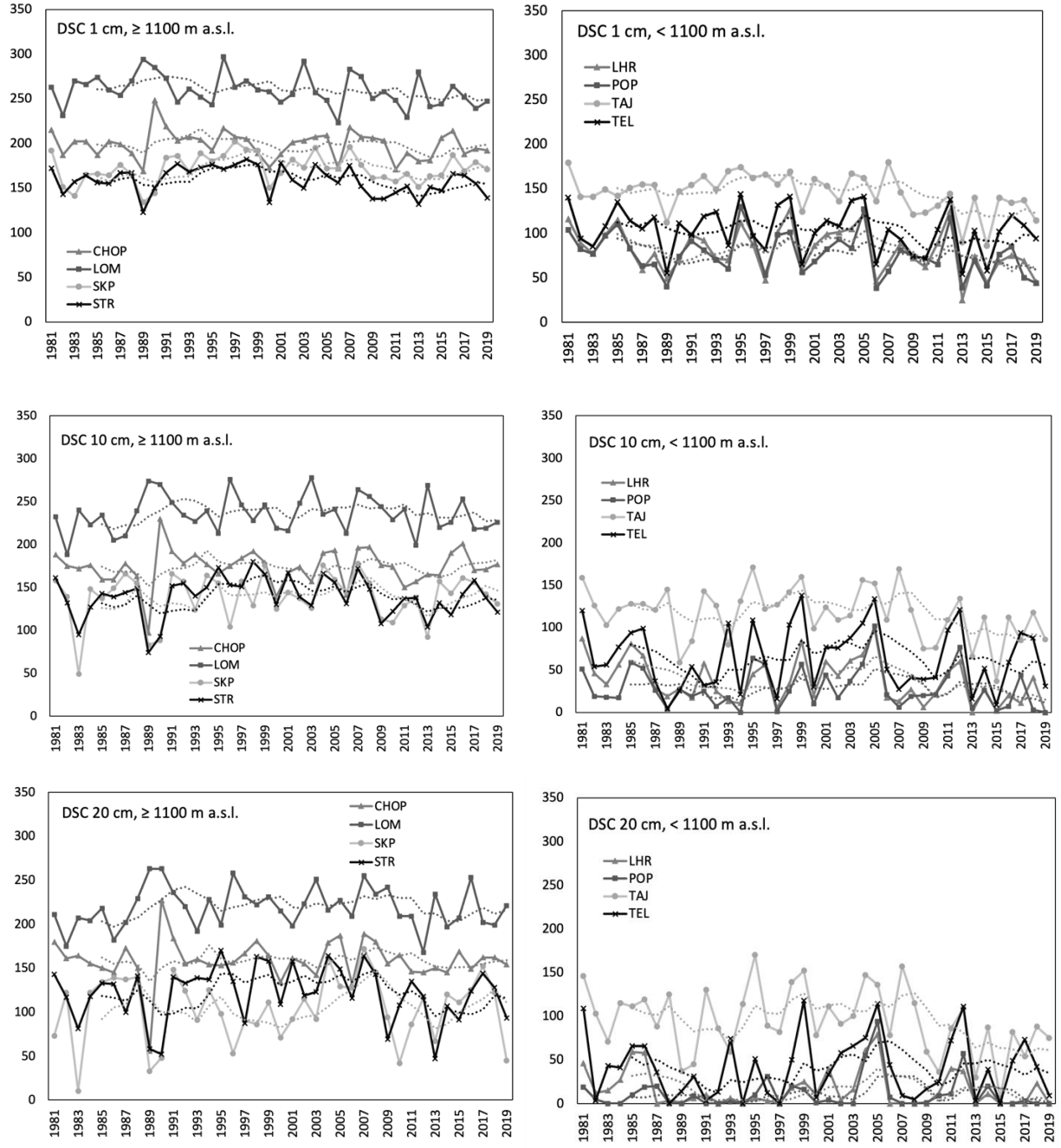

Fig. 1. Interannual course of number of days with snow cover (DSC) with 1 cm, 10 cm and 20 cm for seasons 1981/82 to 2019/20. The dotted lines represent the 5-year moving average.

Following weak trends were observed with regards to the snow depth variations. Two characteristics were analysed: the summed snow depth (SSD) and the mean snow depth (MSD), (Table 3). Mean SSD during the 39 seasons was highest at Lomnický štít (299 m), with the maximum of 509 m in 2007/08 season. The lowest mean SSD was observed at Poprad (7.56 m) but the lowest SSD overall occurred in Liptovský Hrádok during the 2013/14 season and it was only 0.88 m. Trend pointed out to a considerable decadal increase at Lomnický štít (24 m) followed by Chopok (12 m). Other stations showed only a slight decrease. SSD at Liptovský Hrádok has decreased by 1.8 m per decade. Coefficient of variation was obtained as the standard deviation divided by the mean*100 to illustrate the rate of interseasonal changes. The lowest coefficient of variation was at Lomnický štít (30.6%) and the highest occurred at Poprad (82%).

As the MSD depends on the SSD and number of days with 1 cm snow cover, therefore the trends are similar. The maximum values were obtained again for Lomnický štít (1 m) with decadal increase of 8 cm day^{-1} (same as Chopok). These results fit the estimated critical level, above which the snow trends become positive, which lies in 1800 m a.s.l. on northern and in 2300 m a.s.l. on southern slopes (Vojtek et al. 2003). Coefficient of variation reflecting on the interseasonal variability ranged from 30% at Lomnický štít to 73% at Telgárt. Also Poprad and Liptovský Hrádok showed high data variability.

Table 3. Statistical summary and mean estimated decadal differences for summed snow depths (SSD) for the full 12 months and mean snow depths (MSD) based on data for the 1981/82–2019/20 period (in cm). Stations are ordered from highest to lowest elevation. CV is the coefficient of variation

	LOM (2635)	CHOP (2005)	SKP (1778)	STR (1322)	TAJ (1013)	TEL (901)	POP (693)	LHR (640)
SUMMED SNOW DEPTH (SSD)								
Mean [cm]	29927	17210	5224	7769	5106	2237	757	957
SD	9168	6047	2341	3377	2547	1801	623	715
Minimum	14018	3233	1156	2218	751	296	124	88
Maximum	50942	32471	10146	16363	10364	7606	3028	2901
Trend	243	117	-5	-54	-37	-3	-1.53	-17
Difference [cm]	2432	1171	-47	-544	-369	-29	-15	-175
Pearson	0.302	0.221	0.022	0.184	0.165	0.020	0.028	0.279
CV [%]	30.64	35.14	44.82	43.50	49.89	80.54	82.24	74.73
MEAN SNOW DEPTH (MSD)								
Mean [cm]	99.81	71.25	25.77	42.99	32.27	15.70	7.02	9.92
SD	29.77	26.20	11.39	17.31	14.39	11.46	4.46	6.03
Minimum	45.66	12.06	5.78	14	8.16	2.9	1.75	1.87
Maximum	159.65	134.73	48.78	84.78	63.49	48.14	22.10	31.53
Trend	0.809	0.808	0.042	-0.173	-0.041	0.016	-0.002	-0.162
Difference [cm]	8	8	0.4	-1.7	-0.4	0.2	0	-2
Pearson	0.310	0.352	0.042	0.114	0.033	0.014	0.006	0.306
CV [%]	29.83	36.77	44.21	40.25	44.60	73.00	63.59	60.73

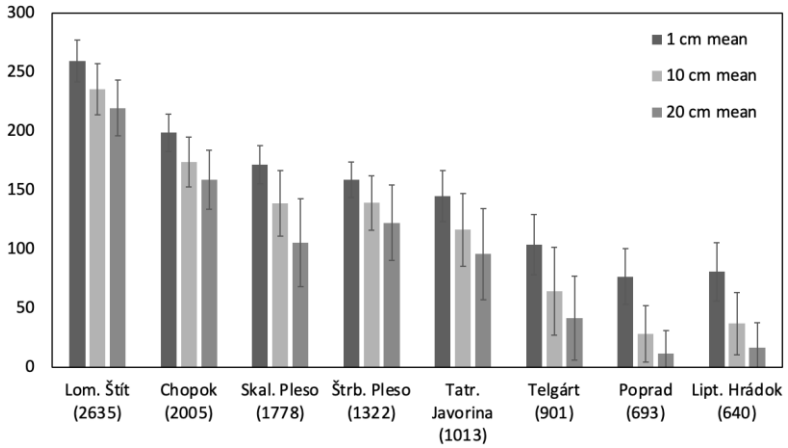

Fig. 2. Mean number of days with characteristic snow cover for studied stations ordered from highest elevation. (The error bars indicate the standard deviation).

To establish the differences amongst the stations, mean number of days with characteristic snow cover (1 cm, 10 cm and 20 cm) was graphically compared (Fig. 2). There were significant differences in all three categories between stations ($P \leq 0.05$). Lomnický štít had the highest number of days in all three characteristics but there was no significant difference between these, and Poprad revealed the lowest values that were very similar to Liptovský Hrádok. Skalnaté Pleso, despite being situated 456 m higher, had slightly lower number of days with 20 cm snow depth than Štrbské Pleso, which could be caused by orography. Also, station in Poprad is situated slightly higher than Liptovský Hrádok, by 53 m, yet had 9 days less with snow cover ≥10 cm. This could be caused by the orographic barrier effects as the Popradská basin is generally drier than Liptovská basin situated to the west. According to Chomitz and Šamaj (1974), based on data from 1901–1960, there was 107 mm year^{-1} less annual rainfall in Poprad than in Liptovský Hrádok. Based on data from Table 1 looking at the study period, this difference was similar, 98 mm year^{-1}.

Additionally, the correlation of elevation with the number of given snow cover characteristic in number of days was evaluated (Fig. 3.). The fitted logarithmic trendlines illustrate an increasing duration of snow cover for each snow depth category ($R^2 \approx 0.9$). All curves have similar shape and direction with the 20 cm data being the lowest. Additionally, some computed data were plotted using equations developed by Briedoň et al. (1974). According to their work, elevation gradient can be established using three equations: (1) $D=43+0.094*E$ for lower situated stations below 1500 m a.s.l.; (2) $D=68+0.077*E$ for stations above 1500 m a.s.l.; (3) $D=177+0.0225*E$, and for peak stations above 2000 m a.s.l., where D is the number of days and E is the elevation. The computed data showed a slight overestimation (e.g. 16 days on average for 1 cm data) based on the data collected at the SHMI stations, but both linear and logarithmic trends had strong fit ($R = 0.99$ and 0.95). However, it must be noted, that these equations were established from field data collected in the 1930 to 1960 period. The mean number DSC/1 cm calculated by Briedoň et al. (1974) came to 163.5 days (± 48.8), while the mean number of days with 1 cm based on the 1981–2020 data was 149.4 (± 58.3), which is a roughly 14 days drop. This result can assume that the equations are valid also today if the effect of shorter snow seasons is taken into the consideration.

The main issue of the temporary trends presented earlier is the small statistical significance presented by the values of Pearson's correlation coefficient up to 0.44 (Tables 2 and 3). Some interesting trends came for the SSD and MSD, for the highest Chopok and Lomnický štít stations, where there was an increase in the amount of snow cover. Other stations showed a drop or occasionally no difference. The visualization of trends (Fig. 4) suggests that there are more negative values at stations below 1100 and positive (increase) especially for SSD and MSD at the stations above 2000 m. Numerous studies e.g. from Swiss Alps pointed out decrease in snow cover since 1980s, especially in stations below 1300 m a.s.l. (Laternser and Schneebeli, 2003) which was attributed to an increase in local temperature. Same conclusions were mentioned also in the study from Slovak Tatra Mountains by Lapin et al. (2007) who reported on the snow cover trends that was attributed to

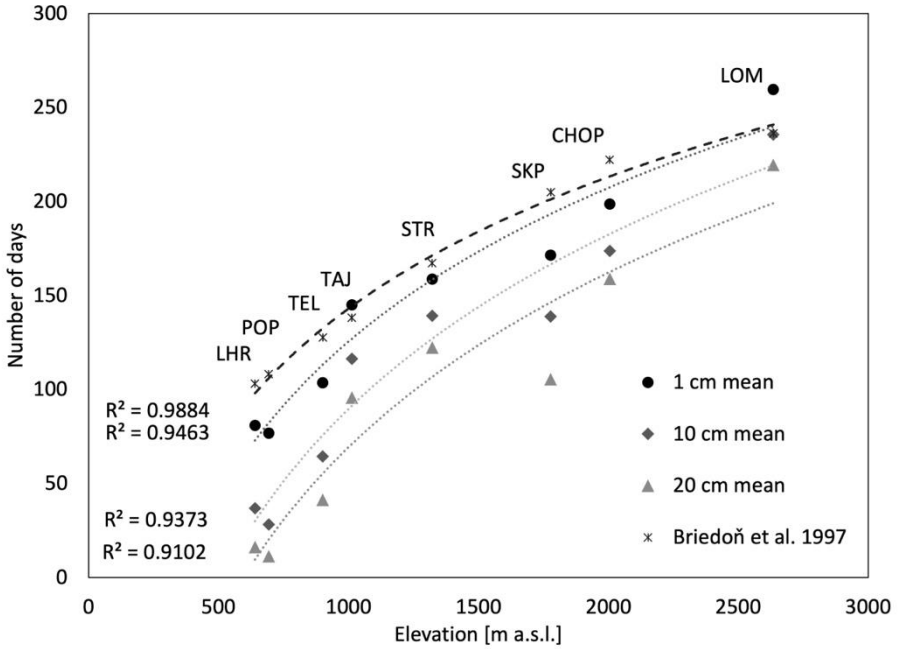

Fig. 3. Mean number of days (y axis) with characteristic snow cover related to elevation in m a.s.l. (x axis). The trendlines are logarithmic trends. The star markers are computed data based on elevation gradient equations by Briedoň et al. (1974) used to estimate the number of days with 1 cm snow cover or more.

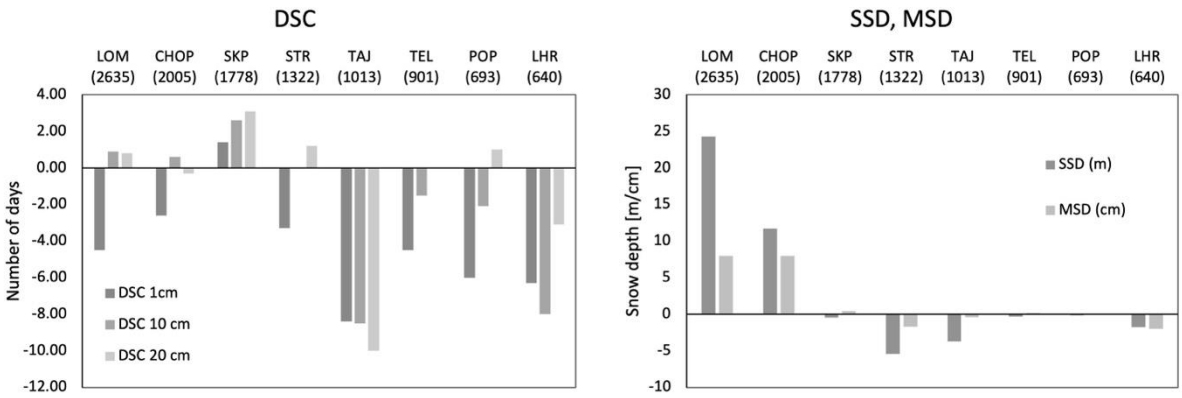

Fig. 4. Graphical interpretation of linear trends for days with snow cover (DSC) for 1 cm, 10 cm and 20 cm characteristic height as number of days expected to rise (positive values) or drop (negative values) per decade (on the left) and expected decadal differences for summed snow depths (SSD) in m and mean snow depths (MSD) in cm.

the air temperature and precipitation variability, but also to the change in atmospheric circulation patterns. For the period 1920–2006 they reported on a significant decrease of snow cover in Slovakia, but pointed out that northern and mountainous regions are exceptions and are more likely to have rising snow trends. Similar conclusions were made by a study Faško et al. (2023), who analysed trends since 1921 and the most significant decrease appeared in the 21st century. Furthermore, a study by Onderka and Pecho (2022) showed that due to ongoing climate change, there was higher occurrence of snow during Christmas for the 1951–1980 period compared to the 1981–2020.

In addition to the elevation, other factors such as slope orientation or relief were mentioned as an important phenomena that has an impact on snow trends (Lapin at al. 2007), however, more stations would be needed to compare the topographic attributes. Our stations were situated on the south-facing slopes, on peaks or in basins, only one station was at north-facing slope. In our study, we have observed the lee effect by lower snow cover at Poprad station. However, it must be stressed, that the complex conditions in the Tatra Mountains make it more difficult to understand the changes that occurred during the studied period. There was higher incidence in increase of snow cover in the stations above 1100 m a.s.l. and the trends in lower lying stations were generally decreasing. Also, there was less interannual data variability in higher situated stations which suggests that climate change related events are more likely to influence the foothill and basin areas rather than the peaks. Another approach with larger number of stations and longer study period could be useful in finding more statistically sound correlations.

Conclusion

Snow cover is one of the most important indicators of climate change, but it also has important functions in creating runoff, water supply, for vegetation dynamics, albedo etc. Numerous studies pointed out the decline in the snowpack and in the duration of the periods with characteristic heights of snow cover worldwide caused by global warming. However, the trends behave differently with increasing elevations and there could be point, where the snow cover could be increasing. It is therefore critical to observe the spatial and temporal trends of the snow cover both at lower and higher elevations.

In Slovakia, SHMI and their predecessors collected data on daily snow heights from Tatra Mountains since 1921. Westerns Carpathians, and their highest ridges, the Tatra Mountains, were chosen for this study to compare five selected snow cover parameters for period of 39 years (1981–2020). Not just winter seasons were considered, but because at some stations snow cover occurs also during warmest months, we divided the seasons from 1 July to 30 June the following year. Eight stations were selected, four with elevation above and four below the 1100 m a.s.l. There was clear relationship between the snow cover and elevation that was in accordance with the gradient equations proposed by Briedoň et al. (1974), but the temporary trends for the study period had weak correlations (maximum Pearson's coefficient was 0.44) so it is questionable whether and how these can be interpreted. However, the graphical visualization of the proposed change per decade suggested that the amount of snow and the number of days with snow cover was generally increasing for the stations above 1100 m a.s.l. and there was a decline expected for the stations situated at lower elevations.

These results are in accordance with the number of international but also national studies analyzing the effect of global warming on snow cover. But the complexity of mountainous terrain, the changes in circulation patterns, wind conditions, slope orientation etc. can have an important effect on the trends. Therefore, more stations or longer periods of data could be useful in establishing reliable trends and patterns in relation to other important factors. Based on our findings, we can conclude that our study was in the agreement with similar ones in the field, but we cannot confidentially suggest

the trends in the snow cover parameters that are likely to be happening in the future solely due to global warming.

Acknowledgement

We would like to thank the Slovak Hydrometeorological Institute for the kind provision of all data used in this study. We are also grateful to dr. Jerzy Zasadni from AGH University of Science and Technology in Krakow for his useful commentary on our manuscript and to dr. Adam Dudáš from the Matej Bel University for technical data support.

References

Beniston, M., Rebetez, M., Giorgi, F., Marinucci, M. R. (1994): An analysis of regional climate change in Switzerland. Theoretical and Applied Climatology, vol. 49, 135–159.

Briedoň V., Chomicz K., Konček, M. (1974): Snehové pomery. In Konček et al. 1974: Klíma Tatier, Veda, Bratislava, 865 s.

Brown, R. D. (2000): Northern Hemisphere snow cover variability and change, 1915–97. Journal of climate, vol. 13, no. 13, 2339–2355.

Brziak, A., Kubáň, M., Kohnová, S., Szolgay, J. (2021): Comparison of the variability of snow cover parameters of the HBV model using lumped and distributed precipitation inputs and multi-basin calibration. Acta Hydrologica Slovaca, vol. 22, no. 1, 2021, 40–49.

Bulygina, O.N., Razuvaev, V.N.–Korshunova, N.N. (2009): Changes in snow cover over Northern Eurasia in the last few decades. Environmental Research Letters, vol. 4, no. 4, 6 p., ISSN 1748-9326.

Chomicz K., Kňazovický L. (1974): Avalanches. In: Konček M. et al.: Klíma Tatier, VEDA, Bratislava, 581–600.

Chomitz, K., Šamaj, F. (1974): Zrážkové pomery (Precipitation characteristics). Klíma Tatier. Veda, Bratislava, 443–536.

Clark, M. P., Serreze, M. C., Robinson, D. A. (1999): Atmospheric controls on Eurasian snow extent. International Journal of Climatology: A Journal of the Royal Meteorological Society, vol. 19, no. 1, 27–40.

EEA (2023): Snow cover. Indicator Assessment. https://www.eea.europa.eu/publications/europes-changing-climate-hazards-1/snow-and-ice/snow-and-ice-snow

EEA (2021): Snow and ice — snow, glaciers and ice sheets. https://www.eea.europa.eu/data-and-maps/indicators/snow-cover-3/assessment

Ellenberg, H. (1988): Vegetation ecology of central Europe. Cambridge University Press, 731 p. ISBN 9780521236423.

Engel, Z., Mentlík, P., Braucher, R., Minár, J., Léanni, L., (2015): Geomorphological evidence and 10Be exposure ages for the Last Glacial Maximum and deglaciation of the Veľká and Malá Studená dolina valleys in the High Tatra Mountains, central Europe. Quaternary Science Reviews, vol. 124, 106–123. https://doi.org/10.1016/j.quascirev.2015.07.015

Faško P., Handžák Š., Lapin M. (1997): Selected snow cover characteristics change in the Low Tatras Region in 1921–1995. Slovak National Climate Program, 7/97, 46–67, MŽP SR, SHMÚ Bratislava.

Faško, P., Markovič, L., Pecho, J., Bochníček, O. (2020): Decadal changes in snow cover characteristics in Slovakia over the period 1921–2020, EGU General Assembly 2020, 4–8 May 2020, EGU2020-3405.

Faško, P., Markovič, L., Bochníček, O. (2023): Changes in snow accumulation and snow depth in Slovakia in the 1921 – 2021 period, EGU General Assembly 2023, Vienna, Austria, 24–28 April 2023, EGU23-5554.

Falarz, M. (2002): Long-term variability in reconstructed and observed snow cover over the last 100 winter seasons in Cracow and Zakopane (southern Poland). Climate Research, vol. 19, no. 3, 247-256.

Falarz, M. (2004): Variability and trends in the duration and depth of snow cover in Poland in the 20th century. International Journal of Climatology: A Journal of the Royal Meteorological Society, vol. 24, no. 13, 1713–1727.

Fiema, A., (2008): Changes of snow coverage in selected synoptical situations in the period 1966/67–1995/96. Meteorologický časopis, vol. 11, no. 1–2, 31–37, ISSN 1335-339X.

Foster, J., Owe, M., Rango, A. (1983): Snow cover and temperature relationships in North America and Eurasia. Journal of Applied Meteorology and Climatology, vol. 22, no. 3, 460–469.

Holko L. (2000): Vyhodnotenie dlhodobých meraní parametrov snehovej pokrývky v horskom povodí (Evaluation of variability of the long-term snow characteristics of a mountain catchment), Acta Hydrologica Slovaca vol. 1, no. 1, 15–22. (in Slovak)

Holko, L., Kostka, Z., Parajka, J. (2001): Snehová pokrývka, Životné prostredie, vol. 35, 138–141. (in Slovak)

Holko, L., Kostka, Z., Pecušová, Z. (2005): Snow. In: Pekárová, P. and Szolgay, J. (eds.); Scenarios of changes of selected components of hydrosphere and biosphere in catchment basin of Hron River and Vah River as consequence of climatic change, 496 p; ISBN 80-224-0884-0; Worldcat; 105–167.

Holko, L., Škvarenina, J., Kostka, Z., Frič, M., Staroň, J. (2009): Impact of spruce forest on rainfall interception and seasonal snow cover evolution in the Western Tatra Mountains, Slovakia. Biologia, vol. 64, no. 3, 594–599.

Holko, L., Gorbachová, L., Kostka, Z. (2011): Snow hydrology in central Europe. Geography Compass, vol. 5, no. 4, 200–218.

Holko, L., Danko, M., Hlavčo, J., Kostka, Z. (2016): Dlhodobé údaje o priebehu vybraných klimatických a hydrologických prvkov v povodí Jaloveckého potoka (Západné Tatry, Liptovská kotlina). Životné prostredie, vol. 50, no. 2, 81 – 86. (in Slovak)

Holko, L., Danko, M., Sleziak, P. (2021): Snowmelt characteristics in a pristine mountain catchment of the Jalovecký Creek, Slovakia, over the last three decades. Hydrological Processes, vol. 35, no. 4, e14128.

Holko, L., Danko, M., Jančo, M., Sleziak, P. (2022): Empirical models to calculate the snow water equivalent in the high mountain catchments of the Western Carpathians. Acta Hydrologica Slovaca, vol. 23, no. 2, 241–248. DOI: https://doi.org/10.31577/ahs-2022-0023.02.0027

Hríbik M., Škvarenina J. (2006): Influence of altitude, exposition, forest stand and type of forest stand on hydrophysical characteristics of snow cover in Biosphere reserve Poľana, in winter times 2003/2004 a 2004/2005), 11th annual snow hydrology meeting, Czech Hydrometeorological Institute, 30–40.

Jaagus, J. (1997): The impact of climate change on the snow cover pattern in Estonia. Climatic Change, vol. 36, no. 1–2, 65–77.

Konček, M., Briedoň, V. (1964): Sneh a snehová pokrývka na Slovensku. Bratislava: Vydavateľstvo SAV. 76 p. (in Slovak)

Lapin, M., Faško, P. (1996): Snow cover and precipitation changes in Slovakia in the 1921–1995 period. In: Proceedings on the 24th International Conference on

Alpine Meteorology, Bled (Slovenia), 9–13 September 1996, 259–266.

Lapin, M., Faško, P., Pecho, J. (2007): Snow cover variability and trends in the Tatra Mountains in 1921–2006. 29th International Conference on Alpine Meteorology. Extended Abstracts. Oral Sessions, vol. 1.

Laternser, M., Schneebeli, M. (2003): Long-term snow climate trends of the Swiss Alps (1931–99). International Journal of Climatology: A Journal of the Royal Meteorological Society, vol. 23, no. 7, 733–750.

Makos, M., Rinterknecht, V., Braucher, R., Tołoczko-Pasek, A., Arnold, M., Aumaître, G., Bourlès, D., Keddadouche, K. (2018): Last Glacial Maximum and Lateglacial in the Polish High Tatra Mountains - Revised deglaciation chronology based on the 10Be exposure age dating. Quaternary Science Reviews, vol. 187, 130–156. https://doi.org/10.1016/j.quascirev.2018.03.006

Onderka, M., Pecho, J. (2022): Fingerprinting the North-Atlantic and Arctic oscillation signals in rainfall and fresh snowpack in the Western Carpathian Mountains. Research Square, https://doi.org/10.21203/rs.3.rs-1587740/v1

Pánek, T., Mentlík, P., Engel, Z., Braucher, R., Zondervan, A., Aster Team. (2017): Late Quaternary sackungen in the highest mountains of the Carpathians. Quaternary Science Reviews, vol. 159, 47–62.

Petrovič, P. (1972): Výpočet výparu zo snehovej pokrývky v povodí Nitry. In: Vodohospodársky časopis, vol. 20, no. 1, 1972, 1–15.

Pribullová, A., Pecho, J., Bičárová, S. (2009): Analysis of snow cover at selected meteorological stations in the High Tatra Mountains. In: Sustainable Development and Bioclimate. Reviewed Conference Proceedings. Stará Lesná, 56–57.

Siman, C., Polčák, N. (2017): Vplyv kontinentality podnebia na vybrané charakteristiky snehovej pokrývky na Slovensku v období rokov 1981/1982–2010/11. Meteorologický časopis. vol. 20, no. 1, 11–18. ISSN 1335-339X. (in Slovak)

Siman, C., Slavková, J. (2019): Vývoj snehovej pokrývky na Slovensku v období rokov 1981/1982–2017/2018 (Development of snow cover in Slovakia in the period 1981/1982 – 2017/ 2018). Bratislava: SHMÚ. (in Slovak)

Šamaj, F., Valovič, Š. (1988): Snehové pomery na Slovensku. In: Zborník prác SHMÚ, zv. 14/III, Bratislava, Alfa, 128 p. (in Slovak)

Vojtek, M., Faško, P., Šťastný, P. (2003): Some selected snow climate trends in Slovakia with respect to altitude. Acta Meteorologica Universitatis Comenianae, vol. 32, no. 1, 17–27.

Vojtek, M. (2010): Climate trends of snow cover in mountainous regions of Slovakia. Meteorologický časopis, vol. 13, no. 2 – 3, 57 – 61. ISSN 1335-339X.

Zasadni J., Kłapyta P., Broś E., Ivy-Ochs S., Świąder A., Christl M., Balážovičová L. (2020): Latest Pleistocene glacier advances and post-Younger Dryas rock glacier stabilization in the Mt. Kriváň group, High Tatra Mountains, Slovakia. Geomorphology, vol. 358, 107093. doi: 10.1016/j.geomorph.2020.107093

Mgr. Lenka Balážovičová, PhD. (*corresponding author, e-mail: lenka.balazovicova@umb.sk)
Department of Geography and Geology
Faculty of Natural Science
Matej Bel University
Tajovského 40
97401 Banská Bystrica
Slovak Republic

Mgr. Cyril Siman, PhD.
Mgr. Katarína Mikulová, PhD.
Slovak Hydrometeorological Institute
Jeséniova 17
83315 Bratislava
Slovak Republic

DOI: 10.31577/ahs-2023-0024.02.0032

ACTA HYDROLOGICA SLOVACA

Volume 24, No. 2, 2023, 294 – 302

An assessment of historical short-time precipitation deficiency in eastern Slovakia and northern Serbia according to the SPI-3

Tatiana SOĽÁKOVÁ, Martina ZELEŇÁKOVÁ*, Hany ABD-ELHAMID, Milan GOCIC, Helena HLAVATÁ, Peter BUJANSKÝ, Miroslav GARAJ

Short-term precipitation deficiency is one of the primary causes of agricultural drought, which can have far-reaching consequences on various aspects such as society, environment, and the economy. This complex natural phenomenon attracts more attention due to changes in precipitation pattern. The use of the SPI-3 index for the quantitative measure of precipitation anomalies over a three-month period across the eastern part of Slovakia and the northern part of Serbia is a valuable approach in understanding and managing drought conditions in these countries with different climate conditions. The SPI-3 can be highly beneficial for the farmers, policymakers, and water resource managers when it comes to making informed decisions about irrigation, crop selection and water allocation during drought events. In northern Serbia and eastern Slovakia, the extreme precipitation anomalies often occur during the autumn season. Predicting extreme rainfall anomalies, especially during the growing season, is highly justified and essential for effective natural risk management in agriculture-dependent countries. The average inter-arrival time of an extreme precipitation deficit is in the north of Serbia ranges from 3.1 to 5.1 years, while in the east of Slovakia it ranges from 3.2 to 5.9 years.

KEY WORDS: precipitation deficiency, agricultural drought, SPI, Slovakia, Serbia

Introduction

Agricultural drought is natural phenomenon that occurs when there is a prolonged deficiency in precipitation or insufficient soil moisture to support crop growth. Drought indices like SPI (Standardized Precipitation Index), SPEI (Standardized Precipitation Evapotranspiration Index) and PDSI (Palmer Drought Severity Index) are crucial tools for characterizing and quantifying agricultural drought. These indices provide valuable information for assessing the severity, duration and spatial extent of drought conditions, in addition to effective drought monitoring and management (McKee et al., 1993; Vincente-Serrano et al., 2010; Palmer, 1965). The European Drought Observatory (EDO) is a useful resource for monitoring and assessing drought conditions in Europe. It utilizes various drought indices to identify drought expansion in European regions as well as to apply adaptation strategies to mitigate future economic losses due to drought. It is essential for governments, businesses, and communities to work together to address this issue and minimize the economic consequences of drought in the EU. Nowadays, the prediction for a future next ten years is that the economic consequences will be 9.68 billion EUR (CGTN, 2023). The analysis of short-term rainfall anomalies and their effects on the environment have been studied throughout Europe by a numer of researchers (e.g. Mohammed et al. (2022) in Hungary, Vergni et al. (2021) in Italy, Popova et al. (2014) in Bulgaria, Potop et al. (2010) in Czech Republic, Pandžić et al. (2022) in Croatia Labedzki (2007) or Kubiak-Wójcicka et al. (2023) in Poland, Kobulniczky et al. (2023) in Romania and Slovenia Payab and Türker (2019) in Cyprus, Tiqkas et al. (2019) in Greece, Kubiak-Wójcicka et al. (2021) in Slovakia.

Also, some researchers have studied soil moisture deficiency in Slovakia. Vido et al. (2019) examined precipitation and evapotranspiration anomalies using SPEI in Arborétem Mlyňany. Kišš et al. (2021) observed the occurrence of physical drought in Nitra River basin. Takáč et al. (2015) investigated agricultural drought events in Danube lowland using Daisy model. Zuzulova and Vido (2018) tested the correlation relationship between normalized difference vegetation index NDVI and Palmer drought severity index PDSI during the time period of 2000–2014 in twelve cities. Portela et al. (2015) calculated three-month standardized precipitation index in whole Slovak country during the reference period 1981–2013. For instance, the following authors addressed the issue of meteorological drought in Slovakia: Škvareninová et al. (2018), Soľáková et al. (2022), Almikaeel et al. (2023).

Mimić et al. (2022) and Strievic et al. (2011) studied soil moisture deficiency and its consequence on agriculture

yields and proposed new methodology for early warning system in northern Serbia. Mimić et al. (2022) studied a level of moisture stress in maize and sunflower yields during the summer in Vojvodina province. Mimić et al. (2022) stated that maize was the most sensitive to drought. Strievic et al. (2011) presented their authentic methodology, which they tested at 9 meteorological stations located at northern Serbia. Northern Serbia is an area with high agricultural production thanks also the USAID project, which supported unemployed people to set up greenhouses for growing crops especially higher-value crops such as peppers, lettuce, tomatoes and cucumbers (USAID, 2023).

The main aim of this study is to compare the short-term deficiency of precipitation using SPI-3 index and predict future drought in different study areas in Slovakia and Serbia.

Material and methods

Eastern Slovakia and northern Serbia (see Fig. 1) have a temperate continental climate with cold winters and hot and humid summers. East Slovakia lowland is the most important region for agriculture in Slovakia and also northern Serbia is an area with high agriculture production too. Eastern Slovakia is represented by five synoptic stations located in Bardejov, Humenné, Ždiar, Medzev a Spišské Vlachy. Mentioned stations lie on the territory of sub-basins: Dunajec and Poprad, Bodrog, Bodva, Hornad with land area 14494 km^2, of which 47.13% is agricultural land. Northern Serbia is represented by five synoptic stations located in Kikinda, Zrenjanin, Sombor, Palić and Novi Sad. These stations belong to the Tisza sub-basin, covering 10057 km^2 in Serbia, with agricultural land making up 86.47% of the total area. Values of monthly precipitation are provided by Hydrometeorological Institute of Serbia and Slovak Hydrometeorological Institute of Košice for the time period (1972–2019). All selected rain gauge stations had complete data on total rainfall for the analyzed time interval.

The agricultural area occupies a smaller area in the territory of eastern Slovakia than in the territory of northern Serbia. In the territory of eastern Slovakia mainly; wheat, barley and maize are grown while in the territory of northern Serbia, mainly; peppers, lettuce, tomatoes and cucumbers are grown (MINZP, 2023; Interreg 2023).

Extreme short-term precipitation deficit in vegetation period is one of the primary causes of agricultural drought, which can lead to deficiency of soil water content and can result in social, environmental and especially economic problems. For the analysis of extreme short-term precipitation deficit we calculated three-month standardized precipitation index (SPI-3).

Computation of the SPI-3 involves fitting a gamma probability density function to obtain cumulative distribution function of three months precipitation totals

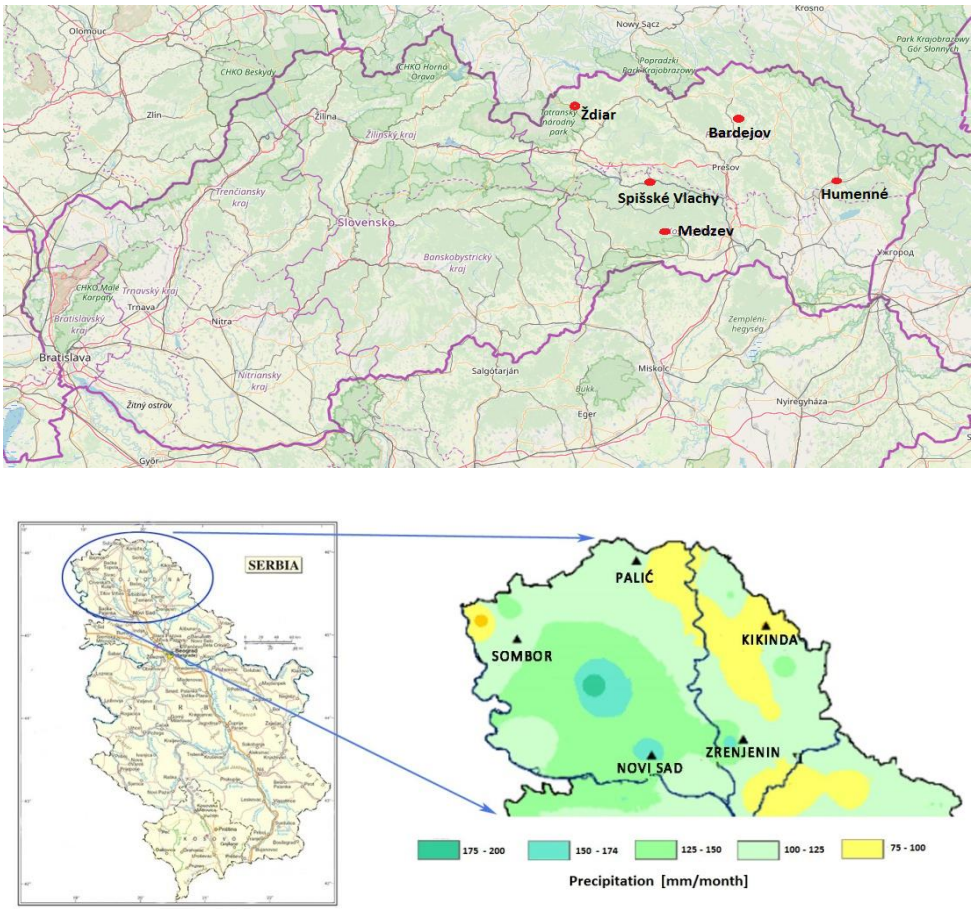

Fig. 1. Studied areas in Slovakia and northern Serbia.

for a given month for a selected rain gauge station. The cumulative distribution function of gamma function is then transformed to the standard normal random variable, which represents the value of the SPI. These mathematical operations were performed in the DrinC program. Then, based on SPI values, we can classify periods into several categories: extremely wet (SPI>2), very wet (SPI between 1.5 and 1.99), moderately wet (SPI between 1.0 and 1.49), near normal (SPI between -0.99 and 0.99), moderately dry (SPI between -1 and -1.49), very dry (SPI between -1.5 and -1.99), extremely dry (SPI<-2) (McKee et al., 1993). In this study we examined the main characteristics of short-time drought conditions such as duration, severity and intensity in eastern Slovakia and northern Serbia. We identified extreme short-time precipitation deficiency during the period (1972–2019).

Results and discussion

For the five stations in the eastern part of Slovakia, the analysis of short-term precipitation deficits for the time period (1972–2019) is shown in the Table 1 and Fig. 2. An assessment of short-term precipitation anomalies for the five stations in the northern part of Serbia is presented in Table 2 and Fig. 3. An extreme short-term precipitation deficit was identified by 3-month SPI, which can be expected in an average of 3.2 to 5.9 years. In Fig. 2 and Fig. 3 is a extreme short-term precipitation deficiency marked by red colour.

Table 1. Characterization of episodes with extreme short-term deficiency of precipitation by SPI-3 in eastern Slovakia

Station	Number of events	Duration	Cumulative severity	Cumulative intensity	Average Inter-arrival time [years]	Years of extreme drought
Bardejov	12	17	-42.4	-29.3	3.7	1973, 1975, 1977 1978, 1983, 1985 1987, 1995, 2007 2012, 2014
Humenné	11	13	-29.9	-25.6	4.3	1974, 1977, 1987 2003, 2004, 2012 2014, 2016, 2017
Ždiar	11	15	-32.9	-24.1	4.2	1983, 1987, 1992 1995, 2001, 2006 2015
Medzev	10	13	-28.6	-21.9	3.2	1987, 1989, 1993 1999, 2001, 2003 2007, 2012, 2016
Spišské Vlachy	8	9	-20.5	-16.3	5.9	1974, 1977, 1983 1984, 1987, 1994

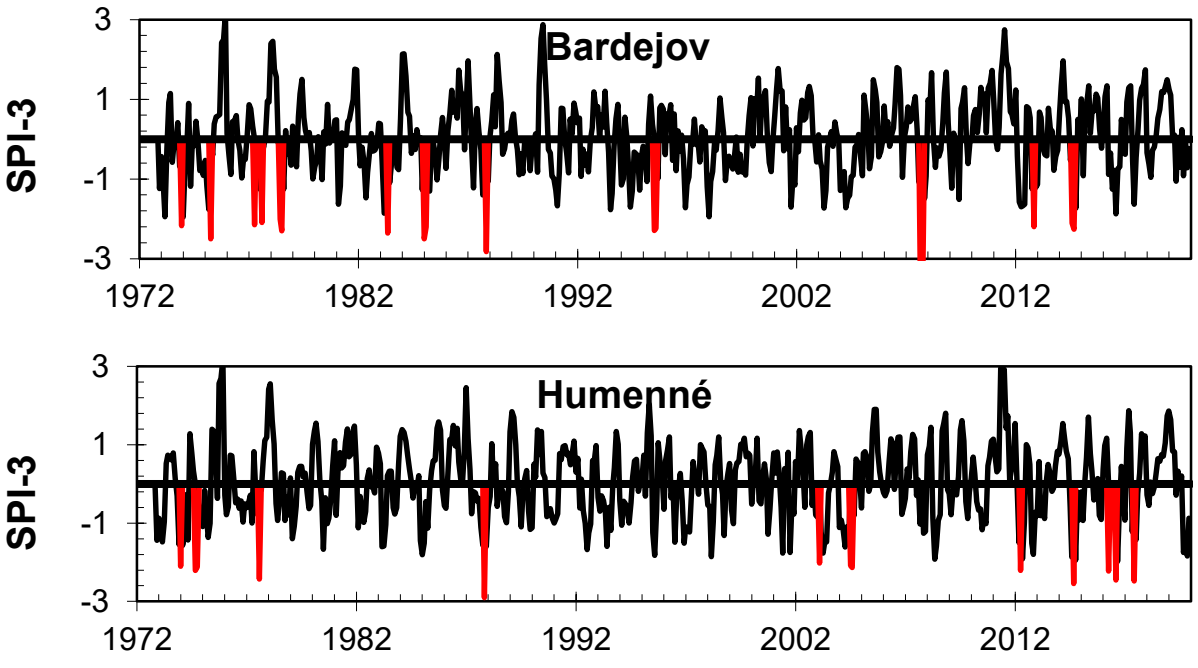

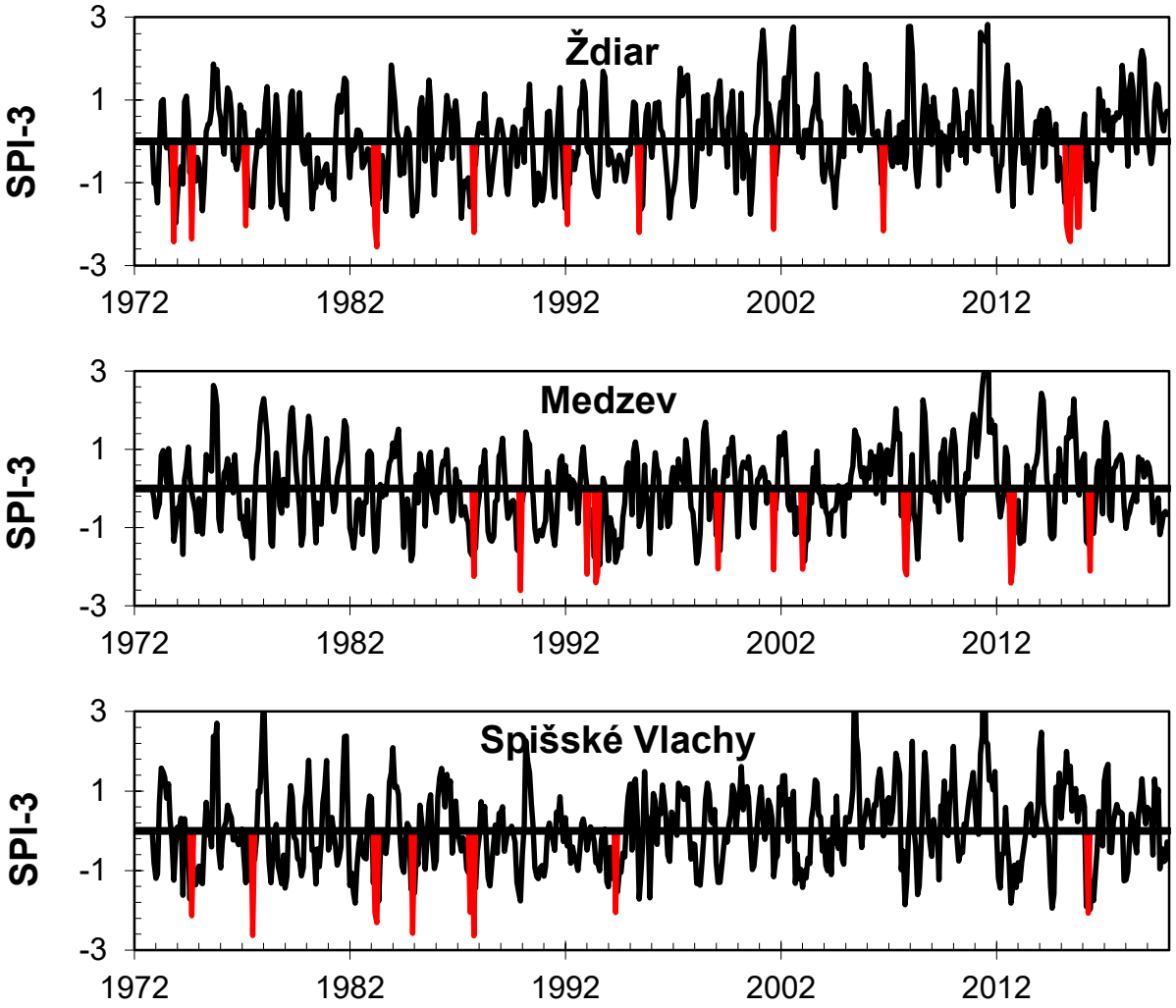

Fig. 2. SPI-3 of five selected stations in eastern Slovakia.

Table 2. Characterization of episodes with extreme short-time deficiency of precipitation by SPI-3 in northern Serbia

Station	Number of events	Duration	Cumulative severity	Cumulative intensity	Average Inter-arrival time [years]	Years of extreme drought
Kikinda	9	19	-45.9	-21.6	5.1	1977, 1987, 1994 2001, 2002, 2005, 2017
Novi Sad	9	14	-32.7	-20.5	3.9	1973, 1976, 1978, 1988, 1990, 1993, 2001, 2004
Palić	13	20	-47.1	-30.0	3.1	1976, 1983, 1986, 1988, 1989, 1990 1993, 1994, 2001, 2004, 2013
Sombor	10	17	-40.8	-24.0	4.2	1976, 1978, 1983, 1988, 1990, 1993, 2001, 2004, 2013
Zrenjanin	12	17	-38.2	-26.9	4.1	1974, 1977, 1979 1987, 1988, 1991, 1994, 2002, 2004 2005, 2019

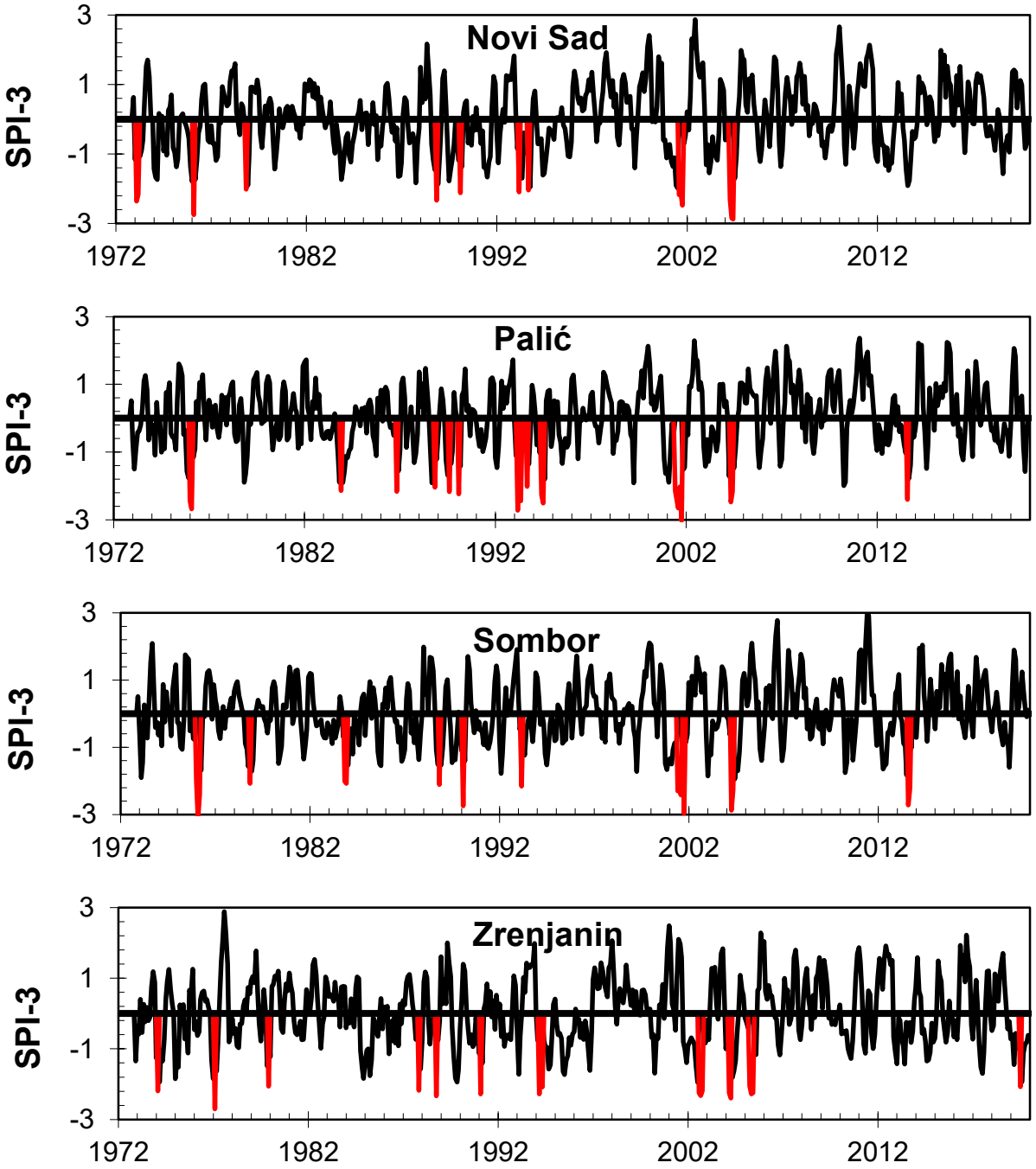

Fig. 3. SPI-3 of five selected stations in northern Serbia.

In total, events with severe insufficient short-term precipitation totals for a five synoptic stations in eastern Slovakia during the years 1972–2019 are 52 with a total duration of 67 months, cumulative severity of -154.3. The most vulnerable year of extreme drought was 1987 in this country, because extreme meteorological drought was recorded in several observed stations based on intensity, severity and duration. Extreme short-term precipitation deficits in eastern Slovakia were recorded especially in the autumn. The longest three-month extreme precipitation deficit was recorded in Ždiar station.

In total, events with extreme insufficient short-term precipitation totals for a five synoptic stations in northern Serbia during the years 1972–2019 are 53 with a total duration of 87 months, cumulative severity of -204.7. The most prone year of extreme droughts in northern Serbia was 1988 in many observed stations based on intensity, severity and duration of drought. Extreme short-term precipitation deficits were identified especially in the autumn. The longest five-month extreme precipitation deficit occurred in stations Kikinda and Palić.

In both observed countries, extreme precipitation deficits most often occur in the autumn period when they do not affect agricultural activity than much. The territory of northern Serbia is more sensitive to the occurrence of extreme precipitation deficits.

Based on the Fig. 4 the duration of these events over 47-year time period ranges from 9 to 20 months, while these events lasted the longest at the Palić station. This station has the greatest cumulative severity and intensity (see the Fig. 5 and Fig. 6). In Medzev and Palić stations, we and expect more frequent occurrence of extreme short-term precipitation deficits.

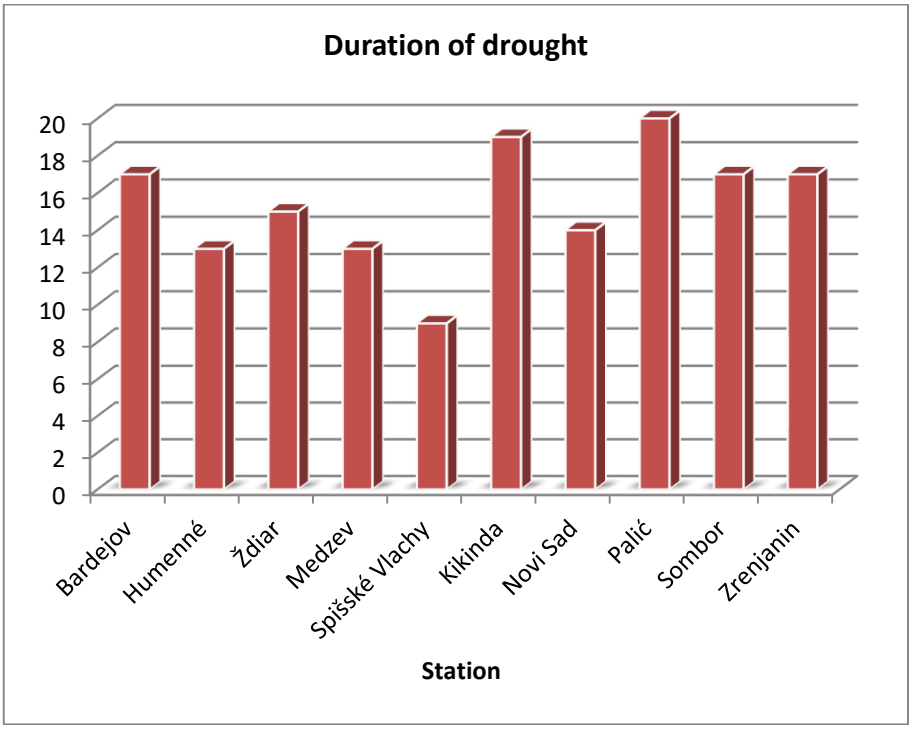

Fig. 4. Duration of extreme precipitation deficiency in eastern Slovakia and in northern Serbia.

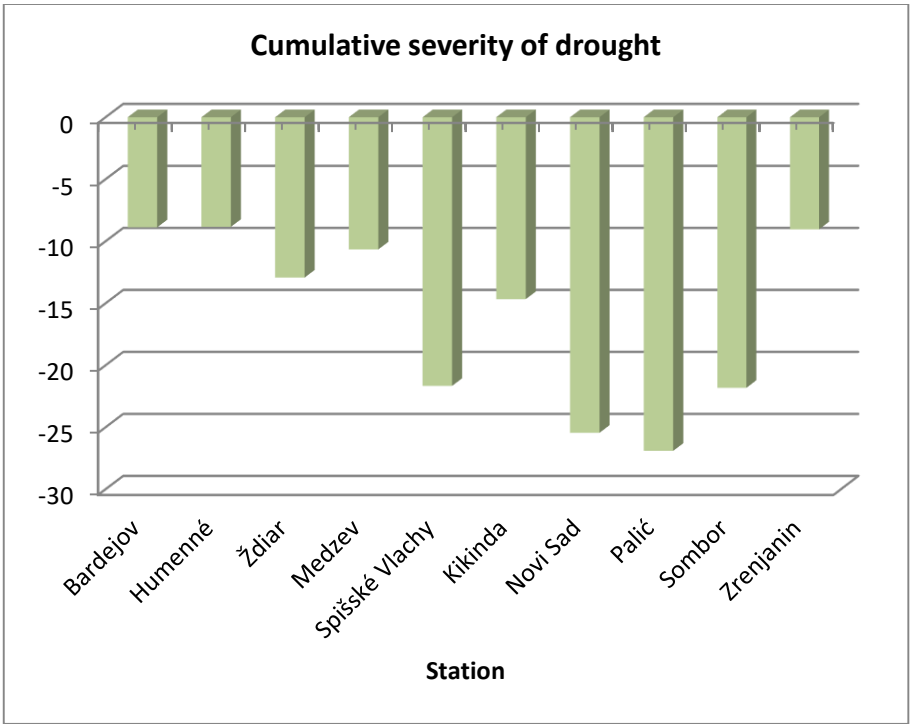

Fig. 5. Cumulative severity of extreme precipitation deficiency in eastern Slovakia and in northern Serbia.

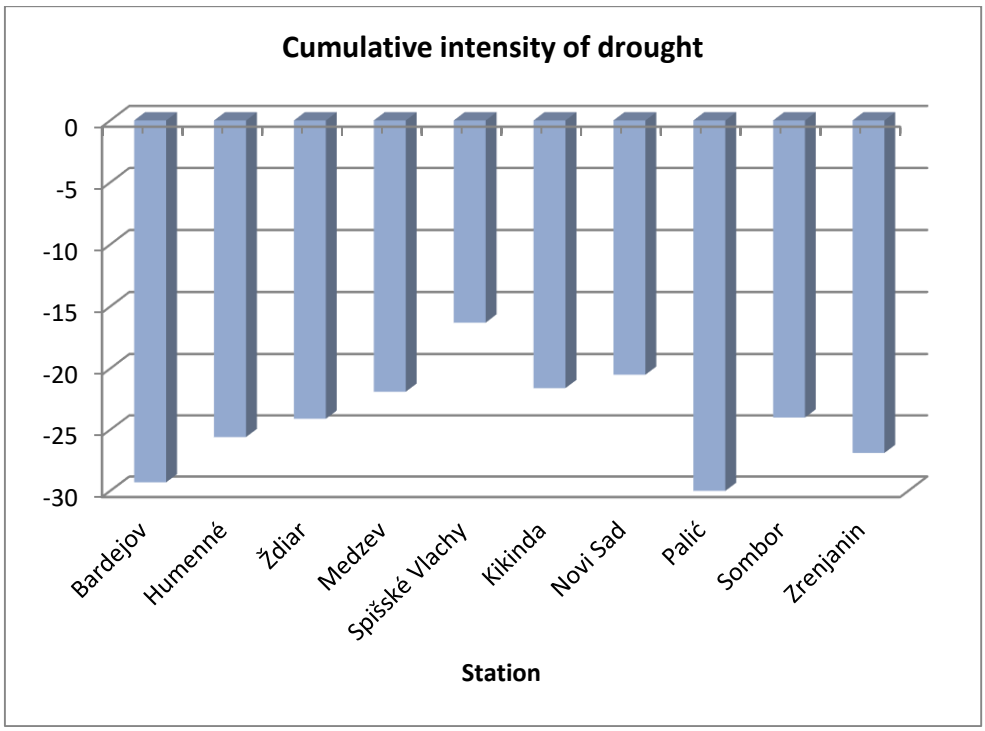

Fig. 6. Cumulative intensity of extreme precipitation deficiency in eastern Slovakia and in northern Serbia.

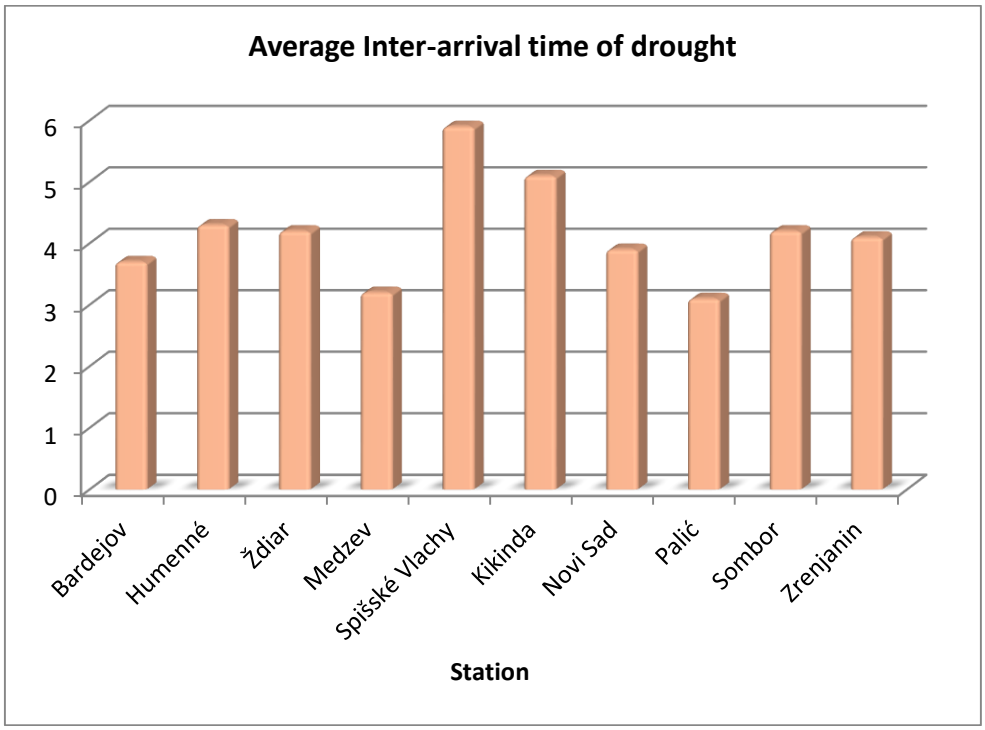

Fig. 7. Average inter-arrival time of extreme short-time precipitation deficiency in eastern Slovakia and in northern Serbia.

Conclusion

Extreme short-term precipitation deficiency mainly in vegetation season can have significant implications for food production and water resources in northern Serbia and in eastern Slovakia. The sixth report of Intergovernmental Panel on Climate Change pointed out that soil moisture will be decrease more than 25% in

analyzed countries (Mimić et al., 2022). Due to their high agricultural production, the countries of the study area are becoming more and more sensitive to persistent precipitation deficits, rising temperatures and increasing evapotranspiration and therefore monitoring, predicting and implementing irrigation systems helps to avoid economical losses in agriculture. By calculating SPI-3 in the studied area, we estimate the occurrence of extreme precipitation deficits on average every 3 to 5 years from the beginning of the last such event.

Acknowledgement

This work was supported by project SK-SRB-2120052 Inovative approaches to the assessment and management of drought risk due to climate change – Inovatívne prístupy k hodnoteniu a riadeniu rizika sucha v dôsledku zmeny klímy.

References

Almikaeel W., Almeida L. C., Čubanová L., Šoltész A., Mydla J., Barolová D (2023): Understanding the impact of drought on Topľa River discharge seasonality Acta Hydrologica Slovaca, vol. 24, issue 1, 63–72.

CGTN, https://newseu.cgtn.com/news/2022-08-14/Europe-s-drought-in-charts-who-s-losing-the-most-money--1coj3XEa9Bm/index.html, last accessed 2023/05/15

Interreg (2023): https://www.interregdanube.eu/uploads/media/approved_project_output/0001/37/ed1b7198ffc57c6d2d528717650cd6d94280004e.pdf, last accessed 2023/05/05

Kišš, V., Tárník, A. and Čimo, J. (2021): Climate Change Impact on Meteorological Drought and Soil Water Storage in the Nitra River Basin for the Period 2015–2019. Sciendo issue 24, 117–123.

Kobulniczky, B., Holobâcă, I.–H., Črepnišek, Z., Pogočar, T., Jiman, A.–M., and Žindaršič, Z. (2013): Comparison of Standardized Precipitation Index (SPI) and Standardized Precipitation Evapotranspiration Index (SPEI) applicability for drought assessment during the maize growing period between Bărăgan (Romania) and Prekmurje (Slovenia) regions. EGU General Assembly 2023, Vienna, Austria, 24–28 Apr 2023, EGU23-499

Kubiak-Wójcicka, K., Nagy, P., Zeleňáková, M., Hlavatá, H., Abd-Elhamid, H. F. (2021): Identification of Extreme Weather Events Using Meteorological and Hydrological Indicators in the Laborec River Catchment, Slovakia. Water 2021, vol. 13, issue. 10, 1413 p.

Kubiak-Wójcicka, K., Owczarek, M., Chlost, I., Olszewska, A., Nagy P. (2023): Assessment of Meteorological Drought Trends in a Selected Coastal Basin Area in Poland–A case Study. Water 2023, vol. 15, issue 15, 2836 p.

Labedzki, L. (2007): Estimation of local drought frequency in central Poland using the standardize precipitation index SPI. Irrigation and Drainage vol. 56, issue 1, 67–77.

McKee, T. B., Doesken, J. N., Kleist, J. (1993): The relationship of drought frequency and duration to time scales. In: Proceedings of the Eighth Comference on Applied Climatology, 179–184. Anaheim, CA, USA.

Mimić, G., Živaljević, B., Blagojević, D., Pejak, B., Brdar, S. (2022): Quantifying the Effects of Drought Using the Crop Moisture Stress as an Indicator of Maize and Sunflower Yield Reduction in Serbia. Atmosphere, vol. 13, issue 11, 1880 p.

MINZP (2023): https://minzp.sk/files/sekcia-vod/hodnotenie-rizika-2018/bodrog/phpr-bodrog.pdf, last accessed 2023/05/05

Mohammed, S., Alsafadi, K., Enaruvbe, G. O., Bashir, B., Elbeltagi, A., Széles, A., Alsalman, A., Harsanyi E. (2022): Assessing the impacts of agricultural drought (SPI/ SPEI) on maize and wheat yields across Hungary. Sci Rep issue 12, 8838 p.

Pandžić, K., Lisko, T., Pejić, I., Šarčević, H., Pecina, M., Šestak, I., Tomšić, D., Mahović, N. S. (2022): Application of the self-calibrated palmer drought severity index and standardized precipitation index for estimation of drought impact on maize grain yield in Pannonian part of Croatia. Natural Hazards issue 113, 1237–1262.

Palmer, W. C. (1965): Meteorological Drought. 1st edn. U.S. DC, USA.

Payab, A. H., Türker, U. (2019): Comparison of standardized meteorological indices for drought monitoring at northern part of Cyprus. Environmental Earth Sciences issue 78, 309 p.

Popova, Z., Ivanova, M., Martins, D., Pereira, L. S., Doneva, K., Alexandrov, V., Karcheva, M. (2014): Vlunerability of Bulgarian agriculture to drought and climate variability with focus on rainfed maize systems. Natural Hazards No. 74, 865–886.

Portela, M. M., Zeleňáková, M., Santos, J. F., Purcz, P., Silva, A. T., Hlavatá, H. (2015): A comprehensive drought analysis in Slovakia using SPI. European Water, issue 51, 15–31

Potop, V., Türkott, L., Kožnarová, V., Možný, M. (2010): Drought episodes in the Czech Republic and their potential effects in agriculture. Theoretical and Applied Climatology, issue 99, 373–388.

Soľáková, T., Zekeňáková, M., Mikita, V., Hlavatá, H., Simonová, D., Abd-Elhamid, H. (2022): Assessment of meteorological and hydrological drought using drought indices: SPI and SSI in eastern Slovakia. Acta Hydrologica Slovaca, vol. 23, issue 2, 267–272.

Stricevic, R., Djurovic, N., Djurovic, Z. (2011): Drought classification in Northern Serbia based on SPI and statistical pattern recognition. In: Meteorological Applications, vol. 18, 60–69. Wiley Online Library.

Škvareninová, J., Hlavatá, H., Jančo, M., Škvarenina, J. (2018): Impact of climatological drought on the leaves yellowing phenophase selected tree species. Acta Hydrologica Slovaca vol. 19, issue 2, 220–226.

Takáč, J., Skalský, R., Morávek, A., Klikušovská, Z., Bezák, P., Bárdyová, M. (2015): Spatial patterns of agricultural drought events in Danube lowland in the 1961–2013 period. In: Šiška et al. (eds.): TOWARDS CLIMATIC SERVICES, Nitra, Slovakia.

Tiqkas, D., Vanqelis, H., Tsakiris, G. (2019): Drought characterisation based on an agriculture-oriented standardized precipitation index. Theoretical and Applied Climatology, issue 135, 1435–1447.

Vergni, L., Vinci, A., Todisco, F. (2021): Effectiveness of the new standardized deficit distance index and other meteorological indices in the assessment of agricultural drought impacts in central Italy. Journal of Hydrology, issue 603, 126986 p.

Vido, J., Nalevanková, P., Valach, J., Šustek, Z., Tadesse, T. (2019): Drought Analyses of the Horné Požitavie Region (Slovakia) in a Period 1966–2013. In: Advances in Meteorology, Hindawi.

Vincente-Serrano, S. M., Begueria, S., López-Moreno, J. I. (2010): A multiscalar drought index sensitive to global warming: the standardized precipitation evapotransipration index. Journal of Climate, vol. 23, issue 7, 1696–1718.

USAID (2023): https://2017-2020.usaid.gov/results-data/success-stories/youth-horticulture-startups-make-first-sales, last accessed 2023/05/12

Zuzulova, V., Vido, J. (2018): Normalized difference vegetation index as a tool for the evaluation of agricultural drought in Slovakia. Ecocycles, vol. 4, issue 1, 83–87.

Ing. Tatiana Soľáková, PhD.
Prof. Ing. Martina Zeleňáková, PhD. (*corresponding author, e-mail: martina.zelenakova@tuke.sk)
Prof. Hany Abd-Elhamid
Ing. Peter Bujanský, MBA
Mgr. art. Miroslav Garaj
Faculty of Civil Engineering
Technical University of Košice
Vysokoškolská 4
040 01 Košice
Slovak Republic

Prof. Milan Gocic
University of Nis
Faculty of Civil Engineering and Architecture
Aleksandra Medvedeva 14
18000 Nis
Serbia

Ing. Helena Hlavatá, PhD.
Slovak Hydrometeorological Institute
Regional Office Košice
Ďumbierska 26
041 17 Košice
Slovak Republic

DOI: 10.31577/ahs-2023-0024.02.0033

ACTA HYDROLOGICA SLOVACA

Volume 24, No. 2, 2023, 303 – 309

Study of the saturated hydraulic conductivity by falling–head method for different soil types amended with different biochar fraction size

Lucia TOKOVÁ*, Natália BOTKOVÁ, Justína VITKOVÁ, Lenka BOTYANSZKÁ, Peter RONČÁK

Saturated hydraulic conductivity is an important soil property related to soil water regime. Generally, loam soil has a convenient moisture regime. However, if this type of soil is gradually drying out, its moisture regime may change for the worse. Our task is therefore to search for methods to increase the hydraulic conductivity of the loamy soils. In contrast, one of the goals of sandy soil management is slowing down flow velocity. In our research, we focused on the effect of biochar particle size on saturated hydraulic conductivity changes in three different soil types. The soils were selected based on their textures – sandy, silt loam and silty clay. Our results confirmed that addition of biochar with particle size <125 μm produced from paper fiber sludge and grain husks significantly ($p<0.05$) reduced saturated hydraulic conductivity in sandy soil by approximately 61% compared to control with sandy soil. Further, the results indicated that biochar with a fraction size >2 mm effectively increased the saturated hydraulic conductivity of silt loam soil by approximately 165% compared to pure silt loam soil. The difference was also statistically significant ($p<0.05$). Biochar amendment to the finest textured soil used in this study (silty clay) also increased the saturated hydraulic conductivity of the soil. The biochar with a fraction size of 125 μm–2 mm and >2 mm significantly ($p<0.05$) increased the saturated hydraulic conductivity by approximately 629% and 1063%, respectively when compared to pure silty clay soil.

KEY WORDS: biochar fraction size, soil type, saturated hydraulic conductivity, falling–head method

Introduction

It is essential to know the hydraulic properties of the soil for better planning and management of water resources. Increasing the velocity, when water enters into the soil is very important for capturing rainfall, soil water retention and overall soil management (Blaco–Canqui, 2017). From this point of view, saturated hydraulic conductivity (*K*) is important soil property in solving problem with the soil water regime. It is also important soil property, especially for modeling water flow and solute transport in soil, irrigation and drainage design, groundwater modeling and other agricultural or engineering processes as well. Some studies state that biochar addition can increase *K* in clay soils and loamy soils (Dan et al., 2015) by increasing the number of connected macropores. Other study (Uzoma et al., 2011) suggests that biochar could effectively suppress water loss in sandy soils. The biochar particle fraction size itself and the particle size of the soil into which the biochar was applied also play an important role (Hardie et al. 2014; Lehmann and Joseph 2015; Esmaeelnejad et al. 2017).

K represents the ease with which water flows through soil when pore spaces are completely filled with water and it reflects the number of pores and their arrangement. It is difficult to characterize it because of its high variability even over short distances, and measurement methods, typically require considerable time and resources. However, accurate estimation of *K* in soil is essential for various hydrological applications (Shwetha and Varija, 2015). *K* depends mainly on soil structure, soil texture, organic matter content and bulk density which can vary in both space and time (Hillel, 1998; Beckwith et al., 2003). Chirico et al. (2007) stated that the relationship between *K* and above-mentioned soil properties is not strong enough to permit accurate estimations of *K*. However, anisotropy of *K* is not routinely determined because practical and validated methods are still lacking (Petersen et al., 2008).

In laboratory conditions, *K* could be affected by the quality of undisturbed soil sample and the content of the preferred water flow pathways in the soil sample. Another factor influencing the measurement could be the number of repetitions of the measurement. Regardless of the determination method of *K* in the field or laboratory, the measured value is representative both for the specific place and time at which the measurement was carried out (Kargas et al., 2021). There are lots of laboratory methods for measuring *K* (e.g. falling–head method, constant–head method) (Antal and Igaz, 2012).

In our study *K* was measured using the falling–head method (FHM) in laboratory conditions. Three different soil types were chosen based on their texture (sandy, silt loam and silty clay) and amended by biochar with three different fraction sizes (<125 μm, 125 μm–2 mm, >2 mm).

Material and methods

Used soils for the laboratory experiment

Soils with different structure were chosen for this experiment. The grain size analysis was determined based on USDA classification protocol. Measurements of the sandy and silty clay soils were performed using the hydrometer method described, e.g., by Novák and Hlaváčiková (2019). The analysis of the silt loam soil was obtained by Šimanský and Klimaja (2017).
Sandy soil used in this experiment was taken from site of Záhorská nížina (area Plavecký Štvrtok). The soil sample contained 91% of sand, 7.5% of silt and 1.5% of clay.
Sample of silt loam soil was taken from site of Nitrianská pahorkatina (area Dolná Malanta). Its content of sand was 15.2%, silt 59.9% and clay 24.9%.
Silty clay soil was taken from site of Východoslovenská nížina (area Senné) and it consisted of 11.1% of sand, 42.9% of silt and 46% of clay.

Used biochar for the laboratory experiment

Biochar used in this experiment was made from paper fiber sludge mixed grain husks at a 1:1 ratio (according to their weight). The feedstock was processed by pyrolysis at 550°C for 30 minutes in a Pyreg reactor (Pyreg GmbH, Görhe, Germany) and provided by Sonnenerde company (Austria) as a final commercial product. Further detailed information of the biochar parameters is shown in Table 1.

Mixtures of soil and biochar

Mixtures of each soil type (sandy, silt loam and silty clay) with biochar were prepared in laboratory conditions. We applied a biochar with concentration of 1.5% (20 t ha^{-1}) in steel cylinders with a volume of 100 cm^3. Overall, three treatments, representing different particle size fractions (< 125 μm, 125 μm–2 mm and > 2 mm), were prepared. For each treatment 3 replicates of soil and biochar mixtures were prepared. These prepared mixtures were compared with the control treatment (without biochar amendment – each for sandy soil, silt loam soil and silty clay soil), which was prepared in 3 replicates as well. The treatments of the laboratory experiment are presented in Table 2.

Laboratory measurement of saturated hydraulic conductivity

Saturated hydraulic conductivity of the soil (*K*) was determined by prepared mixtures of each soil type and biochar in steel cylinders for all treatments of the laboratory experiment. Each treatment was made in three replicates, so 36 samples were measured in total (Table 2). We performed 3 measurements of *K* for each soil sample, which means that we had 9 values (n=9) of *K* for each treatment for further statistical analysis.
We used falling–head (variable) method (FHM) to measure the amount of water that goes through the soil sample in a fixed time interval. The water level above the soil sample decreases over time (Antal and Igaz, 2012; Igaz et al., 2017, Dulovičová et al., 2022) (Fig. 1). A digital caliper (Emil Lux GmbH & Co. KG) was used to measure the water level drop with accuracy +/- 0.2 mm (Fig. 1). *K* was calculated according to Eq. 1:

$$K = \frac{L}{t} \ln\frac{H_2}{H_1} \qquad [\text{cm s}^{-1}] \tag{1}$$

where:
L – soil cylinder height (soil sample) [cm],
t – time of water level decrease from height H_2–H_1 [s],
H_2 – initial water level in the extension [cm],
H_1 – the height of the water in the extension after the drop [cm].

Statistical analysis

In our study we used Microsoft Excel program for descriptive statistics (Mean, Standard deviation – SD) to describe and summarize the basic features of the given dataset and to create the box plots. The effect of biochar application on the saturated hydraulic conductivity of the soil was evaluated using a one–way analysis of variance (one–way ANOVA). Statistically significant effects at $p<0.05$ were determined by least significant difference (LSD) test. All statistical analyses were performed in Statgraphics Centurion XV.I software (Statpoint Technologies, Inc., Warrenton, VA, USA).

Table 1. The chemical and physical properties of biochar (Kondrlova et al., 2018; Šimanský et al., 2019)

SSA* [m^2 g^{-1}]	Size fraction [mm]	pH [–]	Total C [g kg^{-1}]	Total N [g kg^{-1}]	P [g kg^{-1}]	K [g kg^{-1}]	Ca [g kg^{-1}]
21.7	1–5	8.8	531	14	6.2	15	57

** SSA specific surface area*

Table 2. Treatments of the laboratory experiment

Treatment	Replication
sandy soil (control)	3
sand and biochar (<125 μm) mixture	3
sand and biochar (125 μm–2 mm) mixture	3
sand and biochar (>2 mm) mixture	3
silt loam soil (control)	3
silt loam and biochar (<125 μm) mixture	3
silt loam and biochar (125 μm–2 mm) mixture	3
silt loam and biochar (>2 mm) mixture	3
silty clay soil (control)	3
silty clay and biochar (<125 μm) mixture	3
silty clay and biochar (125 μm–2 mm) mixture	3
silty clay and biochar (>2 mm) mixture	3
Total	36

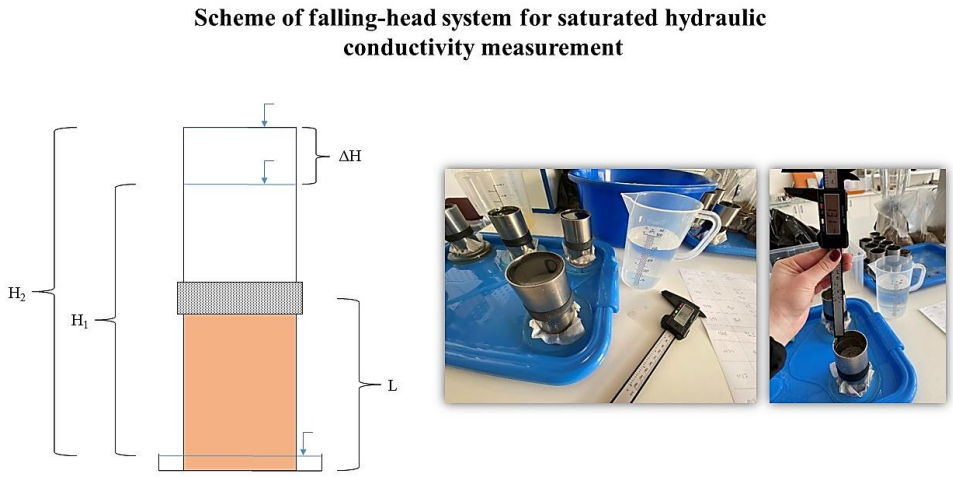

Fig. 1. Scheme of falling–head method for saturated hydraulic conductivity measurement.

Results and discussion

Evaluation of biochar application impact on the soil

The most important observed result of our work was a decrease in *K* after biochar application in sandy soil (Fig. 2) and an increase in *K* after biochar application in silt loam and silty clay soils (Fig. 3 and Fig. 4). According to previous research, biochar is believed to cause slower flow in sandy soils and effectively suppress water loss (Dan et al., 2015). Coarse biochar particles increased intraporosity and fine biochar particles decreased hydraulic conductivity due to reduced macropores. Conversely, in loamy soils, biochar tends to reduce soil bulk density (Toková et al., 2020), increase soil porosity (Vitková et al., 2019), improve soil texture (Sun and Lu, 2014; Walters and White, 2018), and consequently increase *K* (Esmaeelnejad et al., 2017) and soil water content (Vitková et al., 2021). According to previous studies of the effect of biochar on fine textured clay soils, its positive effect is not clearly demonstrable (Castellini et al., 2015). However, from our results, it seems that biochar behaves similarly to loamy soils and thus effectively increases *K* values in clay soils (Fig. 4). Another result observed was a gradual decrease in *K* after application of gradually decreasing the particle size fraction of biochar to sandy soil (Fig. 2), with a statistically significant ($p<0.05$) decrease in *K* observed for the treatment with the smallest size fractions (<125 μm) compared to the control (Table 3). Similar results were also reported by Toková et al. (2022a), where the effect of different biochar sizes (produced from willow tree) on sandy soil was investigated. The authors Lehmann and Stephen (2015) reported that biochar with smaller particles size than the soil particles present in the soil profile can reduce *K* after its application. This statement is consistent with our results as sandy soil contains predominately sandy particles (size fraction in the range of 0.05 to 2 mm) and thus when biochar with a size <125 μm (i.e. 0.125 mm) was applied to soil it could have caused the effect mentioned above. For larger biochar size fractions (125 μm–2 mm and

>2 mm) in combination with sandy soil, this difference was not so obvious (Fig. 2). Further, we observed a gradual increase in *K* after gradually increasing the size fraction of biochar applied to silt loam (Fig. 3), with a statistically significant ($p<0.05$) increase in *K* when the largest particle size fraction (>2 mm) of biochar was used compared to the control (Table 4). Similar results were also reported by Toková et al. (2022b), where the effect of biochar (made from willow tree) applied in different size fractions to clay soil was investigated. Lehmann and Joseph (2015) stated that biochar with larger particles than soil particles could increase *K*. This statement is also consistent with our results, as silt loam soil was used for the experiment and the most obvious *K* enhancement effect was observed for the larger size fractions of used biochar. According to Esmaeelnejad et al. (2017), finer fractions of biochar fill easier the spaces between soil particles. Consequently, the addition of biochar can lead to either clogging (in sandy soil) or enlarging the pores (in silt loam and silty clay). In the case of silty clay soil (Fig. 4), the effect of increasing *K* is more apparent than in the case of silt loam soil. This could be because silty clay soil has a higher representation of the finest clay fraction (<0.002 mm) than silt loam soil.

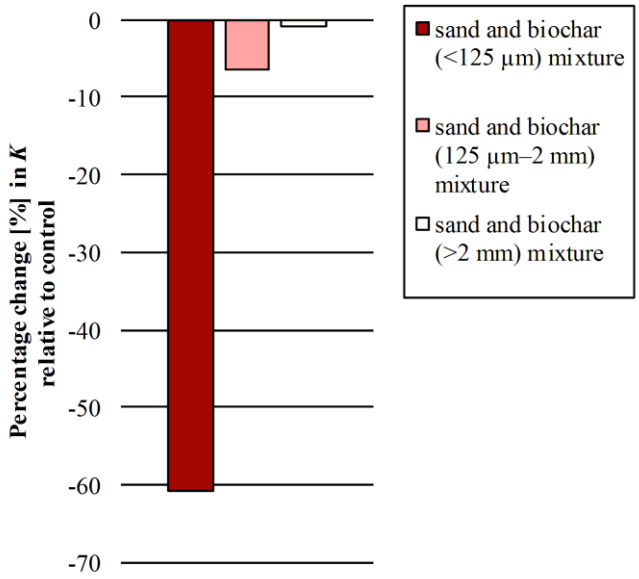

Fig. 2. Graphical representation of the influence of biochar on saturated hydraulic conductivity (K) of the sandy soil expressed as a percentage change relative to control.

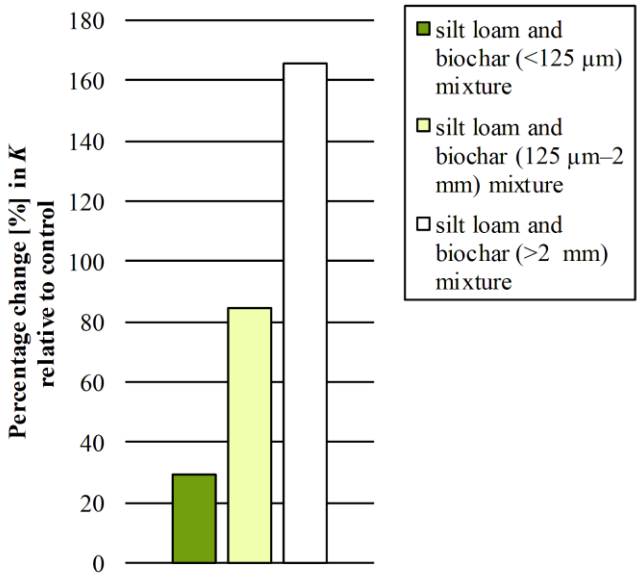

Fig. 3. Graphical representation of the influence of biochar on saturated hydraulic conductivity (K) of the silt loam soil expressed as a percentage change relative to control.

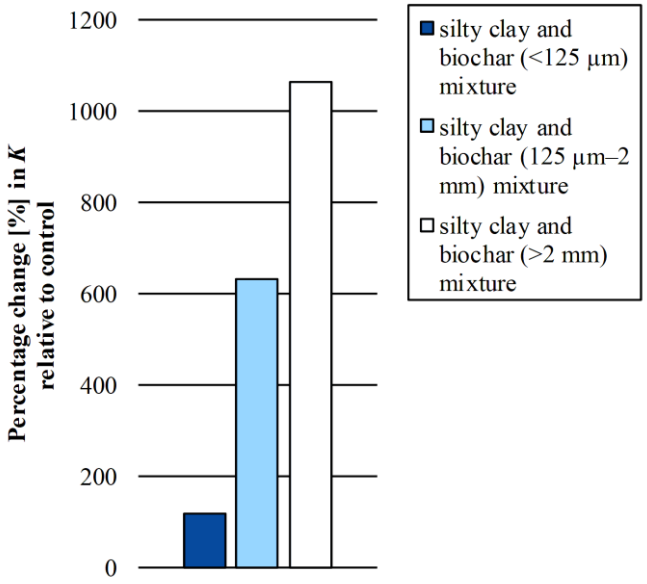

Fig. 4. Graphical representation of the influence of biochar on saturated hydraulic conductivity (K) of the silty clay soil expressed as a percentage change relative to control.

Table 3. Effect of biochar application on saturated hydraulic conductivity (*K*) of the sandy soil (means ± standard deviations)

Treatment	Mean [cm h^{-1}]	SD
sandy soil (control)	48.363[b]	14.920
sand and biochar (<125 µm) mixture	18.958[a]	5.581
sand and biochar (125 µm–2 mm) mixture	45.238[b]	13.965
sand and biochar (>2 mm) mixture	47.940[b]	16.893

Different letters (a, b) indicate that treatment means are significantly different at p<0.05 according to least significant difference test (one-way ANOVA).

Table 4. Effect of biochar application on saturated hydraulic conductivity (*K*) of the silt loam soil (means ± standard deviations)

Treatment	Mean [cm h^{-1}]	SD
silt loam soil (control)	0.966[a]	0.558
silt loam and biochar (<125 µm) mixture	1.247[a]	0.690
silt loam and biochar (125 µm–2 mm) mixture	1.779[ab]	0.685
silt loam and biochar (>2 mm) mixture	2.563[b]	0.893

Different letters (a, b) indicate that treatment means are significantly different at p<0.05 according to least significant difference test (one-way ANOVA).

Table 5. Effect of biochar application on saturated hydraulic conductivity (*K*) of the clay soil (means ± standard deviations)

Treatment	Mean [cm h^{-1}]	SD
silty clay soil (control)	0.083[a]	0.045
silty clay and biochar (<125 µm) mixture	0.182[a]	0.115
silty clay and biochar (125 µm–2 mm) mixture	0.605[b]	0.142
silty clay and biochar (>2 mm) mixture	0.966[c]	0.292

Different letters (a, b, c) indicate that treatment means are significantly different at p<0.05 according to least significant difference test (one-way ANOVA).

Evaluation of the falling–head method used for K measurements

The results showed that FHM is sensitive enough to record high differences in *K* measurements between sandy, silt loam and silty clay soil (Pedescoll et al., 2011) (with or without biochar amendment). Mean values ranged from 18.958 to 48.363 cm h^{-1}, from 0.966 to 2.563 cm h^{-1} and from 0.083 to 0.966 cm h^{-1} for sandy, silt loam and silty clay soil, respectively (Table 3, Table 4 and Table 5). Therefore, FHM appears to be a suitable technique for the evaluation of *K*. However, other authors (Antal and Igaz, 2012) stated that the FHM principle is more suitable to be used for finer soils (loams, clays). For coarser sandy soils, the constant-head method (CHM) measurement principle is recommended. The authors go on to give a cut-off value for "low" saturated soil hydraulic conductivity of 100 cm d^{-1} (i.e. 4.167 cm h^{-1}) and therefore a cut-off value for the use of one or other laboratory K measurement method. Our results showed that FHM exhibits a large standard deviation (SD) between measured values (n=9) within a single treatment in sandy soil (Table 3). In general, the largest SD was recorded in sandy soil (control) (14.920) and with biochar application with fraction >2 mm (16.893) (Table 3). Thus, the greater SD recorded in above mentioned cases was to be expected with the method used. The method used appears to be suitable for use on loamy and clayey soils (Table 4 and Table 5). On these soils, a high standard deviation between the measured values was not observed.

Conclusion

It can be concluded that the saturated hydraulic conductivity of the soil varied depending on the soil type and particle size fraction of the used biochar. Our results showed that biochar with the smallest particle size fraction (<125 μm) (mean value 18.958 cm h^{-1}) in sandy soil effectively retarded flow velocity compared to the control (mean value 48.363 cm h^{-1}). In clay soils, the use of biochar with the largest fraction size (>2 mm) (mean value 2.563 cm h^{-1}) effectively increases the rate of saturated hydraulic conductivity compared to the control (mean value 0.966 cm h^{-1}). As in clay soils, the use of biochar with larger fraction sizes (<125 μm–2 mm and >2 mm) effectively increased saturated hydraulic conductivity velocity (mean value 0.605 cm h^{-1} and 0.966 cm h^{-1}, respectively) compared to the control (mean value 0.083 cm h^{-1}). In all cases, this difference was also demonstrated by statistical analysis (one-way ANOVA). Further investigations are recommended to better understand the influence of biochar particle size on hydraulic conductivity in sandy, silty and clay soils. Our results provide recommendations for farmers that biochar particle size influences the soil hydrological regime. Farmers can choose a biochar fraction that will positively affect a specific soil type.

Acknowledgement

This study was realized with financial support by VEGA 2/0155/21 and APVV-21-0089 projects.

References

Antal, J., Igaz, D. (2012): Aplikovaná agrohydrológia, SPU, Nitra, 210 p. ISBN 978-80-552-0731- 5.

Beckwith, C. W., Baird, A. J., Heathwaite, A. L. (2003): Anisotropy and depth-related heterogeneity of hydraulic conductivity in a bog peat. I: laboratory measurements. Hydrological processes, vol. 17, no. 1, 89–101.

Blanco-Canqui, H. (2017): Biochar and Soil Physical Properties. Soil Science Society of America Journal, vol. 81, 687-711.

Castellini, M., Giglio, L., Niedda, M., Palumbo A. D., Ventrella, D. (2015): Impact of biochar addition on the physical and hydraulic properties of a clay soil. Soil and Tillage Research, vol. 154, 1–13.

Chirico, G. B., Medina, H., Romano, N. (2007): Uncertainty in predicting soil hydraulic properties at the hillslope scale with indirect methods. Journal of Hydrology, vol. 334, no. 3-4, 405–422.

Dan, T., Zhong-Yi, Q., Mang-Mang, G., Bo, L., Yi-Jia, L. (2015): Experimental Study of Influence of Biochar on Different Texture Soil Hydraulic Characteristic Parameters and Moisture Holding Properties. Polish Journal of Environmental Studies, vol. 24, no. 3, 1435–1442.

Dulovičová, R., Schugerl, R., Velísková, Y. (2022): Hydraulic conductivity of saturated bed silts in Chotárny channel, ŽO area, Slovakia. Acta Hydrologica Slovaca, vol. 23, no. 2, 180–189.

Esmaeelnejad, L., Shorafa, M., Gorji, M., Hosseini, S. M. (2017): Impacts of woody biochar particle size on porosity and hydraulic conductivity of biochar-soil mixtures: an incubation study. Communications in soil science and plant analysis, vol. 48, no. 14, 1710–1718.

Hardie, M., Clothier, B., Bound, S., Oliver, G., Close, D. (2014): Does biochar influence soil physical properties and soil water availability? Plant and soil, vol. 376, 347–361.

Hillel, D. (1998): Environmental soil physics. Academic Press, San Diego. Environmental soil physics. Academic Press, San Diego. USA, 771 p.

Igaz, D., Kondrlová, E., Horák, J., Čimo, J., Tárník, A., Bárek, V. (2017): Základné merania v hydropedológií, SPU, Nitra, 110 p. ISBN 978-80-552-1686-7.

Kargas, G., Londra, P. A., Sotirakoglou, K. (2021): Saturated hydraulic conductivity measurements in a loam soil covered by native vegetation: Spatial and temporal variability in the upper soil layer. Geosciences, vol. 11, no. 2, 105 p.

Kondrlova, E., Horak, J., Igaz, D. (2018): Effect of biochar and nutrient amendment on vegetative growth of spring barley ('Hordeum vulgare' L. var. Malz). Australian journal of crop science, vol. 12, no. 2, 178–184.

Lehmann, J., Joseph, S. (2015): Biochar for environmental management: science, technology and implementation. Routledge. 2nd ed. London: Rountledge, Taylor and Francis Group, 976 p. ISBN 978-0-41570415-1.

Novák, V., Hlaváčiková, H. (2019): Applied Soil Hydrology; Theory and Applications of Transport in Porous Media,

Springer International Publishing: Cham, Switzerland, 342 p. ISBN 978-3-030-01805-4.

Petersen, C. T., Trautner, A., Hansen, S. (2008): Spatio-temporal variation of anisotropy of saturated hydraulic conductivity in a tilled sandy loam soil. Soil and Tillage Research, vol. 100, no. 1–2, 108–113.

Pedescoll, A., Samsó, R., Romero, E., Puigagut, J., García, J. (2011): Reliability, repeatability and accuracy of the falling head method for hydraulic conductivity measurements under laboratory conditions. Ecological Engineering, vol. 37, no. 5, 754–757.

Shwetha, P., Varija, K. (2015): Soil water retention curve from saturated hydraulic conductivity for sandy loam and loamy sand textured soils. Aquatic Procedia, vol. 4, 1142–1149.

Sun, F., Lu, S. (2014): Biochars improve aggregate stability, water retention, and pore-space properties of clayey soil. Journal of Plant Nutrition and Soil Science, vol. 177, no.1, 26–33.

Šimanský, V., Horák, J., Polláková, N., Juriga, M., Jonczak, J. (2019): Will the macro and micronutrient content in biochar show in the higher content of the individual parts of corn. J. Elem, vol. 24, no. 2, 525–537.

Šimanský V., Klimaj A. (2017): How does biochar and biochar with nitrogen fertilization influence soil reaction? Journal of Ecological Engineering, vol. 18, 50–54.

Toková, L., Igaz, D., Horák, J., Aydin, E. (2020): Effect of biochar application and re-application on soil bulk density, porosity, saturated hydraulic conductivity, water content and soil water availability in a silty loam Haplic Luvisol. Agronomy, vol. 10, no.7, 1005.

Toková, L., Botková, N., Vitková, J., Šurda, P., Botyanszká, L., Rončák, P., Gaduš, J. (2022a): Saturated hydraulic conductivity of sandy soil under application of two different biochar types. In Veda mladých 2022 – Science of Youth 2022: proceedings of reviewed contributions. – Nitra: Faculty of Horticulture and Landscape Engineering, 138–146. ISBN 978-80-552-2502-9. ISSN 2585-7398.

Toková, L., Botková, N., Vitková, J., Botyanszká, L. (2022b): Influence of fine biochar fraction size application on two different soil texture types. In Interdisciplinary Approach in Current Hydrological Research: electronic book. – Bratislava IH SAS, 2022, 91–95. ISBN 978-80-89139-53-8.

Uzoma, K. C., Inoue, M., Andry, H., Zahoor, A., Nishihara, E. (2011): Influence of biochar application on sandy soil hydraulic properties and nutrient retention. Journal of Food, Agriculture and Environment, vol. 9, no. 3/4 part 2, 1137–1143.

Walters, R. D., White, J. G. (2018): Biochar in situ decreased bulk density and improved soil-water relations and indicators in Southeastern US Coastal plain ultisols. Soil Science, vol. 183, no. 3, 99–111.

Vitková, J., Gaduš, J., Skic, K., Boguta, P., Giertl, T. (2019): Impact of grapevine biochar on some hydro – physical characteristics of silt loam soil. Laboratory measurements. Acta Hydrologica Slovaca, vol. 20, no. 2, 166–171.

Vitková, J., Šurda, P., Rončák, P., Botková, N., Zvala, A. (2021): Statistical analysis of water content differences after biochar application and its repeated application during 2020 drowing season. Acta Hydrologica Slovaca, vol. 22, no. 2, 320–325.

Ing. Lucia Toková, PhD. (*corresponding author, e-mail: tokova@uh.savba.sk)
Ing. Natália Botková
Ing. Justína Vitková, PhD.
Ing. Lenka Botyanszká, PhD.
Mgr. Peter Rončák, PhD.
Institute of Hydrology SAS
Dúbravská cesta 9
841 04 Bratislava
Slovak Republic

Ing. Natália Botková
Institute of Landscape Engineering
Faculty of Horticulture and Landscape Engineering, SUA
Hospodárska 7
949 76 Nitra
Slovak Republic

DOI: 10.31577/ahs-2023-0024.02.0034

ACTA HYDROLOGICA SLOVACA

Volume 24, No. 2, 2023, 310 – 321

Soil and water assessment tool model for runoff reaction to land use variations by SWAT model package

Kaveh OSTAD-ALI-ASKARI*, Mohsen GHANE, Peiman KIANMEHR

Hydro-climatic degeneracies, for example moist and dissipations, have most likely enlarged owing to climatical modification and could due to diffident possessions on socio-economic, mechanical and ecological regions. To plan and concept most hydraulic structures, e.g., dams, it is vital to regulate the runoff of the rivers. If the river absences any position to live the yield, the hydraulic mockups are frequently used to estimate it. SWAT is one of the greatest widely-applied computerized models. In this prototypical, we'd like to feed such influential climatological data as precipitation, temperature, wind speed, radiation and ratio, also as, watershed data including the Curve Number (CN) and roughness coefficient to calculate the watershed runoff. Some watershed contains few weather stations, and there is a risk that the registered data in a station do not represent the whole watershed. Consequently, the amount of the runoff estimation error needs to be determined. The obtained results indicate that with a 32.07% decrease in the average monthly precipitation, sunshine, relative humidity, wind and temperature, we witness 65.36% decrease, 116.82% increase, 46.78% decrease, 127.16% increase, and 39.52% increase in modeled runoff, respectively. The wind speed and therefore the radiation are the foremost sensitive and temperature is that the least sensitive components within the runoff approximation.

KEY WORDS: Meteorological Parameters; Rainfall Runoff; Sensitivity Analysis; SWAT model; Curve Number (CN)

Introduction

So as to shape a dam, it is energetic to regulate the monthly and annular yields of the river to compute the volume and the height of the dam (Varga et al., 2023). A gage station can measure the input water of the dam. In the nonappearance of the gage station, a computerized model, e.g., SWAT, are often want to estimate the present and therefore the input runoff. The high-tech mockups can make accurate and complex designs in a short period. So as to compute the watershed runoff on the one hand, the prototypical needs such powerful climatological information as precipitation, temperature, wind speed, solar radiation and relative humidity, and on the opposite hand we'd like the watershed basin information including the curve number and therefore the roughness coefficient (Khaleghi et al., 2011, Rabiei et al., 2022).

The same perfect was applied and verified from 1999 to 2006.Data from 2007 to 2010 was used to examineing the precision and in the together phases of confirmation and authentication the consequences were acceptable. The SWAT model keeps the ability to produce varied situations to study different decision-making issues. The obtained results indicated a higher sensitivity of the model to the over land roughness coefficient (Behtari Nejad, 2012). It was used SWAT to stimulate the river current in the Gharesar sub-basin northwest of the Karkheh River. The research showed a higher analytical sensitivity to the curve number parameter (Behtari Nejad, 2012). It was dealt with the stimulation of the daily discharge, water balance and land application in Haraz watershed. The results provided by the model were sensitive to the period, that is, the annual and the monthly periods yielded more reasonable results in comparison with the daily period (Saadati, 2003, Ghashghaie et al., 2022). Alavinia and Nasiri-saleh utilized the SWAT model to estimate the discharge and approved the efficiency of the model (Behtari Nejad, 2012, Alavinia and Nasiri Saleh, 2011).

Material and methods

The case to be studied is limited to Haraz watershed (located in Northern forests of Alborz mountain in Iran). The revision zone of this research is situated between 549,026 to 623,239 Eastern longitude and 3,926,045 to 4,012,211 north latitude in zone 40 of UTM. Haraz watershed with a zone of 401932.9 hectares is situated to the south of the area and in the locality of Amol Town. The least height of 300 meters and an extreme height of 5800 meters are the height restrictions. The area of Haraz

watershed is approximately 66.81 square kilometers and the main river stretches for 16.8 kilometers. The geographical coordinates of the rivers are as follows: latitude from 36˚-06' to 36˚-15' N, and longitude from 53˚-15' to 53˚ -29' E. Fig. 1 shows the position of Haraz watershed. The mentioned statistical parameters were retrieved from Karehsang, Chelav and Razan, Panjab places. Haraz River shows a significant part in the exists of the persons of this area, particularly in their agronomic segment. The Haraz plain is located in the Mazandaran province, one of the northern provinces of Iran between the Caspian Sea and the Alborz mountains. This seaside basic is located between the Amlash and Babol rivers (Shrestha et al, 2020). The southern district of the plain is enclosed by mountains and highlands (Schuol et al., 2006). The zone covers from the Damavand peak (5675 m a.s.l.) as the highest height in the highlands to the deepest region with -25 m a.s.l. in the plain. The study zone (6850 km^2) is drained by the two foremost streams Haraz and Babolroud (Bačová Mitková et al., 2023). These stable streams instigate from the Alborz elevations and grasp the Caspian Sea after passing through forestlands, rangelands, urban zones and agronomic land in the Haraz plain. In terms of geomorphology, the Haraz plain can be

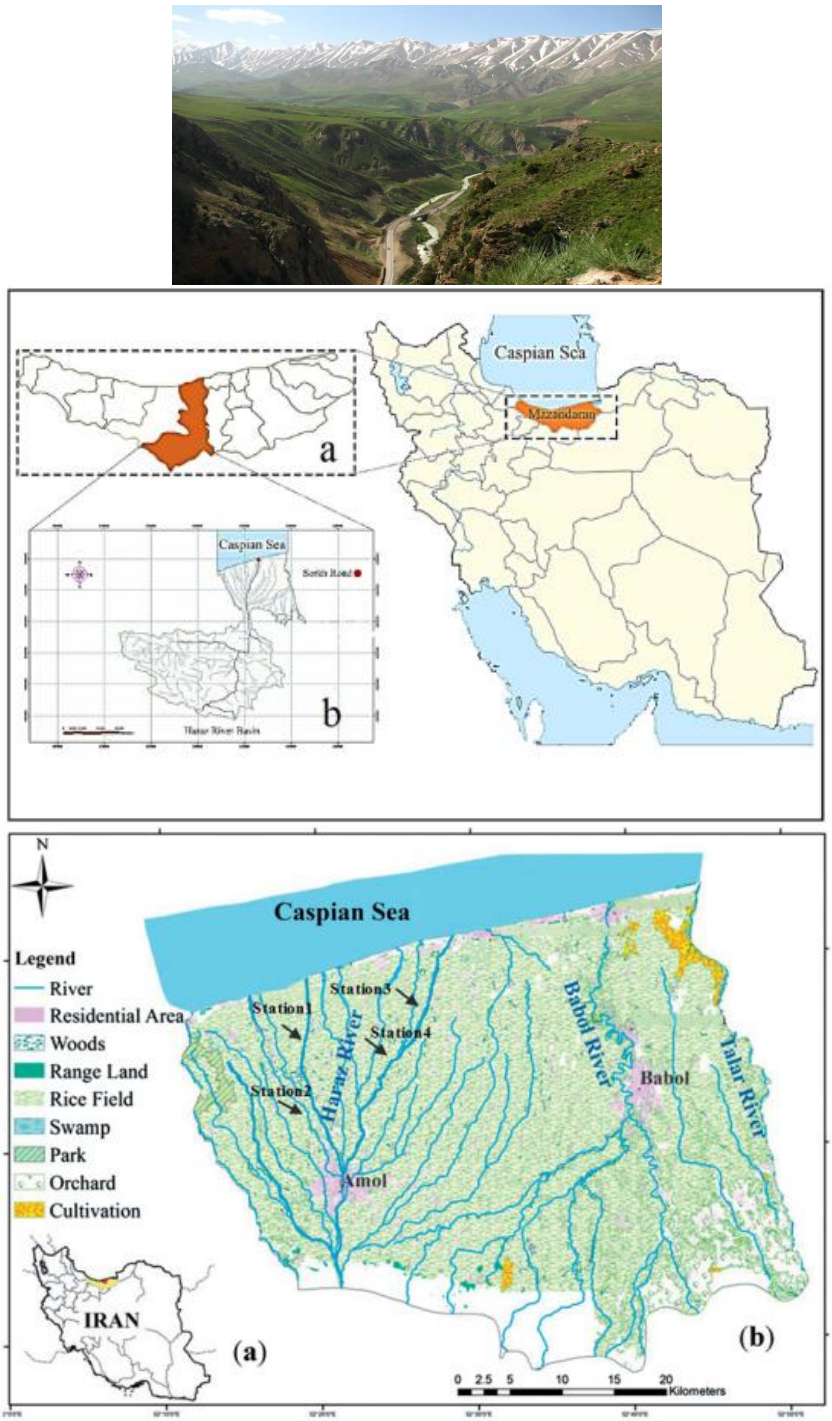

Fig. 1. Show the position of Haraz Watershed (Mazandaran Province, Iran). (Naeeji et al., 2020; Dadar et al., 2016).

confidential into six main units comprising highlands (1.25%), mountains (0.38%), piedmont plain (22.92%), stream sedimentary plain (10.52%), low terrestrial (7.32%), flood plain (52.32%) and beach low sand hills (5.82%). The Haraz natural obtains an average annual precipitation of 675 mm (850 mm in the highland watersheds) with a range of total maximum and minimum temperature among −10 to 38.3 and the mediocre annual moisture is 780% (depend on synoptic data 2000–2020 at Amol). In this plain, Haraz is the chief river with many branches and a extensively industrialised sedimentary fan. Owing to the fertile soil and available basis of superficial water and groundwater, the large quantity of the study zone is enclosed by paddy agronomy. Other foremost land routines are urbanized zones, forestry lands, rangelands, natural wetlands and fish farms. Inceptisols (58.92%), Alfisols (39.82%) and coastal sands (1.56%) are the foremost soil assemblies in the area (Ecological Defence Society, 2021). Soil, geology and digital elevation model maps for the study area are presented in accompanying information. Haraz Stream lies between longitude of 35º 536 and 45 º 62 and latitude of 35 º 463 and 36 º 163. (Mohammadi, 2023).

According to the relevant statistics, the coldest month of the year is from the middle of January to the beginning of February, and the minimum temperature occurred among the stations, according to the average of -95.8 degrees Celsius, corresponding to Haraz station was in the month of February (Amoakowaah Osei et al., 2019). The maximum temperature occurred between the climatology stations according to the absolute maximum of 38.5 degrees Celsius corresponding to Haraz station in the month of August and also according to the average maximum equivalent of 23.1 degrees Celsius corresponding to the Haraz station in the month of August which was recorded (Apostel et al., 2020). According to the available information about the monthly and annual temperature, the relationship between the average annual temperature and altitude is at a significant level of 0.01 based on equation 1. is below:

$$T = 1.68 - 0.0051H \quad (1)$$

In Eq. 1, *T* is the air temperature in degrees Celsius and *H* is the height in meters. Using relation Eq. 1, the average temperature of the lowest point of the basin in Haraz station with an altitude of about 1100 meters is approximately equal to 10.96 degrees Celsius and the average temperature of the highest point at an altitude of 3100 meters is approximately equal to 0.75 degrees Celsius (Chu and Shirmohammadi, 2004). According to this equation, the average gradient of the annual normal temperature drop in the Haraz basin is about 1.7 degrees Celsius per kilometer.

The number of SCS curve is a function of soil permeability, land application and the humidity already retained in the soil. Different types of curve number were considered for humidity condition II in diverse types of land from 69 to 78 based on the SWAT formulas tables and the optimum number for the region was obtained as 72 (SCS Engineering Division 1986, SWAT Theoretical Documentation Version 2009).

SCS runoff equation is an empirical model developed in 1950 after 20 years of studying the relationship between rain and runoff in the small American villages' watersheds. The model estimates the runoff in various land applications and different types of soil (Rallison and Miller 1981, SWAT Theoretical Documentation Version 2009).

Eq. 2 shows the curve number as follows (SCS 1972):

$$Q_{surf} = \frac{(R_{day} - I_a)^2}{(R_{day} - I_a + S)} \quad (2)$$

where Q_{surf} is the accumulated runoff or the excess of precipitation [mm], *R* day is the height of water per day [mm], I_a is the initial leakage of the surface reserve, the diffusion before runoff [mm], and *S* is the water saving [mm]. A change in saving parameter ends in changes in the type of the soil, land application, management, slope and soil content. Saving parameter is defined in Eq.3 (SWAT Theoretical Documentation Version 2009):

$$S = 25.4 \left(\frac{1000}{CN} - 10\right) \quad (3)$$

where *CN* is the Curve Number for day. I_a is approximately estimated as 0.25 and fed to Eq.1. to obtain Eq. 4 (SWAT Theoretical Documentation Version 2009):

$$Q_{surf} = \frac{(R_{day} - 0.2s)^2}{(R_{day} + 0.8s)} \quad (4)$$

Runoff occurs only if $R_{day} > I_a$. The graphical solutions for Eq. 4 with the numerical values of different curves are presented in Fig. 2 (SWAT Theoretical Documentation Version 2009).

Manning over land roughness coefficient value for the intended watershed region and related SWAT tables are in the range of 0.05 to 0.2. The optimum value for this region was calculated as 1 (Engman, 1983; SWAT Theoretical Documentation Version 2009).

The land current concentration time tov is calculated as Eq. 5 (SWAT Theoretical Documentation Version 2009):

$$t_{ov} = \frac{L_{slp}}{3600.v_{ov}} \quad (5)$$

where L_{slp} is the length of sub-basin slope, v_{ov} is the velocity of land current [m s^{-1}] and 3600 is the unit conversion factor. The velocity of the land current was estimated based Eq.6 or Manning equation (SWAT Theoretical Documentation Version 2009):

$$v_{ov} = \frac{q^{0.4}_{ov}.slp^{0.3}}{n^{0.6}} \quad (6)$$

where q_{ov} is the average of the land current (cubic meter per second), slp is the mean slope of sub-basin and n is the Manning roughness coefficient for the sub-basin. The rate of current is assumed as 6.35 [mm h^{-1}] and unit conversion was done through Eq. 7 and Eq. 8 (SWAT

Theoretical Documentation Version 2009).

$$v_{ov} = \frac{0.005.L_{slp}^{0.4}.slp^{0.3}}{n^{0.6}} \quad (7)$$

$$t_{ov} = \frac{L_{slp}^{0.6}.n^{0.6}}{18.slp^{0.3}} \quad (8)$$

A modest method to compute solar declination is:

$$\delta = \sin^{-1}\left\{0.4 \sin\left[\frac{2\pi}{365}(d_n - 82)\right]\right\} \quad (9)$$

Where δ is the solar declination testified in radians, and d_n is the day number of the year.

$$I_{SC} = 1367\, Wm^{-2} = 4.921 MJm^{-2}h^{-1} \quad (10)$$

On any given day, the extraterrestrial irradiance (rate of energy) on a surface normal to the rays of the sun, I_{0n}, is:

$$I_{0n} = I_{SC}E_0 \quad (11)$$

where E_0 is the eccentricity correction factor of the earth's orbit, and I_{0n}has the same unit as the solar constant, I_{SC}.
The extraterrestrial radiation falling on a horizontal surface during one hour is given by the equation:

$$I_0 = I_{SC}E_0(\sin\delta \sin\emptyset + \cos\delta \cos\emptyset \cos\omega t) \quad (12)$$

where I_0 is the extraterrestrial radiation for 1 hour centered around the hour angle ωt.
The temperature for the hour is then calculated with the equation:

$$T_{hr} = \bar{T}_{av} + \frac{(T_{mx}-T_{mn})}{2}.\cos\big(0.2618.(hr - 15)\big) \quad (13)$$

where T_{hr} is the air temperature during hour hr of the day [ºC], $\bar{T}_{av}$ is the average temperature on the day[ºC], T_{mx} is the daily maximum temperature [ºC], and T_{mn} is the daily minimum temperature [ºC].
In SWAT, a minimum difference of 1 meter is specified for canopy height and wind speed measurements. When the canopy height exceeds 1 meter, the original wind measurement is adjusted to (Rallison and Miller, 1981):

$$z_w = h_c + 100 \quad (14)$$

where z_w is the height of the wind speed measurement [cm], and h_c is the canopy height [cm].
The variation of wind speed with elevation near the ground surface is estimated with the equation (Haltiner and Martin, 1957):

$$u_{z2} = u_{z1}.\left[\frac{z_2}{z_1}\right]^{aa} \quad (15)$$

Where u_{z1} is the wind speed [m s^{-1}] at height Z_1 [cm], u_{z2} is the wind speed [m s^{-1}] at height Z_2 [cm], and *aa* is an exponent between 0 and 1 that varies with atmospheric stability and surface roughness. Jensen (1974) recommended a value of 0.2 for aa and this is the value used in SWAT.

$$R_{day} = \mu_{mon} + 2.\sigma_{mon}.\left(\frac{\left[\left(SND_{day} - \frac{g_{mon}}{6}\right).\left(\frac{g_{mon}}{6}\right)+1\right]^3 - 1}{g_{mon}}\right) \quad (16)$$

where R_{day} is the amount of rainfall on a given day [mm H_2O], μ_{mon} is the mean daily rainfall [mm H_2O] for the month, σ_{mon} is the standard deviation of daily rainfall [mm H_2O] for the month, SND_{day} is the standard normal deviate calculated for the day, and g_{mon} is the skew coefficient for daily precipitation in the month.
The standard normal deviate for the day is calculated:

$$SND_{day} = \cos(6.283.rnd2).\sqrt{-2\ln(rnd1)} \quad (17)$$

where $rnd1$ and $rnd2$ are random numbers between 0.0 and 1.0.
Relative humidity is defined as the ratio of the actual vapour pressure to the saturation vapour pressure at a given temperature:

$$R_{hmon} = \frac{e_{mon}}{e_{mon}^0} \quad (18)$$

where R_{hmon} is the average relative humidity for the month, e_{mon} is the actual vapour pressure at the mean monthly temperature [KPa], e_{mon}^0 is the saturation vapour pressure at the mean monthly temperature [KPa]. The saturation vapour pressure, e_{mon}^0, is related to the mean monthly air temperature with the equation:

$$e_{mon}^0 = \exp\left[\frac{16.78.\mu ump_{mon}-116.9}{\mu ump_{mon}+237.3}\right] \quad (19)$$

where e_{mon}^0 is the saturation vapour pressure at the mean monthly temperature [KPa], and μump_{mon} is the mean air temperature for the month [ºC] (Neitsch at al., 2005).

Soil Type

In this investigation, we consider the optimal curve number and Overland Roughness factor of watershed. The precipitation data was chosen from the different meteorological parameters to obtain the optimum curve number and the Overland Roughness coefficient of the watershed. SWAT was initially run with the curve number, CN_2=69 and the Overland Roughness coefficient 0.12. The consequences are offered in (Fig. 2). To optimize parameters different values for the curve number and roughness coefficient were utilized and the correlation of the Discharge variations with each one of parameters introduced in Table 1 and Table 2. In comparison with runoff amounts registered in hydrometer station and the calculated amount of current, the most optimum curve number was 69 and the Roughness coefficient of watershed was 0.12 (Frizzle et al., 2021; Neitsch et al., 2005). Subsequently, based on the obtained values, variations in SWAT input parameters were used to simulate the river runoff. The properties of difference in separately of climatological components on overflow was computed

and contrasted with the experiential overflow. It should be stated that in this phase of computations individual rainfall information were fed into the prototypical. Fig. 3 shows difference CN2 Simulated Discharge. Fig. 4 shows difference Manning Overland Roughness coefficient with Simulated Discharge.

Sympathy Investigation of Climatological Components in Stream Overflow

In this phase of investigation, other essential climatological component with temperature, relative humidity, wind speed and solar radiation in addition to

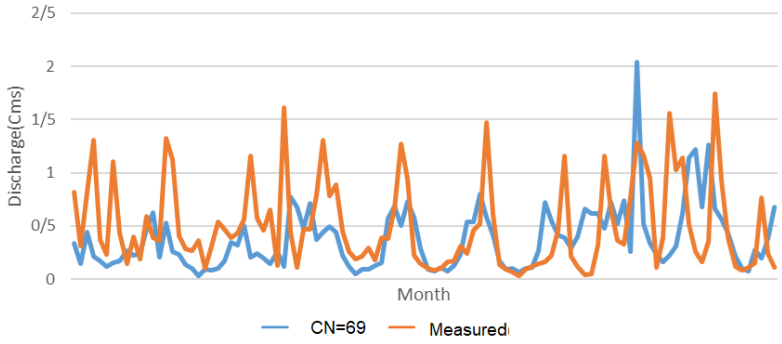

Fig. 2. Comparation Monthly Simulated Release of the SWAT with Quantified overflow.

Table 1. Examine effective curve number in the Average Simulated Discharge

Curve Number	68	70	73	77
Average Simulated Discharge [m^3 s^{-1}]	0.375793	0.377234	0.38093	0.388232
Average Measured Discharge [m^3 s^{-1}]	0.498963	0.498963	0.498963	0.498963
Error [m^3 s^{-1}]	0.123169	0.121736	0.118126	0.11085
Percent change or variable	0	0.4025%	1.3614%	3.4361%

Table 2. Inspect operative Over land Roughness factor in the Average Discharge design

Manning Overland Roughness coefficient	0.07	0.12	0.17	0.22
Average Simulated Discharge [m^3 s^{-1}]	0.375793	0.375793	0.375793	0.375793
Average Measured Discharge [m^3 s^{-1}]	0.498966	0.498966	0.498966	0.498966
Difference Average Measured Discharge and Simulated Discharge [m^3 s^{-1}]	0.123179	0.123179	0.123181	0.123183
Percent change or variable	0	0	-0.0009%	-0.0037%

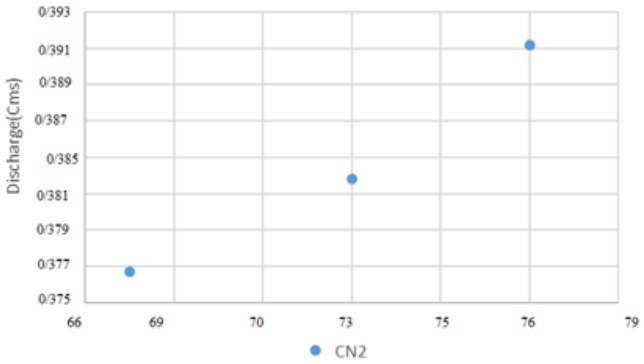

Fig. 3. Difference CN_2 with Simulated Discharge.

precipitation were due to SWAT and the medium runoff, as is shown in the third row if the Table 3, was calculated as 0.5715 cubic meters per second (Novak, 2023).
Fig. 5 shows simulated Discharge river with variable curve number to compare Measured Discharge. Fig. 6 shows Simulated Discharge river with variable Manning Overland Roughness coefficient to compare Measured Discharge.

Precipitation Effect

In order to study the sensitivity of the runoff estimated by the model to precipitation, initially, all precipitation values were multiplied to 1.52 and the runoff was

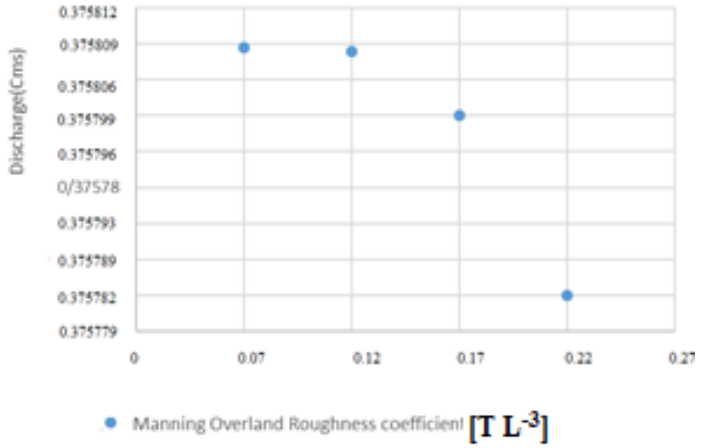

Fig. 4. Difference Manning Overland Roughness coefficient with Simulated Discharge.

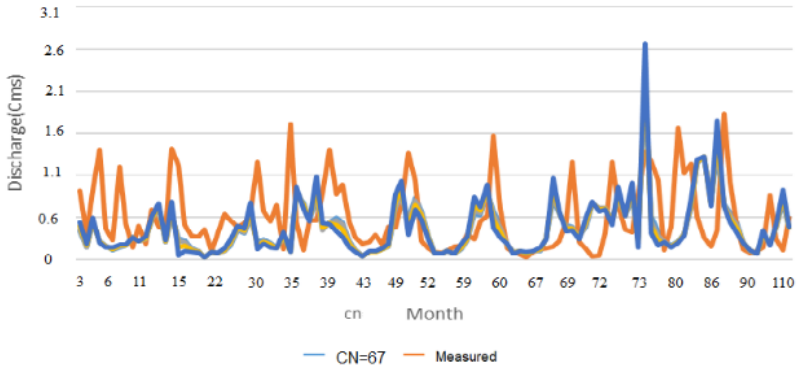

Fig. 5. Simulated Discharge river with variable curve number to compare Measured Discharge.

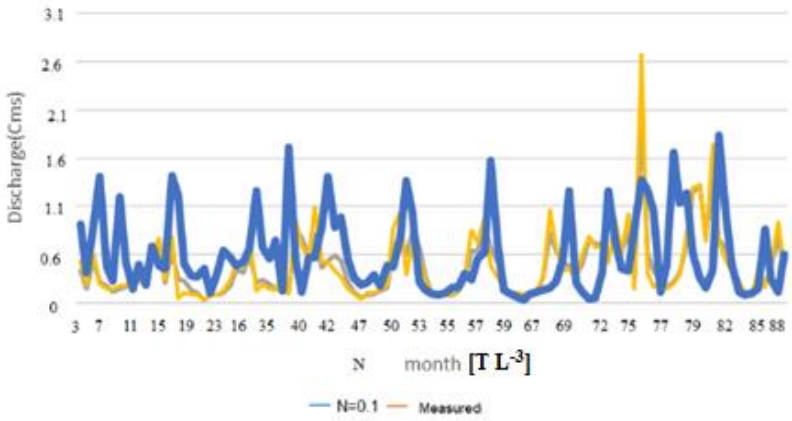

Fig. 6. Simulated Discharge river with variable Manning Overland Roughness coefficient to compare Measured Discharge.

calculated. The real amount of precipitation was used to obtain the average long-term runoff of the river (0.5704232). With a 60% increase in the precipitation, the river runoff was increased to 1.285224121 (a 132% increase). With a 20% decrease in precipitation, the average runoff decreased for 62% (0.203889562 cubic meters per second). Consequently, we face 0.7153 increase and 0.3671 decrease in monthly runoff. As apparent in Fig. 7, the regular runoff tendency is rising depend on the rainfall. With a 60% rise and a 20% decline in input rainfall, the stimulated overflow will be 0.82 and 0.31 which are higher and lower than the mean experiential regular overflow, individually.

Solar Radiation

Effect with a 30% increase and a 40% decrease in the input solar radiation, the simulated runoff varied from 0.61 cubic meters per second to 0.63 and 1.31 cubic meters per second, respectively. The monthly variations are presented in Table 4 and Fig. 8. with a 30% increase and a 50% decrease in the input solar radiation, the simulated runoff would increase 0.16 and 0.86 cubic meters per second respectively.

Humidity Effect

By a 20% rise and a 30% diminution in the input relative humidity, the average monthly runoff would alter from 0.5704 to 0.6947 and 0.3084, correspondingly. These 21.79% increase and 45% decrease are presented in the Table 5 and Fig. 9. By a 20% rise and 30% decrease in input comparative moisture, the simulated runoff was 39.25% advanced, and 38.18% lesser than medium quantified monthly runoff, correspondingly.

Wind Speed

With a 55% increase and a 20% decrease in input wind speed, the obtained average monthly runoff would be

Table 3. Result variable Simulated Discharge that change precipitation

Precipitation [mm]	Average Simulated Discharge [$m^3 s^{-1}$]	Average Measured Discharge [$m^3 s^{-1}$]	Difference Average Measured Discharge and Simulated Discharge [$m^3 s^{-1}$]	Percent variable Simulated Discharge
PCP×1.6=3.11196	1.28522412	0.49895316	0.7878	131.26%
PCP×0.8=1.452191	0.203889561	0.49895402	0.2963	-66.32%
PCP= 2.07467	0.5704235	0.49895316	0.0725	0

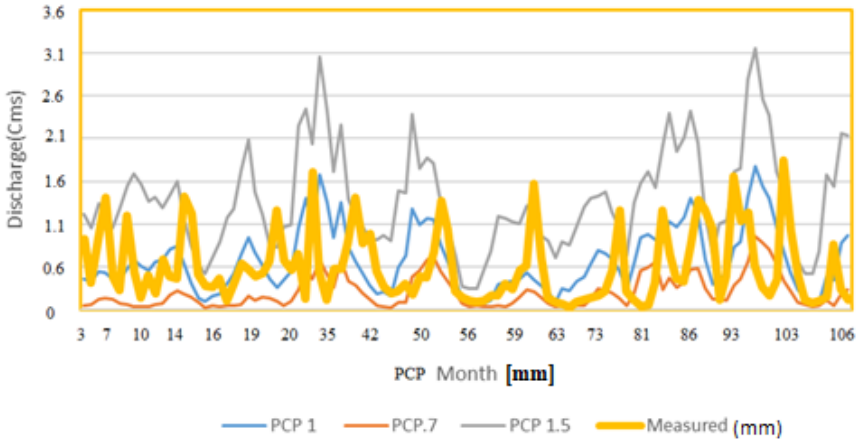

Fig. 7. Result Simulated Discharge with change precipitation.

Table 4. Alteration Simulated Release of the prototypical SWAT with Change data input solar radiation

Average Solar Radiation [MJ/[m^2/Day]]	Average Simulated Discharge [$m^3 s^{-1}$]	Average Measured Discharge [$m^3 s^{-1}$]	Difference Average Measured Discharge and Simulated Discharge [$m^3 s^{-1}$]	Percent variable Simulated Discharge
solar ×1.3=23.19	0.59279362	0.498653806	0.0942	3.9156%
solar ×0.8=14.15	1.224632	0.498653806	0.7263	117.78%
solar=18.63	0.5704362	0.498653806	0.0722	0

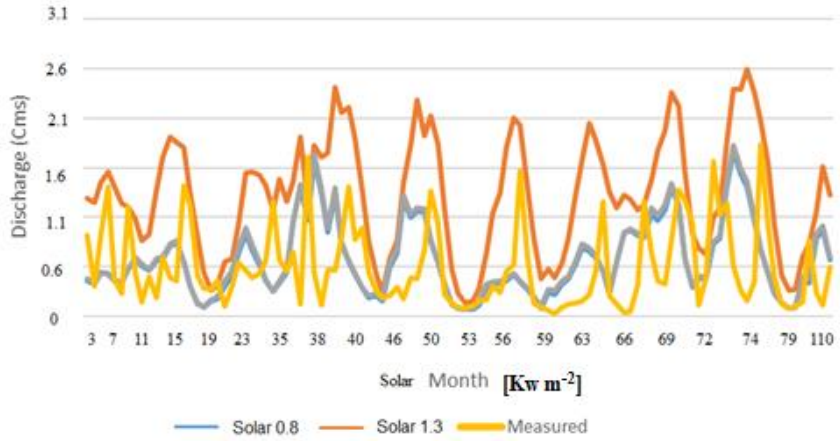

Fig. 8. Result Simulated Discharge with Difference information input Solar Radiation.

Table 5. Difference Simulated Discharge with changing information input humidity

Average Humidity [%]	Average Simulated Discharge [$m^3 s^{-1}$]	Average Measured Discharge [$m^3 s^{-1}$]	Difference Average Measured and Discharge Simulated Discharge [$m^3 s^{-1}$]	Percent Difference Simulated Discharge
0.4581 =Rh	0.5704232	0.498966	0.0723	0
0.56322=Rh×1.3	0.694742122	0.498966	0.1963	21.83%
0.3223=0.8 Rh×	0.308425123	0.498966	0.1915	-46.93%

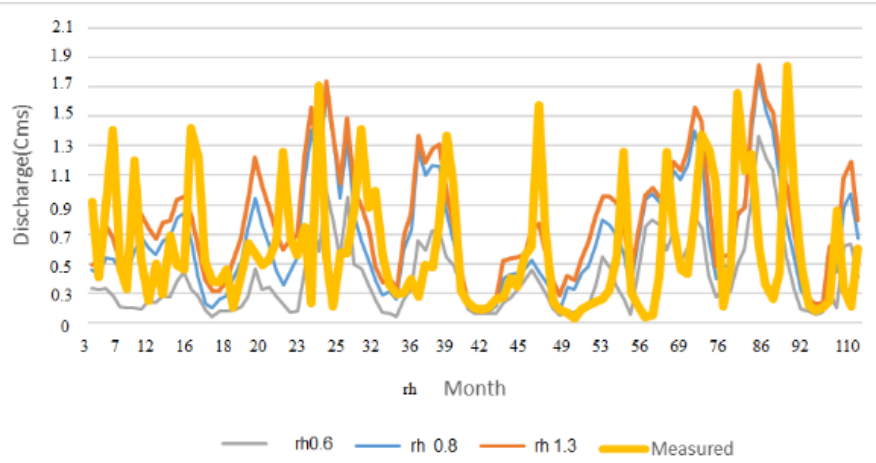

Fig. 9. Consequence Replicated Release Average Monthly with Alteration data input Relative Moisture.

1.32 and 1.42 cubic meters per second. The simulated values are 0.81 and 0.86 higher than the observed average monthly runoff (Fig. 10, Table 6).

Temperature

With a 60% increase and a 20% decrease in the input temperature, the average monthly runoff varied from 0.5704235 to 0.242062696 and 0.79410478, that is, a 58.64% increase and a 40.32% decrease in the monthly runoff. The Simulated results are 52% lower and 62.32% higher than the Measured Average Monthly Runoff (Fig. 11, Table 7).

Results and discussion

1. With 14.56% increase in the curve number, the Simulated Average Monthly Runoff would 2.63% close to the Measured average runoff. With a 1.7% increase in the roughness coefficient of watershed,

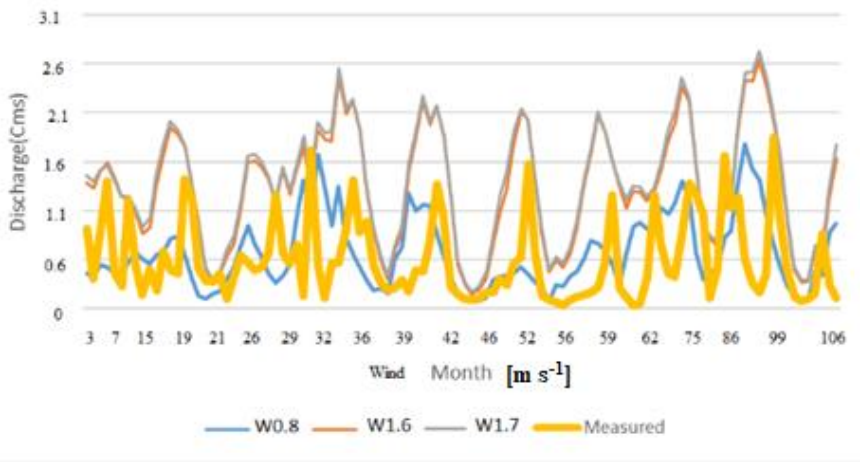

Fig. 10. Simulated Discharge with Difference information input Wind Speed.

Table 6. Difference Simulated Discharge with changing information input humidity

Average Wind Speed [m s^{-1}]	Average Simulated Discharge [m^3 s^{-1}]	Average Measured Discharge [m^3 s^{-1}]	Difference Average Measured Discharge and Simulated Discharge [m^3 s^{-1}]	Percent variable Simulated Discharge
0.8 wind×=1.764	1.2898432	0.498953716	0.7916	132.12%
wind× 1.6 =3.78	1.23933897	0.498953716	0.7416	121.26%
Wind=2.52	0.5704232	0.498953716	0.0725	0

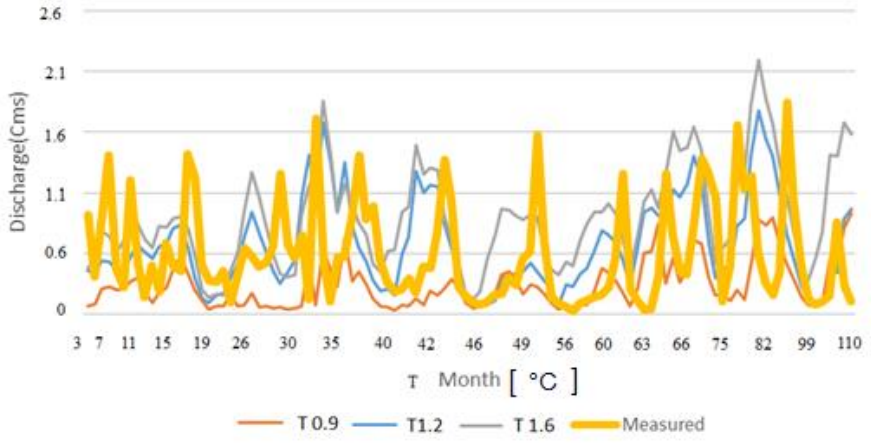

Fig. 11. Simulated Discharge with Difference information Input Temperature.

Table 7. Alteration Simulated Release with Change data Input Temperature

Temperature [°C]	Average Simulated Discharge [m^3 s^{-1}]	Average Measured Discharge [m^3 s^{-1}]	Difference Average Measured Discharge and Simulated Discharge [m^3 s^{-1}]	Percent variable Simulated Discharge
T×0.9 =7.762742	0.79410478	0.498953715	0.2963	39.32 %
T×1.6 =16.635596	0.242062699	0.498953715	0.2572	-57.63 %
T= 11.08987	0.5704246	0.498953715	0.0719	0

the Simulated runoff would come 0.02% closer to the Measured Discharge.

2. SWAT software is a good tool to estimate Average Monthly runoff using the precipitation, temperature and other required data. A 33% decrease in the average monthly precipitation, solar radiation, relative humidity, wind and temperature would cause a 65.33% decrease, 115.78% increase, 47.99% decrease, 129.14% increase and 39.46% increase, respectively. It is evident that the precipitation and the relative humidity face the most decreases. The most increase in runoff was a function of wind, then solar radiation and finally temperature.
3. With a 55% increase in the Average Monthly precipitation, a 30% increase in the radiation and relative humidity and a 55% increase in wind and temperature, the amount of modeled runoff would face a 126.36% increase, 3.9114% increase, 21.89% increase, 117.32% increase and 57.63% decrease, respectively. Precipitation then wind and relative humidity reason the greatest intensifications. The least runoff sensitivity is related to the solar radiation.
4. Discharge is steady flexible measurement which display a foremost part on water accessibility, environmental conservation and ecohydrological effective of a watershed. So as to inspect their spatial-temporal altering features, hydrological models, are evaluation devices. But, to reduce doubts of the prototypical estimations, good quality spread investigational data recognized are important for realist prediction. The aim of this examination is to apply the Soil and Water Assessment Tool (SWAT) in a affectionate watershed of Haraz watershed, and to measure the possessions of using together issue and soil humidity data's on the prototypical doubts and predictions. For streamflow, the values of the Nash–Sutcliffe prototypical efficiency (NS) amongst tool positions varied from 0.75 to 0.91 in the calibration stage for the yearly period stage, and amongst 0.61 and 0.86 in the monthly period stage. In the justification stage, NS standards fluctuated from 0.61 to 0.81 for the yearly period stage and amongst 0.65 and 0.84 for the once-a-month period stage. These significances mean "satisfactory" and "very good" routines for discharge. Whereas there is still some measurement of uncertainty, the preparation of balancing data, for instance soil humidity, to regulate and approve the SWAT model is valuable, predominantly as soon as discharge data is uncommon, as for some watersheds in the humid area. Water scarcity and the absence of water resources expansion and association are foremost tasks for get-together approaching water problems and dipping civilization powerlessness. Hydrological models afford a global contemplation of measurements refinements that occur in the soil–plant atmosphere association, while donating a mark of uncertainty in their significances. Increasingly, such devices have been useful for expansion, group and water resources approach. Reviews associated to the examination of uncertainties of distributed models have been increasing performed. calibration and examination of doubts of semi-dispersed watershed models are subject to a measurement of issues, for instance their parameterization, the non-eccentricity of an established of parameters, the description of what is a "calibrated model", are the proper restrictions of its practice, and the calibration in watersheds somewhere land usages or rivers have been importantly adapted. Furthermore, input data and three-dimensional gauge descriptions are similarly measured as bases of uncertainties.
5. The Haraz watershed is portion of the Haraz River washbasin, which is situated in the central district of northern Iran south of the Caspian Sea. The smallest and supreme advancements in the washbasin are 292 and 3292 m, consistently. The zone's global category is hilly with average grade of 16.6% and, conferring to the Iranian biological organization, this washbasin depends to the central Alborz with its superficial rocks fitting to the primary, another, and 3rd ages. The popular of this washbasin is bounded to different forestry kinds that have earthly uses for example rangeland and agronomy, in addition to forestry terrestrial usage. The soil in this washbasin is chiefly of the podzolic, brown forest, and sedimentary kinds. Iran has a warm, dry weather considered by extensive, warm, dehydrated summers. Rainfall is occasionally focused in local then fierce hurricanes, causation corrosion and local overflowing, particularly in the winter months. A minor region alongside the Caspian coastline has a very diverse climatological form. Now, precipitation is heaviest from late summer to mid-winter, then, in over-all, falls through the year. The instruction region has an average yearly rainfall of 753 mm and the environment is semi-humid and cool. The Haraz watershed is situated in Mazandaran domain, which hosts the greatest data of splits interesting in inner movement, typically due to satisfactory situation circumstances compared to the dry situation in the rest of the country.

Conclusion

SWAT prototypical routine in simulating the hydrogeological management has been assessed for the Haraz watershed, Mazandaran province (Iran) applying different soil shapes. The consequences of the calibration process show a deteriorating of the routine if a collective number of soil units are measured. Discharge presented a respectable routine and was consequently additional utilized in the validation process. The shaped map displays that some sub-basins are constantly considered by a high quantity of runoff. The runoff exposure map, comprehended examining the yearly maps shows the same sub-basins as high disposed to runoff. Exclusive these zones, considered by high development, short runoff periods could happen, rising the peak current downriver and accordingly the flood hazard. This explanation denotes an appreciated instrument for supervision application strategies and deterrent goal

schedules for those zones more disposed to runoff efficiency. The overall method here used can be accepted in many other minor watersheds categorized by Haraz (Mazandaraan Province, Iran) environment. This investigation consider the sensitivity of the runoff approximation for streams, applying the SWAT model, depend on differences in such climatological components as precipitation, solar radiation, wind, humidity and temperature. The obtained results indicate that with a 32.07% decrease in the average monthly precipitation, sunshine, relative humidity, wind and temperature, we witness 65.36% decrease, 116.82% increase, 46.78% decrease, 127.16% increase, and 39.52% increase in modeled runoff, respectively.

COI Declarations Statement
Data Availability statement

Some or all data, models, or code generated or used during the study are available from the corresponding author by request.

Acknowledgment

This research was supported by the Department of Civil Engineering, School of Engineering. We thank our all authors who provided insight and expertise that greatly assisted the research.

References

Alavinia, M., Nasiri Saleh, F. (2010): Comparsion Of HSPF and SWAT Model to simulate Sediment ;(Case Study: Watershed Abro); Fifth National Congress On Civil Engineering Ferdowsi University Of Mashhad(In Persian).

Amoakowaah Osei, M., Kofitse Amekudzi, L., Dotse Wemegah, D., Preko, K., Serwaa Gyawu, E., Obiri-Danso, K. (2019): The impact of climate and land-use changes on the hydrological processes of Owabi catchment from SWAT analysis. Journal of Hydrology: Regional Studies. Volume 25, October 2019, 100620. https://doi.org/10.1016/j.ejrh.2019.100620.

Apostel, A., Kalcic, M., Scavia, D. (2020): Simulating internal watershed processes using multiple SWAT models. Science of The Total Environment. Volume 759, 10 March 2021, 143920. https://doi.org/10.1016/j.scitotenv.2020.143920.

Bačová Mitková, V., Pekárová, P., Halmová, D. (2023): Investigation of water temperature changes in the Hron River in the context of expected climate change. Acta Hydrologica Slovaca, Vol. 24, No. 1, 2023, 52–62, doi:10.31577/ahs-2023-0024.01.0007.

Behtari Nejad, B. (2012): Estimation of erosion, sedimentation and nutrient loss in Gorganrood catchment with SWAT model.A Thesis Presented for a Degree Master of Science (M.Sc) in Soil Physics & Conservation (In Persian).

Chu, T. W., Shirmohammadi, A. (2004): Evaluation of the SWAT model's hydrology component in the piedmont physiographic region of Maryland. Trans. ASAE.47: 1057–1073.

Dadar, M., Adel, M., Ferrante, M., Nasrollahzadeh Saravi, H., Copat, C., Oliveri Conti, G. (2016): Potential risk assessment of trace metals accumulation in food, water and edible tissue of rainbow trout (Oncorhynchus mykiss) farmed in Haraz River, northern Iran. Toxin Reviews 35(3–4). DOI: 10.1080/15569543.2016.1217023.

Engman, E. T. (1983): Roughness coefficients for routing surface runoff. Proc Spec. Conf. Frontiers of Hydraulic Engineering.

Frizzle, C. A., Fournier, R. E., Luther, J. (2021): Using the Soil and Water Assessment Tool to develop a LiDAR-based index of the erosion regulation ecosystem service. Journal of Hydrology. Volume 595, April 2021, 126009. https://doi.org/10.1016/j.jhydrol.2021.126009.

Haltiner, G. J., Martin, F. l. (1957): Dynamical and physical meteorology. Mcgraw-Hill, New York.

Jensen, M. E. (ed.) (1974): Consumptive use of water and irrigation water requirements. Rep. Tech. Com. on Irrig. Water Requirements, Irrig. and Drain. Div., ASCE.

Khaleghi, M. R., Gholami, V., Ghodusi, J., Hosseini H., (2011): Efficiency of the geomorphologic instantaneous unit hydrograph method in flood hydrograph simulation. Catena. Volume 87, Issue 2, November 2011, 163–171.

Mohammadi, M., Egli, M., Kavian, A., Lizaga, I. (2023): Static and dynamic source identification of trace elements in river and soil environments under anthropogenic activities in the Haraz plain, Northern Iran. Science of The Total Environment. Volume 892, 20 September 2023, 164432. https://doi.org/10.1016/j.scitotenv.2023.164432.

Naeeji, N., Rafeei, M., Azizi, H., Hashemi, M., Eslami, A. (2020): Data on the microplastics contamination in water and sediments along the Haraz River estuary, Iran. Volume 32, October 2020, 106155. https://doi.org/10.1016/j.dib.2020.106155.

Neitsch, S. L., Arnold, J. G., Kiniry, J. R., Williams, J. R. (2005): Soil and Water Assessment Tool Theoretical Documentation, SWAT 2005.

Neitsch, S. L., Arnold, J. G., Kiniry, J. R., Williams, J. R. (2011): SWAT Soil and Water Assessment Tool Theoretical Documentation Version 2009.

Novak, V. (2023): The influence of land use change on transport of water and energy in ecosystem and climate change. Acta Hydrologica Slovaca, Vol. 24, No. 1, 2023, 3–8, doi: 10.31577/ahs-2023-0024.01.0001.

Ghashghaie, M., Eslami, H., Kaveh Ostad-Ali-Askari, K. (2022): Applications of time series analysis to investigate components of Madiyan-rood river water quality. Appl Water Sci 12, 202 (2022). https://doi.org/10.1007/s13201-022-01693-5

Rabiei, J., Sadat Khademi, M., Bagherpour, S., Ebadi, N., Karimi, A., Ostad-Ali-Askari, K. (2022): Investigation of fire risk zones using heat–humidity time series data and vegetation. Appl Water Sci 12, 216 (2022). https://doi.org/10.1007/s13201-022-01742-z

Rallison, R. E., Miller, N. (1981): Past , present and future SCS runoff procedure.p. 353-364. In V.P. Singh (ed). Rainfall runoff relationship. Water Resources Publication, Littleton, CO.

Saadati, H. (Fall 2003): Effect Of Land Use On Simulating Daily Discharge Flow Using SWAT Mathematical Model (Case Study: BabolRod Catchment Area); A Thesis Presented For The Degree Of Master in Watershed Management.; Tarbiat Modares University Natural Science Faculty (In Persian).

Schuol, J., Abbaspour, K. C., Yang, H., Reichert, P., Srinivasan, R., Schar, Ch., Zehnder, A. J. B. (2006): Estimation of freshwater availability in the west Africa subcontinent. J. Hydrol. 254:58–69.

Shrestha, N. K., Akhtar, T., Daggupati, P., (2020): Can-GLWS: Canadian Great Lakes Weather Service for the Soil and Water Assessment Tool (SWAT) modelling. Journal of Great Lakes Research. Volume 47, Issue 1,

February 2021, Pages 242–251. https://doi.org/10.1016/j.jglr.2020.10.009.
Soil Conservation Service (1964): Chapter 17: Flood routing, Section 4, Hydrology, National engineering handbook. U.S. Department of Agriculture. U.S.Gov't Printing Office, Washington, D.C.
Soil Conservation Service (1972): Section 4: Hydrology In National Engineering Handbook. SCS.
Soil Conservation Service Engineering Division (1986): Urban hydrology for small watersheds. U.S. Department of Agriculture, Technical Release 55.U.
USDA Soil Conservation Service (1983): National Engineering Handbook Section 4. Hydrology, Chapter 19.
Werneck, F. P. (2011): The diversification of eastern South American open vegetation biomes: historical biogeography and perspectives. Quat. Sci. Rev. 30, 1630–1648, http://dx.doi.org/10.1016/j.quas- cirev.2011.03.009.
Xue, C. M., Asce, B. C., Wu, H. (2014): Parameter uncertainty analysis of surface flow and sediment yield in the Huolin Basin, China. J. Hydrol. Eng. 19, 1224–1236, http://dx.doi.org/10.1061/(ASCE)HE.1943-5584. 0000909.
Varga, A., Velísková, Y., Sokáč, M., Sočuvka, V., Mikula, P. (2023): Analysis of seasonal changes of thermal stratification in reservoir for drinking water supply (Slovakia, Turček reservoir). Acta Hydrologica Slovaca, Vol. 24, No. 1, 2023, 33–42, doi: 10.31577/ahs-2023-0024.01.0005.
Yang, J., Reichert, P., Abbaspour, K. C., Xia, J., Yang, H., (2008): Comparing 1150 uncertainty analysis techniques for a SWAT application to the Chaohe Basin in China. J. Hydrol. 358, 1–23, http://dx.doi.org/10.1016/j.jhydrol.2008.05.012.
Zare, M., Panagopoulos, T., Loures, L. (2017): Simulating the impacts of future land use change on soil erosion in the Talar watershed, Iran. Land Use Policy. Volume 67, September 2017, Pages 558–572.
Zettam, A., Taleb, A., Sauvage, S., Boithias, L., Belaidi, N., Sa´nchez-Pe´rez, J. M. (2017): Water 9, 216–234, http://dx.doi.org/10.3390/w9030216.
Zhang, D., Chen, X., Yao, H., Lin, B., (2015): Improved calibration scheme of SWAT by separating wet and dry seasons. Ecol. Model. 301, 54–61, http://dx.doi.org/10.1016/j.ecolmodel.2015.01.018.
Zhang, X., Liang, F., Srinivasan, R., Van Liew, M. (2009): Estimating uncertainty of streamflow simulation using Bayesian neural net- works. Water Res. Res. 45, 1–16, http://dx.doi.org/10.1029/2008WR007030.

Dr. Kaveh Ostad-Ali-Askari (*corresponding author, e-mail: ostadaliaskari.k@of.iut.ac.ir; kaveh.oaa2000@gmail.com)
Department of Civil Engineering, School of Engineering
American University in Dubai
Dubai, 28282
United Arab Emirates

Department of Natural Sciences
Manchester Metropolitan University
Manchester
M1 5GD
United Kingdom

World Top 2-Percent Researcher, Standford University
USA, 2022

Mr. Mohsen Ghane
Department of Water Resources Management and Water Engineering
Semnan University
Semnan
Iran

Dr. Peiman Kianmehr
Department of Civil Engineering, School of Engineering
American University in Dubai
Dubai, 28282
United Arab Emirates